



**A Novel Mass Spectrometer for Atmospheric Measurements
&
Halocarbons During the CARIBIC and SAMBBA
Aircraft Campaigns**



By

ADAM WISHER

School of Environmental Sciences
UNIVERSITY OF EAST ANGLIA

April 2015

A thesis submitted to the
School of Environmental Sciences of the
University of East Anglia in partial
fulfilment of the requirements for the
degree of Doctor of Philosophy

Copyright © Adam Wisher 2015
All rights reserved.

For Emma and Charlotte

Abstract

Identification and monitoring of halocarbons in the atmosphere remains important for the purposes of regulation and prediction of stratospheric ozone depletion. Measurements of these and other compounds have created a demand for techniques that improve the number of atmospheric compounds analysable. A prototype time-of-flight gas chromatography-mass spectrometer (GC-MS) was characterised for atmospheric measurements. Instrument performance was found to be at the lower end of expectations. A comparison to a quadrupole GC-MS indicated that the TOF GC-MS would be suitable for measurements in polluted environments.

As part of this comparison, a number of halocarbons were analysed in London, U.K. as part of the ClearLo campaign. HCFCs were found at higher concentration than their Northern Hemispheric (NH) baseline values. Furthermore, HFC-134a and HFC-227ea were almost double their NH baseline. CH_2Cl_2 , C_2Cl_4 and C_2HCl_3 were encountered at high concentrations and sources of very short-lived bromomethanes (VSLB) were identified close to London.

As part of the CARIBIC project, five VSLB were measured in the mid-latitude upper troposphere/lower stratosphere and tropical troposphere. Higher mixing ratios were encountered over Southeast Asia, likely due to a locally longer CH_2Br_2 lifetime. Total bromine derived from these five VSLB is at the lower end of the quantity required to balance the stratospheric bromine budget.

During the SAMBBA project, biomass burning and natural sources of COS, methyl halides and other halocarbons were assessed over Brazil. Methyl halide emissions from rainforest and savannah fires were quantified. The Cerrado savannah was found to be a strong source of COS. Regional biomass burning emission estimates indicate that this is an important region for emissions of these compounds. Terrestrial, natural sources of CH_3Cl , CH_3Br and CHCl_3 were confirmed over the Amazon rainforest. Emissions from a localised source of CHCl_3 were identified and wetlands or agricultural soil disturbance were hypothesised as a likely cause.

Acknowledgements

Firstly I would like to thank my supervisor David Oram for his support and understanding throughout my studies. I would also like to thank my co-supervisors Johannes Laube and Bill Sturges for their invaluable discussions and suggestions. Thanks also go to Graham Mills for his technical genius and for maintaining the TOF by not touching it, and to Stephen Humphrey for his general help around the lab.

I am very grateful for the generosity of spirit of the project groups that I have been involved in and to those individuals who shared their data with me. I am especially grateful to everyone working on the CARIBIC project who all make great effort to include and enthuse those they work with.

On a more personal note, I would like to thank everyone in the office for cheering me along and the coffee/lunchtime gang for making breaks worth it. I would especially like to thank Mike and Emma for their constructive criticism and thoughts as well as their friendship and support. Special thanks go to the Albert Sloman Library, staff, staffroom and paternoster lift (when it's on). Lastly, and most importantly, I would like to thank my ever-loving wife Emma for her patience, encouragement, support and love, and to Charlotte for being the best daughter in the world.

Contents

1	Introduction	1
1.1	Atmospheric structure	1
1.2	Atmospheric circulation	2
1.2.1	Stratospheric transport at the ITCZ	3
1.3	Stratospheric ozone	3
1.3.1	Chlorine and ozone	4
1.3.2	Bromine and ozone	5
1.3.3	Heterogeneous chemistry	6
1.3.4	Ozone depletion potentials (ODPs)	7
1.4	A note on atmospheric concentrations	7
1.5	Ozone depleting substances (ODSs)	9
1.5.1	Chlorocarbons	9
1.5.1.1	Chlorofluorocarbons (CFCs)	9
1.5.1.2	Hydrochlorofluorocarbons (HCFCs)	10
1.5.1.3	Methyl chloride	10
1.5.1.4	Other long-lived chlorocarbons	11
1.5.1.5	Very short-lived chlorocarbons	12
1.5.2	Bromocarbons	13
1.5.2.1	Halons	13
1.5.2.2	Methyl bromide	14
1.5.2.3	Very short-lived bromocarbons (VSLB)	14
1.5.3	Iodocarbons	16
1.5.3.1	Methyl iodide	16
1.5.4	Carbonyl sulfide (COS)	17
1.6	Greenhouse gases	17
1.6.1	Global warming potentials (GWPs)	18
1.6.2	Fluorocarbons and other fluorinated gases	18
1.6.2.1	Hydrofluorocarbons (HFCs)	18
1.6.2.2	Perfluorocarbons and other perfluorinated compounds	19
1.7	Aims and rationale	19
1.7.1	The ClearLo campaign	20
1.7.2	The CARIBIC project	21

1.7.3	The SAMBBA project	21
1.7.4	Summary of aims	22
2	Experimental Theory & Methods	23
2.1	Gas chromatography	23
2.1.1	Chromatographic theory	23
2.1.2	Carrier gases	24
2.1.3	GC columns	24
2.1.4	Detectors	25
2.2	Mass spectrometry	26
2.2.1	Quadrupole mass analyser	26
2.2.2	Time of flight mass spectrometry (TOF MS)	27
2.2.2.1	Orthogonal time-of-flight analysers (oa-TOF)	28
2.2.2.2	Reflectron time-of-flight analysers (re-TOF)	30
2.2.2.3	Applications of TOF to Atmospheric Science	31
2.2.3	Ionisation techniques	32
2.2.3.1	Electron ionisation (EI)	32
2.2.3.2	Negative ion chemical ionisation (NICI)	33
2.2.4	Summary of time-of-flight vs. quadrupole mass spectrometry	34
2.3	General calibration processes	36
2.4	GC-MS technique usage	36
3	A GC Time of Flight Mass Spectrometer for Atmospheric Measurements	39
3.1	Inlet system	39
3.2	GC system	40
3.2.1	GC×GC capability	40
3.2.2	Agilent™ GC system	41
3.3	Time-of-flight (TOF) mass spectrometer	42
3.3.1	MS alterations and upgrades	43
3.3.1.1	30 kHz and 100 kHz sampling modes	44
3.3.1.2	High-voltage accel-decel Einzel lens assembly	44
3.3.1.3	Other alterations and repairs	45
3.4	Instrument characterisation	45
3.4.1	Manual analysis method	45
3.4.2	Compound identification	46
3.4.3	Reproducibility	46
3.4.4	Mass dependency	49
3.4.4.1	Signal-to-noise dependency	49
3.4.5	Sensitivity drift	54
3.4.6	Linearity	54
3.5	Preliminary comparison	58
3.5.1	The ClearLo Project	58
3.5.2	Analysis and supporting measurements	59
3.5.2.1	Dual MS analysis method	59

3.5.2.2	TOF analysis method	60
3.5.2.3	Supporting measurements	61
3.5.3	Comparison to the ClearfLo in situ data	61
3.6	ClearfLo Results	68
3.6.1	Air mass influences at the summer IOP site	69
3.6.2	Summer IOP averages	72
3.6.3	Long-lived halocarbons	72
3.6.3.1	Chlorofluorocarbons (CFCs)	73
3.6.3.2	Hydrochlorofluorocarbons (HCFCs)	74
3.6.3.3	Other chlorocarbons	76
3.6.3.4	Hydrofluorocarbons (HFCs)	76
3.6.3.5	PFCs	77
3.6.3.6	Other fluorinated compounds	77
3.6.3.7	Halons	78
3.6.4	Short-lived halocarbons	78
3.6.4.1	Short-lived chlorocarbons	78
3.6.4.2	Very short-lived bromo-and iodo-methanes	79
3.7	Summary	82
3.7.1	ClearfLo results	82
3.7.2	TOF GC-MS	86
4	Very short-lived bromocarbons in CARIBIC	89
4.1	The CARIBIC project	89
4.2	Methods	90
4.2.1	Calibration of short-lived halocarbons	92
4.3	Results and discussion	93
4.3.1	Central American flights	93
4.3.1.1	Latitudinal distribution and averages	93
4.3.1.2	Potential temperature	96
4.3.1.3	Ozone and height above the tropopause	97
4.3.2	South African flights	102
4.3.3	South-East Asia flights	105
4.3.4	Enhancements in the mixed bromochloromethanes	107
4.4	Summary and conclusions	107
5	Biomass burning and background emissions in SAMBBA	109
5.1	The SAMBBA campaign	109
5.2	Analysis and supporting measurements	109
5.2.1	Instrumental set-up and methods	109
5.2.2	Carbon monoxide measurements	110
5.3	Emission ratios and emission factors	113
5.3.1	Normalised emission ratio (NEMR)	113
5.3.2	Emission factor (EF)	114
5.3.3	Modified combustion efficiency (MCE)	115

5.4	Results and discussion	115
5.4.1	Flight classification	115
5.4.2	Biomass burning	117
5.4.2.1	Halomethane background mixing ratios	117
5.4.2.2	Halomethane normalised emission ratios (NEMRs)	119
5.4.2.3	Halomethane emission factors (EFs)	121
5.4.2.4	Chlorobenzene burning emissions	124
5.4.2.5	Carbonyl sulfide NEMRs and EFs	125
5.4.2.6	Regional and global biomass burning emission estimates	129
5.4.3	Background measurements	132
5.4.3.1	Carbon monoxide	133
5.4.3.2	Methyl chloride	134
5.4.3.3	Methyl bromide	136
5.4.3.4	Methyl iodide	136
5.4.3.5	Chloroform	137
5.4.3.6	Dichloromethane	142
5.4.3.7	Dibromomethane and bromoform	143
5.4.3.8	Perchloroethene, PCE	144
5.5	Summary	144
6	Conclusions and future research	147
6.1	Outline of major research findings	147
6.1.1	TOF GC-MS	147
6.1.2	Halocarbons in London	147
6.1.3	Very short-lived bromocarbons in the upper troposphere	148
6.1.4	Biomass burning and background emissions over Brazil	148
6.1.4.1	Biomass burning	148
6.1.4.2	Background rainforest emissions	149
6.2	Discussion and future work	149
6.2.1	TOF-GC MS	149
6.2.2	Halocarbons in London	151
6.2.3	VSLB in the mid-upper troposphere	152
6.2.4	Brazilian biomass burning and background emissions	153
	References	167
	List of figures	171
	List of tables	174
	Major abbreviations and chemical formulae	176

Introduction

In recent years there has been increased interest in chemical perturbations of the atmosphere. Key environmental concerns highlighted in the past few decades include urban air pollution, acid rain, the ozone hole and man-made climate change. These issues have become areas of public as well as scientific concern due to their deleterious effects on human health and the environment. Increasingly, governments and the public have accepted that current changes to the atmosphere are not sustainable. One key issue that highlights the significance of human perturbations to the atmosphere, and the near-global response possible, is the destruction of the ozone layer. The discovery of the Antarctic ozone hole and subsequent identification of the gases responsible, e.g. CFCs, led to a large-scale response systematised by the Montreal Protocol and its subsequent amendments. The Montreal Protocol has generally been deemed, at least in the public eye, to be one of the greatest successes in environmental recovery of recent decades. However, continued vigilance is required by the scientific community and policy-makers in order to maintain the effectiveness of current legislature, identify non-adherents, prevent relapse and recognise emergent threats.

This work is mainly concerned with atmospheric trace gases which deplete stratospheric ozone. A small number of anthropogenic greenhouse gases which contribute to global warming are also covered. This chapter will introduce some of the basic concepts of atmospheric structure and circulation, and outline the chemistry of stratospheric ozone depletion. There follows an introduction to the main compounds considered in subsequent chapters.

1.1 Atmospheric structure

The atmosphere can be divided vertically into four major regions: the troposphere, stratosphere, mesosphere and thermosphere, Figure 1.1. The troposphere extends from the surface to approximately 8–18 km altitude dependent on the location and season. The stratosphere extends from the top of the troposphere to 45–55 km. The transition between the troposphere and stratosphere is termed the tropopause; the equivalent at the top of the stratosphere, at the transition into the mesosphere, is termed the stratopause. This work is only concerned with tropospheric chemistry and its effects on the stratosphere.

These regions, and the boundaries between them, are mainly defined by temperature. In the troposphere, the main heat source is radiation from the Earth's surface, leading to an average

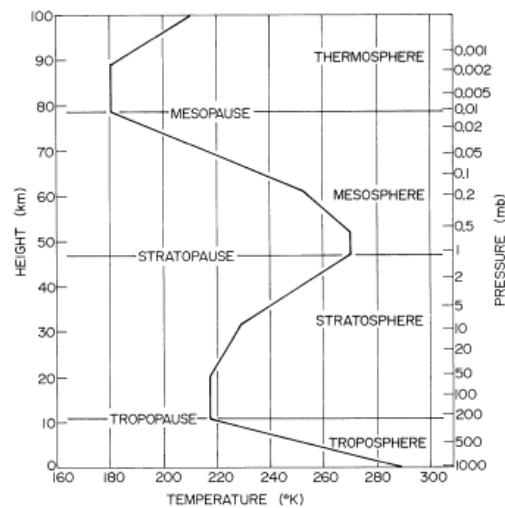


Figure 1.1: Example of the vertical temperature profile in the atmosphere. Courtesy of Wallace & Hobbs (1977).

decrease in temperature with height (termed the lapse rate) of $\sim 6.5 \text{ K km}^{-1}$ (Wayne, 1996). This gives rise to instability in the troposphere, driven by convective processes and leads to a high degree of vertical transport. Hot, moist air rising in the troposphere is dried by the condensation of moisture as the temperature drops with altitude. The subsequent release of latent heat by condensation increases the convective instability and further drives the up-welling of air. At the tropopause there is a temperature inversion, termed the tropopause, created by the the formation and destruction of ozone in the stratosphere (see Section 1.3).

In contrast to the troposphere, the stratosphere is characterised by slow vertical transport due to the temperature inversion which inhibits convective transport. The exception is for warm air saturated with water, as is frequently encountered in the tropics, which may release enough latent heat energy to drive air through the tropopause.

1.2 Atmospheric circulation

The general circulation of the atmosphere is driven by the temperature differential between the warm tropical regions and the cold polar regions. As the atmosphere attempts to equilibrate the temperature difference, warm air is transported from the equator to the poles. The conservation of angular momentum in the atmosphere, the Coriolis force, drives the poleward circulation to form into three circulation cells termed Hadley cells. For the purposes of this work, the most significant region of circulation is where warm air is transported across the surface from the subtropics and uplifted at the tropics; a region called the Intertropical Convergence Zone (ITCZ).

The ITCZ is a narrow region close to the equator characterised by strong vertical transport in the troposphere and is the main region for transport of trace gases into the stratosphere. The ITCZ has a seasonal, latitudinal oscillation generally moving northwards during Northern Hemispheric summer and southwards during Southern Hemispheric summer. However, the position of the ITCZ is also determined by the location of land masses and ocean circulation.

1.2.1 Stratospheric transport at the ITCZ

At the ITCZ, air is uplifted towards the tropopause by ascent in convective clouds towards a region termed the tropical tropopause layer (TTL). This layer is defined as the region above the level of maximum convective outflow (~ 12 km altitude) and below the cold point tropopause (~ 17 km). The TTL acts as a source region for the stratospheric overworld and the extra-tropical lowermost stratosphere. Net transport into the stratospheric overworld is dominated by large-scale ascent in the Brewer-Dobson circulation, the slow circulation of stratospheric air from the equator to the poles. The strength of this circulation is determined by large-scale dynamical processes. Stratospheric transport from the tropics to the poles occurs most strongly in the upper stratosphere with large-scale descent occurring at high latitudes. In the lowermost stratosphere at mid-latitudes, there is greater mixing and transport across the tropopause. Substances entering the stratosphere from the mid-latitudes are not likely to be transported into the upper stratosphere and have an impact on stratospheric ozone over the poles where ozone depletion is most significant.

1.3 Stratospheric ozone

The chemistry of the stratosphere is dominated by the reactions of ozone (O_3). The catalytic processes of ozone production and loss are the main source of heat in the stratosphere and are responsible for the temperature inversion at the troposphere/stratosphere boundary, the tropopause. Additionally, the ozone layer absorbs most of the UVB (280–315 nm) portion of the spectrum. This shields the troposphere and surface from intense short-wave UVB radiation, preventing damage to biological organisms.

The chemistry of atmospheric ozone involves a number of chemical cycles. The production and loss of ozone in the ‘unperturbed’ stratosphere was first described by Chapman (1930). Ozone is produced by the photolytic breakdown of oxygen (O_2) (Equation 1.1) and the recombination of atomic oxygen, O with O_2 (Equation 1.2), where M is a third body required to carry off the excess energy of formation of O_3 . In the atmosphere M is largely O_2 or N_2 . The overall reaction produces two ozone molecules for every three oxygen (Equation 1.3).



Ozone is lost by photolysis (Equation 1.4) and by reaction with O (Equation 1.5) to give the overall reaction of three O_2 produced for every two ozone lost (Equation 1.6).



The oxygen-only stratospheric cycle proposed by Chapman over-predicts ozone in the stratosphere. This is due to the presence of a series of ozone destroying catalytic cycles. The most basic of these can be generalised as in Equations 1.7, 1.8 and 1.9. The most important species suggested for the catalytic X in the natural atmosphere are H, OH, NO, Cl, Br and, to a lesser extent, I. Stratospheric NO_x , i.e. NO and NO_2 , is present in the stratosphere due to the breakdown of the long-lived gas nitrous oxide (N_2O). HO_x (H, OH and HO_2) is mostly created from the reaction of H_2O and CH_4 with energetically excited oxygen, $\text{O}(^1\text{D})$. Stratospheric Cl, Br and I are produced from natural and anthropogenic, halocarbon trace gases.



This work is mainly concerned with halogenated species with respect to ozone depletion. Therefore, only the ozone depletion chemistry of chlorine and bromine will be considered further. Iodine-ozone chemistry is not discussed further as stratospheric ozone depletion by iodine is poorly understood with few measurements of active iodine species in the stratosphere (e.g. IO). It is assumed that, although the ozone depleting efficiency is theoretically high, little iodine crosses into the stratosphere as iodinated species readily photolyse at high wavelengths.

1.3.1 Chlorine and ozone

The catalytic destruction of ozone by chlorine was proposed by Molina & Rowland (1974), prompted by the escalating use of halogenated compounds in applications such as refrigeration. The ozone destruction cycle involving chlorine is shown in Equations 1.10 and 1.11. The chlorine species involved are generally referred to as ClO_x where $x = 0, 1, \text{ or } 2$. The net ozone destruction is shown in Equation 1.12.



Stratospheric ClO_x is derived from natural and anthropogenic species. For instance, the most abundant natural precursor for ClO_x is methyl chloride (CH_3Cl). The tropospheric lifetime of CH_3Cl is ~ 1 yr (Montzka & Reimann, 2011) allowing some CH_3Cl to be transported across the tropopause. Once in the stratosphere, CH_3Cl is mainly removed by reaction with hydroxyl radical (OH), with photolysis becoming more significant at higher altitudes.

The catalytic cycle shown in Equations 1.10–1.12 can be terminated by reaction with NO_x , HO_x or ClO_x species to form ‘reservoir’ compounds. These species can act as temporary holding cycles, when not efficiently removed from the atmosphere, or as sinks for ClO_x when removed from the stratosphere. For instance, the formation of chlorine nitrate (ClONO_2) forms a temporary reservoir for ClO as does hypochlorous acid (Equations 1.13 and 1.14) and can lead to a non-linear response of ozone to chlorine perturbations (Holloway & Wayne, 2010).



For ClO_x , the main reservoir species is hydrochloric acid (HCl) which can be removed from the stratosphere by slow transport to the troposphere where it is subsequently dissolved by water and ‘rained out’. The production of HCl and regeneration of Cl are shown in Equations 1.15 and 1.16 with the net process shown in Equation 1.17. Approximately, 70 % of stratospheric ClO_x is thought to be present as HCl , though this is dependent on heterogeneous processes (Holloway & Wayne, 2010).

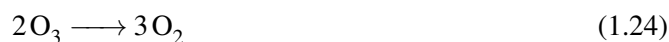
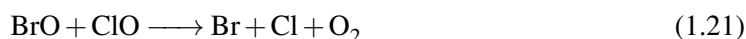
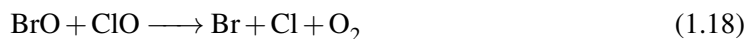


1.3.2 Bromine and ozone

Bromine is, on average and on a per-atom basis, ~ 60 times more efficient at destroying ozone than chlorine (Sinnhuber et al., 2009). Three factors contribute to the ozone destruction efficiency of bromine:

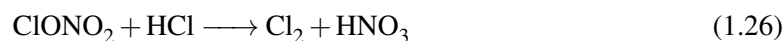
1. Brominated compounds are photolysed at longer wavelengths than chlorinated analogues giving rise to a higher proportion of free bromine.
2. Bromine reservoir species are formed inefficiently and are readily photolysed.
3. Coupling between bromine- and chlorine-catalysed processes potentiates chlorine and bromine for further ozone destruction.

The coupling between BrO and ClO can proceed via three branches, two of which (Equation 1.18 and 1.19) directly produce Br and Cl atoms that can enter a catalytic cycle with ozone as in Equations 1.21–1.23. The other branch (Equation 1.20) generates BrCl which can be further photolysed to Br and Cl.



1.3.3 Heterogeneous chemistry

The reactions described thus far in Section 1.3 are all gas phase reactions. However, heterogeneous reactions on stratospheric particles, e.g. ice, soot, nitric acid hydrate and sulfuric acid, are all significant for stratospheric chemistry. These heterogeneous processes are particularly important for the re-partitioning of reservoir species. For instance, the hydrolysis of ClONO₂, formed by the route given in Equation 1.14, occurs on stratospheric particles as in Equation 1.25. Reactive chlorine can also be liberated by the reaction of ClONO₂ and HCl followed by photolysis to Cl as in Equations 1.26 and 1.27. Numerous other reactions occur on stratospheric particle surfaces involving the interconversion of reservoir species.



Heterogeneous stratospheric chemistry is important in the polar stratosphere. This is especially the case with regard to the Antarctic ozone hole. First discovered in 1985 by Farman et al. (1985), the Antarctic ozone hole forms as total column ozone dramatically reduces in Austral spring. A number of factors influence the chemistry of polar ozone depletion most of which are beyond the scope of this work. However, key among them is the formation of polar stratospheric clouds (PSCs). Low stratospheric water-vapour pressure and low polar temperatures lead to the formation of cloud droplets composed of hydrates of sulfuric acid (H₂SO₄) and nitric acid (HNO₃). PSCs form below a critical temperature of -78°C , a temperature achieved for on average 1–2 months over

the Arctic and 5–6 months over the Antarctic (Holloway & Wayne, 2010). Once photochemistry is triggered by sunlight in spring, the ‘normal’ chemistry of ozone formation and destruction is perturbed by heterogeneous reactions on the PSC particles, leading to activation of reservoir species, and runaway ozone depletion.

The formation of PSCs is partially determined by stratospheric aerosol loading. Therefore, the quantities of potentially aerosol-forming gases transported into the stratosphere are of interest to the study of ozone depletion. Sulfur in the atmosphere can be converted into SO_2 , SO_3 and H_2SO_4 and, hence, acts as a precursor to aerosol formation. Of the sulfur-containing gases in the atmosphere, carbonyl sulfide (COS) and carbon disulfide (CS_2) are thought to be the main precursors to atmospheric sulfate aerosols. Due to its lifetime of 2–8 years (Table 1.1), COS is thought to be the dominant source of sulfur to the stratospheric aerosol layer along with transport of sulfur dioxide (SO_2) to the stratosphere (Montzka & Reimann, 2011). CS_2 is oxidised in the troposphere to COS and acts as an indirect source.

1.3.4 Ozone depletion potentials (ODPs)

In order to assess the relative impact of halogenated gases on stratospheric ozone chemistry, a standardised method of comparing the ability of halocarbons to deplete ozone has been developed. The ozone depletion potential (ODP) is a calculated quantity used to quantify the potential of a gas released at the Earth’s surface to destroy stratospheric ozone. The ODP of a gas is given relative to a similar mass of CFC-11 (CCl_3F). Therefore, CFC-11 is defined as having an ODP of 1.0. ODPs of compounds discussed in this work are presented in Table 1.1.

1.4 A note on atmospheric concentrations

The compounds discussed in this work are termed trace gases; defined as gases that represent less than 1 % of the Earth’s atmospheric composition. However, the trace gases in this work each generally make up less than 0.0000001 % of the atmosphere. One method of expressing the amount of a substance in the atmosphere is the number of molecules of that substance per cubic centimetre of air (units of cm^{-3}), called the number density. This is well suited to calculations, especially for very low abundance compounds such as radicals. However, this method of expressing atmospheric concentrations does not give a sense of the significance of gases in terms of their contribution to atmospheric composition. An alternative is to express the quantity of a compound as a proportion of the atmosphere in a manner analogous to a percentage contribution. To this end, the molar mixing ratio is more commonly used. The molar mixing ratio is the number of moles of a substance per mole of air. Common molar mixing ratios, for trace gases, are $\mu\text{mol mol}^{-1}$, nmol mol^{-1} and pmol mol^{-1} . In order to aid readability, these are often abbreviated to ppm (parts-per-million), ppb (parts-per-billion) and ppt (parts-per-trillion) respectively. These abbreviations are used throughout this work.

Table 1.1: Global mean mixing ratios (MR), atmospheric lifetimes, ozone depletion potentials (ODP) and 100-year time horizon global warming potentials (GWP_{100}) for compounds discussed in this work. Due to their short lifetimes and high spatial and temporal variability, short-lived compounds cannot be assigned a single ODP or GWP. Lifetimes for long-lived compounds are global lifetimes. Those for the short-lived compounds are local lifetimes and do not represent global lifetimes. Mixing ratios are global mean values for 2012 from AGAGE measurements (Prinn et al., 2000) unless otherwise stated. ODPs and lifetimes have been taken from Montzka & Reimann (2011) except where indicated.

Compound	Formula	MR [ppt]	Lifetime [yrs]	ODP	GWP_{100}
<i>Long-lived</i>					
CFCs					
CFC-12	CCl_2F_2	527.7	100	0.82	10900
CFC-11	CCl_3F	235.6	45	1.0	4750
CFC-112	$C_2Cl_4F_2$	0.44 ¹	51 ¹	~0.88	-
CFC-113	$C_2Cl_3F_3$	74.0	85	0.85	6130
CFC-113a	CCl_3CF_3	0.48 ¹	51 ¹	0.68	-
CFC-115	C_2ClF_5	8.4	1020	0.57	7230
HCFCs					
HCFC-133a	$C_2H_2ClF_3$	0.37 ¹	4.3	0.02 ¹	-
HCFC-141b	CH_3CCl_2F	22.5	9.2	0.12	717
HCFC-142b	CH_3ClF_2	21.9	17.2	0.06	2220
HCFC-22	$CHClF_2$	219.2	11.9	0.04	1790
HFCs					
HFC-134a	$C_2H_2F_4$	67.7	9.7	0	1370
HFC-152a	CH_3CHF_2	6.8	1.5	0	133
HFC-227ea	CF_3CHCF_3	0.74	44.5	0	3580
Halons					
H-1202	CBr_2F_2	0.027 ²	2.9	1.7	-
H-1211	$CBrClF_2$	4.0	16	7.9	1890
H-1301	CBr_3F	3.3	65	15.9	7140
H-2402	$C_2Br_2F_4$	0.47 ²	20	13.0	1640
PFCs					
PFC-218	C_3F_8	0.57	2600 ³	0	8830
PFC-C318	<i>c</i> - C_4F_8	1.2 ⁴	3200	0	10300
<i>n</i> -perfluorobutane	<i>n</i> - C_4F_{10}	0.171 ⁵	2600	0	8850
<i>n</i> -perfluoroheptane	<i>n</i> - C_7F_{16}	0.105 ⁵	~3000	0	-
Other					
Carbon tetrachloride	CCl_4	84.2	26	0.82	1400
Methyl bromide	CH_3Br	7.1	0.8	0.66	5
Methyl chloride	CH_3Cl	538.2	1.0	0.02	13
Methyl chloroform	CH_3CCl_3	5.2	5.0	0.16	146

Continued on next page ...

Table 1.1: *Continued from previous page.*

Compound	Formula	MR [ppt]	Lifetime [yrs]	ODP	GWP ₁₀₀
Sulfur hexafluoride	SF ₆	7.6	3200	0	22800
Trifluoromethyl sulfur pentafluoride	SF ₅ CF ₃	0.15 ⁶	650–950	0	17800
Carbonyl sulfide	COS	491 ²	2–8	-	-
<i>Short-lived</i>					
Chlorocarbons					
Chloroform	CHCl ₃	7.5	149 days	-	-
Dichloromethane (DCM)	CH ₂ Cl ₂	26.0	144 days	-	-
Perchloroethene (PCE)	C ₂ Cl ₄	1.2	90 days	-	-
Trichloroethene (TCE)	C ₂ HCl ₃	0.099	4.9 days	-	-
Bromocarbons					
Bromochloromethane	CH ₂ BrCl	0.09	137 days	-	-
Bromodichloromethane	CHBrCl ₂	0.11	78 days	-	-
Bromoform	CHBr ₃	0.50	24 days	-	-
Dibromochloromethane	CHBr ₂ Cl	0.11	59 days	-	-
Dibromomethane	CH ₂ Br ₂	0.86	123 days	-	-
Iodocarbons					
Methyl iodide	CH ₃ I	0.13	7 days	-	-

¹ Laube et al. (2014), mixing ratios from late 2012. ² Montzka & Reimann (2011), mixing ratios from 2008.

³ Metz et al. (2005). ⁴ Oram et al. (2012), Southern Hemispheric mixing ratios from 2010. ⁵ Laube et al. (2012), Southern Hemispheric mixing ratios from 2010. ⁶ Sturges et al. (2012).

1.5 Ozone depleting substances (ODSs)

1.5.1 Chlorocarbons

Anthropogenic chlorinated ozone depleting substances (ODSs), i.e. those entirely or partially emitted by human activity, make up approximately 83.4 % of chlorine derived from source gases entering the stratosphere. Approximately 61.2 % of this total chlorine is derived from the three major chlorofluorocarbons (CFCs); CFC-12, CFC-11 and CFC-113. The CFC-substitutes, hydrochlorofluorocarbons (HCFCs) account for 7.5 % of the total. The historically most important non-fluorinated chlorocarbons, carbon tetrachloride (CCl₄) and methyl chloroform (CH₃CCl₃) account for 11.8 % leaving the remaining 19.5 % to minor ODSs and naturally sourced methyl chloride (CH₃Cl) (Montzka & Reimann, 2011).

1.5.1.1 Chlorofluorocarbons (CFCs)

CFC-12, CFC-11 and CFC-113 are the most abundant CFCs in the atmosphere and represent ~ 61.2 % of the source gas chlorine entering the stratosphere. CFC-11 and CFC-12 each have ODPs close to 1 (see Table 1.1) and are the most abundant ODSs in the atmosphere with mixing ratios of ~528 and ~236 ppt respectively in 2012. Their long lifetimes (100 years for CFC-12 and 45 years for CFC-11) have limited their decline in the atmosphere.

Due to the Montreal Protocol, production and consumption of these CFCs in developed countries ended in 1996 and in developing countries in 2010. Consequently, CFC-11 and CFC-113 abundances have peaked in the atmosphere and have been declining for more than a decade. CFC-12, owing to its longer lifetime, has only shown a decrease in the past few years. Continuing emissions from CFC-12 banks, e.g. refrigeration and air conditioning equipment, have also contributed to this slow decline. These three compounds are expected to continue to decline throughout this century.

A number of other lower abundance CFCs have been identified in the atmosphere. CFC-114 and CFC-115 are the next most abundant CFCs at ~ 16 and 8 ppt respectively, as measured in 2008 (Montzka & Reimann, 2011). These are both decreasing in the atmosphere but with lifetimes of 190 and 1020 years respectively, they are decreasing slowly. Other minor CFCs, such as CFC-113a, CFC-112 and CFC-112a have recently been identified. These CFCs have low atmospheric mixing ratios and both CFC-112 and its isomer CFC-112a are decreasing in line with other CFCs controlled by the Montreal Protocol (Laube et al., 2014). Interestingly, and perhaps worryingly, CFC-113a is increasing in the atmosphere though its current global mixing ratio is low at ~ 0.45 ppt.

1.5.1.2 Hydrochlorofluorocarbons (HCFCs)

HCFCs are short-term substitute gases for ODSs with higher ODPs, e.g. the CFCs. They are used in refrigeration, insulating foam manufacture and as solvents i.e. applications for which CFCs were primarily used. HCFCs contain hydrogen in addition to chlorine fluorine and carbon. The hydrogen moiety makes HCFCs more vulnerable to hydrogen abstraction reactions by OH radicals. Their tropospheric reactivity makes HCFCs 88–98 % less effective than CFC-12 in depleting stratospheric ozone (Montzka & Reimann, 2011). The provisions of the Montreal Protocol require the complete phaseout of HCFCs in all countries by 2030.

By far the most abundant HCFC, at approximately 10 times the atmospheric concentration of the next most abundant, is HCFC-22. Global mean mixing ratios of HCFC-22 were 219.2 ppt in 2012 with a growth rate, in 2007–2008, of 8.6 ppt yr^{-1} . The next most abundant are HCFC-141b and HCFC-142b with global mean mixing ratios of 22.5, and 21.9 ppt respectively in 2012. A number of minor HCFCs are present in the atmosphere including HCFC-133a discussed in Section 3.6.3.2. The HCFCs are all growing in the atmosphere in line with their expected increased usage in response to the phase out of CFCs. It is expected that future atmospheric concentrations will decrease as HCFCs are phased out by the Montreal Protocol and are increasingly replaced by HFCs and other proposed replacement compounds such as hydrofluoro-olefins (HFOs).

1.5.1.3 Methyl chloride

Methyl chloride, CH_3Cl , is the most abundant organic chlorocarbon in the atmosphere, at 538 ppt in 2012, and contributes ~ 16 % to chlorine derived from long-lived gases in the troposphere (Montzka & Reimann, 2011). As CH_3Cl effectively forms the baseline of tropospheric and stratospheric chlorocarbon emissions, understanding the sources and their relative strengths is important for an accurate understanding of the effects of anthropogenic emissions.

The main sources of CH_3Cl to the atmosphere are tropical vegetation (e.g. Gebhardt et al., 2008; Saito et al., 2008; Yokouchi et al., 2002, 2007), biomass burning (e.g. Lobert et al., 1999;

Akagi et al., 2011, and references therein), oceans (Hu et al., 2013) and salt marshes (Rhew et al., 2000). Minor contributions come from industrial sources such as waste incineration and fossil fuel burning (e.g. Keene et al., 1999), mangroves (Manley et al., 2007; Yokouchi et al., 2007), fungi (Moore et al., 2005; Mead et al., 2008a) and senescent or dead plant material (Hamilton et al., 2003). A summary of major sources and sinks is provided in Table 1.2. Xiao et al. (2010) suggest, using a 3-D global chemistry transport model, that ~55 % of global emissions can be accounted for by terrestrial sources. Umezawa et al. (2014) indicate that strong tropical sources and outflow of tropical air are the main controllers of the global-scale distribution of CH₃Cl in the atmosphere. CH₃Cl concentrations are relatively stable in the atmosphere due to natural sources forming the majority of emissions. Due to the dominance of natural emissions, factors such as climate change and human land usage may well become significant.

Methyl chloride is becoming increasingly important, in relative terms, as a supplier of chlorine to the stratosphere as the atmospheric abundances of anthropogenic chlorocarbons such as CFCs decrease in the atmosphere. Additionally, significant uncertainties exist in the budget with sinks outweighing sources, as can be seen in Table 1.2. Consequently, there has been recent interest in increasing the accuracy of CH₃Cl source estimates and in identifying new sources. Biomass burning as a source of CH₃Cl has been recognised for some time. However, measurements of fire emissions in the field can be difficult, and while laboratory studies have been undertaken to simulate fires from different fuel-types and ecosystems, these are not always truly representative of fires in the field. This can be due to a combination of factors such as the burning properties of the fire and the physical transport of smoke into the free troposphere. For instance, fuel undergoing flaming combustion produces more heat (Akagi et al., 2011) and aids transport of smoke into the free troposphere whereas lower temperature smoldering combustion is less efficient for vertical transport of smoke. CH₃Cl is mainly produced in smoldering combustion as are most reduced species such as non-methyl hydrocarbons (Akagi et al., 2011). The height at which a gas in a fire plume is injected into the free troposphere, the ‘injection height’, is key to accurate modelling of these emissions (Akagi et al., 2011). Furthermore, geopolitical factors have complicated accurate measurements in some countries and/or ecosystems. Fire and background emissions of CH₃Cl from Brazil are discussed in Chapter 5.

1.5.1.4 Other long-lived chlorocarbons

The historically most significant non-fluorinated anthropogenic halocarbon compounds are carbon tetrachloride (CCl₄) and methyl chloroform (CH₃CCl₃). CCl₄ was present in the atmosphere at 84.2 ppt in 2012. The major use of CCl₄ was as a feedstock for CFCs and was phased out by the Montreal Protocol in 2010. As a result atmospheric abundances have been in decline for more than two decades. However, CCl₄ is declining less rapidly than expected. This suggests that emissions are larger than reported or that the lifetime of CCl₄ is not accurately understood. CH₃CCl₃ is mainly used as a solvent and has shown the largest reduction in abundance of the ODSs; approximately a factor of 10 decrease since the early 1990s (Montzka & Reimann, 2011). This exponential decrease is a consequence of the relatively short lifetime of CH₃CCl₃ (~5 years). CH₃CCl₃ has been phased out in developed countries since 1996 and is scheduled to be phased out in developing countries in January 2015.

Table 1.2: Estimated sources and sinks for methyl chloride (CH_3Cl) based on Clerbaux & Cunnold (2007) and references therein.

Sources	Range	Sinks	Range
Tropical and subtropical plants	820–8200	OH reaction	3800–4100
Tropical senescent or dead leaves	30–2500	Loss to stratosphere	100–300
Biomass burning	325–1125	Cl reaction	180–550
Oceans	380–500	Soils	100–1600
Salt marshes	65–440	Loss to polar oceans	93–145
Fungi	43–470		
Wetlands	48		
Rice paddies	2.4–4.9		
Fossil fuel burning	5–205		
Waste incineration	15–205		
Industrial processes	10		
Total	1743–1357	Total	4273–6695

All values are given in units of Ggyr^{-1}

1.5.1.5 Very short-lived chlorocarbons

Short-lived compounds are defined by Law & Sturges (2007) as “...substances that have atmospheric lifetimes comparable to, or less than, average tropospheric transport time scales of about 6 months.”. A number of short-lived chlorocarbons have been identified in the background atmosphere. Principal among these are dichloromethane (CH_2Cl_2), chloroform (CHCl_3), chloroethane ($\text{C}_2\text{H}_5\text{Cl}$), 1,2-dichloroethane ($\text{CH}_2\text{Cl}-\text{CH}_2\text{Cl}$), trichloroethene (TCE, C_2HCl_3) and perchloroethene (PCE, C_2Cl_4). All of these compounds have anthropogenic sources. Other short-lived chlorocarbons include the mixed bromochloromethanes. These are discussed in Section 1.5.2.3 in the context of short-lived bromocarbons.

CH_2Cl_2 is mainly used as a paint remover and also as a solvent, degreaser, foam production agent and fumigant. PCE and TCE are used in the textile industry, dry-cleaning applications and as degreasing agents. Simmonds et al. (2006) indicate that 90 % of emissions of CH_2Cl_2 and PCE emanate from the Northern Hemisphere (NH) indicating that they are mainly anthropogenic in origin. Current industrial inventories indicate that only 1 % of industrial emissions are present in the Southern Hemisphere (SH) suggesting that other sources, such as biomass burning, might be responsible (McCulloch et al., 1999). The contribution of biomass burning to global CH_2Cl_2 may have been overestimated (Montzka & Reimann, 2011) and it is unlikely that biomass burning represents a large source of CH_2Cl_2 . Biomass burning is thought to contribute $\leq 1\%$ to emissions of PCE and TCE (Montzka & Reimann, 2011). Dichloromethane has been increasing in the atmosphere since 2000 (Leedham Elvidge et al., 2014; Montzka & Reimann, 2011) at a rate of 1.8 pptyr^{-1} during 2007–2008. PCE also increased in the global atmosphere during 2007–2008 at a slower rate of 0.01 pptyr^{-1} . TCE may be increasing, however, due to its short lifetime of 4.9 days, averaged measurements do not give an accurate impression of atmospheric concentrations. Global average mixing ratios of TCE in Table 1.1 should be treated as an approximation.

$\text{C}_2\text{H}_5\text{Cl}$ is mostly used in the manufacture of ethyl cellulose, dyes and pharmaceuticals. 1,2-dichloroethane is used in the production of polymers and rubbers, as a solvent and a fumigant. Montzka & Reimann (2011) indicate that there might be a substantial non-industrial source.

Table 1.3: Estimated sources and sinks of chloroform (CHCl_3) based on McCulloch (2003).

Sources	Range	Sinks	Range
Open oceans	270–450	OH reaction	370–830
Soil processes	120–320	Soils	n.y.q.
Volcanic and geological processes	9–15		
Anaerobic fermentation	2–4		
Pulp and paper manufacture	26–42		
Water treatment	8–34		
Other industrial sources	9–13		
Biomass burning †	2		
Total	446–880	Total	370–830

All values are given in units of Ggyr^{-1} , n.y.q. = not yet quantified.

† Value from Lobert et al. (1999).

However, there are very few measurements of $\text{C}_2\text{H}_5\text{Cl}$ and $\text{CH}_2\text{ClCH}_2\text{Cl}$ in the literature.

CHCl_3 is used in the production of HCFC-22 and fluoropolymers. It is also released as a by-product of paper and pulp bleaching. Approximately 25–29 % of CHCl_3 emissions were estimated to be from industrial sources according to Worton et al. (2006). Biomass burning contributes ≤ 1 % to CHCl_3 emissions. The major natural sources of CHCl_3 are oceans and soil processes (McCulloch, 2003, and references therein). However, sources and sinks are poorly characterised. Table 1.3 summarizes the known sources and sinks of CHCl_3 . Biomass burning and natural sources of CHCl_3 are discussed further in Chapter 5.

1.5.2 Bromocarbons

As highlighted in Section 1.3.2, bromine is approximately 60 times more effective at destroying ozone than chlorine. The increased efficacy of bromine, due to the catalytic coupling with stratospheric chlorine, leads to high ODPs of up to 15.9 for H-1301. The halons represent a completely anthropogenic source of bromine to the atmosphere. Methyl bromide (CH_3Br) also has an anthropogenic source from fumigation however, ~ 90 % of emissions in 2008 were natural in origin.

1.5.2.1 Halons

Halons are the most destructive brominated ODSs. The majority of stratospheric bromine comes from natural sources with approximately 42.4 % of bromine derived from brominated source gases entering the stratosphere (Montzka & Reimann, 2011). H-1211 and H1301 constitute 34 % of bromine in stratospheric source gases. Halons have mainly been used in fire extinguishers, fire prevention systems and explosion protection applications due to their inertness. An additional two halons, H-2402 and H-1202, are also present in the atmosphere at lower concentrations than H-1301 and H1211. H-2402 was produced and used mainly in the Soviet Union. H-1202 is mainly produced as a by-product of H-1211 manufacture (Newland et al., 2013). All of these compounds have been banned under the Montreal Protocol since 2010 except for some users with critical use exemptions. H-1211, H-2402 and H-1202 have either levelled off or are in decline. H-1301 continues to increase in the atmosphere probably due to release from existing fire extinguishers

and stockpiled 'halon banks'. Though halons are no longer being produced, halon stockpiles are still providing a source to the atmosphere. A large proportion of banked halons are used in military applications where alternatives are not readily available.

1.5.2.2 Methyl bromide

Peak atmospheric CH_3Br was 9.2 ppt during 1996–1998 (Yvon-Lewis et al., 2009). Global mean mixing ratios of CH_3Br in 2012 were 7.1 ppt. This decline was due to the regulation of global production and consumption of CH_3Br as a fumigant (Montzka & Reimann, 2011). Based on a pre-industrial SH mixing ratio of 5.8 ppt, Montzka & Reimann (2011) suggest that SH mixing ratios have declined 50–60 % of the way back to pre-industrial levels. CH_3Br accounts for approximately 50 % of naturally-sourced organic bromine in the troposphere, the other 50 % is comprised of very short-lived gases such as bromoform (CHBr_3 , see Section 1.5.2.3). In a similar vein to methyl chloride (Section 1.5.1.3), decreasing anthropogenic bromocarbon emissions increase the relative importance of methyl bromide, especially its potential response to factors such as climate change.

Methyl bromide shares many similar sources and sinks to methyl chloride. Table 1.4 summarises the best estimates for sources and sinks of CH_3Br . There are significant uncertainties in the atmospheric budget of CH_3Br , with sinks outweighing sources by $\sim 32 \text{ Ggyr}^{-1}$. The major natural source of CH_3Br is oceanic (e.g. Yvon-Lewis et al., 2009) and biomass burning (e.g. Akagi et al., 2011, and references therein) with minor contributions from peatlands (White et al., 2005), rice paddies, (e.g. Lee-Taylor & Redeker, 2005) salt marshes, (Manley et al., 2006) rapeseed (Mead et al., 2008b) and fungi (e.g. Mead et al., 2008a). A number of terrestrial sources have also been identified but not well quantified (see Table 1.4).

As with methyl chloride, biomass burning emissions are not well quantified for all regions and ecosystems. Biomass burning emissions of CH_3Br are lower ($10\text{--}40 \text{ Ggyr}^{-1}$) than for CH_3Cl ($30\text{--}2500 \text{ Ggyr}^{-1}$). This is probably reflective of the lower concentrations of bromine in plant tissues compared with chlorine. However, biomass burning remains an important source of CH_3Br . Fire and background emissions from Brazil are discussed in Chapter 5

1.5.2.3 Very short-lived bromocarbons (VSLB)

Chlorinated and brominated organic compounds have the potential to catalytically destroy ozone in the stratosphere via processes involving the inorganic products of photochemical decomposition. The influence of long-lived anthropogenic species such as chlorofluorocarbons (CFCs), bromochlorofluorocarbons and bromofluorocarbons (halons) is well documented. However, short-lived compounds with lifetimes of less than ~ 6 months, termed very short-lived substances (VSLS), can also transport significant quantities of reactive halogens to the stratosphere. The most significant biogenic brominated VSLS are bromoform (CHBr_3), dibromomethane (CH_2Br_2), dibromochloromethane (CHBr_2Cl), bromodichloromethane (CHBrCl_2) and bromochloromethane (CH_2BrCl). These very short-lived brominated compounds (VSLB) are emitted predominantly from natural sources, namely, macroalgae in coastal regions and oceanic phytoplankton (e.g. Leedham et al., 2013; Brinckmann et al., 2012; Carpenter et al., 2009; Montzka & Reimann, 2011). There are also minor contributions of trihalomethanes from drinking water chlorination and power plant cooling water (Quack & Wallace, 2003).

Table 1.4: Estimated sources and sinks of methyl bromide (CH₃Br) based on Montzka & Reimann (2011) and references therein.

Sources	Range	Sinks	Range
Fumigation	11.7–17.1	Ocean	45–52
Ocean	34–49	OH & photolysis	63.6
Biomass burning	10–40	Soils	28–33
Leaded gasoline	< 5.7		
Temperate peatlands	–0.1–1.3		
Rice paddies	0.1–1.7		
Coastal salt marshes	0.6–14		
Mangroves	1.2–1.3		
Shrublands	0–1		
Rapeseed	4.0–6.1		
Fungus (litter decay)	0.5–5.2		
Fungus (leaf-cutter ants)	0.5		
<i>Tropical trees</i>	n.y.q.		
<i>Temperate woodlands</i>	n.y.q.		
<i>Tropical ferns</i>	n.y.q.		
<i>Abiotic decomposition</i>	n.y.q.		
Total	69.2–142.9	Total	136.6–148.6

All values are given in units of Ggyr⁻¹, n.y.q. = not yet quantified.

Recent WMO reports (Law & Sturges, 2007; Montzka & Reimann, 2011) indicate that natural halocarbon emissions are associated with significant stratospheric O₃ depletion. Bromine has an ~60 times higher efficiency, on average and on a per atom basis, to destroy ozone than chlorine (Sinnhuber et al., 2009). This, combined with the highly variable spatial and temporal distribution of VSLS in the troposphere, indicates that even at low mixing ratios, brominated VSLS species could contribute significantly to stratospheric ozone depletion. Hossaini et al. (2012a) suggest that VSLS source gas injection into the stratosphere is likely to increase in response to future climate change. Furthermore, as levels of anthropogenic halogenated source gases are predicted to decrease (e.g. Montzka & Reimann, 2011), as a result of the Montreal Protocol, biogenic halocarbons including bromomethanes will become proportionally more significant in the future. Additionally, there is a relative paucity of measurements in the region of the upper troposphere/lower stratosphere (UTLS); an important region when considering the transport of compounds into the stratosphere.

Currently, the best estimate of the contribution of brominated VSLS to inorganic bromine in the stratosphere, as inferred from measurements of inorganic decomposition products such as BrO, is 6 (range 3–8) ppt (Montzka & Reimann, 2011) which represents ~27% (13–36) of total stratospheric bromine. Uncertainties in this estimate include the high degree of variability in source emissions, limited understanding of transport pathways to the upper tropical tropopause, differences in calibration scales between measurements, limited spatial and temporal data coverage and uncertainties in kinetic parameters used to calculate decomposition rates.

Within the tropics, the region between the level of maximum convective outflow (345 K potential temperature, ~12 km) and the cold point tropopause (380 K potential temperature, ~17 km) is termed the tropical tropopause layer (TTL) (Law & Sturges, 2007). The TTL acts

as a source region for the stratospheric overworld and the extra-tropical lowermost stratosphere. Therefore, mixing ratios of halogenated compounds (including VSLB) in this region are crucial for understanding stratospheric ozone depletion in the lower and upper stratosphere.

Although it is not as significant for upper stratospheric ozone depletion, the extra-tropical UTLS is of interest as bidirectional transport influences the chemistry of the upper troposphere (UT) and lower stratosphere (LS). This region is also of significance due to its strong influence on surface climate, climate feedbacks and tropospheric weather regimes (e.g. Gettelman et al., 2011). The chemical, radiative and dynamical properties of this region are coupled. Therefore, changes in chemistry in the UTLS may have consequences for tropospheric chemistry (Anderson et al., 2012) and climate (Riese et al., 2012). Additionally, it is possible that future climate change may impact on VSLB transport into the UTLS through changes in oceanic emissions as ocean temperature and acidity change and also through atmospheric processes such as increased convection and large-scale vertical transport (Dessens et al., 2009) or sea surface temperature, wind speed and marine boundary layer height (Hepach et al., 2014). These factors might increase the quantity of VSLB transported to the UTLS and hence, impact on stratospheric ozone.

1.5.3 Iodocarbons

Iodine is important in the atmosphere in a number of ways. Iodine is an essential dietary element and the atmosphere provides a means of transport from the main oceanic source to the continents (Whitehead, 1985). Iodine is also important in its influence on the oxidative capacity of the atmosphere via reaction with ozone and changes to the OH radical (e.g. Chameides & Davis, 1980). Iodine has also been of interest in the formation of ultra-fine aerosol particles and in the removal of atmospheric mercury (Saiz-Lopez et al., 2011). Though iodine's role in tropospheric ozone depletion is important, iodine containing trace gases are generally considered to have a minimal role in the stratosphere. This is due to the rapid photolysis of iodinated compounds at long wavelengths leading to their rapid breakdown and hence, very short atmospheric lifetimes on the order of days. However, stratospheric iodine chemistry is poorly understood with sparse measurements of active species.

1.5.3.1 Methyl iodide

Numerous iodocarbon species have been identified in the atmosphere including methyl iodide (CH_3I), ethyl iodide ($\text{C}_2\text{H}_5\text{I}$), 1- and 2-propyl iodide ($\text{C}_3\text{H}_7\text{I}$) and more reactive iodocarbons such as bromiodomethane (CH_2BrI) and diiodomethane (CH_2I_2). Of these, CH_3I is generally the most abundant and longest lived of the iodocarbons with a mean atmospheric lifetime of ~ 7 days. Oceans represent the largest source of CH_3I with generally higher mixing ratios in coastal regions (Saiz-Lopez et al., 2011). Bell (2002) gives a range of oceanic emissions, based on a number of studies, of $140\text{--}1300 \text{ Ggyr}^{-1}$. This value is greatly dependent on the time of year, latitude and particular ocean where measurements were made. Terrestrial sources include rice paddies, peatlands and wetlands (Bell, 2002). Biomass burning is not well quantified, with values reported of 3.4 Ggyr^{-1} (Blake et al., 1996) and $< 10 \text{ Ggyr}^{-1}$ (Andreae et al., 1996) but represents a minor source of CH_3I . Significant anthropogenic emissions of CH_3I have not been reported and are probably negligible in comparison to the natural background.

Table 1.5: Estimated sources and sinks of carbonyl sulfide (COS) based on Montzka et al. (2007).

Sources/sink	Range
<i>Sources</i>	
Oceanic	–110–190
Oxidation of CS ₂ and S(CH ₃) ₂	149–330
Anthropogenic	32–96
Oxidation of anthropogenic CS ₂	58–170
Biomass burning	68–144
Other (wetland, soils. . .)	13–119
Total	210–1049
<i>Sinks</i>	
Vegetation	730–1500
Soils	74–180
OH oxidation	2–110
COS photolysis (stratosphere)	11–21
O atom oxidation	5–16
Total	902–1827

All values are given in units of Ggyr⁻¹.

1.5.4 Carbonyl sulfide (COS)

As alluded to in Section 1.3.3, carbonyl sulfide (COS) contributes to the formation of sulfur aerosol in the stratosphere and, indirectly, to stratospheric ozone depletion via the formation of polar stratospheric clouds. COS is the most abundant sulfur-containing gas in the atmosphere at 491 ppt in 2012. The major primary sources of COS are the oceans and biomass burning, with the oxidation of other sulfur gases as a secondary source (Montzka et al., 2007). COS is also taken up by vegetation which is its major sink. Sources and sinks are summarised in Table 1.5. Emissions of COS are seasonally variable due to the seasonality of oceanic emissions and vegetative uptake (Montzka et al., 2007). Other sources, such as biomass burning, are also seasonal. However, variations in these fluxes are much lower than for oceanic and vegetative fluxes. The current background mixing ratio is approximately 60 % higher than the pre-industrial value of ~300 ppt (Montzka & Reimann, 2011). This is due to a combination of direct anthropogenic emissions and oxidation of anthropogenic CS₂. Anthropogenic emissions of sulfur gases are closely linked with anthropogenic fossil fuel consumption (Montzka et al., 2007).

1.6 Greenhouse gases

All halocarbons have a warming effect on the atmosphere. This is due to strong absorption in the infra-red region of the spectrum. The absorption bands that these compounds cover are, coincidentally, in regions of the infra-red spectrum where CO₂ absorbs weakly. Therefore, they have the potential to close the atmospheric ‘windows’ through which radiation escapes to space and, consequently, may have a global warming contribution greater than the simple additive effect of radiation trapped by halocarbons alone.

The heating effect that halocarbons have on the atmosphere can be described by their radiative

forcing. Radiative forcing is defined as the rate of energy change per unit area of the globe as measured at the top of the atmosphere (Solomon et al., 2007). For an atmospheric species, the radiative forcing is given as $\text{W m}^{-2} \text{ppb}^{-1}$. Greenhouse gases all have a positive radiative forcing.

1.6.1 Global warming potentials (GWPs)

The Global Warming Potential (GWP) of an atmospheric gas is used to quantify the total effect on radiative forcing of an emission relative to that of a reference gas on a per kilogram basis. GWP takes into account the radiative forcing of a gas and its atmospheric lifetime. A short lifetime gas might have a strong effect on radiative forcing over a short time-horizon but a negligible effect over a longer period. Therefore, the value of a compound GWP is dependent on the time-horizon over which it is calculated. The most common time-horizon reported is 100 years and is usually referenced to CO_2 , i.e. CO_2 has a GWP of 1.0.

1.6.2 Fluorocarbons and other fluorinated gases

The fluorocarbons do not pose a threat to stratospheric ozone depletion due to their lack of chlorine, bromine or iodine atoms. However, they are significant for their effect on global climate due to their high GWPs and lifetimes (in the case of perfluorocarbons, PFCs). Hydrofluorocarbons (HFCs) are the current replacement compounds for the CFCs and HCFCs. Hence, they are expected to increase in the atmosphere in the future as HCFCs are phased out under the terms of the Montreal Protocol. Perfluorocarbons (PFCs) are used in a variety of applications such as the electronics industry and as heat exchange fluids. Two other gases of note are the fluorinated sulfur-containing gases sulfur hexafluoride (SF_6) and trifluoromethyl sulfur pentafluoride (SF_5CF_3).

1.6.2.1 Hydrofluorocarbons (HFCs)

As the preferred refrigerant in refrigeration and mobile conditioning units, e.g. vehicle air-conditioning, HFC-134a is the most abundant HFC in the atmosphere at 67.7 ppt in 2012 (Table 1.1). According to Montzka & Reimann (2011), due to its long lifetime and relatively high GWP_{100} of 1370, HFC-134a will eventually be phased out in Europe. However, there is potential for increased emission of HFC-134a in developing countries. The next most abundant HFC is HFC-23, mainly as a by-product of over fluorination of chloroform during production of HCFC-22. There are a large number of less abundant HFCs that have been identified in the atmosphere as a consequence of the increased interest in this class of compound as a chlorocarbon replacement. Of interest for this work are HFC-152a and HFC-227ea. HFC-152a is used as a foam-blowing agent and as an aerosol propellant. It has the smallest GWP_{100} of all the major HFCs and a short lifetime of 1.5 years. The short life-time of HFC-152a and the growth rate during 2007–2008 imply large increases in emissions in recent years (Montzka & Reimann, 2011). HFC-227ea is a low abundance HFC, with a mixing ratio of 0.74 ppt in 2012, mainly used in fire suppression but also in metered dose inhalers, refrigeration and foam blowing. The growth rate of HFC-227ea has been accelerating in recent years (Laube et al., 2010).

1.6.2.2 Perfluorocarbons and other perfluorinated compounds

Perfluorocarbons (PFCs) have very high GWPs and long lifetimes. PFC-14 (CF_4) is the only PFC with a natural source from crustal out-gassing. It is also the most abundant PFC at ~ 77 ppt in 2008 (Montzka & Reimann, 2011). C_2F_6 is the next most abundant at ~ 4 ppt followed by cyclic perfluorobutane, $c\text{-C}_4\text{F}_8$. A number of sources of $c\text{-C}_4\text{F}_8$ have been reported including the electronics and semi-conductor industries. However, discrepancies still remain in the atmospheric budget. $c\text{-C}_4\text{F}_8$ was ~ 1.2 ppt in 2010 and growing at a rate of 0.03 ppt yr^{-1} (Oram et al., 2012). A number of minor PFCs have been recently identified in the background atmosphere. $n\text{-C}_4\text{F}_{10}$ and $n\text{-C}_7\text{F}_{16}$ were reported by Laube et al. (2012). $n\text{-C}_4\text{F}_{10}$ is used in refrigeration, air conditioning, as a fire suppressant and in semiconductor manufacture. $n\text{-C}_7\text{F}_{16}$ is used as a solvent and heat transfer agent. Laube et al. (2012) suggest that growth of $n\text{-C}_4\text{F}_{10}$ has recently slowed but not for $n\text{-C}_7\text{F}_{16}$. Despite the slowdown in growth rate of these compounds, atmospheric levels will not decrease notably for some time in the future due to their long atmospheric lifetimes.

Sulfur hexafluoride (SF_6) and trifluoromethyl sulfur pentafluoride (SF_5CF_3) are both greenhouse gases because of their high radiative efficiencies and very long lifetimes (see Table 1.1). SF_6 increased in the atmosphere at a rate of 0.2 ppt yr^{-1} during 2007–2008. Trace quantities of SF_6 are produced in the Earth's crust, however, the main sources are from the electricity sector, magnesium production and semiconductor manufacture (Levin et al., 2010). SF_5CF_3 was thought to be produced from electrical arc discharge in equipment containing SF_6 (Huang et al., 2005), however, Sturges et al. (2012) give evidence that SF_5CF_3 was being used in the production of fluorosurfactants, mainly by one company (3M). Production of fluorosurfactants using SF_5CF_3 has largely ceased and emissions appear to have halted.

1.7 Aims and rationale

The initial aim of this thesis was to test and refine, with assistance from the manufacturer (SAI), a time-of-flight gas chromatography mass spectroscopy (TOF GC-MS) instrument for the measurement of a wide range of volatile organic compounds (halocarbons, hydrocarbons etc.). When purchased, in around 2006, the SAI TOF GC-MS was one of the first of its type. It was bought, as something of a prototype, with the expectation that it would achieve similar detection limits working to that achieved by the market leading Agilent MSD systems operating in selected ion, electron ionisation mode. Chapter 3 discusses the characterisation of the TOF GC-MS. The main purpose of this study was to determine the operational strengths and limitations of the TOF GC-MS as an instrument for the analysis of atmospheric trace gases. The features assessed in determining the suitability of the instrument were:

- **Sensitivity:** the response of the instrument to analytes and the degree to which they are distinguishable from the background noise.
- **Reproducibility:** the degree of agreement between measurements of repeat samples.
- **Drift:** the change in response of the mass spectrometer over time.
- **Linearity:** the degree of linearity in the response of the GC-MS system under varying sample size.

Ideally, a direct comparison would have been made to an instrument under similar analysis conditions i.e. an Agilent MSD quadrupole mass spectrometer. However, due to instrumental issues, detailed in Chapter 3, the TOF GC-MS was not able to participate in any appropriate fieldwork. Instead, a preliminary comparison was made on a set of samples collected during the Clean Air for London (ClearfLo) campaign in 2012. This provided an initial look at the suitability of the TOF GC-MS as an instrument for atmospheric analysis. The main purpose of this comparison was to assess the TOF GC-MS, however, a cursory analysis was also made of halocarbons during the ClearfLo campaign.

Due to numerous technical issues, upgrades and replacements, the TOF GC-MS was not operationally reliable enough to be used during field campaigns or for most lab-based analyses. Consequently, the majority of this work is concerned with measurements made with different mass spectral techniques on other instruments. Chapters 4 and 5 are based on results from the CARIBIC and SAMBBA projects.

1.7.1 The ClearfLo campaign

The main aims of the ClearfLo campaign were to assess air quality and chemistry in an urban centre, namely London, U.K. Measurements from ClearfLo reported in this work are focused on atmospheric halocarbons. Very few measurements have been made of halocarbons in the U.K. and, to my knowledge, none have been made in London. Emissions of long-lived halocarbons are important for stratospheric ozone depletion (e.g. CFCs and HCFCs) and for their global warming potentials as discussed in this chapter. It was not expected that elevated concentrations of CFCs, halons and other long-lived chlorocarbons, such as Cl_4 and CH_3CCl_3 would be encountered in London as these compounds have been phased out of production and usage, by the Montreal Protocol, in all participating developed and developing countries. However, HCFCs, the short-term replacement compounds for CFCs, have yet to be fully phased out. Levels of HCFCs and their long-term replacement compounds, the HFCs, might be expected to be higher than background levels depending on their usage. As these compounds are frequently used in refrigeration and air-conditioning applications, London is likely to be a source of these compounds. Additionally, some perfluorinated compounds might also be present at elevated levels due to their usage in a variety of applications.

Short-lived chlorocarbons in London might be of anthropogenic origin, such as CH_2Cl_2 and other short-lived chlorocarbons, or natural origin, such as CHBr_3 . Short-lived chlorocarbons might be important as a source of reactive chlorine in the urban environment. Reactive chlorine can initiate ozone formation by reaction with hydrocarbons (e.g. Tanaka et al., 2003). CH_2Cl_2 and CHCl_3 are long-lived enough, with average lifetimes of ~ 144 and ~ 149 days respectively, to be distributed throughout the atmosphere and impact air quality at a remove from their sources. Short-lived bromocarbons, are mainly marine sourced but might impact air quality in London via the formation of aerosol particulates (e.g. Saiz-Lopez et al., 2011) and ozone destruction (e.g. Read et al., 2008). They are also potential tracers of marine air and its influence on urban air quality.

1.7.2 The CARIBIC project

The CARIBIC project (Containerised Aircraft for the Regular Investigation of the atmosphere Based on an Instrument Container) has made measurements with a fully automated container-based atmospheric laboratory on board a Lufthansa Airline A340–600 aircraft since 1997. Further details can be found in Chapter 4. This work is concerned with measurements of the very short-lived bromomethanes, CHBr_3 , CH_2Br_2 , CHBr_2Cl , CHBrCl_2 and CH_2BrCl . There is a discrepancy between stratospheric inorganic bromine (Br_y), calculated from measurements of BrO , and the total bromine available from halons and methyl bromide (Dorf et al., 2006, 2008). This discrepancy is assumed to be due to short-lived brominated species. The best candidates are the bromomethanes. As mentioned in Section 1.5.2.3, the best estimate of the contribution of VSLB is 6 (3–8) ppt, $\sim 27\%$ of total stratospheric bromine. These compounds are highly variable, both spatially and temporally, due to their biological sources and short lifetimes. Measurements of these compounds in the upper troposphere, especially in the tropics where air is rapidly transported to the TTL, is key to understanding and better quantifying the contribution of these compounds to stratospheric bromine. Additionally, measurements at the interface between the stratosphere and troposphere in the mid-latitudes, the UTLS, are rare especially for VSLB.

The purpose of this study was to better quantify the VSLB in the tropical upper troposphere and mid-latitude UTLS and to gain insight into the horizontal and vertical distributions of these compounds. Source regions are difficult to pinpoint at the altitudes of the CARIBIC aircraft (typically 10–12 km). However, it was hoped that emissions from presumed strong source regions, such as the western Pacific (e.g. Aschmann et al., 2009; Fueglistaler et al., 2009), would be detectable at these altitudes.

1.7.3 The SAMBBA project

The South American Biomass Burning Analysis (SAMBBA) was an airborne field experiment to quantify biomass burning and background emissions over the Brazilian rainforest and savannah during summer 2012. Analysis of results from this campaign are presented in Chapter 5. Both biomass burning and natural emissions of halocarbons and carbonyl sulfide are important in this region. The tropics are a key source region for transport into the TTL and, hence, the stratosphere. Biomass burning has been known to be a source of halogenated species for over two decades (e.g. Crutzen et al., 1979). The methyl halides (CH_3Cl , CH_3Br and CH_3I) are the major halogenated species emitted. However, uncertainties remain in emissions of other halocarbons such as CHBr_3 and PCE (C_2Cl_4). COS is also known to be emitted from biomass burning but is not well reported in some regions. Differences in emissions are known to exist for biomass burning of different vegetation types in different ecological biomes and there have not been a large number of measurements made of emissions from biomass burning over the Amazon rainforest and Cerrado savannah regions. This has led to a high degree of uncertainty in emission estimates of fire-emitted species. One of the aims of SAMBBA was to make repeat measurements of smoke plumes close to source in order to better quantify the emission of trace gases. Halocarbons such as CH_3Cl , CH_3Br and CHCl_3 are also thought to have terrestrial sources. For instance, CH_3Cl has recently been identified as having a source in tropical vegetation (Yokouchi et al., 2007) and CHCl_3 has a source from soil processes (Hoekstra et al., 2001).

The purpose of the study presented in this work was to better quantify the emissions of

halocarbons and carbonyl sulfide from biomass burning in Brazil and to provide a regional estimate of emissions. Additionally, terrestrial sources were to be assessed and potential local sources identified.

1.7.4 Summary of aims

To summarise, Chapter 3 is mainly concerned with the characterisation and assessment of the TOF GC-MS instrument for atmospheric analysis. An additional, brief analysis is made of anthropogenic and natural, long- and short-lived halocarbon levels in London as part of the ClearLo project. Very short-lived bromomethanes in the mid-latitude upper troposphere/lower stratosphere and the tropical troposphere are discussed in Chapter 4. Chapter 5 is concerned with halocarbon and carbonyl sulfide emissions, both biomass burning and natural background, made over the Brazilian rainforest and savannah during the SAMBBA project. Chapter 2 provides an overview of the analytical techniques applied in this work and Chapter 6 presents a summary of the results from these analyses. The following is a chapter-by-chapter breakdown of the aims of this thesis.

Chapter 3

- Assess the performance of the TOF GC-MS.
- Analyse atmospheric levels and possible sources of halocarbons in London.

Chapter 4

- Analyse the atmospheric levels of VSLB in the upper troposphere over potential tropical source regions.
- Elucidate the vertical structure of VSLB in the mid-latitude UTLS and tropical troposphere.

Chapter 5

- Quantify emissions of methyl halides and carbonyl sulfide in Brazilian biomass burning.
- Compare emissions between rainforest and savannah fires.
- Provide regional and global biomass burning emission estimates for rainforest and savannah fires.
- Assess natural background emissions of halocarbons from the Amazon rainforest and identify potential sources.

Experimental Theory & Methods

2.1 Gas chromatography

Gas chromatography (GC) was first introduced as an analytical technique by James & Martin in 1952. The basic operating principle of gas chromatography involves volatilisation of a sample via heating (except in the case of volatile gases or atmospheric trace substances), injection onto an appropriately prepared column, separation of the components of the mixture by interaction with the column, and detection of each component by a detector. Analytes are delivered through the system in a stream of carrier gas such as hydrogen or helium. The column or column packing contains a stationary phase. Interactions with the stationary phase and distribution between it and the mobile phase (carrier gas) determine the separation of components. For instance, a component that spends little time, or interacts weakly, with the stationary phase will elute quickly.

2.1.1 Chromatographic theory

The theoretical plate concept of chromatography assumes that a chromatographic column can be approximated as a series of separate layers called ‘theoretical plates’. Analytes move through the column by equilibrated transfer of mobile phase from one plate to the other. Equilibration is assumed to be infinitely fast. This model allows the measurement of efficiency by calculation of the number of plates in a column, N , as in Equation 2.1, where t_R is the retention time of an analyte, t_0 is the column dead volume and W_h is the full-width-at-half-maximum of the analyte peak, Hübschmann (2009).

$$N = \frac{5.54 \cdot (t_R - t_0)}{W_h} \quad (2.1)$$

An alternative measure of efficiency is the height equivalent to a theoretical plate, h which is related to N (see Equation 2.2, where L is the column length). A larger value of N or a smaller value of h indicate a greater efficiency.

$$h = \frac{L}{N} \quad (2.2)$$

An alternative model, which more realistically represents the processes occurring in the column, is given by the van Deemter equation (Equation 2.3). A simplified form of the van

Deemter equation is given in Equation 2.3, below:

$$h = A + B/u + C \cdot u \quad (2.3)$$

where u is the average velocity of the mobile phase. A , B and C are factors which contribute to band broadening.

A: Eddy diffusion. This term quantifies the the broadening of the solute band due to the variation in random path lengths as molecules pass through a packed stationary phase. For non-packed columns, i.e. capillary columns, this is zero.

B: Longitudinal diffusion. This term represents the peak broadening arising from diffusion of the analyte from the centre of the band to the edges, due to the analyte concentration being higher in the centre. This is reduced with increasing velocity of the mobile phase.

C: Resistance to mass transfer As the analyte takes a finite time to equilibrate between the stationary and mobile phases, the analyte in mobile phase can move ahead of the analyte in the stationary phase, broadening the band. Higher mobile phase velocities increase broadening.

The expanded version of the van Deemter equation given in Equation 2.3 can be used to derive the optimal flow velocity of a mobile phase and can inform the choice of carrier gas for a particular application.

2.1.2 Carrier gases

For atmospheric trace gas analysis, and especially in gas chromatography mass spectroscopy (GC-MS) techniques, helium is the most common carrier gas. Hydrogen is used less commonly due to the safety concerns of using a flammable gas. The linear velocity of the gas through the system is an important factor with regard to choice of carrier gas and optimal set-up of chromatographic parameters. For most applications it is necessary to balance the efficiency and speed of separation. This is dependent on the number and similarity of the components of interest. However, for each carrier gas there is an optimal flow rate where speed and efficiency of separation are balanced as determined by the solution of the full van Deemter equation, of which Equation 2.3 is a simplification, over a range of flow rates. Figure 2.1 shows the application of the van Deemter equation (Equation 2.3) to different carrier gases. As can be seen, each carrier gas has a different optimal gas velocity where h is minimised. For He, the optimal gas velocity is $\sim 25 \text{ cm s}^{-1}$. In practise, a gas velocity of 30 cm s^{-1} is used to compensate for lower starting temperatures in a GC temperature program.

2.1.3 GC columns

Gas chromatography columns can be classified into two broad categories: packed columns and capillary columns. Packed columns consist of a metal or glass tubing packed with an inert support material coated in a liquid stationary phase. The efficiency of a packed column is limited by band broadening processes e.g. term A in Equation 2.3. To a large extent capillary columns have replaced packed columns, especially in the analysis of atmospheric trace gases at sub-ppb mixing ratios.

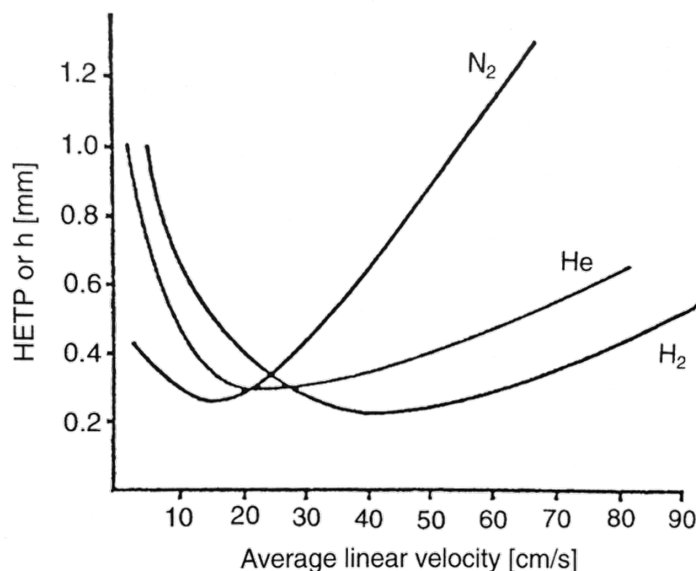


Figure 2.1: van Deemter curves for nitrogen, helium and hydrogen carrier gases. The values given are based on a $250\ \mu\text{m} \times 30\ \text{m}$ column with a film thickness of $0.25\ \mu\text{m}$. Adapted from Hübschmann (2009).

Capillary columns consist of a long narrow piece of tubing usually made of fused silica coated externally with polyimide to increase flexibility and strength, though occasionally made of steel. The tubing has an internal coating; either a liquid such as a silicone-based polymer (termed a wall coated open tubular, WCOT, column), or a solid such as alumina or molecular sieve (termed a porous layer open tubular, PLOT, column). Typically, capillary columns are 20–100 m long with internal diameters $100\text{--}320\ \mu\text{m}$. Capillary columns have the advantage of giving a higher resolution in a shorter time than a packed column. However, distortions caused by overloading capillary columns limit the quantity of sample that can be injected.

2.1.4 Detectors

A number of detectors can be utilised in conjunction with gas chromatography. These include the electron capture detector (ECD) which is one of the most sensitive detectors available and is particularly sensitive to electronegative compounds such as chlorinated, brominated and iodinated species. Other detectors widely used include the flame ionisation detector (FID), used for hydrocarbon analysis, and the flame photometric detector (FPD), used for sulfur-containing compounds. One of the main limitations of these detection techniques is that they cannot positively identify a compound i.e. they rely on the retention time as the main means of identification. This is subject to interferences especially in a situation where there are a large number of potentially unidentified compounds e.g. a polluted atmosphere. The technique of gas chromatograph-mass spectroscopy (GC-MS) combines the separation of compounds, by gas chromatography, with the means to identify chemical species. As a result, this technique is less susceptible to interferences and they are easier to identify when they do occur.

2.2 Mass spectrometry

2.2.1 Quadrupole mass analyser

Commercial development of the quadrupole mass analyser (also known as the quadrupole mass filter, QMF) began in the 1960s. QMFs have become popular in GC applications, and arguably are the current standard mass spectrometric technique in atmospheric science. QMFs offer the advantages of low cost, simple operation, durability, ease of maintenance and transportability.

A QMF analyser consists of four parallel rods, ideally with a hyperbolic cross-section. Direct current (DC) and radio frequency (RF) electrical potentials are applied to the rods to induce a fluctuating field within the central space. Ions extracted from an ion source are accelerated into the central space along the longitudinal axis of the quadrupole. The magnitude and frequency of the electric fields can be varied to selectively allow passage of ions of a specific m/z value to pass through the central space and reach the detector; all other ions collide with the quadrupole surfaces. This is illustrated in Figure 2.2.

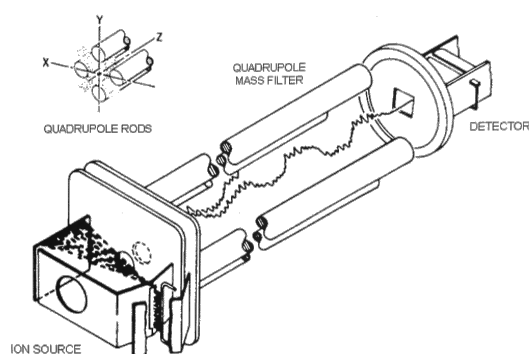


Figure 2.2: Schematic of a quadrupole mass filter, showing ion trajectories. Only ions of one m/z value have a stable enough trajectory to reach the detector. Courtesy of Watson & Sparkman (2007).

QMFs are commonly operated in one of two modes: scan mode and single ion monitoring (SIM) mode. Scan mode is often used for preliminary identification of compounds or for compounds at high concentration. The QMF scans across a range of m/z values in each window of time. Sensitivity in QMF is proportional to the time spent acquiring ion counts on each ion. As the time taken for each scan is dependent on the number of ions required for analysis, scan mode has a large trade-off between sensitivity and rate of acquisition (i.e. the number of spectra captured per second).

The alternative mode of operation, SIM mode, is frequently used when the number of components requiring analysis is small or when components are at low concentrations. In SIM a small number of ions are filtered by the QMF in any window of time. In order to maintain a useful rate of acquisition over the course of a single analysis, this is commonly on the order of <10 ions depending on the number of GC peaks requiring analysis within that time window. As the number of ions is small, sensitivity is greatly increased compared to scan mode. However, the main trade-off with SIM is that increased sensitivity comes at the cost of a smaller number of analysable compounds. Additionally, in most cases SIM requires a larger amount of pre-analysis preparation in order to correctly identify compounds of interest and set-up the appropriate selection

ion windows and ions to ensure reliable peak capture and sensitivity.

2.2.2 Time of flight mass spectrometry (TOF MS)

The concept of time-of-flight (TOF) for separation of ions in mass spectroscopy was first reported in the 1930s (Smythe & Mattauch, 1932). However, it was not until the publication of a seminal paper (Wiley & McLaren, 1955) on ion focusing in TOF mass spectroscopy (TOF MS) that time-of-flight instrument development took off. By 1962 it was estimated that a third of all mass spectrometers in use in the United States were TOF instruments. Since then, the universal popularity of TOF MS has waned mainly due to the commercialisation of transmission quadrupole mass spectrometers in the mid-1960s (Watson & Sparkman, 2007, and references therein). However, TOF MS still remains popular for some applications e.g. matrix-assisted laser desorption/ionisation (MALDI) (e.g. Mlynski & Guilhaus, 1996) and mass spectroscopy/mass spectroscopy (MS/MS) techniques (Campbell et al., 1998), and is rapidly gaining wider popularity with recent improvements in nano- and pico-second timing electronics and resulting increases in sensitivity.

The principle of TOF MS involves measuring the time required for an ion to travel from an ion source to a detector over a known distance (Figure 2.3). If all ions receive the same kinetic energy during instantaneous acceleration from the source they will, due to their different mass to charge ratios (m/z), have different velocities. In linear TOF MS instruments (i.e. Figure 2.3) the region between the source and the detector has no accelerating potential i.e. it is ‘field free’. Therefore, as ions move through the region between source and detector, they will separate into packets according to their velocity, which is a function of m/z . As a consequence, ions of all m/z values can, theoretically, be detected in the initial ion packet without the need to scan across a range of ions.

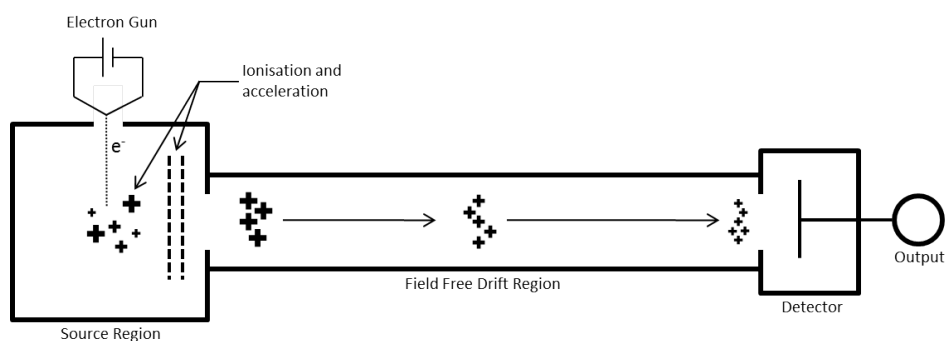


Figure 2.3: Schematic representation of a linear time-of-flight mass spectrometer.

The kinetic energy gained by an ion in the accelerating section of the TOF MS is equal to the potential energy gained between the accelerator plates:

$$zeV = \frac{1}{2}mv^2 \quad (2.4)$$

where z is the charge on the ion, e the elementary charge, V the accelerating potential, m the mass of the ion and v the velocity of the ion. Solving for v and substituting for $v = L \cdot \text{tof}$ (where tof is

the time-of-flight from source to detector separated by distance L gives:

$$\text{tof} = L\sqrt{\frac{m}{2zeV}} \quad (2.5)$$

Therefore, in principle, there is no upper limit to the m/z that can be separated (it is only dependent on how long the ions take to reach the detector). This is the main reason why TOF MS has found favour in some applications, such as matrix-assisted laser desorption/ionisation (MALDI), where higher m/z species are of interest. Another major advantage of TOF MS over other techniques, such as quadrupole MS, is the ability of TOF MS to follow high speed chromatography. This is especially the case if it is desirable to analyse a large m/z range e.g. for compound identification. Quadrupole MS and other scanning techniques are limited by the transit time for ions through the mass analyser. Narrow chromatographic peaks require a higher number of scans across that peak in order to ensure accurate peak shape and integration. In practice, this requires that the observation time at a specific m/z diminishes to near or below the transit time of ions through the mass spectrometer (Guilhaus et al., 1997). As this limit was reached or exceeded, the performance of the mass spectrometer would be expected to rapidly deteriorate. This limit is easily reached when a large m/z range and a high scan rate are required for compound identification and good peak shape during high speed chromatography. TOF MS sidesteps this issue as ions are detected *near* simultaneously giving full mass spectra on the microsecond timescale.

Similarly, TOF MS also avoids the issue of spectral skewing in transmission quadrupole MS (TQ-MS) and other scanning MS techniques (Dallüge et al., 2002). Skewing in TQ-MS results when the partial pressure of the analyte in the ion source changes on the timescale of a mass spectral scan. Figure 2.4 shows an exaggerated example of spectral skewing. Spectra taken on the leading and tailing edges of the chromatographic peak (Scan #1 and Scan #3) show significant distortion in the relative intensities of ions as compared to the hypothetical mass spectrum. This can lead to difficulties in pattern recognition when using mass spectral library databases. Averaging over the width of a peak can reconstruct a near-ideal spectrum. However, this requires chromatographic peaks to be relatively symmetrical and to represent only a single compound. Additionally, a slow scan rate relative to elution time will not provide enough data points across a chromatographic peak to reconstruct the chromatographic profile. TOF analysers acquire spectra from pulsed ion packets which are then combined to form a mass spectrum. As each ion packet is formed discretely, the partial pressure of components does not change during each acquisition. Therefore, each packet's ion distribution is representative of the 'true' ion distribution.

Linear TOF instruments produce ion packets by pulsing or gating of the ion source. However, the limitations that this imposes on ion sampling efficiency led to the development of orthogonal sampling from a continuous ion beam (Guilhaus et al., 2000).

2.2.2.1 Orthogonal time-of-flight analysers (oa-TOF)

In orthogonal time-of-flight (oa-TOF) instruments ion packets are pushed out of a continuous, collimated ion beam perpendicular to the axis of the flight path (Figure 2.5). Because the original ion beam is collimated, and some collision cooling can take place within the ion beam, there is

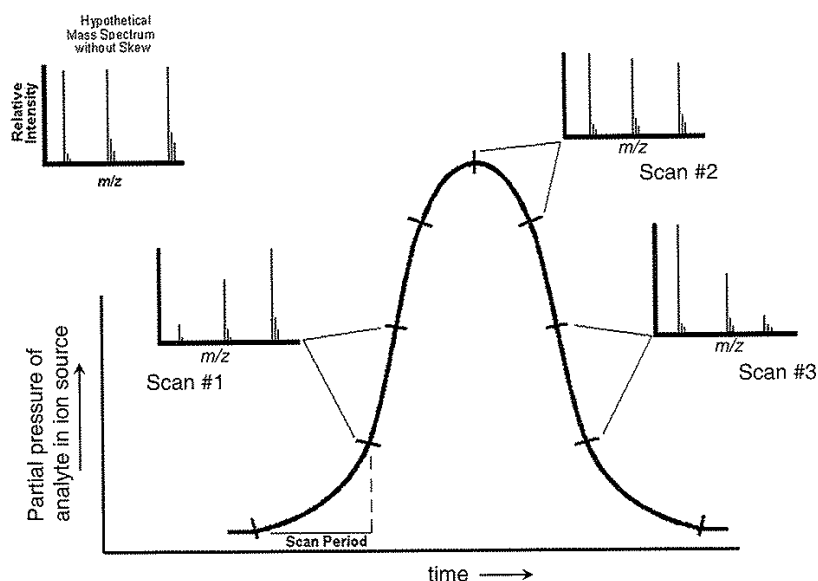


Figure 2.4: An illustration of spectral skewing due to dynamic changes in analyte partial pressure in an instrument that scans across an m/z range, from low to high masses, during GC elution (distortion has been exaggerated for clarity). During the leading and trailing portions of the peak, where the concentration of the eluent is rapidly changing, the mass spectrum is distorted (Scans #1 and #3). For instance, during a spectral acquisition on the leading edge of the peak, higher masses are recorded at slightly higher eluent concentration than the lower masses, skewing the mass spectrum towards higher m/z . The equivalent occurs on the trailing edge but with mass spectra skewed towards lower m/z . Adapted from Watson & Sparkman (2007).

reduced radial energy dispersion of ions. This translates into an improved resolving power and sensitivity of the instrument over that of a linear TOF or purely reflecting TOF instrument (see Section 2.2.2.2).

The formation of the continuous ion beam is an important factor in optimising the performance of oa-TOF instruments (Guilhaus et al., 2000). A nearly parallel ion beam will minimise the spread of magnitudes of the velocity component in the ‘drift’ direction and a narrow beam will minimise the spatial spread of ions. Therefore, the design of the ion optics controlling the ion beam is an important factor in oa-TOF design.

Individual ion packet ‘shots’, pushed out of the ion beam, are summed together over a set time interval to produce a mass spectrum. For instance, in an instrument operating with a 30 kHz push signal producing two spectra per second, each spectrum will be the sum of 15000 shots. The frequency of the push signal can be varied so that more shots are summed together in the same time period to give greater sensitivity. For instance, a 100 kHz push signal would give 50000 shots per spectrum for two spectra per second, theoretically giving a three times sensitivity enhancement. However, this is at the cost of a reduced detectable mass range; a consequence of the time between individual shots approaching the flight time of higher m/z ions in the drift region of the TOF analyser. This leads to the lowest m/z ions from one packet overlapping with the highest m/z ions of the preceding packet thereby reducing the range over which the timing of the push voltage and the detection of ions are correlated. Additionally, if a greater number of spectra are required over the width of a chromatographic peak, the number of shots summed per spectrum will be reduced, leading to reduced sensitivity.

Though the ions in oa-TOF do not have a significant spread of velocities in the drift direction,

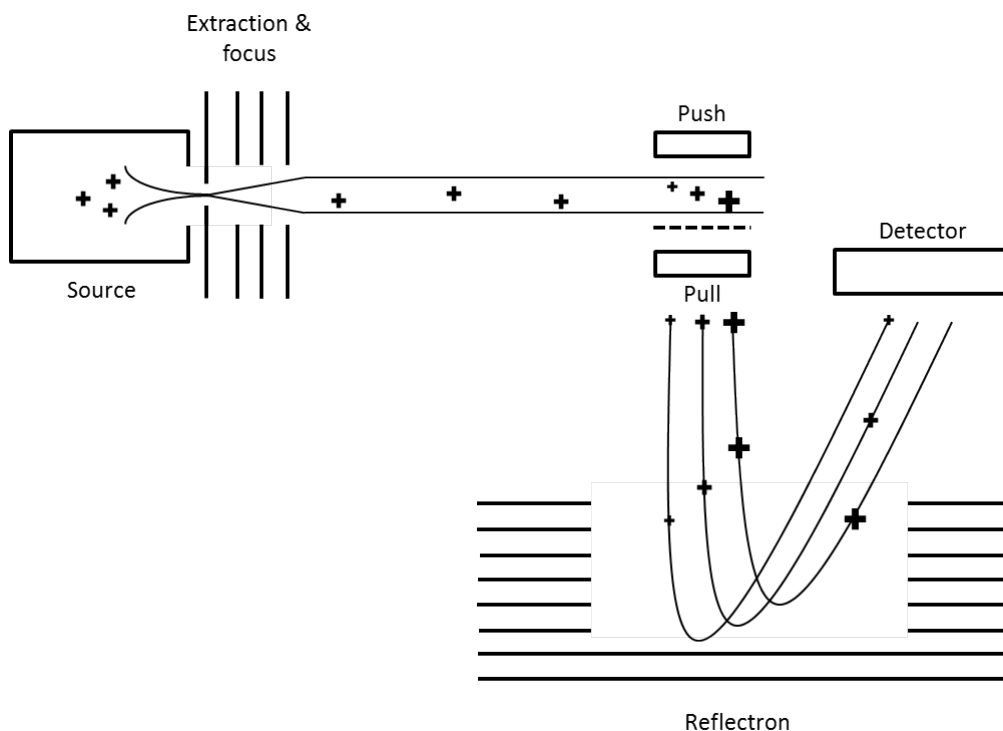


Figure 2.5: Schematic of an orthogonal TOF mass spectrometer with reflectron. Ion packets are cut out of a continuous, collimated ion beam before ion separation.

they do have a significant velocity spread orthogonal to the drift direction. This acts to disperse the ions over the detector plane but is insignificant as long as the detector is large enough to intercept most of the ions as “it matters when the ions hit the detector but it does not matter where they hit it” (Guilhaus et al., 2000). The detector in the TOF MS used in this work is a discrete-dynode electron multiplier (SGE Analytical Science, Trajan Scientific, Australia). A dynode is an electrode in a vacuum that amplifies the signal from an impacting ion (in the case of MS), electron or neutral particle. When an incoming particle impacts a dynode surface, a number of secondary electrons are released. The number of electrons depends on the incident particle, its angle of impact, energy and the characteristics of the surface. A typical discrete dynode electron multiplier has between 12 and 24 individual dynodes arranged in series to provide an operating gain of between 10^5 and 10^8 depending on the application.

2.2.2.2 Reflectron time-of-flight analysers (re-TOF)

Along with orthogonal sampling of the ion beam, the reflectron represents an important innovation in TOF analysers. The reflectron is an ion mirror with an electric field that opposes and is of greater magnitude than the electric field of the ion acceleration region, and replaces the field free region of linear TOF. In non-orthogonally accelerating instruments, the mirror is positioned at an angle of less than 180° to avoid reflection of ions directly back into the source (Figure 2.6). In oa-TOF instruments, the reflectron can be mounted at 180° as the residual velocity component of the ion beam prevents direct reflection back into the push/pull region (Figure 2.5). The reflectron serves two purposes: to reduce the dimensions of the instrument and to improve the resolving power of the TOF MS. This is achieved by adjusting, within an ion ‘packet’ of the same m/z , the length of the flight path of individual ions in proportion to their kinetic energy. This provides

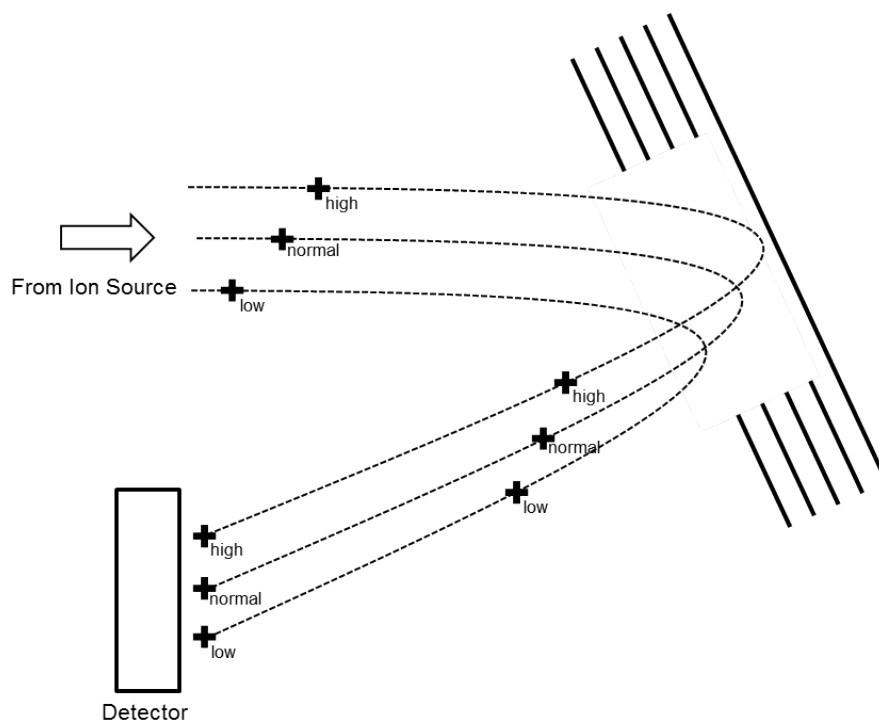


Figure 2.6: Schematic of a reflectron ion mirror. Ions retain their original velocity (high, normal or low) but are detected at the same time because of the difference in residence time in the reflectron.

an additional temporal focus for the ions within a packet.

Improvements in resolving power are a result of the reflectrons ability to focus ions with the same m/z but which differ slightly in initial kinetic energy. As in Figure 2.6, a discrete ‘packet’ of ions of the same m/z but differing kinetic energies enter the opposing field of the reflectron and they penetrate to different extents depending on their kinetic energies; the ions with highest kinetic energies penetrating the furthest. The ions decelerate until their kinetic energies reach zero, at which point they are accelerated by the electric field in the opposite direction. As ions with the highest initial kinetic energy penetrated the deepest, they will gain more kinetic energy during re-acceleration. Therefore, though the ions leave the reflectron with the same distribution of kinetic energies, the lengths of their flight paths have been altered in proportion to their initial kinetic energies. Hence, ions with a distribution of initial kinetic energies will be focused at the detector with respect to arrival time (they will be temporally focused) as in Figure 2.6. This only applies to ions with the same m/z ; ions with different m/z values will still arrive at the detector after different flight times. However, mass spectral peaks will be sharper as a result of the reduced spread of flight times within an m/z ‘packet’.

2.2.2.3 Applications of TOF to Atmospheric Science

The recent innovations in TOF instrument design, especially in the design of high speed electronics, have attracted interest from the atmospheric sciences. It is hoped that GC-TOF instrumentation will be able to overcome some of the shortcomings of current techniques especially TQ-MS (transmission quadrupole mass spectrometry, see Section 2.2.1), the most widely used GC-MS technique in atmospheric science. The main benefit of GC-TOF is in being able to assess the full range of ions during an analysis whilst maintaining sensitivity. This potentially allows for

immediate identification of known compounds, de-convolution of co-eluting compounds and minimizes the steps required to identify unknown compounds. In theory, TOF MS could also make redundant the need for multiple individually optimised GC-MS instruments for analysis of the full spectrum of atmospheric compounds. In practise, however, TOF instrumentation may not yet be sensitive enough to replace some of these techniques e.g. chemical ionisation TQ-MS for the analysis of sub-ppt mixing ratio halocarbons.

The effectiveness of GC-TOF in the analysis of hydrocarbons in gasoline has been highlighted by Hamilton et al. (2004). GC-TOF was found to be especially useful for high speed analysis of a mixed hydrocarbon standard due to the fast scan rate. Hamilton et al. also speculated that combining GC-TOF with comprehensive gas chromatography (GCxGC), in which the sample undergoes two independent separations before analysis, would be a very powerful technique for atmospheric analysis. This technique has since been used for atmospheric studies, especially component analysis of organic aerosol (e.g. Hamilton et al., 2004; Kallio et al., 2006; Laitinen et al., 2010; Ozel et al., 2010; Vogt et al., 2007). There is great scope for GC-TOF measurements especially direct measurement of trace gases in the atmosphere.

2.2.3 Ionisation techniques

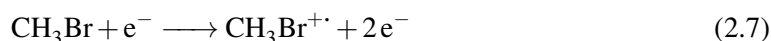
2.2.3.1 Electron ionisation (EI)

The ionisation technique used in mass spectrometry depends on the type of sample and the results required of the analysis. The most common method is electron ionisation (EI). In the EI source, analyte molecules are ionised by a beam of high energy electrons produced by thermoelectric emission from a heated metal filament (usually made of tungsten). The electrons are accelerated by a potential difference commonly set to 70 eV (electron volts). The electrons enter the source through a small slit into the ionisation chamber.

When an electron in the source collides with a neutral molecule (M), another electron may be ejected from the molecule giving a positively charged radical ion as in Equation 2.6. The $M^{\cdot+}$ ion is referred to as the molecular ion. Removal of one electron from an organic molecule requires about 10 eV. If the energy of the impacting ion is greater than this, the molecular ion may be left with enough excess energy to fragment into lower mass ions. The pattern of fragmentation and number of ions produced are dependent on the energy of the impacting electrons. Provided that the ionisation energy is known, the fragmentation pattern of a compound should be similar between instruments using an electron ionisation technique.



As an example, Equations 2.7-2.9 show possible ions resulting from fragmentation of the molecular ion formed from electron ionisation of CH_3Br .



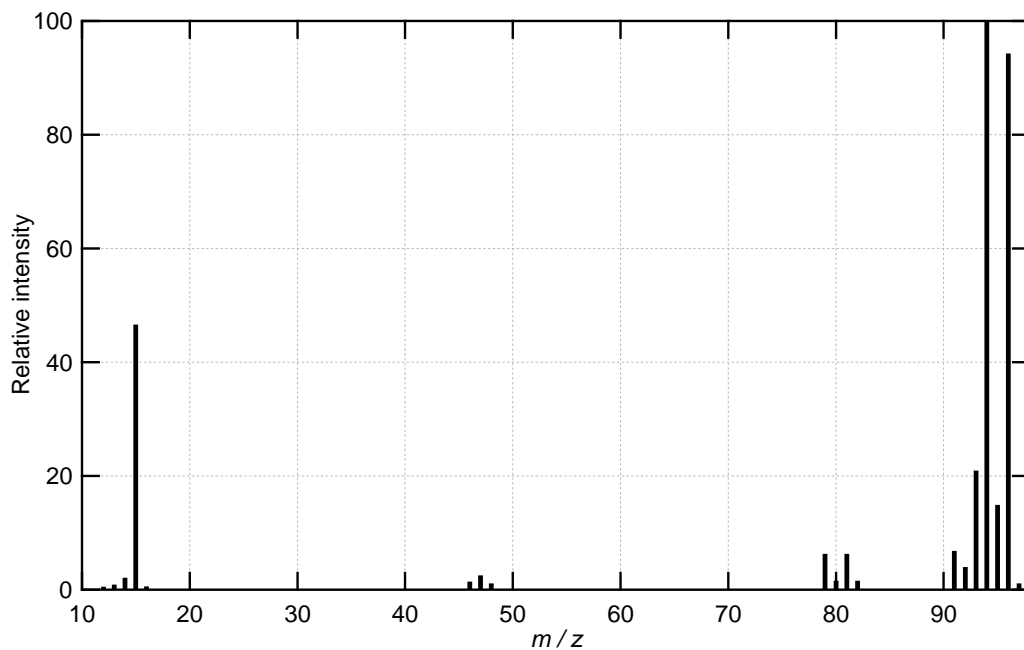


Figure 2.7: Typical mass spectrum for methyl bromide, CH₃Br. Intensities are given relative to the most intense ion in this case m/z 79. Based on data from the NIST Chemistry WebBook (Lindstrom & Mallard, 2014).

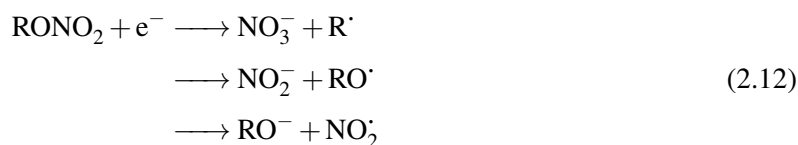
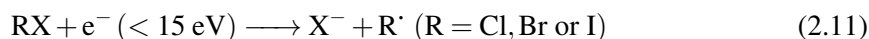
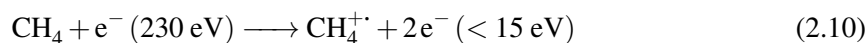
As bromine (Br) has two stable isotopes, mass 79 and 81, the molecular ion (Equation 2.7) would give ion peaks at mass 94 and 96. Loss of Br[•] (Equation 2.8) would give a peak at mass 15 due to the CH₃⁺ ion. Similarly, peaks at mass 79 and 81 would be expected due to the Br⁺ ion. An example of the resultant mass spectrum is shown in Figure 2.7. The intensities of mass spectral peaks are governed by a combination of the efficiency of ionisation and fragmentation processes, coupled with the stability of the resultant ion.

2.2.3.2 Negative ion chemical ionisation (NICI)

Although electron ionisation is the most common form of ionisation technique, fragmentation can result in loss of information about the molecular ion. An alternative technique is chemical ionisation (CI) where analyte molecules are ionised by an ion transfer process or by dissociative electron capture.

Negative ion chemical ionisation, NICI (sometimes referred to as electron capture ionisation, ECI), is used for compounds with high electron affinity. The source in NICI is designed to accommodate a relatively high pressure (20–50 times higher than the surrounding vacuum) of a reagent gas e.g. methane or argon. High energy primary electrons (~ 230 eV) are thermionically emitted from a heated filament. These electrons are decelerated by interaction with the reagent gas to form low energy electrons (< 15 eV) and positively charged radical ions (Equation 2.10). The high pressure of reagent gas serves two purposes: ensuring a sufficient number of collisions during the dwell time of reactants in the source, and shielding the analyte molecules from the high energy primary electrons and, therefore reducing competing EI reactions and fragmentation (Watson & Sparkman, 2007). The primary electrons are necessarily of higher energy (~ 230 eV) than standard EI (commonly 70 eV) in order to effectively penetrate the reagent

gas. Methane is the most common reagent gas, however, argon can be used and has the advantages of reducing the frequency of source cleaning compared to methane and being a non-flammable gas.



The lower energy electrons created in NICI can be captured by a variety of species, especially those with electron affinity e.g. halocarbons. Fragmentation is reduced due to the low energy of captured electrons leading to higher sensitivity during detection. Halocarbons and alkyl nitrates produce anions during NICI (Equations 2.11 and 2.12). Alkyl nitrates produce three anions during NICI (Reaction 2.12). Halocarbon gases give the corresponding halogen anion (Reaction 2.11). In the case of multiply halogenated molecules, the anion formed is usually, though not exclusively, that of the halogen with highest electron affinity (Worton et al., 2008). Table 2.1 shows the typical sensitivity enhancement in NICI when compared to EI, for a number of trace atmospheric compounds. For halocarbons, the sensitivity enhancement of NICI is dependent on the halogen atom present, with sensitivity increasing with increasing atomic number i.e. $\text{Cl} < \text{Br} < \text{I}$. This is illustrated by the three methyl halides, MeCl, MeBr and MeI in Table 2.1. NICI sensitivity is also dependent on the number of each halogen atom in the molecule with increasing sensitivity to more highly halogenated molecules though the relationship is not always simplistic e.g. MeBr, CH_2Br_2 and CHBr_3 .

2.2.4 Summary of time-of-flight vs. quadrupole mass spectrometry

One of main advantage of time-of-flight mass spectrometry as compared to quadrupole MS is that a large range of ions can be analysed simultaneously without loss of sensitivity. This allows for positive identification of compounds during analysis. This is in addition to routine identification based on previous identification of key (usually two) ions and the retention time of a compound. Being able to identify compounds during analysis and data work-up is especially beneficial in polluted atmospheres where compound mixing ratios might vary over a large range and have many co-elutants. This also allows for the simultaneous analysis of a larger number of compounds than in quadrupole MS. This is especially advantageous when analysing for low abundance compounds where quadrupole dwell times would have to be increased to improve sensitivity and, hence, decrease the number of ions simultaneously analysable. A related feature of TOF MS, in atmospheric analysis, is that the large number of ions measured and recorded allows for easier reanalysis of the data e.g. for previously unidentified compounds.

TOF MS also has the advantage of higher 'scan' rates compared to quadrupole MS. The

Table 2.1: Comparison of the limit-of-detection (LOD) for similar analyses made with negative ion chemical ionisation (NICI) and electron ionisation (EI) sources. The sensitivity enhancement is given as the ratio of LODs from the two techniques (NICI/EI). Compounds have been grouped to highlight the effects of functional group e.g. Cl, Br, I or ONO₂, and in the case of halocarbons, the number of halogen atoms in the molecule. Based on data from Worton et al. (2008).

Species	LOD [ppt]		NICI/EI
	NICI	EI	
MeCl	50	2.0	0.04
CHCl ₃	0.01	0.07	6
CH ₃ CCl ₃	0.03	0.2	6
CCl ₄	0.01	0.05	3
MeBr	2	0.2	0.1
CH ₂ Br ₂	0.001	0.02	20
CHBr ₃	0.001	0.02	10
CHBrCl ₂	0.0008	0.2	300
CHBr ₂ Cl	0.001	0.1	100
CCl ₂ F ₂	0.07	0.1	2
CCl ₃ F	0.05	0.2	3
CBrClF ₂	0.003	0.3	100
C ₂ Br ₂ F ₄	0.001	0.02	20
MeI	0.002	0.3	100
MeONO ₂	0.002	0.3	100
EtONO ₂	0.0008	0.05	60
<i>i</i> -PrONO ₂	0.003	0.2	40

number of spectra per second that a quadrupole MS instrument can record is limited by the number of ions and dwell times required for the analysis. As TOF MS sum averages a number of high frequency shots into one 'scan', the number of spectra per second can be varied as required. For standard capillary GC, a scan frequency of approximately 2 spectra per second is necessary to provide an appropriate number of points across a chromatographic peak for accurate peak integration. For applications, such GC×GC, peak widths are much narrower than in standard GC and might require scan rates of 50–100 spectra per second. This is not achievable on a quadrupole MS instrument when analysing for a large number of compounds.

The major disadvantages of TOF mass spectrometry are that, until recently, the power supply units and high frequency electronics have not been readily available. Large power supplies have limited the portability of TOF instruments for many field applications. The availability of high frequency electronics, required for the nanosecond timing of ion-packet pulses in TOF, has impeded the necessary sensitivity, reliability and reproducible behaviour of TOF MS. Quadrupole mass spectrometers have found favour in atmospheric chemistry partly due their robust, portable and stable nature. Current developments in TOF electronics are likely to overcome these limitations in the near future.

2.3 General calibration processes

The process used for assigning compound mixing ratios in samples analysed at UEA is based on individual compound response factors determined by comparison to a working standard with known mixing ratios. The working standard varies between campaigns and sampling runs depending on availability. The mixing ratios of compounds in the working standard are determined by repeat comparison to calibrated gas standards. The calibrated gas standards used at UEA are supplied by the Global Monitoring Division of NOAA ESRL in 34 L electropolished stainless steel or Aculite-treated aluminium canisters (Essex Cryogenics, St. Louis, MO, US). Mixing ratios of a number of compounds in these standards are determined, at the Central Comparison Laboratory of the Global Monitoring Division of NOAA ESRL, by comparison to a set of primary standards that are prepared using pure vapour or pure liquid of the compound (NOAA: ESRL, 2008). For compounds that are not calibrated for by NOAA, a similar process of comparison to a pure-liquid/vapour-derived standard is followed at UEA. Not all compounds are stable with time when stored in canisters. For some working standards, e.g. those in aluminium tanks, time-correction based on a number of inter-comparisons is necessary in order to correct for drift. For instance, drift correction was applied to working standard mixing ratios of bromocarbons analysed as part of the CARIBIC campaign (Chapter 4).

As a general note, units for mixing ratios for compounds measured at UEA are-dry air mole fractions e.g. nmol mol^{-1} and pmol mol^{-1} . For the sake of readability, these have been abbreviated to ppb (parts per billion) for nmol mol^{-1} (dry air) and ppt (parts per trillion) for pmol mol^{-1} (dry air). For supporting data analysed by a gas chromatography technique (e.g. GC-MS or GC-FID) it is usually the case that air had been dried prior to analysis. Therefore, units of ppt and ppb indicate dry-air mole fractions for these measurements. For some measurements of gaseous species (such as O_3 in Chapter 4 or CO in Chapter 5) the air is not dried prior to analysis. In this case ppb and ppt refer to wet-air mole fractions. In practice the difference between wet- and dry-air fractions is minimal.

2.4 GC-MS technique usage

GC-MS techniques have been used throughout this work in the analysis of atmospheric trace gases. Quadrupole GC-MS was used for analysis of samples during the ClearfLo, CARIBIC and SAMMBA campaigns (Chapters 3, 4 and 5 respectively). A TOF GC-MS in EI mode was characterised and compared to a quadrupole mass spectrometer in Chapter 3. The following summarises the techniques used in each chapter. Within each chapter, a more detailed description of the experimental methods and techniques used during the specific analysis has been given.

Chapter 3:

The initial aim this thesis was to characterise a new TOF GC-MS instrument and use it for analysis on a number of field and lab-based projects. Ultimately, instrumental problems led the TOF GC-MS not being used for the projects discussed in this work excepting a comparison to a dual electron ionisation/negative ion chemical ionisation (EI/NICI) GC-MS using data from the ClearfLo campaign.

Chapter 4:

Due to the high sensitivity to halogens especially bromine and iodine (Section 2.2.3.2), NICI GC-MS was used to study short-lived bromo- and chloro-methanes in the upper troposphere/lower stratosphere (UTLS) as part of the CARIBIC campaign. These compounds are present at sub part-per-trillion (sub-ppt) levels and are generally close to or below the detection limit of standard quadrupole EI GC-MS techniques.

Chapter 5:

Though NICI GC-MS has an increased sensitivity to halogenated compounds, this enhancement is also proportional to the number of halogen atoms in a molecule. The main aim of the analysis for the SAMBBA campaign, described in Chapter 5, was to characterise emissions of methyl halides from biomass burning in the Amazon rainforest. NICI GC-MS has comparatively poor sensitivity, compared to EI GC-MS, for methyl chloride and methyl bromide (see Table 2.1). Additionally, a number of species are not well characterised in the NICI GC-MS instrument. Therefore, EI GC-MS was used in the analysis of samples from the SAMBBA campaign.

A GC Time of Flight Mass Spectrometer for Atmospheric Measurements

The time-of-flight gas chromatography-mass spectrometer (TOF GC-MS) system described in this chapter was provided by Scientific Analysis Instruments Ltd. (SAI, <http://www.saiman.co.uk/>). As provided, the instrument consisted of an SAI Kronus™ TOF MS combined with a rebuilt Perichrom (now Alpha MOS, <http://www.alpha-mos.com/>) PR 2100 GC combined in a single case (see Figure 3.1) with a proprietary trapping system. The provided inlet was rapidly determined to be insufficient for atmospheric analysis and was replaced with a manual system (Section 3.1). The GC unit had a number of problems and was bypassed eventually with a replacement Agilent GC system and transfer line (Section 3.2). The TOF GC-MS, though still somewhat unreliable, was used to analyse bottle samples of real air from a London-based campaign where in situ measurements were made of a number of halocarbons. The resolution of technical problems with the TOF GC-MS was hindered by the limited technical support provided by the suppliers.

3.1 Inlet system

In order to use the GC-TOF system for the analysis of air samples, a suitable inlet system had to be built. The original specifications of the system were for an automated system ready for sampling air and other gases. To this end, an air-sampling system was provided but was rapidly determined to be insufficient for the quantitative and reproducible trapping required for trace-gas sampling from real-air samples.

In order to provide the best possible measurement reproducibility, a manual inlet system was built. This manual inlet system was based on a commonly used layout for air sampling incorporating a 6-port sampling valve (Figure 3.2).

Samples are dried prior to trapping with a magnesium perchlorate (MPC) drier to remove water vapour. Samples are pre-concentrated before injection onto the GC column by cryogenic trapping of the compounds of interest with subsequent separation from the majority gases in an air sample (mainly N₂, O₂ and Ar). Cryogenic trapping is performed using a 1/8 inch stainless steel tubing sample loop packed with Haysep D, 80/100 mesh (Valco) at -72 °C by immersion in an ethanol/dry-ice mixture. Samples are trapped at ~100 ml min⁻¹ regulated with a needle



Figure 3.1: Photograph of the time-of-flight gas chromatography mass spectrometer (GC-TOF) provided by SAI (Scientific Analysis Instruments) Ltd. The left-hand panel houses the time-of-flight mass spectrometer (TOF), the central panel houses the gas chromatograph (GC) and the right-hand panel houses the GC control panel with a void that can be utilised for housing a controlling computer workstation.

valve between the sample and sampling loop. Sample volume and sampling rate are controlled by monitoring the pressure change on a 6 L reference volume with an eBaratronTM capacitance manometer (MKS Instruments, Massachusetts, USA) labelled “vacuum gauge” in Figure 3.2. After pre-concentration, the sample loop and reference volume are isolated from the sample flow and the pressure allowed to equilibrate prior to thermal desorption from the loop at 100 °C with boiling water and injection onto the analytical column. Injection is performed via switching of the 6-port injection valve heated to 100 °C (see Figure 3.2). Gases eluted from the sample loop are transferred to the head of the GC column via ~30 cm of neutral polarity unfunctionalised fused silica capillary (320 μm ID) heated to 100 °C.

3.2 GC system

3.2.1 GC \times GC capability

The original instrument design specification included a comprehensive two-dimensional gas chromatography (GC \times GC) capability. This would have been achieved via a dual jet cryojet modulator utilising liquid N₂. TOF-MS systems are ideally suited to this GC technique; due to the re-focusing of analytes and high speed conditions of the secondary column, very sharp peaks are obtained with base widths of typically 200 μs (e.g. Hübschmann, 2009). However, as the two dimensional (2D) GC setup provided with the instrument was found to be unsuitable for routine

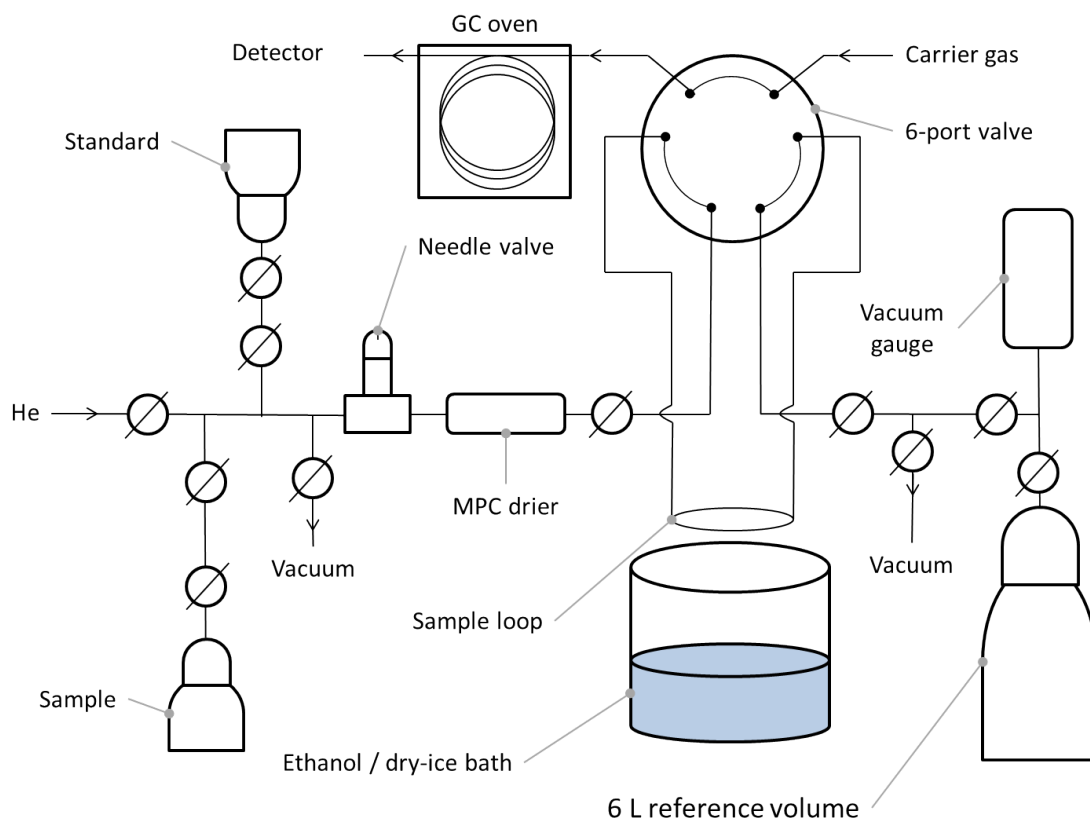


Figure 3.2: Diagrammatic representation of the inlet system used for the GC-TOF. The MPC drier is a glass tube packed with magnesium perchlorate.

use in GC-TOF analysis, the GC×GC unit was not tested.

3.2.2 Agilent™ GC system

The as-delivered GC-TOF system included a PR2100 from Perichrom (now Alpha MOS, Toulouse, France) rebuilt for the GC-TOF case (see Figure 3.1). A notable disadvantage of the as-delivered GC-TOF system was the unreliable nature of the GC system. Several problems were encountered including the following:

- Sticking of the oven ventilation flaps that help the oven maintain temperature and cool rapidly between GC runs, causing overheating of the heating filament and subsequent shorting on the casing of the oven. This was successfully fixed, however, if the GC software crashed and reset, as was frequently the case, the ventilation flaps had to be manually checked to ensure the controlling stepper motor had reset to the default position.
- Crashing of the GC control software built into the oven. No reproducible cause could be determined for this fault.
- Poor maintenance of flow conditions by the electronic pressure control (EPC) unit and/or poor thermo-regulation of the GC oven, causing baseline oscillations in the resulting chromatogram. An example of the baseline oscillations can be found in Figure 3.3. It was not possible to determine the exact cause of these oscillations but it is likely that they were caused by temperature and/or pressure fluctuations. Air-leaks were eliminated as a cause.

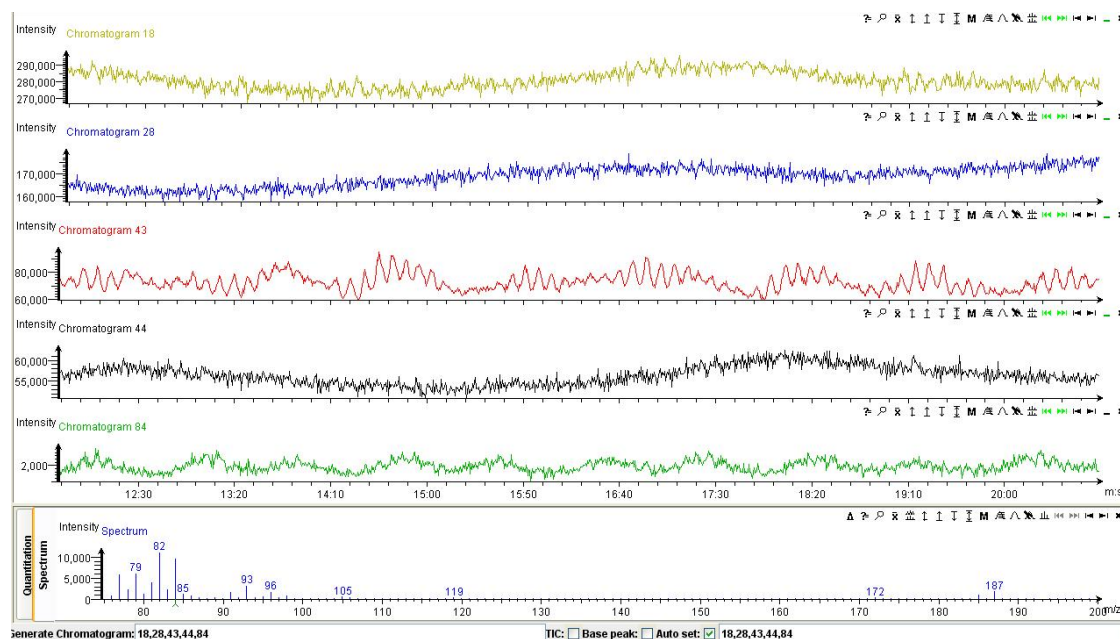


Figure 3.3: Screen-shot of the software output for selected ions acquired at constant temperature showing oscillations in the baseline. These oscillations are assumed to have been caused by pressure fluctuations due to either poor thermo-regulation in the GC oven or poor pressure regulation from the GC electronic pressure control.

The problems encountered in using the existing GC system were considered of a fundamental nature and not worth pursuing further with the manufacturers. As a consequence the existing GC system was bypassed and an Agilent 6890N gas chromatograph (Agilent Technologies) was inserted into the carrier gas flow between the inlet and the mass spectrometer. A heated transfer line ~ 45 cm long was used between the GC and the TOF inlet. The transfer line consists of a length of neutral polarity unfunctionalised fused silica capillary ($320 \mu\text{m}$ ID) heated to 180°C with a rope heater and temperature controller. The last ~ 15 cm of capillary are heated by the TOF GC-MS transfer line heater to 150°C , the maximum temperature attainable. The Agilent 6890N provides the advantages of stability (both in terms of thermo-/pressure-regulation and computer control), more comprehensive programmability, the option of a constant flow pressure regime and of being a better understood and well-used system within the group of potential users. Baseline oscillations were eliminated with the Agilent GC system and usability was improved. However, the instrument was too large to be of practical use in fieldwork. Removal of the original GC system from the TOF, i.e. using the TOF as a standalone instrument, would bring the system back to a field-usable state however, this was beyond the scope and time-constraints of the development of this instrument and will be carried out in the future.

3.3 Time-of-flight (TOF) mass spectrometer

The TOF mass spectrometer is an orthogonal time-of-flight (oaTOF) mass analyser with a reflectron ion mirror as outlined in Sections 2.2.2.1 and 2.2.2.2 and similar in layout to the diagram in Figure 2.5. Figure 3.4 shows the layout of the mass spectrometer with key components highlighted. The TOF instrument was designed with a number of considerations relevant for use in analysis of atmospheric trace gases. These considerations will be further discussed in Section 3.7.2. However,

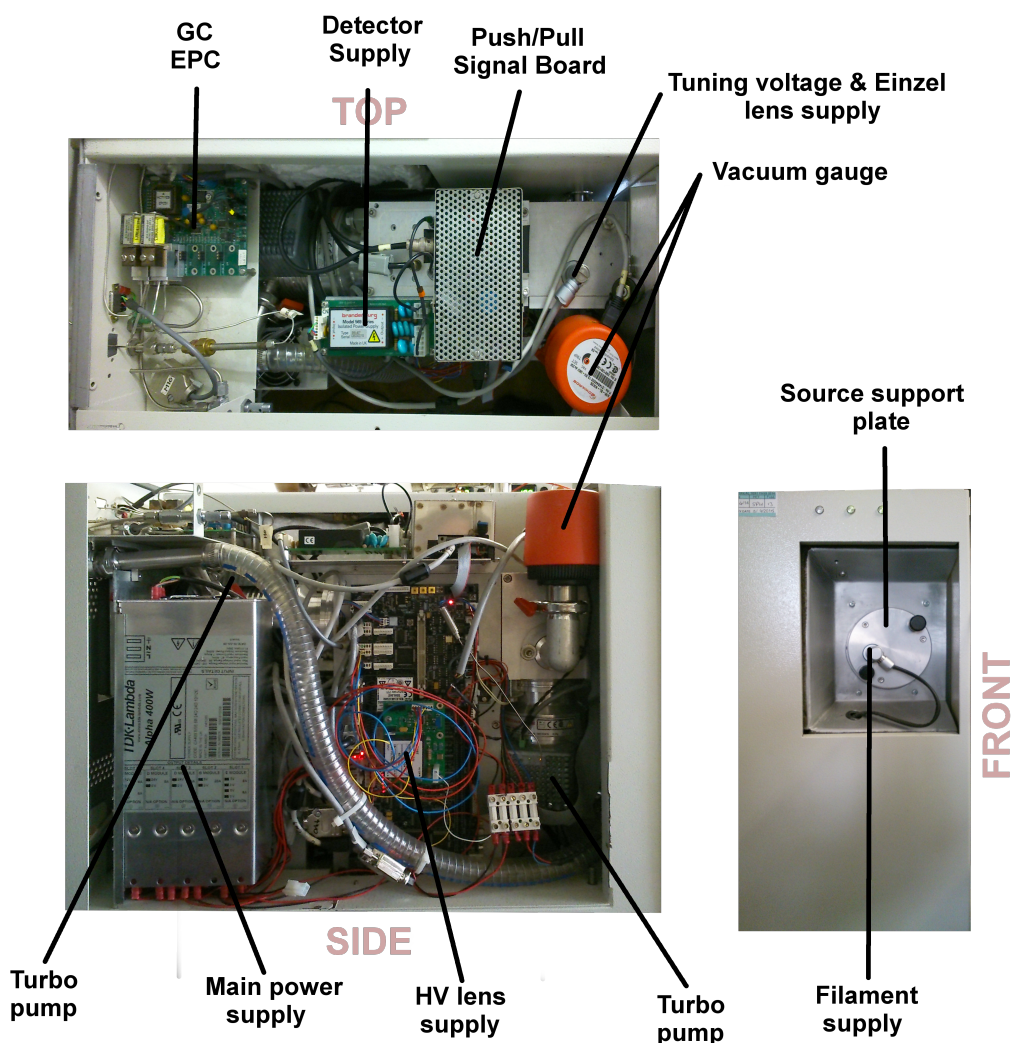


Figure 3.4: Internal layout of the TOF MS showing the location of key elements.

an important factor in the instrument design was portability for fieldwork. Hence, it should be noted that there is no separate power source for the mass spectrometer and that the MS footprint is similar to a conventional quadrupole instrument. The internal layout of the TOF MS is shown in Figure 3.4.

3.3.1 MS alterations and upgrades

After receipt of the GC-TOF system, a number of alterations were made to the instrument by supporting engineers. These improvements were made as an attempt to increase the sensitivity of the instrument in order to better match the original specification of a sensitivity similar to that of a quadrupole mass spectrometer (roughly better than a limit-of-detection of 0.1 ppt). Additionally, some of the capability of the instrument, namely the 100 kHz sampling mode, was of an experimental design and not proven for use in routine analysis. The main alterations and untested features added to the GC-TOF system are discussed here.

3.3.1.1 30 kHz and 100 kHz sampling modes

The time-of-flight mass spectrometer is capable of operating at different ‘shot’ sampling rates (see Section 2.2.2.1). Two sampling frequencies were provided with the instrument for use with atmospheric samples: 30 kHz and an experimental 100 kHz mode. A 10 kHz mode is also provided but does not have any advantages over the other sampling frequencies for the intended application of the instrument. As mentioned in Section 2.2.2.1, when individual ‘shots’ are averaged to the same number of spectra per second, the 100 kHz mode offers a theoretical three-fold increase in sensitivity over the 30 kHz mode. Additionally, the 100 kHz mode would provide increased sensitivity and sampling across chromatographic peaks when working with GC×GC chromatography where the chromatographic peak widths are on the order of 200 μ s (see Section 3.2.1).

The 100 kHz mode was found to provide approximately double the sensitivity, based on peak area, than the 30 kHz mode. However, the pay-off of m/z range coverage, discussed in Section 2.2.2.1, limits the 100 kHz mode to an m/z range of 14–150 compared to the 30 kHz mode range of 14–460. Unfortunately, this limited range reduces the number of atmospheric trace gases analysable and can complicate positive identification of some compounds. For instance, bromoform (CHBr_3) would be difficult to identify due to the three most abundant ions being m/z 173, 171 and 175. Additionally, at the typical sub-part-per-trillion mixing ratios of CHBr_3 , analysis based on less abundant ions would be impractical. During initial testing, the experimental 100 kHz mode was found to be too unstable for routine use due to factors such as distorted mass spectral peaks, unusual spiking in chromatograms and software issues. Due to these issues, it was considered that the sensitivity increase was not large enough to be worth pursuing further and the instrument was run in 30 kHz mode for all further usage.

3.3.1.2 High-voltage accel-decel Einzel lens assembly

In order to provide a focused packet of ions for acceleration in to the ‘drift’ section of the time-of-flight mass spectrometer, it is necessary to create a narrow, collimated ion beam (see Section 2.2.2.1 and Figure 2.5). Beam focusing is achieved with an ion lens arrangement between the extraction plate and the push/pull shot slicer. It is possible, with different arrangements of this ion lens, to affect the sensitivity of the instrument.

The lens arrangement provided with the TOF instrument was an ‘Einzel’ lens in decel-accel mode with the lens focus in the direction of the extraction plate (see Liebl, 2008, for a detailed description). The lens consists of three apertured electrodes with the first and third electrode at the same potential (in this case grounded) and the second plate at a tunable voltage similar to that of the source. An alternative Einzel lens arrangement is to have a much larger voltage on the second plate with opposite polarity to that of the source. This provides the potential advantage of a narrower ion beam than in the decel-accel mode.

SAI engineers found that it was possible to rearrange the original Einzel lens arrangement from a decel-accel mode to an accel-decel lens. With the provision of a separate, high-voltage power supply (see Figure 3.4), the instrument could be operated in either lens mode. When running with the high-voltage (accel-decel) lens, mass spectral responses were found to be enhanced by a factor of $\sim 3\times$. However, mass spectral peaks were broader with the high-voltage lens arrangement. Mass spectral m/z values are output as the sum average of peak intensity over an m/z range of

0.5 either side of the peak centroid. The broader peaks, produced with the high-voltage lens, led to individual m/z peaks overlapping with the integration range of neighbouring peaks especially when high-intensity ions were detected. This led to sharp spikes in the signal of many ions. Therefore, at the engineer's recommendation, the high-voltage lens was abandoned in favour of the more stable, though less sensitive, decel-accel lens arrangement.

3.3.1.3 Other alterations and repairs

In addition to the major upgrades and experimental modes of operation mentioned in Sections 3.3.1.1 and 3.3.1.2, faults were identified with the detector and push/pull signal board. These faults were corrected with a modification to the detector and a replacement push/pull circuit board to replace the original prototype. No improvement was made to sensitivity etc., as a result of these changes and the instrument was considered operationally normal.

Additionally, a number of replacements and repairs had to be undertaken including the installation of a new source housing, replacement source cartridge heaters, source parts, several filaments including new filament designs, ceramic spacers, re-soldering of joints and replacement of wiring inside the mass spectrometer. Several software upgrades were also applied in response to software bugs and usability issues. These replacements, upgrades and repairs all delayed the development of the GC-TOF instrument for use in routine measurements.

3.4 Instrument characterisation

3.4.1 Manual analysis method

Routine analysis of whole-air samples on the GC-TOF system was carried out using the manual inlet system described in Section 3.1. The following method represents a typical analysis. Deviations from the method are noted where necessary. Accurately measured samples (~ 750 mL) were dried with a magnesium perchlorate (MPC) moisture trap at a flow rate of 100 mL min^{-1} prior to pre-concentration on an 1/8 inch HayeSep D, 80/100 mesh (Valco) at -72°C and thermally desorbed at 100°C for 15 min using boiling water. Chromatographic separation was achieved using an Agilent J&W GS-GasPro column ($60 \text{ m} \times 320 \mu\text{m OD}$) using research grade helium ($\geq 99.9995\%$ purity) as the carrier gas and by temperature programmed gas chromatography (-10°C hold for 2 min, $15^\circ\text{C min}^{-1}$ to 200°C hold 9 min, $120^\circ\text{C min}^{-1}$ to 230°C hold for 8 min) at a constant flow rate of 1.5 mL min^{-1} . The column eluent was subjected to electron impact ionisation prior to detection by the time-of-flight (TOF) mass spectrometer. Mass spectra were acquired at a rate of 30 kHz averaged to 2 spectra s^{-1} .

In order to assign mixing ratios and uncertainties to analytes, air samples were run against a working standard of known composition. Samples were bracketed between repeat runs of standards with a maximum of three samples between repeats. Two standards were run at the beginning of an analysis set to account for the rapid drift in sensitivity that occurs after the instrument had been powered on (see Section 3.4.5). Analytical uncertainties, unless otherwise stated, are calculated on a per run basis and are the 1σ standard deviation of the working standard, corrected for drift by linear interpolation of the nearest two standards, on the respective measurement day.

3.4.2 Compound identification

The main advantage of the time-of-flight instrument, from the perspective of routine atmospheric trace gas measurements, is the ability to simultaneously measure multiple compounds without the accompanying loss in sensitivity usually encountered in quadrupole instruments. For instance, in a quadrupole instrument, analysis of halocarbons would usually entail the exclusion of most hydrocarbons due to the limitations of ion-window selection in single ion mode (SIM) or reduced sensitivity in scan mode. The large range of masses measured allows many co-eluting compounds to be identified and deconvolved from each other in order to be quantified. The number of identifiable and quantifiable compounds can be greatly improved by the use of a GC×GC system (e.g. Hamilton, 2010).

Table 3.1 shows a list of compounds identified in a GC-TOF chromatogram. The list is not exhaustive, as many compounds, such as long-chain hydrocarbons with a large number of isomers, are difficult to identify based on fragmentation pattern and retention time alone. Furthermore, in order to positively identify these compounds it is necessary to compare chromatograms with known standards or pure compounds. However, this table of compounds gives an indication of the range of compounds identifiable, and potentially quantifiable, with a GC-TOF system. Figure 3.5 shows an example chromatogram with some of the compounds identified in Table 3.1. Note that traces for individual masses extend across the whole chromatogram rather than being limited to individual ion windows. Figure 3.6 shows example spectra for CFC-115 and H-1211 produced by the TOF GC-MS.

All retention times in Table 3.1 are derived from the method given in Section 3.4.1. The sample was ~750 ml of real-air, collected from the roof of the School of Environmental Studies building at the University of East Anglia. The full mass range of the GC-TOF system is m/z 14–460 however, masses up to m/z ~45 are gated off to protect the detector from high mixing ratio air components such as N_2 and CO_2 . Therefore, the most intense ion detected by the TOF MS is not always the most intense ion found in the equivalent EI chromatogram. For example, a large number hydrocarbons have significant ions at $m/z < 50$ which may not be as intense in the GC-TOF spectrum. Coupled with the possibility that co-eluting or closely eluting compounds may have similar ion fragments, the primary ion used for quantification of a compound is frequently not the most intense ion. For most compounds, the best ion for quantification is determined by a balance of best reproducibility and interferences from compounds that are chromatographically close to the analyte. Therefore, after identification of compounds using the full range of ions detected by the TOF detector, one or two ions were selected for quantification of each compound, following the criteria given.

3.4.3 Reproducibility

The reproducibility is an important component in the characterisation of a system and the precision of a measurement. The reproducibility of the GC-TOF was assessed using a real-air stainless steel bottle sample collected from the roof of the School of Environmental Sciences, University of East Anglia filled to a pressure of ~60 bar. The reproducibility is $\pm 1 \sigma$ standard deviation from the mean of a drift-corrected run of 12 standards during one day of analysis. The first two samples of the run were rejected due to exponential drift at the beginning of the run as discussed further in Section 3.4.5. All samples were analysed using the manual inlet system described in Section 3.1

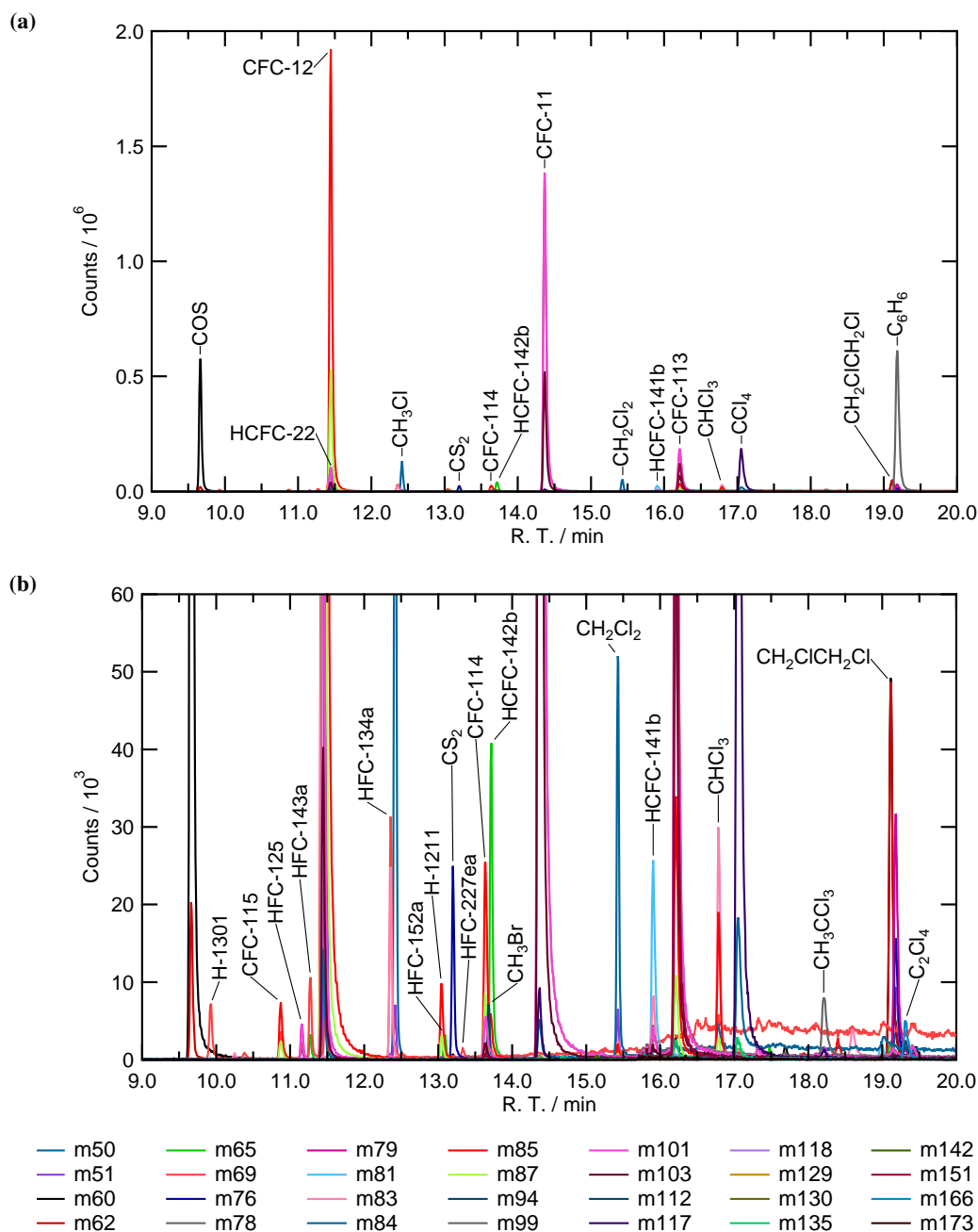


Figure 3.5: A typical gas chromatogram from the TOF GC-MS highlighting a number of identified compounds (also see Table 3.1). (a) shows some of the compounds with higher responses, (b) shows an expanded view of the chromatogram highlighting some of the lower response compounds.

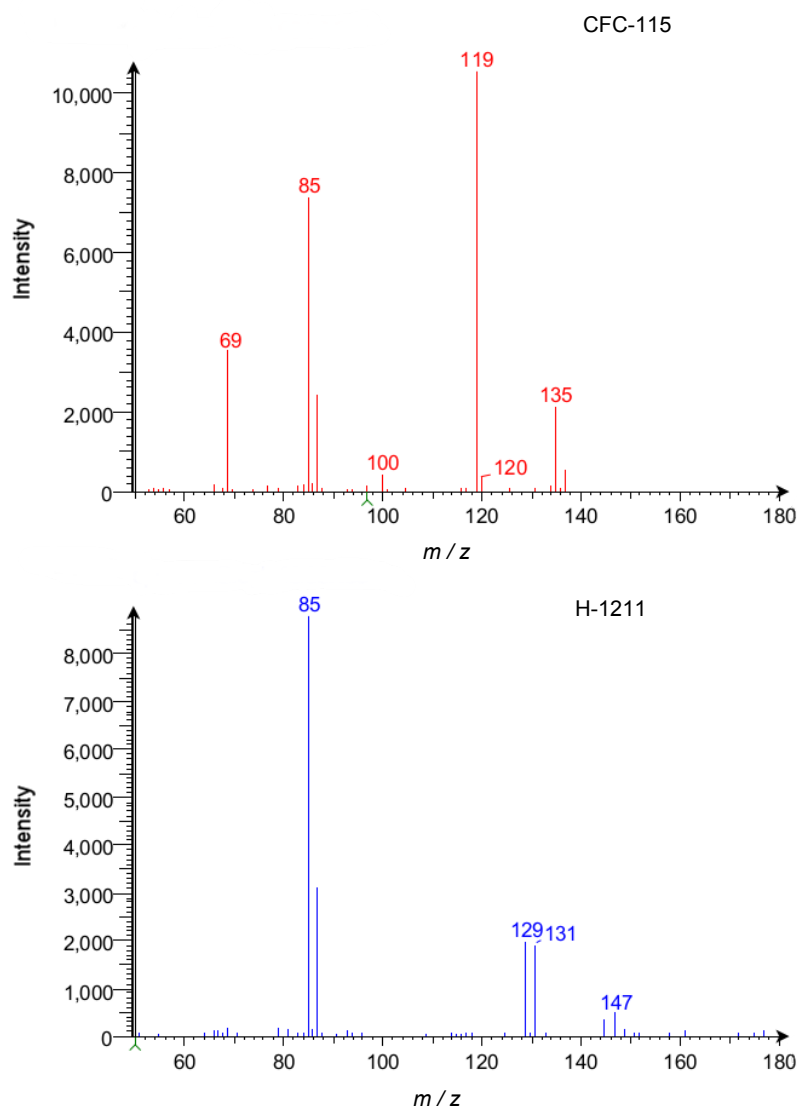


Figure 3.6: Example mass spectra for CFC-115 (top) and H-1211 (bottom). Signal intensity is given in ion counts.

and the analysis method in Section 3.4.1. Manual inlet systems tend to give better reproducibilities than commercially available automated trapping methods, such as the UNITY2TM and Online Air Server (Markes International Ltd.). These techniques rely on mass flow controllers to regulate flow and trapping volume, and are difficult to calibrate. Therefore, it is preferable to use a manual inlet system for system characterisation as this minimises potential effects on reproducibility from the inlet system. Best reproducibilities (dependent on the ion analysed) for compounds with a known mixing ratio in the standard are shown in Table 3.1. The mean reproducibility, across all of the compounds with given reproducibilities in Table 3.1, is 3.9%. It is possible that this represents the upper limit achievable with the TOF GC-MS. Time constraints limit the number of manual samples analysable in a day. Hence, sensitivity has not had time to settle in to a minimal drift regime where reproducibility would ideally be measured.

In order to more thoroughly characterise the performance of the TOF with respect to reproducibility, a number of compounds were assessed over a range of m/z values. Figure 3.7a shows the distribution of m/z values across the range of retention times analysed. Using the

reproducibility data for these compounds, the TOF system was assessed for the mass dependency, retention time dependency and signal-to-noise ratio dependency of system reproducibility.

3.4.4 Mass dependency

Some aspects of the TOF system, especially the detector and the push/pull slicing voltages, might introduce a mass dependent non-linearity to the mass spectrometer. It has been observed, though not verified, that very low masses, i.e. $m/z < 30$, show a greater response than would be expected. This is especially evident when minimizing the response of m/z 18 and 28 relative to m/z 69 in the internal MS PFTBA (Perfluorotributylamine) standard during leak checking. A standard quadrupole instrument will give a relative response on m/z 18 of $\sim 1\%$ when leak tight. However, the TOF system gives a minimum response of $\sim 50\%$ relative to m/z 69 of PFTBA. It is uncertain whether this is a genuine characteristic of the instrument or an issue with contamination giving interferences with masses such as m/z 18 and 28. Assessing the reproducibility across a range of m/z values, as shown in Figure 3.7b, shows no obvious trend in reproducibility with m/z . A least squares linear fit gives a gradient close to zero and an R^2 of 0.013 indicating a poor fit to the data. Therefore, over the range of masses measured (limited to > 50 by the gating of lower masses as described in Section 3.4.2) there does not appear to be a mass dependent effect on reproducibility. In addition, as masses are unevenly distributed across the range of retention times (Figure 3.7a), it might be expected that reproducibility would have a trend with retention time. However, Figure 3.8a shows that reproducibility shows no trend or pattern of reproducibility with retention time.

3.4.4.1 Signal-to-noise dependency

The reproducibility of the system would be expected to improve (i.e. decrease in value) with increasing signal-to-noise ratio. Figure 3.7c shows a negative trend with increasing root-mean-square signal-to-noise ratio (RMS-S/N) and supports the expected behaviour. The masses in Figure 3.7c have been grouped into low (m/z 40–70), medium (m/z 71–100) and high (m/z 101–180) mass ranges. Each group of masses shows a similar trend with increasing RMS S/N. This supports the assertion that there is no mass-dependent effect on reproducibility (Section 3.4.4).

Reproducibility would be expected to have a negative trend with compound mixing ratio. This is due to mixing ratio, in general, indicating the response in an EI GC-MS system. This is, of course, dependent on a number of factors such as fragmentation pattern. Figure 3.8b shows that the TOF reproducibilities have a decreasing trend with increasing mixing ratio. In order to incorporate the RMS S/N with the influence of mixing ratio, reproducibility can be plotted against the limit-of-detection (LOD) of a compound. LOD is the limit at which a compound gas chromatogram peak can be distinguished from baseline noise. This is commonly defined as three times the noise in the region of the peak. LODs in this study were calculated as in Equation 3.1 where MR is the mixing ratio and RMS is the root-mean-square signal-to-noise ratio of the compound.

$$LOD = 3 \times \frac{MR}{RMS} \quad (3.1)$$

Figure 3.8c shows reproducibility plotted against the compound dependent limit-of-detection

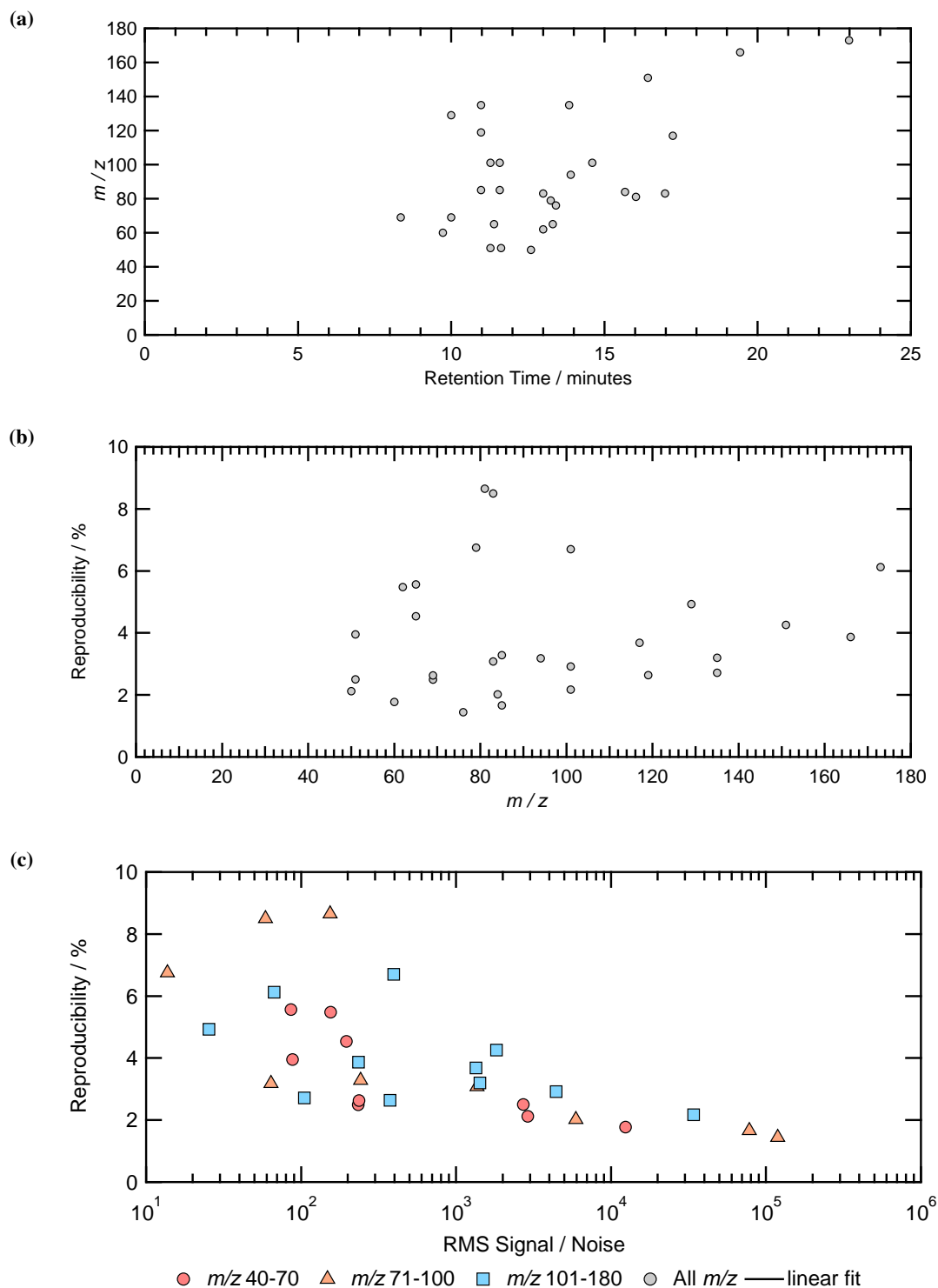


Figure 3.7: (a) Mass-to-charge ratio (m/z) plotted against retention time, (b) compound dependent reproducibilities plotted against the mass-to-charge ratio (m/z) of the ion used for integration and a linear least squares fit to the data and (c) compound dependent reproducibilities plotted against the root-mean-square (RMS) signal-to-noise ratio of the compound analysed (separated in to low, medium and high m/z groups.)

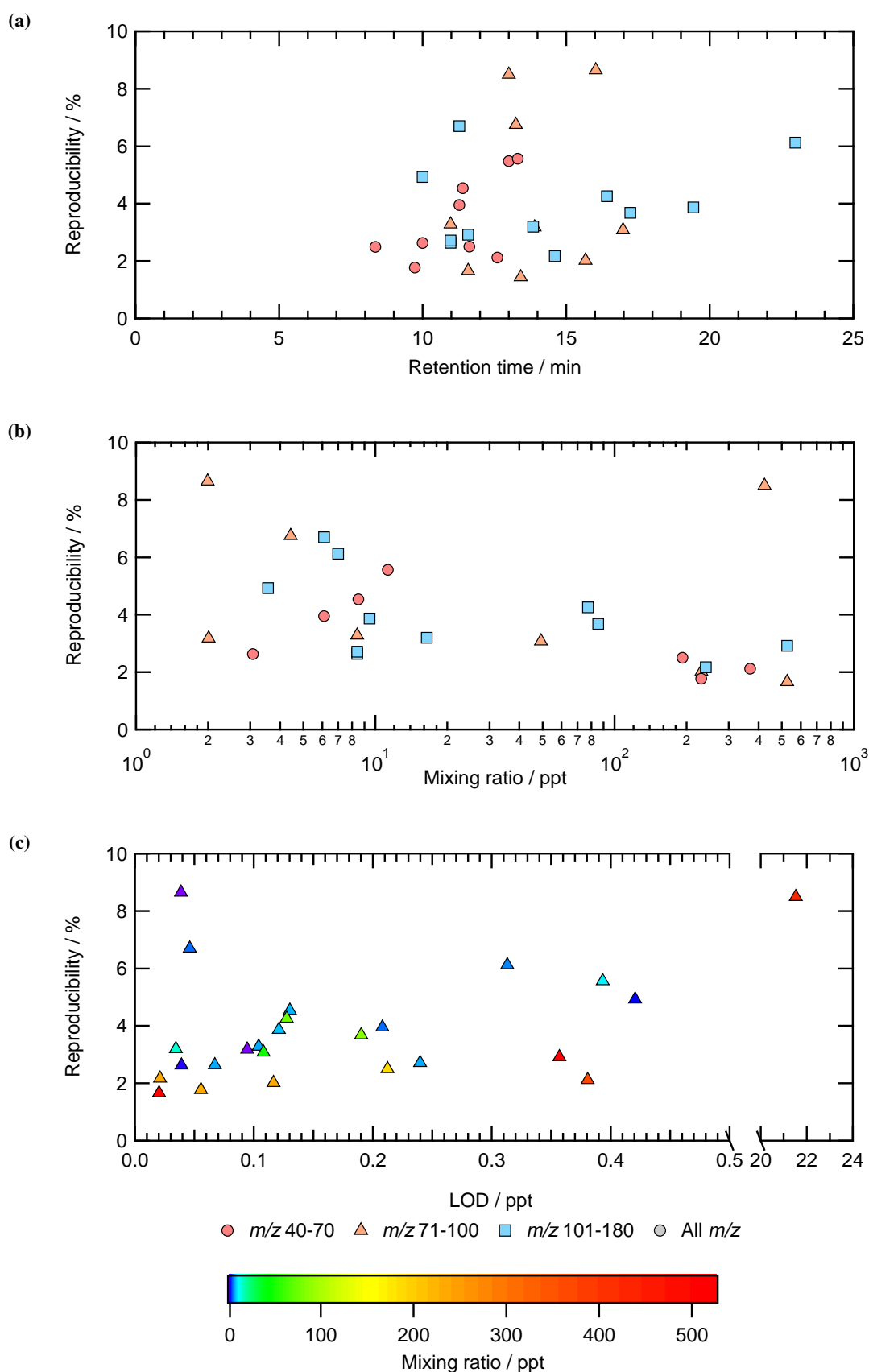


Figure 3.8: Compound dependent reproducibilities for the GC-TOF system plotted against (a) the retention time of the compound analysed and (b) the mixing ratio of compounds with known mixing ratio, with data points separated into low, medium and high m/z groups. (c) Shows compound dependent reproducibilities plotted against the limit-of-detection (LOD) coloured by mixing ratio.

Table 3.1: List of compounds identified using the GC-TOF system, retention times (R.T.), the major ions used for identification. Reproducibilities and limits-of-detection (LODs) for selected compounds are also given (see Section 3.4.3). The listed ions are the primary (1°) ion used for quantification and the secondary (2°) and tertiary (3°) ions used for validating identification. It should be noted that, for identification of most trace gases, all other ions are potentially available due to the nature of TOF MS analysis.

Compound	Formula	R.T. [min]	Reproducibility [%]	LOD [ppt]	Major Ions		
					1°	2°	3°
Carbonyl sulfide	COS	9.73	1.8	0.056	60	62	-
Halon 1301	CBrF ₃	9.92	2.6	0.42	69	129	131
HFC-32	CH ₂ F ₂	10.05	-	-	51	52	-
CFC-115	C ₂ ClF ₅	10.87	2.7	0.24	135	119	85
HFC-125	C ₂ HF ₅	11.48	4.0	0.21	51	101	69
HFC-143a	CH ₃ CF ₃	11.28	4.5	0.13	65	69	51
CFC-12	CCl ₂ F ₂	11.58	1.7	0.02	85	87	101
HCFC-22	CHClF ₂	11.63	2.5	0.21	51	67	69
<i>i</i> -Butane	CH ₃ CH(CH ₃) ₂	12.36	-	-	57	58	-
Methyl chloride	CH ₃ Cl	12.60	2.1	0.38	50	52	-
<i>n</i> -Butane	C ₄ H ₁₀	12.69	-	-	58	57	-
HFC-134a	CH ₂ FCF ₃	12.36	8.5	21.5	83	69	51
Chloroethene	C ₂ H ₃ Cl	12.80	-	-	62	64	-
Halon 1211	CF ₂ BrCl	13.04	6.8	0.97	79	85	129
Carbon disulfide	CS ₂	13.19	-	-	76	78	-
HFC-227ea	CF ₃ CHFCF ₃	13.45	-	-	151	82	69
CFC-114	C ₂ Cl ₂ F ₄	13.63	3.2	0.034	135	137	85
HCFC-142b	CH ₃ CClF ₂	13.72	-	-	65	85	87

Continued on next page ...

Table 3.1: *Continued from previous page.*

Compound	Formula	R.T. [min]	Reproducibility [%]	LOD [ppt]	Major Ions		
					1°	2°	3°
Methyl bromide	CH ₃ Br	13.67	3.2	0.094	94	96	79
HFC-152a	CH ₃ CHF ₂	13.71	5.6	0.4	65	51	47
CFC-11	CCl ₃ F	14.36	2.2	0.021	101	103	105
HCFC-133a	CH ₂ ClCF ₃	14.82	-	-	118	120	99
Methyl iodide	CH ₃ I	15.14	-	-	142	127	-
Dichloromethane	CH ₂ Cl ₂	15.43	2.0	0.12	84	86	49
HCFC-141b	CH ₃ Cl ₂ F	15.92	8.7	0.039	81	61	101
Isoprene	CH ₂ C(CH ₃)CHCH ₂	16.37	-	-	67	68	53
CFC-113	C ₂ Cl ₃ F ₃	16.21	4.3	0.13	151	153	101
Chloroform	CHCl ₃	16.79	3.1	0.11	83	85	87
Carbon tetrachloride	CCl ₄	17.05	3.7	0.19	117	119	82
Ethyl iodide	C ₂ H ₅ I	17.64	-	-	156	127	-
Trichloroethene (TCE)	C ₂ HCl ₃	17.68	-	-	130	132	95
Methylchloroform	CH ₃ CCl ₃	18.37	-	-	99	97	61
1,2-Dichloroethane	CH ₂ ClCH ₂ Cl	19.11	-	-	62	64	-
Benzene	C ₆ H ₆	19.18	-	-	78	77	51
Perchloroethene (PCE)	C ₂ Cl ₄	19.30	3.9	0.12	166	164	129
Bromoform	CHBr ₃	22.88	6.1	0.31	173	171	175
Toluene	C ₇ H ₈	23.29	-	-	91	92	-
Chlorobenzene	C ₆ H ₅ Cl	23.67	-	-	112	114	77

coloured by the mixing ratio of the analyte. There is no distinct trend in reproducibility with LOD though reproducibility would be expected to improve (i.e. decrease) at lower detection limits. There is a large degree of scatter in the data due to the large range of mixing ratios of analysed compounds. However, if the two high values at an LOD of <0.05 ppt are removed, reproducibilities increase with higher LOD as expected. These two data points are for halon 1211 and carbonyl sulfide (COS). These two compounds are among the earliest eluting compounds on the Gas-Pro column. This implies that the higher than expected reproducibilities of these compounds is likely due to chromatography. It is possible that CO_2 is affecting these early eluting compounds as they are chromatographically close to CO_2 . This might indicate that ionisation processes are affected by high concentrations of some compounds. LOD calculations are limited to the compounds with known mixing ratios in the standard. A larger number of calibrated compounds would improve interpretation of the system reproducibility.

3.4.5 Sensitivity drift

The sensitivity of the GC-TOF system drifts over the course of a day of measurements. Figure 3.9 shows examples of the drift in sensitivity of six compounds from repeat measurements of ~ 1 L real-air samples from a stainless steel high pressure canister following the method outlined in Section 3.4.1. In general, for compounds with peak areas on the order of 10^6 counts e.g. CFC-12 and CFC-11 (Figures 3.9a and 3.9b), sensitivity drops rapidly over the first two samples then steadily improves over the course of a day of sampling. For compounds with smaller peak areas, approximately 10^3 counts, the pattern is more variable. However, there is an overall improvement in sensitivity throughout the day as shown in Figures 3.9c to 3.9f. This is typical of the instrument drift, and is unusual, compared to quadrupole and sector instruments used in atmospheric analysis, which tend to decrease in sensitivity throughout the day. It is likely that decreasing sensitivity would also be the case for the TOF GC-MS if analysis runs were longer.

As the first two samples have an exponential drop in sensitivity for some compounds, the first two standards of a run are discarded so that sampling is only undertaken during a period of less rapidly changing sensitivity where drift corrections can be applied. This behaviour is frequently seen in EI mass spectrometers and discarding the first one or two standards is a common practice.

Due to the manual nature of the pre-concentration and sample injection processes, it is not possible to run the instrument for an extended continuous period. Therefore, the long-term sensitivity drift of the instrument has not been assessed in this study. However, the TOF-MS tune parameters, i.e. source voltage, extraction voltage, steering voltages etc., appear to be stable over periods of weeks to months with manual retuning providing no improvement to sensitivity over these time-scales. This implies that sensitivity is stable over relatively long periods assuming no component wear or failure.

3.4.6 Linearity

Ideally a GC-MS system would have a linear response to injected sample mixing ratio. A number of factors may introduce non-linearities into the MS system. In general, at the higher concentration end of a calibration line, 'deviations' from linearity arise from the effect of sample molecules no longer acting independently from each other. For instance, a space charge effect related to the absolute number of ions in an ion source can act to decrease the expected signal. Additionally, in

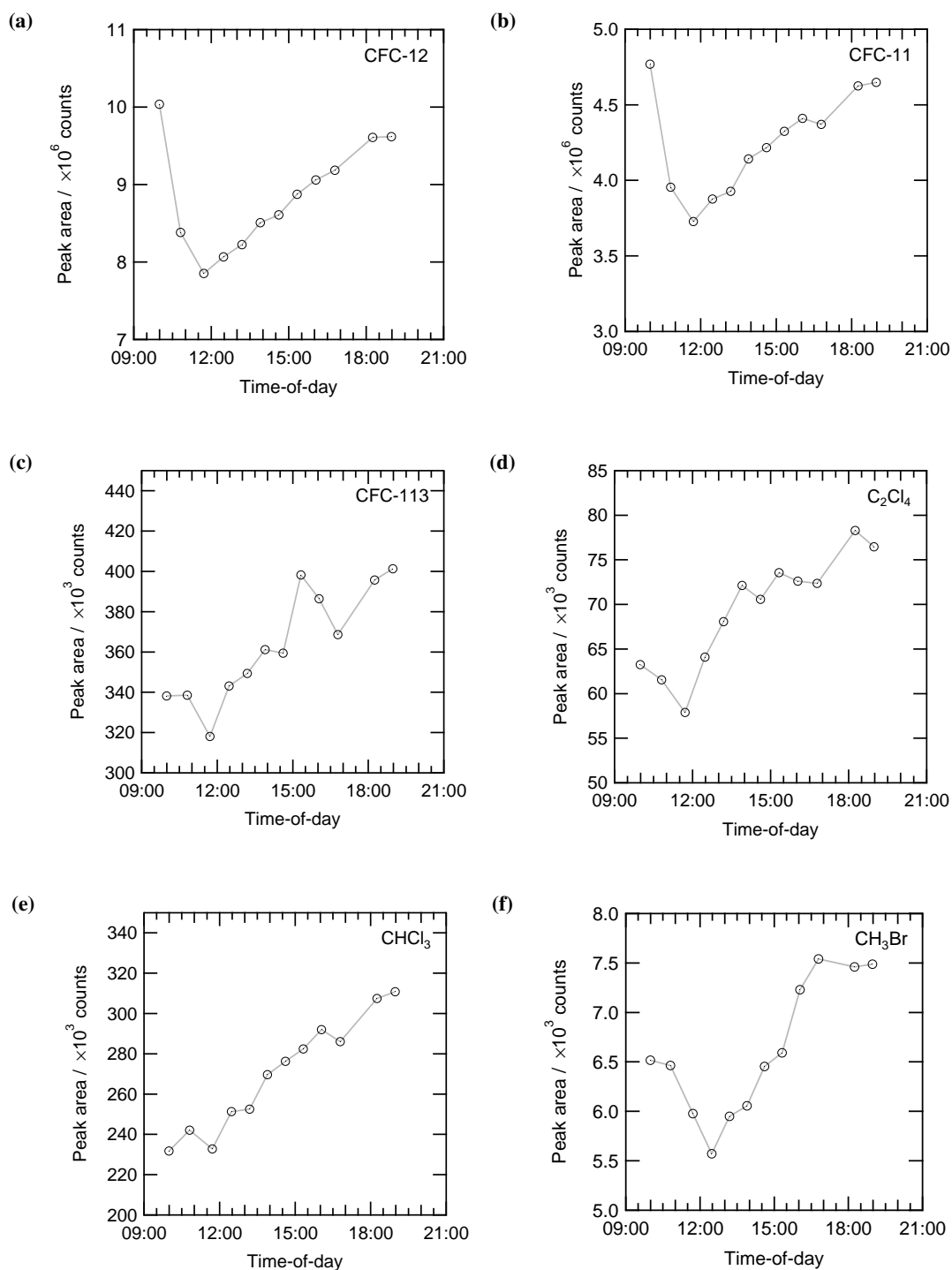


Figure 3.9: Peak area responses plotted against time for repeat standards analysed over one day for (a) CFC-12, (b) CFC-11, (c) CFC-113, (d) C_2Cl_4 (PCE), (e) $CHCl_3$ and (f) CH_3Br .

absorption-based sample pre-concentration systems, commonly utilised in GC-MS systems and the GC-TOF system, trapping may not be quantitative for high mixing ratio compounds and some compounds may not be quantitatively desorbed from the pre-concentration trap.

At the lower end of a calibration line, deviations are usually attributed to unspecified sample losses. These losses are usually assumed to occur in the GC column or the inlet system. Losses could occur on mass spectrometer components, however, as these parts usually involve ions

under vacuum, far removed from active adsorption sites, losses are usually limited to the sample introduction and ionisation source components.

In order to assess the linearity of response of the TOF instrument, it was necessary to create a calibration curve covering a range of sample quantities. For this study a volume series of real air samples, from a stainless steel high pressure canister, was analysed using the method described in Section 3.4.1. Two separate analyses were run approximately one month apart (see Figure 3.10). The first analysis (run #1 in Figure 3.10) consisted of accurately measured volumes at 66, 83, 100, 117, 133 and 150 % of a 750 mL sample. The second analysis (run #2 in Figure 3.10) consisted of accurately measured volumes at 33, 67, 100, 133 and 167 % of a 750 mL sample. The volume series was interspersed with ‘standard’ samples of ~ 750 mL for the purposes of drift correction. A volume of 750 mL had been previously determined, on other GC-MS systems with a similar manual HayeSep D injection set-up, to be an appropriate balance between increased sensitivity and CO₂ trapping (J. Laube, personal communication). Analytical errors for the first analysis were determined as the precision of the ‘standard’ samples. In order to better assess the effect of precision at low sample volumes, where precision would be assumed to be worse than at higher volumes, a repeat of the smallest (33 %) sample was performed during the second run. Therefore, analytical errors for the second run were determined as the root-mean-square sum of the ‘standard’ precision and the 1σ standard deviation of the mean of a repeat of the smallest (33 %) sample.

Peak area responses for selected compounds in the volume series and the ‘standard’ were ratioed to the volume injected to provide the response per mL for each compound. In theory, for a linear system, the response per unit volume should be invariant with sample volume or concentration. These ‘volume-corrected’ responses were then ratioed to a linear interpolation of the response per mL for the ‘standard’ samples. This gives the drift-corrected, and normalised relative response to the standard for volume series samples as presented in Figure 3.10. A number of compounds were analysed for linearity i.e. those with reproducibility and LOD data in Table 3.1. The compounds in Figure 3.10 have been selected to span a range of mixing ratios in the analysed air sample: CFC-12 (529 ppt), CFC-11 (241 ppt), CFC-113 (77 ppt), CHCl₃ (49 ppt), PCE (9.5 ppt) and CH₃Br (2.0 ppt).

In an idealised linear system the normalised fractional responses should all lie on the $y = 1$ line in Figure 3.10. Of the species shown in Figure 3.10, CFC-113 and CHCl₃ show a behaviour during run #1 that could be considered linear within the errors. However, the repeat run #2 does not reproduce this. For most compounds, the lowest volume samples analysed, at 33–67 % (~ 250 – 500 mL), have a negative deviation from the $y = 1$ line. Figure 3.10 also shows that there is a large degree of scatter in the data e.g. CFC-113, CHCl₃ and CH₃Br. Across the majority of compounds, deviation from the ideal response is within ~ 10 %.

A negative deviation from the idealised $y = 1$ line is usually attributed to loss of compound on surfaces in the inlet, GC or MS system and would suggest that sample volumes should be no less than ~ 750 mL. However, it is not clear, given the large degree of scatter, whether trapping of high mixing ratio components, such as CO₂ or H₂O, is affecting linearity at higher trapping volumes. It is not clear, from Figure 3.10, whether analyte mixing ratio alone is affecting linearity, or if the non-linearities in the system arise from a combination of factors. CFC-12 (Figure 3.10a) has the highest mixing ratio of compounds in Figure 3.10. PCE has a mixing ratio approximately $1/50$ of CFC-12 and shows a similar pattern of normalised relative response with sample volume.

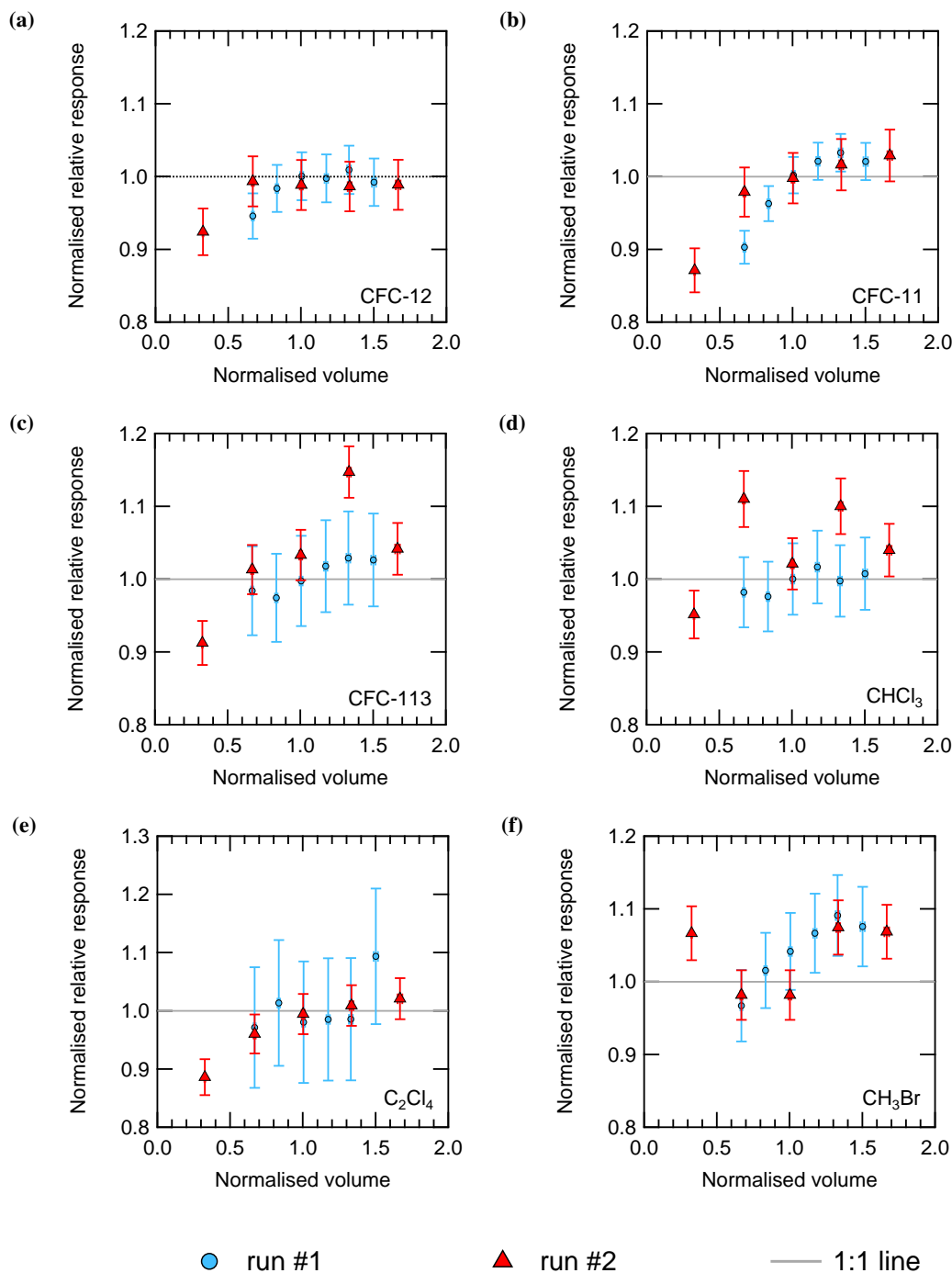


Figure 3.10: Normalised relative responses plotted against normalised sample volumes for two volume series analysed ~1 month apart for (a) CFC-12, (b) CFC-11, (c) CFC-113, (e) C_2Cl_4 (PCE), (d) CHCl_3 and (f) CH_3Br . Error bars represent the analytical uncertainties.

However, CFC-113, CHCl_3 and CH_3Br do not show a similar pattern despite the range of mixing ratios these compounds cover. As discussed above, high concentration components can introduce space charge effects in the ion source. Additionally, compounds such as CO_2 can effect the ionisation patterns of compounds in the ion source. Further investigation is required in order to fully assess the linearity of the TOF MS system. For instance, analysis of a dilution series alongside the volume series would aid the disentanglement of concentration and sample volume effects. A dilution series normally consists of a real air sample accurately diluted to a number of dilutions with a pure gas e.g. research grade nitrogen. A dilution series was not available for analysis on the TOF MS during the period of instrument characterisation. As the linearity tests indicate that the largest deviations occur at low sample volumes, a preliminary comparison was made between the TOF MS and quadrupole MS instruments using ~ 750 mL samples on the TOF GC-MS.

3.5 Preliminary comparison

In order to assess the performance of an instrument under realistic atmospheric analysis conditions it is common practice to make a comparison to an existing and well characterised instrument. In the case of the TOF MS, the most suitable comparison would be to a quadrupole MS analyser as this is the type of ‘workhorse’ instrument that the TOF was intended to replace. Ideally, for an in-the-field instrument, a comparison would be made between in situ measurements made at the same time with separate instruments. Alternatively, a comparison can be made on a set of bottle samples collected at the same time as in situ analysis by the comparison instrument. This method of comparison is not ideal as it does not compare instruments under comparable sampling conditions.

Due to the poor reliability of the TOF MS instrument, it was not possible to make in situ measurements during a field campaign. A comparison on the same set of bottle samples was not possible as suitable comparison instruments were not available for the analysis. Therefore, the TOF MS was used to analyse bottle samples collected during the ClearfLo campaign in London, UK during 2012. These results were compared to in situ measurements made with a dual negative ion chemical ionisation/electron ionisation gas chromatography-mass spectrometry (NICI/EI GC-MS) technique.

3.5.1 The ClearfLo Project

The ClearfLo (Clean Air for London) Project was a collaborative scientific project to investigate boundary layer pollution across London. The project consisted of measurements made at sites within central London and at three rural sites (Figure 3.11). Long-term measurements were made across several sites within London (Marylebone Road, BT Tower, KCL Strand, RGS, NGT, NTT and NDT in Figure 3.11) and the three rural sites from January 2010. Two intensive observation periods (IOPs) were carried out during winter (6th January to 11th February) and summer (21st July to 23rd August) 2012. Extra instrumentation was deployed within London at Sion Manning School, Marylebone Road and the BT Tower. The main aims of ClearfLo were to assess particulate and gaseous chemistry and their interaction with surface meteorology such as boundary layer effects and sea breezes in the urban environment.

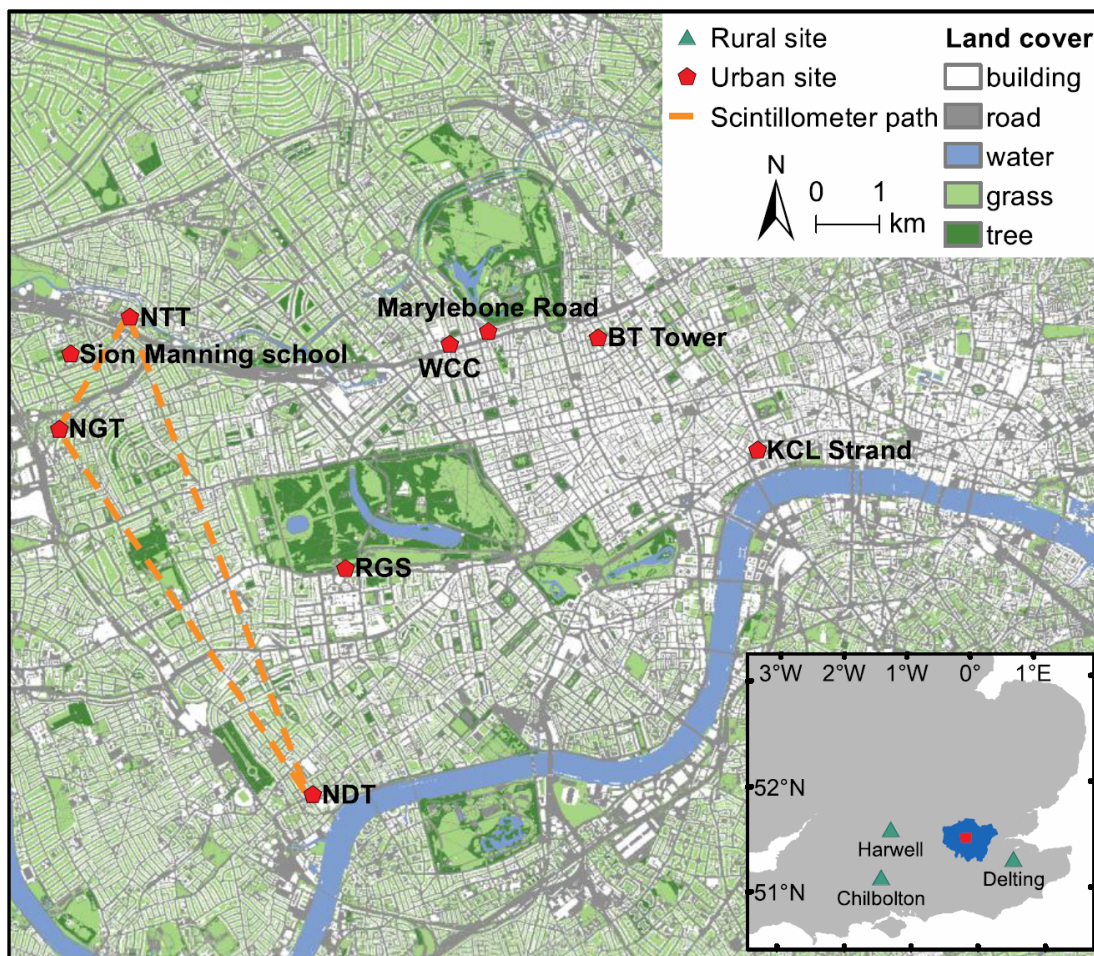


Figure 3.11: Locations of ClearfLo measurement sites. Urban observations were made at several locations in central London (main map). Measurements were also undertaken at three rural locations (see inset). UEA measurements were undertaken at the Sion Manning school site at the middle left of the main map. Image courtesy of Bohnenstengel et al. (2014).

Measurements were made by the University of East Anglia (UEA) during both the winter and summer IOPs at the Sion Manning school site in North Kensington, London (Figure 3.11).

3.5.2 Analysis and supporting measurements

In situ measurements were made with a dual mass spectrometer system with two quadrupole MS analysers running negative chemical ionisation (NICI) and EI in parallel. The GC-dual MS (Agilent Technologies GC 6890/MS 5973N/MS 5973N) was coupled to a thermal desorption pre-concentrator (UNITY2TM and Online Air Server; Markes International Ltd.) similar to that described in Worton et al. (2008) and Chapter 4, Section 4.2. The dual MS system has the advantages that NICI provides an improved response to compounds containing bromine and iodine atoms and to the alkyl nitrates. This is combined with the detection in EI of species that NICI is insensitive to or that have not been identified in NICI.

3.5.2.1 Dual MS analysis method

Dual MS measurements were made by Dr G. Mills, UEA following the method given below. The dual MS is a relatively new instrument which was itself being assessed for performance in the

field. Accurately measured samples (~ 1200 mL, flow rate ~ 40 mL min $^{-1}$) were sampled from an $1/8$ inch PFA (perfluoroalkoxy alkane) sample line from a $3/8$ inch PFA main air line at continuous flow (15–20 standard L min $^{-1}$) with an inlet ~ 3 m above the ground. Samples were dried with a counterflow nafion drier (PermapureTM, 100 mL min $^{-1}$ counterflow of dry nitrogen) prior to pre-concentration on a packed capillary cold trap at -10 °C and thermally desorbed at a rate > 60 °C s $^{-1}$ to a maximum of 250 °C for 10 min. Chromatographic separation was achieved using an RTX-502.2 capillary column (105 m \times 320 μ m OD, 1.8 μ m film, RestekTM Corporation) using research grade helium (≥ 99.9995 % purity) as the carrier gas and by temperature-programmed gas chromatography (35 °C hold 6 min, 12 °C min $^{-1}$ to 160 °C hold 5 min, 14 °C min $^{-1}$, to 260 °C hold 15 min) with a carrier gas pressure ramp of 31 psi hold 6 min, 1.8 psi min $^{-1}$ to 41 psi. The column eluent was split into two streams and fed into two mass spectral detectors. The column eluent was subjected, in parallel, to negative ion chemical ionisation in the presence of argon gas (research grade, ≥ 99.9995 %) prior to detection by a quadrupole mass selective detector operating in selective ion mode (SIM) monitoring the Cl $^-$ ion (m/z 35) for chlorinated compounds, the Br $^-$ ion (m/z 79, 81) for brominated compounds, the I $^-$ ion (m/z 127) for iodinated compounds and the NO $_2^-$ ion (m/z 46) for alkyl nitrates. Simultaneously, the column eluent was subjected to electron ionisation (EI) prior to detect by a quadrupole mass selective detector operating in single ion mode and monitoring a selection of ions (see Table 3.2).

Mixing ratios were determined by comparison to a real air working standard with known mixing ratios. The working standard was a 34 L electro-polished stainless steel canister filled ~ 3 bar with ambient air at UEA. Mixing ratios of the working standard were determined by comparison to a UEA standard (named “Dave”) with mixing ratios determined by repeat comparison to calibrated gas standards supplied by the Global Monitoring Division of NOAA-ESRL in 34 L electro-polished stainless steel canisters (Essex Cryogenics, St. Louis, MO, US). Gases not calibrated for by NOAA-ESRL are determined by comparison to primary standards made by dilution of pure vapour or liquid with research grade nitrogen. Mixing ratios in these standards are known to be stable over a period of years for many halocarbons (e.g. Hall et al., 2014; Butler et al., 2007, supplemental). These comparisons are performed periodically and allow an assessment of any potential changes in the absolute mixing ratio of halocarbons in our working standard over time. During the field analysis, samples from the standard were analysed after every seven samples. Additionally a carrier gas blank was run once every 24 hours. Analytical uncertainties were calculated as the 1σ standard deviation of four standards, drift-corrected by linear interpolation of the surrounding standards, during a prolonged period of measurement (continuous running of the instrument was occasionally interrupted for maintenance etc.). Estimated limits of detection in parts per trillion (ppt), average compound-dependent analytical precisions, the mixing ratios of the working standard at which the measurements were made and the method (EI or NICI) used for analysis are shown in Table 3.2.

3.5.2.2 TOF analysis method

A number of bottle samples were also collected on site during the summer IOP. Bottle samples were collected in SilcosteelTM-coated or electro-polished stainless steel 3 L bottles pressurised to ~ 3 bar. Bottle samples were analysed at UEA on the TOF-GC system ~ 18 months after collection. The long period between sampling and analysis was due to a number of problems with the TOF

GC-MS which did not allow analysis any earlier than this. Samples were analysed using the method in Section 3.4.1. Mixing ratios were determined by comparison to a working standard with known composition. The working standard was a 34 L electro-polished stainless steel canister (SX706077, Essex Cryogenics, St. Louis MO, US). Long- and short-lived halocarbons are known to be stable in these canisters over a period of years (e.g. Hall et al., 2014; Butler et al., 2007, supplemental). Analytical uncertainties were calculated on a per-run basis and are the root-mean-square sum of the 1σ standard deviation of duplicate samples, drift-corrected to a linear interpolation of the standard, and the 1σ standard deviation of the drift-corrected working standard on the respective run day. Estimated limits of detection (LODs) in parts per trillion (ppt), average compound-dependent analytical precisions and the mixing ratios of the working standard are shown in Table 3.2.

3.5.2.3 Supporting measurements

A number of additional measurements were made at the North Kensington site by UEA and partner institutions. These included OH, HO₂, RO₂, formaldehyde, peroxide, peroxyacetylnitrate (PAN), NO_x, non-methane hydrocarbons (NMHCs), oxygenated volatile organic compounds (oVOCs), numerous particulate measurements and meteorological measurements. See Bohnenstengel et al. (2014) for more details of instrumentation and measurements. Additionally, in order to determine the origin of air arriving at London during the IOP periods, the Met Office Numerical Atmospheric-dispersion Modelling Environment (NAME) model (Jones et al., 2007; Bohnenstengel et al., 2014) was used to track the pathways of air to the ClearfLo sites. A separate set of 12 bottle samples, in addition to those run on the TOF GC-MS, were analysed for a suite of halocarbons by Dr. J. Laube at UEA. The samples were analysed within ~7 months of collection during the ClearfLo summer IOP by GC-MS with a high sensitivity tri-sector mass spectrometer described in detail in Laube et al. (2010).

3.5.3 Comparison to the ClearfLo in situ data

The comparison of TOF MS analysed bottle samples and in situ NICI/EI GC-MS data is limited to a small subset of compounds that are stable over long periods in steel bottles and are calibrated for in both the TOF working standard and the ClearfLo standard. Most long-lived halocarbons, such as CFCs, halons, some chlorocarbons and HCFCs are stable over long periods in steel canisters. Comparisons for CFC-11, CFC-113 and HCFC-141b are shown in Figures 3.12a, 3.12b and 3.12c respectively. Comparisons for CCl₄, halon 1211 and CH₂Cl₂ are shown in Figures 3.13a, 3.13b and 3.13c respectively. Unfortunately, only a subset of bottle samples collected during the campaign were available for analysis and therefore do not span the entire in situ analysis period. Additionally, there are gaps in the in situ data where instrument failure or maintenance required the dual system to be off-line. It should be noted that the fill time for bottle samples is ~2 min whereas the dual MS sampling time is ~30 min. Therefore, the bottle samples represent a spot measurement and the dual MS samples are a time-averaged measurement over the 30 min sampling period.

Values derived from TOF-analysed bottle samples agree well with the in situ data within the errors of both measurements. Table 3.3 shows the mean mixing ratios of the compounds given in Figures 3.12 and 3.13. Mean mixing ratios for the TOF GC-MS analysis are calculated

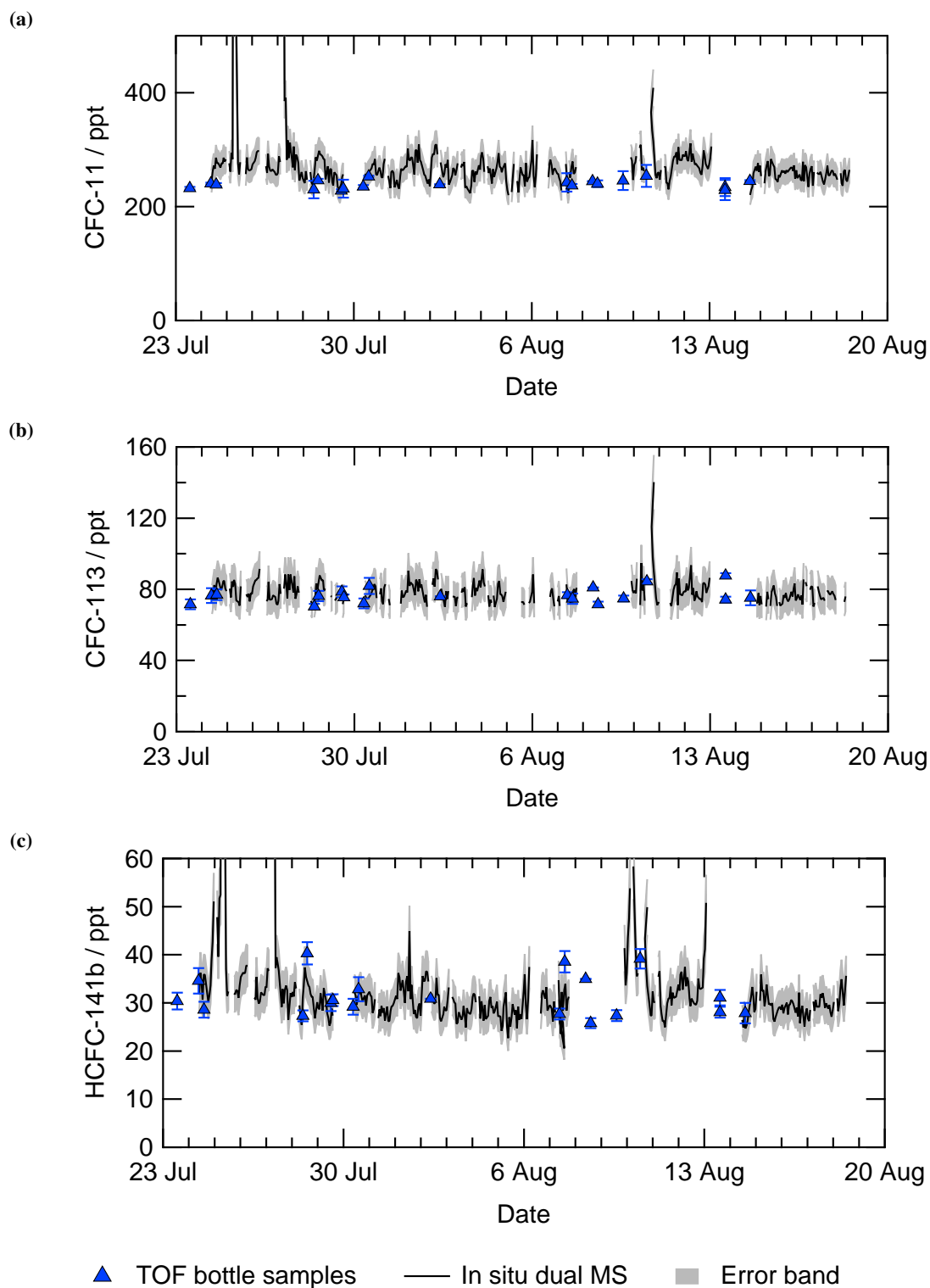


Figure 3.12: Comparison of ClearLo data from bottle samples analysed by TOF GC-MS and in situ dual GC-MS for (a) CFC-11, (b) CFC-113 and (c) HCFC-141b analysed by EI. Analytical errors for the TOF GC-MS data are indicated by error bars. Errors in the in situ data are indicated by the shaded band.

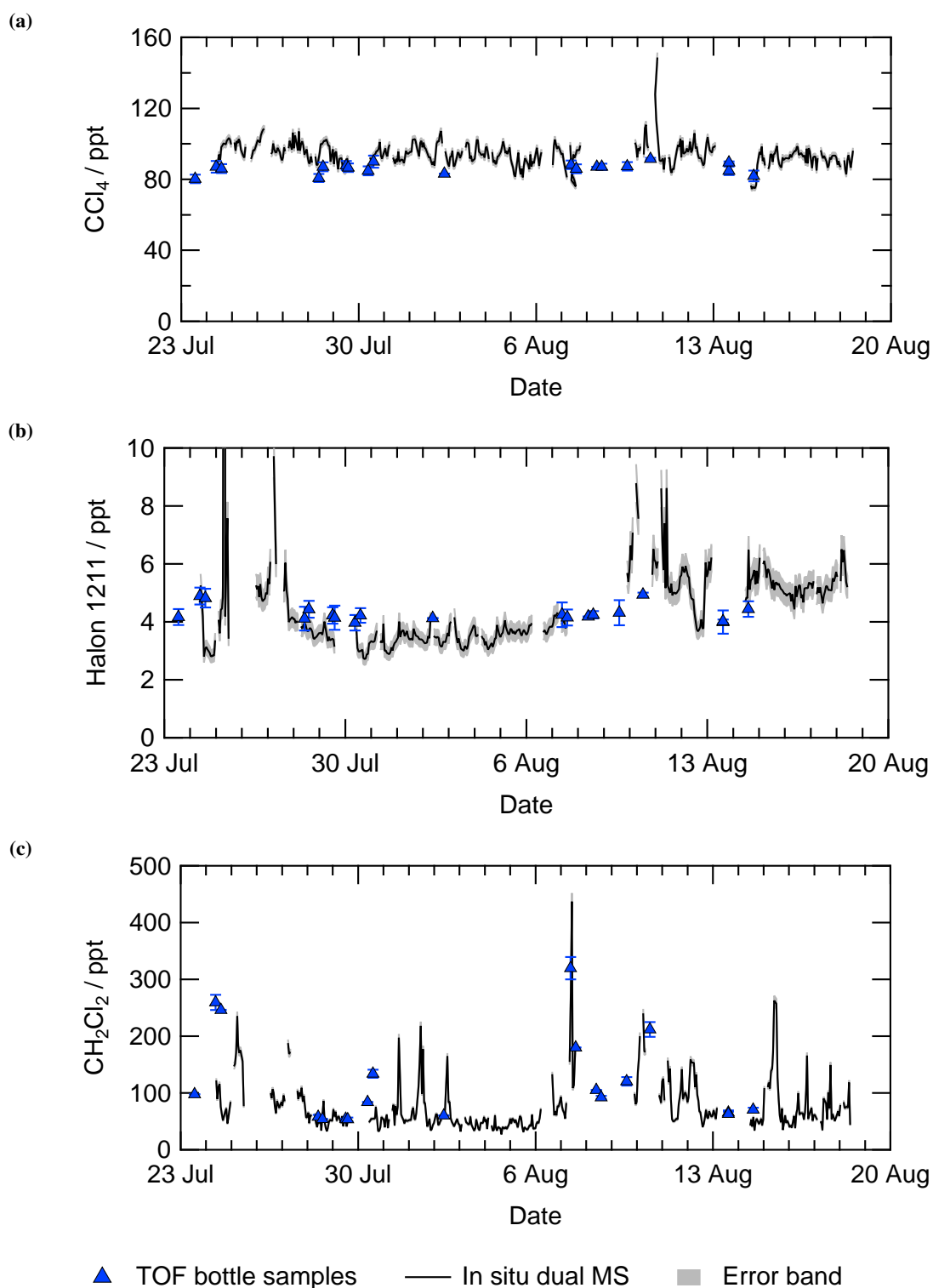


Figure 3.13: Comparison of ClearfLo data from bottle samples analysed by TOF GC-MS and in situ dual GC-MS for (a) CCl_4 , (b) halon 1211 and (c) CH_2Cl_2 . CCl_4 was analysed by EI. Halon 1211 and CH_2Cl_2 were analysed by NICI. Analytical errors for the TOF GC-MS data are indicated by error bars. Errors in the in situ data are indicated by the shaded band.

Table 3.2: List of compounds analysed during ClearLo for the in situ dual EI/NICI GC-MS system and bottle measurements made with the TOF GC-MS. Included are the limit-of-detection (LOD) in parts-per-trillions (ppt), the compound dependent percentage precisions, the mixing ratio (M.R.) in the working standard and the m/z of the ion used for quantification.

Compound	Formula	LOD [ppt]	Precision [%]	M.R. [ppt]	m/z
NICI GC-MS					
<i>Long-lived chloro-carbons</i>					
Carbon tetrachloride	CCl ₄	0.026	0.48	93.1	35
CFC-11	CCl ₃ F	0.026	0.81	521	35
CFC-113	C ₂ ClF ₃	0.058	1.7	64.8	35
Methylchloroform	CH ₃ CCl ₃	0.058	1.4	5.91	35
<i>Long-lived bromo-carbons</i>					
Halon 1202	CBr ₂ F ₂	0.0034	7.4	0.0314	79
Halon 1211	CBrClF ₂	0.011	7.5	4.91	79
Halon 2402	C ₂ Br ₂ F ₄	0.0045	1.4	0.453	79
<i>Short-lived chloro-carbons</i>					
Chloroform	CHCl ₃	0.072	1.2	9.91	35
Dichloromethane	CH ₂ Cl ₂	15	3.4	309	35
Perchloroethene (PCE)	C ₂ Cl ₄	0.016	12	2.80	35
Trichloroethene (TCE)	C ₂ HCl ₃	-	11	-	35
<i>Short-lived bromo-carbons</i>					
Bromochloromethane	CH ₂ BrCl	0.0077	4.1	0.139	79
Bromodichloromethane	CHBrCl ₂	0.0024	1.7	0.269	79

Continued on next page ...

Table 3.2: *Continued from previous page.*

Compound	Formula	LOD [ppt]	Precision [%]	M.R. [ppt]	<i>m/z</i>
Bromoform	CHBr ₃	0.0082	1.7	1.59	79
Dibromochloromethane	CHBr ₂ Cl	0.0025	2.4	0.191	79
Dibromomethane	CH ₂ Br ₂	0.0022	0.64	0.889	79
<i>n</i> -Propylbromide	C ₃ H ₇ Br	-	20	-	79
<i>Short-lived iodo-carbons</i>					
Bromoiodomethane	CH ₂ BrI	-	8.7	-	127
Ethyl iodide	C ₂ H ₅ I	0.0077	4.6	0.043	127
Methyl iodide	CH ₃ I	0.0092	15	1.4	127
<i>i</i> -Propyl iodide	CH ₃ CH ₂ (I)CH ₃	-	4.2	-	127
<i>n</i> -Propyl iodide	C ₃ H ₇ I	-	21	-	127
<i>Alkyl nitrates</i>					
2-Butyl nitrate	CH ₃ CH(ONO ₂)CH ₂ CH ₃	0.026	3.1	4.81	46
<i>n</i> -Butyl nitrate	C ₄ H ₉ ONO ₃	0.045	3.5	1.48	46
Ethyl nitrate	C ₂ H ₅ ONO ₂	0.0045	5.4	2.45	46
2-Methyl-3-butyl nitrate	(CH ₃) ₂ (CH) ₂ (ONO ₂)CH ₃	0.068	3.1	1.49	46
Methyl nitrate	CH ₃ ONO ₂	0.0028	13	1.95	46
2/3-Pentyl nitrate	C ₅ H ₁₁ ONO ₂	1.83	5.1	3.96	46
<i>i</i> -Propyl nitrate	CH ₃ C(ONO ₂)CH ₃	0.0098	4.9	4.82	46
<i>n</i> -Propyl nitrate	C ₃ H ₇ ONO ₂	0.0052	3.7	0.698	46

Continued on next page ...

Table 3.2: *Continued from previous page.*

Compound	Formula	LOD [ppt]	Precision [%]	M.R. [ppt]	<i>m/z</i>
EI GC-MS					
<i>Long-lived chloro-carbons</i>					
Carbon tetrachloride	CCl ₄	0.22	1.8	93.1	117
CFC-11	CCl ₃ F	0.68	7.9	262	101
HCFC-141b	CH ₃ CClF ₂	0.49	12	26.3	81
HCFC-22	CHClF ₂	2.2	6.8	310	67
CFC-113	C ₂ Cl ₃ F ₃	1.2	11	76.7	151
<i>Short-lived chloro-carbons</i>					
Chlorobenzene	C ₆ H ₅ Cl	-	16	-	112
TOF GC-MS					
<i>Long-lived chloro-carbons</i>					
Carbon tetrachloride	CCl ₄	0.055	3.0	91.1	117
CFC-11	CCl ₃ F	0.017	1.7	244.5	101
CFC-113	C ₂ Cl ₃ F ₃	0.055	4.6	78.1	151
CFC-12	CCl ₂ F ₂	0.014	3.0	535.1	85
HCFC-141b	CH ₃ CClF ₂	0.13	6.0	21.5	81
HCFC-22	CHClF ₂	0.11	6.9	206	51
HFC-134	C ₂ H ₂ F ₄	0.19	4.4	54	83
HFC-152a	CH ₃ CHF ₂	0.23	8.2	8.4	65
Methyl chloride	CH ₃ Cl	0.47	5.3	639	50

Continued on next page ...

Table 3.2: Continued from previous page.

Compound	Formula	LOD [ppt]	Precision [%]	M.R. [ppt]	<i>m/z</i>
Methyl chloroform	CH ₃ CCl ₃	0.13	3.6	10.3	99
<i>Long-lived bromo-carbons</i>					
Halon 1211	CBrClF ₂	1.3	6.2	4.3	79
Halon 1301	CBr ₃ F	0.18	10	3.1	129
Methyl bromide	CH ₃ Br	0.11	3.5	8.4	94
<i>Short-lived chloro-carbons</i>					
Dichloromethane	CH ₂ Cl ₂	0.16	4.0	62.3	84
Chloroform	CHCl ₃	0.075	12	11.6	83
Perchloroethene	C ₂ Cl ₄	0.060	4.2	3.7	166
<i>Short-lived bromo-carbons</i>					
Bromoform	CHBr ₃	0.10	7.30	0.68	173
<i>Short-lived iodo-carbons</i>					
Methyl iodide	CH ₃ I	0.0086	15	0.18	142
<i>Hydrocarbons</i>					
Benzene	C ₆ H ₆	-	4.2	-	78
Isoprene	CH ₂ C(CH ₃)CHCH ₂	-	6.9	-	67
<i>Other</i>					
Carbonyl sulfide	COS	0.66	9.1	551	60

from the bottle samples where there is in situ data close to the fill time. In situ means are calculated as a linear interpolation of the two nearest samples either side of the selected bottle sample. Variabilities are given in Table 3.3 as $\pm 1\sigma$ standard deviations of the mean. Within the variabilities, means values agree well for CFC-11, CFC-113, HCFC-141b and CCl_4 . The TOF analysis overestimates halon 1211 and CH_2Cl_2 . CFC-11, CFC-113, HCFC-141b, CCl_4 and halon 1211 are all long-lived compounds with lifetimes of 9.2–85 years (Montzka & Reimann, 2011) and would be expected to be relatively stable in bottle samples over the 18 months between sampling and analysis. CH_2Cl_2 is a short-lived compound with a lifetime of 144 days (Montzka & Reimann, 2011) and would be expected to be less stable in steel bottles. Overestimation of halon 1211 mixing ratios might indicate a calibration issue. Halon 1211 mixing ratios are close to the LOD of the TOF system (LOD of 1.3 ppt, Table 3.2).

Figure 3.13c shows that the TOF instrument can capture, to some extent, the variability in CH_2Cl_2 e.g. the peak during 7th August. However, there is some deviation from the in situ data for instance, at the beginning of the in situ sampling period. This might be explained by variation due to the ~ 18 month period between collection and analysis of bottle samples. Variations in analysed compounds are discussed further in Section 3.6.

There is good agreement between the in situ NICI/EI GC-MS and the TOF GC-MS bottle measurements for selected long-lived species. However, the large time-scale between collection and analysis of the bottle samples as well as the limited coverage of bottle samples during the campaign, means that the TOF GC-MS results are not suitable for further data analysis. Further discussion of results from the ClearfLo campaign will be based on in situ measurements and the 12 bottle samples (separate from those analysed on the TOF GC-MS) analysed on a high sensitivity sector GC-MS (see Section 3.5.2.3).

3.6 ClearfLo Results

The following is a cursory analysis of halocarbon measurements during the summer IOP of ClearfLo. This analysis includes results from the on-site dual MS and bottle measurements made on a high-sensitivity sector instrument by Dr. J. Laube at UEA. As this is a preliminary analysis, comparison to other on-site measurements and measurements made during the winter IOP have not been made. Due to the issues encountered with the TOF GC-MS, it was decided that the main focus for analysis would be the CARIBIC and SAMBBA projects (Chapters 4 and 5). The ClearfLo results and bottle samples were revisited in order to assess the performance of the TOF instrument. This is the main reason for the long gap between sample collection and analysis on the TOF GC-MS. The IOP site was not ideal nor intended for halocarbon sampling, especially for compounds such as HCFCs and HFCs. Possible on-site pollution issues are discussed further in Section 3.6.3.

One of the features of the TOF instrument that made it attractive for analysis of air samples in a polluted environment, such as London, was the possibility of monitoring a large number of compounds simultaneously as a consequence of the large range of ions captured by the TOF. This was not possible at the time of the campaign due to the instrumental problems already discussed. Additionally, measurements of a large range of volatile organic compounds (VOCs), such as hydrocarbons and halocarbons, on the TOF is not as simple as expected. Separating out known

Table 3.3: Table of mean values of ClearfLo bottle samples analysed by TOF GC-MS and in situ data analysed by NICI/EI GC-MS. In situ data are based on a linear interpolation between the two closest samples to the bottle sample. Variabilities are given as $\pm 1\sigma$ standard deviation of the mean. Halon 1211 and CH_2Cl_2 in situ values are from the NICI channel of the dual GC-MS.

Compound	Bottle samples [ppt]	In situ [ppt]
CFC-11	238 ± 6.1	267 ± 18
CFC-113	75 ± 2.4	77 ± 5.7
Halon 1211 [†]	4.4 ± 0.33	3.4 ± 0.37
HCFC-141b	32 ± 4.8	32 ± 3.2
CCl_4	85 ± 2.7	87 ± 2.7
CH_2Cl_2 [†]	131 ± 85	56 ± 9.3

compounds from the large number of pollutants in the urban atmosphere and the high background in chromatograms would probably require a GC×GC solution.

There are several reasons to be interested in halocarbons in London. Wide-spread use of CFCs, Halons and some long-lived compounds has been phased out in Europe due to the Montreal Protocol. However, replacement compounds for CFCs, HCFCs and HFCs, are still in use and continue to provide a threat, albeit reduced, to stratospheric ozone depletion and, in the case of HFCs, to global warming. Short-lived chlorocarbons, such as CH_2Cl_2 and PCE (C_2Cl_4), though not regulated by the Montreal Protocol, are still long-lived enough to be distributed through the global atmosphere. These compounds are used in a wide variety of applications as solvents. CH_2Cl_2 has recently been reported as growing in the atmosphere (Leedham et al., 2013). It is important, from the point of view of governmental policy-makers, to assess whether urban centres, such as London, are a source of these compounds. The ClearfLo project is a significant contribution to the sparse measurements made of halocarbons in the U.K. and is a rare opportunity to investigate the atmospheric composition of halocarbons and other compounds in London.

Very short-lived bromocarbons (VSLB), such as bromoform (CHBr_3), and iodocarbons, such as methyl iodide (CH_3I), are unlikely to have much direct impact on air quality in London, nor do they represent a large anthropogenic source. Brominated and iodinated compounds can play a role in particulate formation in the troposphere (e.g. Mäkelä et al., 2002; Saiz-Lopez et al., 2011), and tropospheric ozone destruction (e.g. Read et al., 2008). With regard to stratospheric ozone destruction, the tropics are more important for production of VSLB e.g. see Chapter 4 on the CARIBIC project. However, concentrations measured during ClearfLo are frequently higher than those encountered during campaigns in the tropics, for instance Sala et al. (2014). As discussed in Section 3.6.4.2, these emissions might be linked to seaweed farming in Normandy, France. Tropical VSLB emissions, especially CHBr_3 have been linked to tropical seaweed farming with planned increases in seaweed production likely to have greater future impact. VSLB were also of interest in London as potential tracers of marine air and its impact on air quality.

3.6.1 Air mass influences at the summer IOP site

The Sion Manning IOP site was chosen as a background urban location away from busy roads. The site was located away from major roads in an area surrounded by 2–3 storey buildings. This means that wind speed and direction measurements made on site approximately 10 m above the ground are not an accurate representation of the flow over London during the campaign. Therefore,

the results of an atmospheric dispersion model were used to estimate likely influences on air arriving at the site.

In order to identify some of the influences on air quality and composition in London, it is useful to understand the proportional influence and origins of air masses arriving at the Sion Manning site. To this end, the NAME dispersion model was used to indicate the regional-scale influences at the Sion Manning site. Model runs were performed by Zoe Fleming, University of Leicester. The NAME model was run in backwards mode, 1-day backwards in time at 3 hourly intervals. Inert tracer particles were released from the site location close to ground level (25 m). All instances where the particles were near the ground (10–100 m) were recorded to indicate surface emissions from different marine and terrestrial geographical regions. The regions used for the 1-day backwards runs are shown in Figure 3.14.

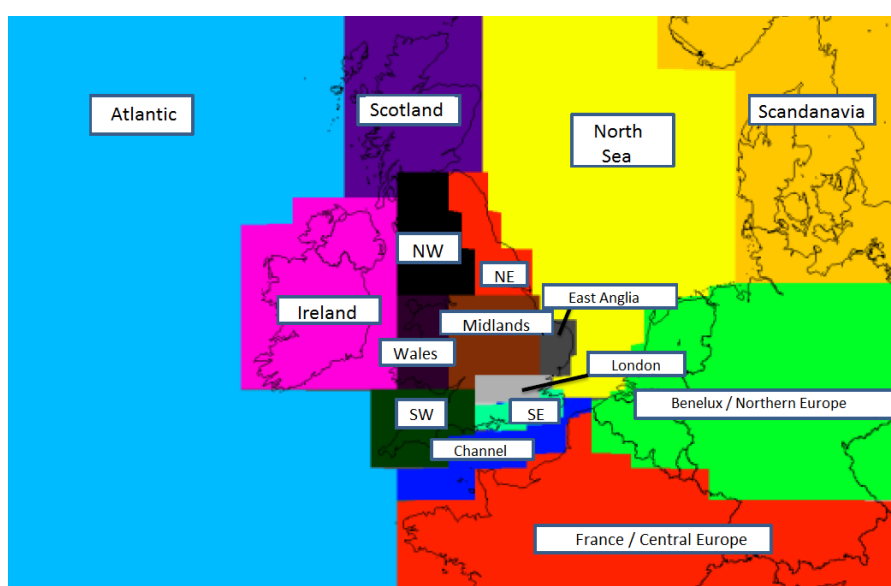


Figure 3.14: Diagrammatic map of the areas used for determining the potential source region contributions at the Sion Manning school site using the NAME 1-day model.

The NAME output represents the 10,000 inert tracer particles released during each 3 hour period. The output is an integration of the number of particles that have passed over a grid cell over the 1-day period. The distribution of tracer particles that pass over each, arbitrarily chosen, geographical region can be shown as a percentage of the total number of particles in the domain from each 3 hourly release period (see Fleming et al. (2012) and Jones et al. (2007) for further details of the NAME model and the method of representing source regions).

Figure 3.15 shows the 1-day contributions from the regions indicated in Figure 3.14. Percentage contributions can sum to $>100\%$ as particles can re-enter a region and be counted multiple times. During the summer IOP period, the Sion Manning site was mainly influenced by air originating near the surface in London and the surrounding area (i.e. South East and South West UK regions). However, there were periods where marine source regions, i.e. Atlantic, Channel, North Sea, have an impact on air arriving in London e.g. 1st to 6th August and continental Europe contributed to a large portion air arriving in London.

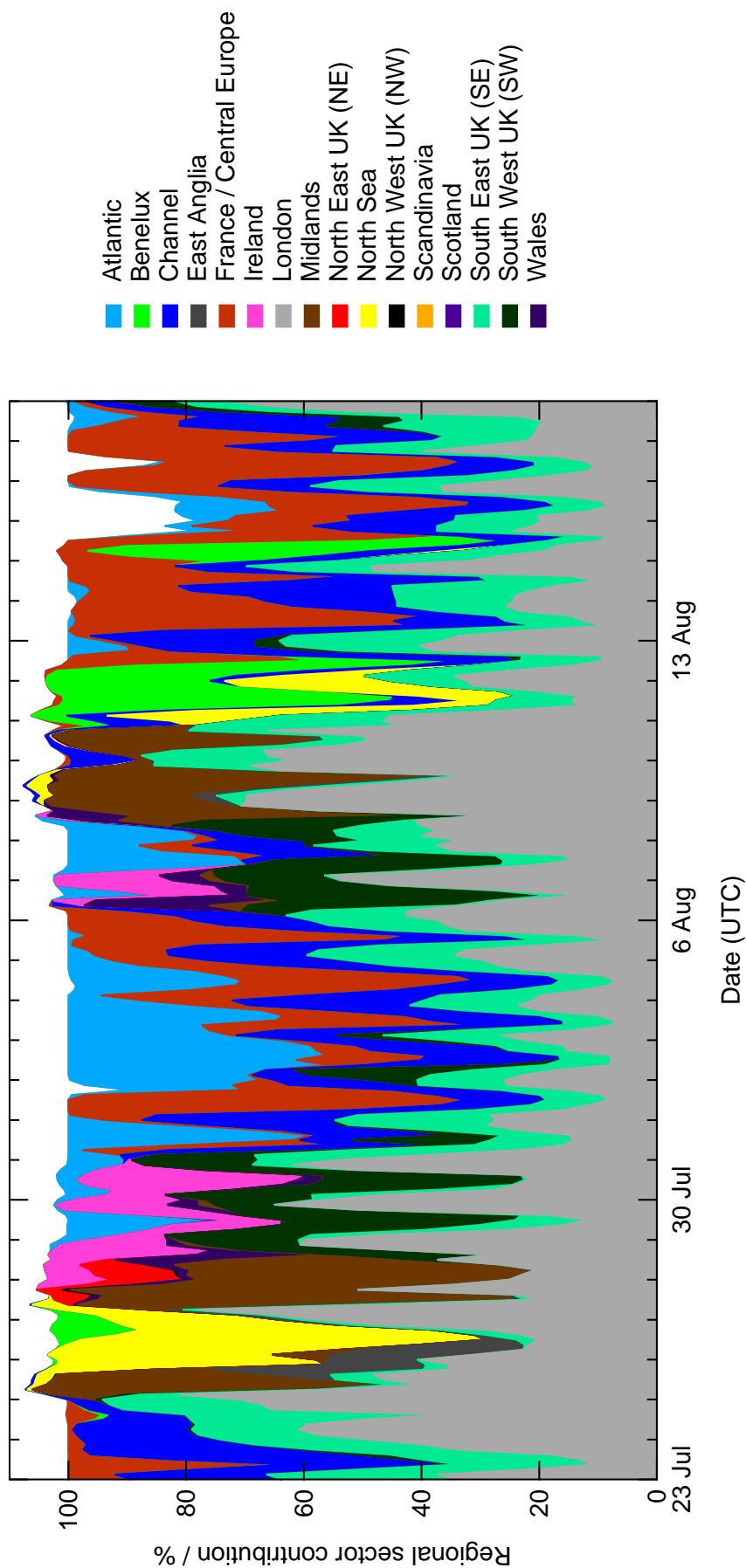


Figure 3.15: Regional influences of air arriving at the Sion Manning school site. Air mass footprints are derived from the NAME particle dispersion model (Jones et al., 2007). The contribution of each geographical region represents the proportion of released particles found within 100 m of the surface of each region over a 1-day backwards mode model run following a process similar to that described in Fleming et al. (2012), Section 5. The geographical regions defined for this analysis are shown in Figure 3.14.

3.6.2 Summer IOP averages

Averages (means and medians) across the whole summer IOP for halocarbons measured on the dual NCI/EI GC-MS are shown in Table 3.4. Long-lived halocarbons, i.e. the CFCs, HCFCs, halons, CH_3CCl_3 and CCl_4 , show a high degree of variability over the campaign. As these compounds are well mixed in the atmosphere, due to their long lifetimes, such a large range of values would not be expected unless close to source. There are three periods where there are substantial peaks in some long-lived halocarbons. Peaks can be seen on 25th July, 27th July and 10th August in CFC-11, CFC-113, HCFC-141b and H-1211 (see Figures 3.12 and 3.12a and 3.12c). Peaks can also be seen in CH_3CCl_3 , HCFC-22 and halon 1301. There is also a substantial peak for HCFC-141b on 13th August. Mixing ratios for these periods exceed, in the case of CFC-11, 1 ppb.

The two periods in July coincide with periods of slack air and high temperatures where the site was heavily influenced by the local area. Instrumental error is unlikely in these cases. Measurements of CFC-11 made in both EI and NCI MS show similar peaks. Furthermore, the limited range of compounds with large peaks, each analysed on different ions, indicates that this is not an MS error or trapping error. The most likely explanation is venting air-conditioning units and other refrigeration units on site. Very low wind speeds and high temperatures probably created a build-up of refrigerants (i.e. CFCs and HCFCs) in the 'urban canyon' formed by the surrounding buildings. This would suggest that some of the air-conditioning units require maintenance and replacement of old refrigerant. Simultaneous peaks in H-1211 might possibly be explained by fire-extinguishers, a number of which would have been present on site. It should be noted that these peak concentrations might not accurately represent emissions from London.

High variability in the short-lived halocarbons is expected as these are not evenly distributed in the atmosphere. All four chlorocarbons in Table 3.4, CH_2Cl_2 , CHCl_3 , TCE (C_2HCl_3) and PCE (C_2Cl_4), have anthropogenic sources. The majority of anthropogenic emissions of these compounds is found in the Northern Hemisphere, so higher mixing ratios and variability might be expected. The short-lived bromo- and iodo-carbons measured in this study are almost exclusively natural and marine in origin with a small anthropogenic source of CHBr_3 identified from water purification and power plant cooling (Quack & Wallace, 2003). These compounds are highly temporally and spatially variable and this is reflected in the summer IOP averages.

As the periods of high halocarbon concentrations mentioned above are likely to be due to on-site contamination, further analysis of the long-lived halocarbons has been constrained to the 31st July to 8th August. This also coincides with a set of bottle samples that were analysed on a high sensitivity sector GC-MS instrument by Johannes Laube at UEA.

3.6.3 Long-lived halocarbons

For the following discussion of long- and short-lived halocarbons during ClearfLo the period 31st July to 8th August is used for calculation of means from ClearfLo and baseline data from an AGAGE monitoring station at Mace Head, Ireland (Prinn et al., 2000). This period was chosen as one of relatively stable wind direction from the south west. Additionally, the choice of period was constrained by the dates of the samples analysed on the sector GC-MS instrument.

It should be noted that UEA results are calibrated on the NOAA calibration scale, as described in Section 3.5.2.1, whereas the Mace Head results are based on an independent AGAGE calibration

Table 3.4: Means $\pm 1\sigma$ standard deviations and medians with ranges in parentheses for dual NICI/EI GC-MS compounds measured during the summer IOP of ClearfLo at Sion Manning school in North Kensington. Errors on the mean represent variability.

Compound	Mean $\pm 1\sigma$	Median (range)
<i>Long-lived</i>		
CFCs		
CFC-11 †	272 \pm 63	264 (220–1098)
CFC-113 †	78 \pm 6.6	77 (70–140)
HCFCs		
HCFC-141b †	33 \pm 17	31 (21–231)
Other		
CH ₃ CCl ₃	6.3 \pm 1.1	6.1 (4.7–19)
CCl ₄	92 \pm 4.3	91 (81–107)
Halons		
Halon-1211	4.5 \pm 2.8	4.0 (2.7–52)
Halon-1202	0.025 \pm 0.012	0.024 (0.018–0.25)
Halon-2402	0.39 \pm 0.02	0.39 (0.34–0.46)
<i>Short-lived</i>		
Chlorocarbons		
CH ₂ Cl ₂	76 \pm 46	59 (27–437)
CHCl ₃	13 \pm 3.4	12 (8.2–30)
C ₂ HCl ₃	1.4 \pm 0.61	1.3 (0.56–7.2)
C ₂ Cl ₄	31 \pm 35	18 (3.4–312)
Bromocarbons		
CH ₂ BrCl	0.18 \pm 0.058	0.17 (0.11–0.59)
CHBrCl ₂	1.1 \pm 0.69	0.93 (0.39–5.3)
CH ₂ Br ₂	1.2 \pm 0.38	1.2 (0.60–3.0)
CHBr ₂ Cl	0.72 \pm 0.41	0.62 (0.19–2.8)
CHBr ₃	4.4 \pm 2.7	3.9 (0.70–17)
Iodocarbons		
CH ₃ I	1.6 \pm 0.83	1.4 (0.42–5.9)

† Measured in EI. All other compounds were measured in NICI.

scale. Differences are known to exist between the scales, however, they are likely to be small.

3.6.3.1 Chlorofluorocarbons (CFCs)

The chlorofluorocarbons (CFCs) are the most abundant anthropogenic chlorinated gases. The three most abundant CFCs (CFC-12, CFC-11 and CFC-113) contribute $\sim 61.4\%$ to the total sum chlorine from stratospheric source gases (Montzka & Reimann, 2011). A small number of CFCs were measured on site during ClearfLo. Emissions of CFC-12, CFC-11 and CFC-113 peaked in the 1990s. All three of these compounds are now decreasing in the atmosphere. It was not expected that CFCs would show large mixing ratios over Northern Hemispheric (NH) baseline values measured in London. In situ measurements of the three major CFCs (CFC-12, CFC-11 and CFC-113) show good agreement, within the variability, with baseline mixing ratios measured by the AGAGE network (Table 3.5).

A selection of minor CFCs were measured in bottle samples (CFC-112, CFC-113a and CFC-115). The in situ instrument does not have the requisite sensitivity to detect these compounds on the most suitable ions. Furthermore, chromatography has to be optimised for some of these minor CFCs e.g. CFC-113a (CCl_3CF_3), which elutes close to its isomer CFC-113 ($\text{CCl}_2\text{FCClF}_2$). CFC-115 agrees well with the baseline measurements made at Mace Head. Montzka & Reimann (2011) indicate that global mixing ratios of CFC-115 did not change appreciably from 2000 to 2008 and gave a global mean mixing ratio of 8.4 ppt. This is similar to ClearfLo and Mace Head values and suggests that levels have not changed substantially since 2008. Laube et al. (2014) report Southern Hemispheric (SH) mixing ratios from late 2012 of 0.48 ppt for CFC-113a and 0.44 ppt for CFC-112. Mean values from ClearfLo bottle samples are 0.11 ppt higher for CFC-113a. Values for CFC-112 are similar to Laube et al. (2014). Laube et al. (2014) indicate a dominantly NH source for these compounds. Additionally, they infer, from firm air collected in Greenland, that CFC-113a has been growing in abundance from the 1960s to 2012 with a sharp acceleration in emissions in the past few years. Therefore, higher NH mixing ratios might be expected for CFC-113a. Laube et al. (2014) indicate that CFC-113a is used as an intermediate in the production of pesticides and as an intermediate in the production of HFCs. However, Laube et al. also suggest that that emissions, either as a feedstock chemical or direct emission, might have been under reported as the Montreal Protocol does not require the separate reporting of isomeric compounds.

3.6.3.2 Hydrochlorofluorocarbons (HCFCs)

Hydrochlorofluorocarbons (HCFCs) were introduced as a short-term replacement for CFCs due to their shorter lifetimes (years compared to 10s to 100s of years for CFCs). This is due to a number of hydrogen atoms in the molecule (usually 1–3). The presence of hydrogen atoms reduces the lifetime relative to hydroxyl (OH) radical (τ_{OH}) by allowing hydrogen abstraction reactions to take place. Therefore, the proportion of HCFCs reaching the stratosphere is reduced by up to 80–90 % (Montzka & Reimann, 2011) due to greater tropospheric processing. However, by definition, HCFCs still contain chlorine atoms and, in spite of their shorter tropospheric lifetimes, they have a significant impact on stratospheric chlorine loading and hence, stratospheric ozone depletion. In 2008 HCFCs contributed $\sim 7.5\%$ to stratospheric chlorinated source gases (Montzka & Reimann, 2011).

Four HCFCs were measured during ClearfLo; HCFC-22, HCFC-133a, HCFC-141b and HCFC-142b. The most abundant HCFC in the atmosphere is HCFC-22 with a NH baseline mixing ratio at Mace Head of 230 ppt. ClearfLo HCFC-22 is 29 ppt higher than this value at 259 ppt (Table 3.5). HCFC-141b and HCFC-142b are both slightly higher (~ 6 ppt) than the Mace Head values. However, the variability in ClearfLo measurements is high at ± 36 ppt, ± 3.2 and ± 8.9 ppt for HCFC-22, HCFC-141b and HCFC-142b respectively. Unlike, the CFCs which were phased out in developed and developing countries by 2010, gradual phaseout of HCFCs in developed and developing countries is still under way and will be completed in 2030. It is likely that the high variability in ClearfLo measurements reflects the continued use of these substances in London. It should be noted that variability in the in situ measurements could also be dependent on measurement precision. Sector GC-MS measurements reported in Table 3.5 have an average precision of $< 2\%$. Therefore, the variability of, for instance, HCFC-142b is probably

Table 3.5: Comparison of ClearfLo in situ NICI/EI GC-MS, a set of nine bottle samples analysed on the sector GC-MS at UEA by Johannes Laube and AGAGE baseline measurements from Mace Head, Ireland (Prinn et al., 2000; Fraser et al., 1996; Cunnold et al., 1997; O’Doherty et al., 2001, 2004). AGAGE means are for the period 31st July to 8th August except where data was unavailable in which case AGAGE global baseline means for August 2012 have been used (indicated by curly brackets). This period during the summer IOP was chosen to allow best comparison between the in situ and bottle measurements. Errors represent the root mean square sum of variability and analytical errors. Compounds where there is a notable enhancement compared to Mace Head values are highlighted.

Compound	ClearfLo		AGAGE
	In situ [ppt]	Bottles [ppt]	Mace Head [ppt]
<i>Long-lived</i>			
CFCs			
CFC-11	260 ± 22 †	239 ± 2.5	{235 ± 0.30}
CFC-12	-	524 ± 4.5	{527 ± 0.17}
CFC-112	-	0.44 ± 0.0058	-
CFC-113	74 ± 7.7 †	78 ± 0.45	74 ± 0.11
CFC-113a	-	0.55 ± 0.010	-
CFC-115	-	8.9 ± 0.11	8.4 ± 0.047
HCFCs			
HCFC-22	-	259 ± 36	230 ± 0.67
HCFC-133a	-	0.52 ± 0.014	-
HCFC-141b	30 ± 3.2 †	-	24 ± 0.088
HCFC-142b	-	29 ± 8.9	23 ± 0.08
HFCs			
HFC-134a	-	140 ± 35	74 ± 0.34
HFC-227ea	-	1.6 ± 1.7	0.81 ± 0.014
Other chlorinated			
CH ₃ CCl ₃	6.0 ± 0.42 †	-	5.2 ± 0.088
CCl ₄	93 ± 5.5	88 ± 0.66	{84 ± 0.38}
Halons			
Halon-1301	-	3.2 ± 0.084	3.3 ± 0.037
Halon-1211	3.5 ± 0.33	-	4.0 ± 0.019
Halon-1202	0.024 ± 0.0026	-	-
Halon-2402	0.38 ± 0.016	-	-
PFCs			
C ₃ F ₈	-	0.61 ± 0.015	0.58 ± 0.0097
<i>c</i> -C ₄ F ₈	-	1.4 ± 0.014	-
<i>n</i> -C ₄ F ₁₀	-	0.21 ± 0.016	-
<i>n</i> -C ₇ F ₁₆	-	0.71 ± 0.33	-
Other perfluorinated			
SF ₆	-	7.9 ± 0.29	7.8 ± 0.027
SF ₅ CF ₃	-	0.16 ± 0.011	-
<i>Short-lived</i>			
Chlorocarbons			
CH ₂ Cl ₂	64 ± 47	-	34.8 ± 0.59
CHCl ₃	11 ± 1.7	-	11 ± 0.49
C ₂ HCl ₃ (TCE)	1.3 ± 0.59	-	{0.063 ± 0.015}
C ₂ Cl ₄ (PCE)	23 ± 32	-	1.5 ± 0.044

† Measured in EI on the dual GC-MS. Otherwise measured on the CI channel.

an accurate reflection of the atmospheric variability at the site. It is likely that measurements of HCFC-22, HCFC-141b and HCFC-142b are influenced by local sources e.g. refrigeration and air conditioning. Most instruments at the ClearfLo site were housed in shipping containers, each equipped with an air conditioning unit. Therefore, elevated measurements at the ClearfLo site might have been influenced somewhat by out-gassing from these units.

Laube et al. (2014) report SH mixing ratios for HCFC-133a of 0.37 ppt, in late 2012, which is 0.15 ppt lower than ClearfLo mean value. Similarly to CFC-113a, HCFC-133a has a dominantly NH source and has been rapidly increasing in the atmosphere in recent years and is used in the production of HFCs. Laube et al. also suggest that HCFC-133a may have been under-reported and it is unclear as to whether current atmospheric abundances are due to emissions as feedstocks and intermediates or unsanctioned production. Laube et al. (2014) also point out that, as HCFC-133a appeared in the atmosphere before widespread replacement of CFCs with HCFCs, it is likely that HCFC-133a has sources unrelated to CFC replacement.

3.6.3.3 Other chlorocarbons

Two other long-lived chlorocarbons were measured during ClearfLo; methyl chloroform (CH_3CCl_3) and carbon tetrachloride (CCl_4). Methyl chloroform is decreasing in the atmosphere at a near-constant exponential rate (Montzka & Reimann, 2011). Clerbaux & Cunnold (2007) reported that, in 2004, the AGAGE Mace Head, Ireland site was no longer experiencing elevated concentrations of CH_3CCl_3 during pollution events. ClearfLo CH_3CCl_3 is ~ 0.8 ppt higher than the Mace Head baseline concentration. However, the difference between ClearfLo and Mace Head measurements is as little as 0.29 ppt when variability in the measurements is taken into account. Calibration differences may also account for this difference and it is unlikely to indicate a source of CH_3CCl_3 in the region.

CCl_4 was originally mainly used as a feedstock for CFCs. As CFC production was reduced in the 1990s as a result of the Montreal Protocol, atmospheric levels of CCl_4 have also decreased and continue to decline. However, it is not declining as quickly as expected (Montzka & Reimann, 2011). ClearfLo results are in good agreement with Mace Head baseline values within the variabilities.

3.6.3.4 Hydrofluorocarbons (HFCs)

Hydrofluorocarbons (HFCs) are used as a long term substitute for CFCs and HCFCs. As HFCs do not contain chlorine, bromine or iodine they do not contribute to stratospheric ozone depletion and are not regulated by the Montreal Protocol. However, HFCs (and all other halocarbons) are radiatively active and contribute to anthropogenic climate change. HFCs are regulated by the Kyoto protocol which seeks to control emission of key gases linked to climate change. HFCs are expected to grow substantially in the future as demand for their use as a substitute grows. The warming effects of HFCs can be minimised by selecting HFCs with low global warming potentials (GWPs, see Section 1.6.1).

Two HFCs were measured during ClearfLo; HFC-134a and HFC-227ea (Table 3.5). HFC-134a is ~ 66 ppt and HFC-227ea is ~ 0.79 ppt higher than Mace Head baseline mixing ratios for the period. Both HFCs are used as replacements for CFCs and HCFCs in aerosol, refrigeration, and air-conditioning applications (e.g. Laube et al., 2010; Montzka et al., 1996). HFC-134a is

the preferred refrigerant used in refrigeration and vehicle air-conditioning (Montzka & Reimann, 2011). HFC-227ea is also widely used in fire protection systems. Therefore, similarly to HCFCs, higher mixing ratios of HFCs during ClearfLo are likely to be due to local sources from, for example, refrigeration and air-conditioning. As noted in the discussion of HCFCs (Section 3.6.3.2), it is possible that these measurements are influenced by on-site emissions.

3.6.3.5 PFCs

Perfluorocarbons (PFCs) are completely fluorinated hydrocarbons with very long atmospheric lifetimes and high GWPs (Forster et al. (2007), also see Section 1.6.1 and Table 1.1). PFC sources are industrial except for CF_4 which has a source from crustal degassing and a pre-industrial background of 39 ppt (Montzka & Reimann, 2011). PFCs sources include aluminium manufacture, fire protection and solvent applications (e.g. Bennett et al., 2005; Mühle et al., 2010).

Four PFCs were measured during the ClearfLo campaign; C_3F_8 , $c\text{-C}_4\text{F}_8$, $n\text{-C}_4\text{F}_{10}$ and $n\text{-C}_7\text{F}_{16}$. C_3F_8 agrees well with baseline measurements from Mace Head (Table 3.5). Oram et al. (2012) report a mean NH mixing ratio for $c\text{-C}_4\text{F}_8$ of ~ 1.2 ppt from samples collected at 10–12 km as part of the CARIBIC project in 2010 (see Chapter 4 for more details on CARIBIC). $c\text{-C}_4\text{F}_8$ measurements made during ClearfLo give a mixing ratio of 1.4 ppt, ~ 0.2 ppt higher than Oram et al. (2012). Oram et al. give a growth rate, based on archived air from Cape Grim, Tasmania as well as CARIBIC flights, of 0.03 ppt yr^{-1} . Assuming that this growth rate has not changed since 2010, this would give an expected concentration of ~ 1.26 ppt at 10–12 km. ClearfLo measurements are 0.14 ppt greater than this which might indicate either that emissions have increased since 2010 or that there is a local source of $c\text{-C}_4\text{F}_8$. However, as Oram et al. (2012) values are from aircraft measurements made at 10–12 km, it is not possible to draw definitive conclusions from comparison with these measurements.

Mixing ratios for $n\text{-C}_4\text{F}_{10}$ and $n\text{-C}_7\text{F}_{16}$, based on Cape Grim archived air in 2010 were 0.178 ± 0.002 ppt and 0.103 ± 0.005 ppt for $n\text{-C}_4\text{F}_{10}$ and $n\text{-C}_7\text{F}_{16}$ respectively (Laube et al., 2012, supplementary material). NH mixing ratios of $n\text{-C}_4\text{F}_{10}$, reported by Laube et al. (2012), were up to ~ 0.18 ppt in March 2011 at 10–12 km. ClearfLo values for $n\text{-C}_4\text{F}_{10}$ are only slightly higher (0.03 ppt) than NH values given by Laube et al. (2012). It is unlikely that this represents a significant difference. Laube et al. (2012) measured tropical mixing ratios of $n\text{-C}_7\text{F}_{16}$ of $\sim 0.23\text{--}0.24$ ppt. No Northern Hemispheric values are available for C_7F_{16} . ClearfLo values for $n\text{-C}_7\text{F}_{16}$ are higher by $\sim 0.45\text{--}0.6$ ppt higher than those from Laube et al. (2012). It is likely that the higher values encountered during ClearfLo are due to a Northern Hemispheric source, possibly close to London. Laube et al. (2012) give the main usage of $n\text{-C}_7\text{F}_{16}$ as a heat transfer fluid with additional usage as a solvent.

3.6.3.6 Other fluorinated compounds

SF_6 and SF_5CF_3 are perfluorinated compounds with long atmospheric lifetimes and high radiative forcing. This leads to very high 100-year GWPs of 22,800 for SF_6 and 17,700 for SF_5CF_3 (Forster et al., 2007). SF_6 has a small background emission from production in the Earth's crust, however, emissions are dominated by usage in high voltage insulation as well as additional contributions from magnesium production and semiconductor manufacture (Levin et al., 2010, and references

therein). ClearfLo measurements of SF₆ (Table 3.5) are similar to the baseline measurements from Mace Head. It is unlikely that there are any strong sources in London.

SF₅CF₃ has been used in the production of fluorosurfactants in the manufacture of foams and stain-resist coatings (Sturges et al., 2012). Sturges et al. indicate that significant emissions of SF₅CF₃ have ceased and that the mixing ratio has equilibrated throughout the atmosphere at ~0.15 ppt. This figure is in good agreement with ClearfLo values. Sturges et al. (2012) give evidence that the cessation of emissions is largely due to the change in production methods of one major manufacturer of fluorosurfactants. According to Sturges et al. (2012), a number of companies worldwide continue to manufacture similar fluorosurfactants but they do not appear to be contributing substantial emissions of SF₅CF₃.

3.6.3.7 Halons

Halons are long-lived halocarbons that contain bromine and fluorine. They may also contain chlorine atoms. As bromine has an approximately 60 times higher, on a per atom basis, ozone destruction efficiency (Montzka & Reimann, 2011), halons have high ozone destruction potentials (ODPs, Section 1.3.4). Halon emissions are thought to be accounted for by leakage from stockpiles or banks. However, they are also used in small quantities as chemical feedstocks and fire suppressant applications (Montzka & Reimann, 2011).

ClearfLo measurements were made of halons 1301, 1211, 1202 and 2402 (abbreviated here to H-1301, H-1211, H-1202 and H-2402). ClearfLo values for H-1301 agree well with baseline measurements from Mace Head (Table 3.5). H-1301 was increasing in the atmosphere at a rate of 0.03–0.04 ppt, yr⁻¹ during 2007–2008 (Montzka & Reimann, 2011) but there do not appear to be local emissions in London. ClearfLo measurements of H-1211 are ~0.5 ppt lower than baseline Mace Head measurements. This might be explained by a calibration offset between Mace Head and ClearfLo measurements.

Newland et al. (2013) report mean mixing ratios, from archived air at Cape Grim, Tasmania during 2011, of 0.020 ± 0.001 and 0.39 ± 0.01 for H-1202 and H-2402. ClearfLo results match these SH values well. H-1202 and H-2402 are both decreasing in the atmosphere at rates of -2.6 ± 0.2 and -3.3 ± 2.5 ppq yr⁻¹ (parts per quadrillion i.e. fmol⁻¹ mol⁻¹) respectively during 2005–2011 (Newland et al., 2013). Newland et al. state that H-2402 emissions are largely limited to countries that use ex-Soviet military equipment. Past emissions were as a consequence of direct production and as a by-product from over-bromination during H-1211 manufacture. H-1202 emissions have also been linked to H-1211 production. However, Newland et al. (2013) point out that current emissions are likely to be linked to either banked H-1202 or to contaminated H-1211 in, for instance, halon-charged fire extinguishers.

3.6.4 Short-lived halocarbons

3.6.4.1 Short-lived chlorocarbons

CH₂Cl₂ is primarily used as a paint remover with other uses as a solvent, degreaser and foam-blowing agent. TCE and PCE are used in dry-cleaning applications and degreasing. CHCl₃ is primarily used in the production of HCFC-22 and fluoropolymers, and is released as a by-product of bleaching in the paper and pulp industry (Montzka & Reimann, 2011). The anthropogenic

fraction (industrial plus biomass burning emissions) of these compounds has been estimated from modelling studies as 25 % for CHCl_3 , 90 % for CH_2Cl_2 and 100 % for TCE and PCE (Montzka & Reimann, 2011). However, the majority of anthropogenic emissions of all four compounds are found in the Northern Hemisphere. The majority of natural sources of CHCl_3 are the open ocean and soil processes with small contributions from geological and anaerobic processes (McCulloch, 2003). CH_2Cl_2 also has a small but poorly quantified oceanic source.

Four short-lived chlorocarbons were measured at Sion Manning school; perchloroethene (PCE, C_2Cl_4), trichloroethene (TCE, C_2HCl_3), chloroform (CHCl_3) and dichloromethane (DCM, CH_2Cl_2). A number of short-lived halocarbons are measured at the AGAGE (Advanced Global Atmospheric Gases Experiment) monitoring station at Mace Head, Ireland. Mean mixing ratios $\pm 1\sigma$ standard deviation for 23rd July to 19th August of AGAGE data under baseline conditions are 1.4 ± 0.45 ppt, 0.2 ± 0.1 ppt, 31 ± 10 ppt and 3.3 ppt respectively for PCE, CH_2Cl_2 and CHCl_3 (Prinn et al., 2000; O'Doherty et al., 2001). AGAGE measurements of TCE are not available for the ClearfLo summer IOP. ClearfLo measurements of these three very short-lived (VSL) compounds are elevated above this background level throughout the campaign excepting CH_2Cl_2 which has a minimum value of 27 ppt. However, this is encountered in only one sample. PCE, TCE, CH_2Cl_2 follow a similar pattern of high mixing ratio peaks reflecting the similar anthropogenic source of these compounds. A striking feature of these compounds during the IOP is the intense peak in PCE, TCE and CH_2Cl_2 mixing ratios on 7th August with CH_2Cl_2 mixing ratios approaching 0.5 ppb. During this peak, NAME 1-day air mass footprints indicate possible source influence from the south coast of Ireland, the Bristol Channel and Southwest UK (e.g. Figure 3.19c). However, considering the sharpness of the peak and the high mixing ratios encountered, this is likely to be due to a local source.

3.6.4.2 Very short-lived bromo-and iodo-methanes

Bromoform (CHBr_3) during the summer IOP is shown in Figure 3.17a. Bromoform is mainly marine in origin and has sources identified in coastal macroalgae (seaweeds) and oceanic phytoplankton (e.g. Leedham et al., 2013; Brinckmann et al., 2012; Carpenter et al., 2009; Montzka & Reimann, 2011). Minor anthropogenic sources have been identified from drinking water chlorination and power plant cooling water (Quack & Wallace, 2003). For further details on VSLB see Section 1.5.2.3 and Chapter 4.

Bromoform reaches a minimum of ~ 1 ppt over the summer IOP period peaking at up to ~ 17 ppt with a median value (and range) of 4.6 (0.70–17) ppt. Median global marine boundary layer (MBL) mixing ratios are 1.6 (0.5–2.4) ppt (Montzka & Reimann, 2011). Carpenter et al. (2005) observed CHBr_3 mixing ratios of up to 25 ppt at Mace Head, Ireland during August and attribute this to macroalgae production and indicate that high levels of CHBr_3 are dependent on light levels and macroalgal coverage which are both higher in spring and summer. The large peaks of up to ~ 16 ppt CHBr_3 in ClearfLo results indicate that London is relatively close to a source of CHBr_3 . Enhanced mixing ratios of CHBr_3 are associated with regional influences that indicates a greater marine influence on air arriving at the site. This is especially clear during the period between 31st July to 7th August (Figure 3.17b). Typically, higher mixing ratios during this period have a 1-day NAME foot print that indicates that air is close to the surface in the region of Brittany and Lower Normandy, France (Figure 3.19a). Higher mixing ratios between

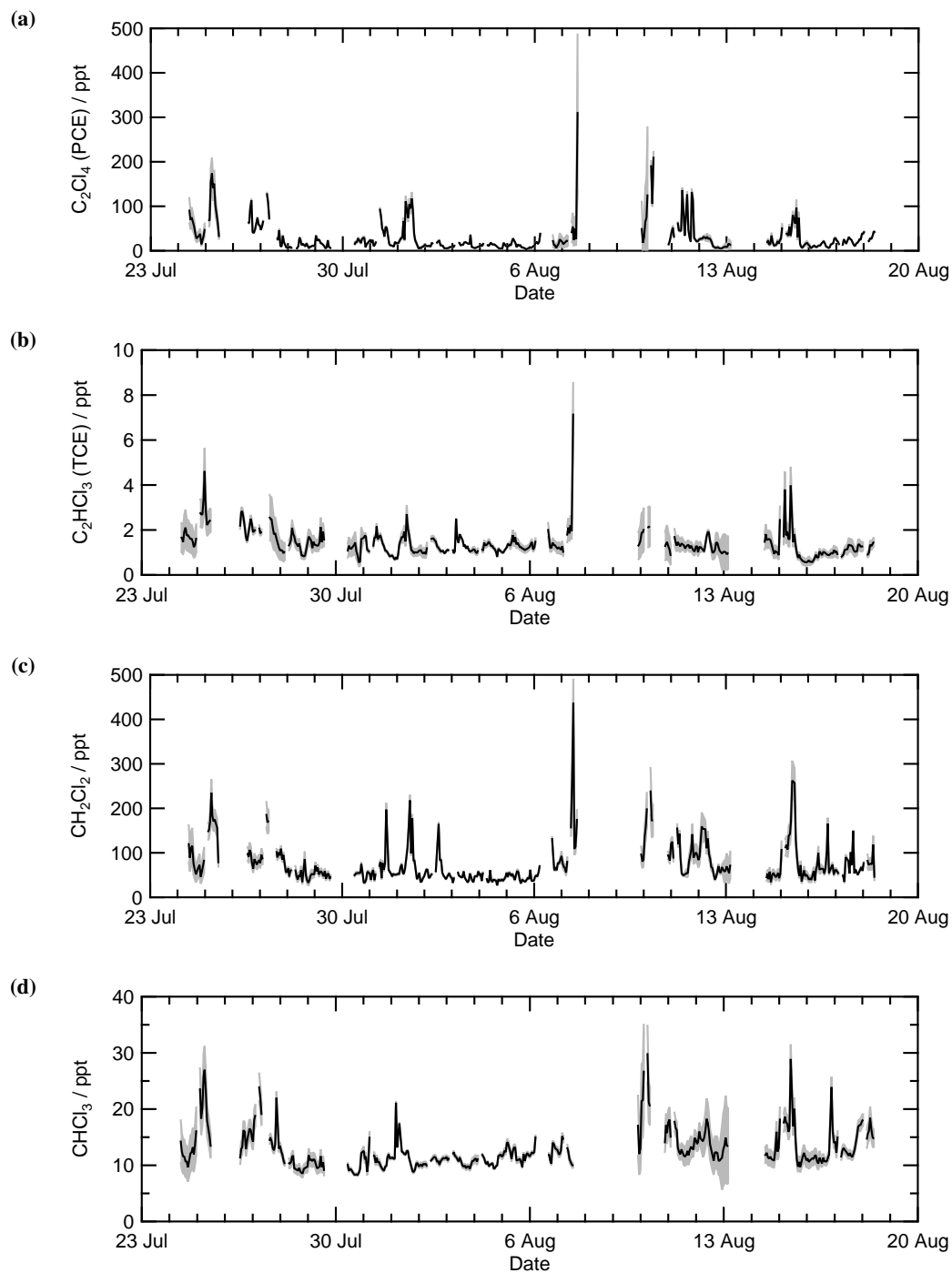


Figure 3.16: Short-lived chlorocarbon species measured during the ClearfLo campaign summer IOP at Sion Manning school in North Kensington. Mixing ratios are plotted against time for (a) C_2Cl_4 (PCE), (b) C_2HCl_3 (TCE), (c) CH_2Cl_2 and (d) $CHCl_3$.

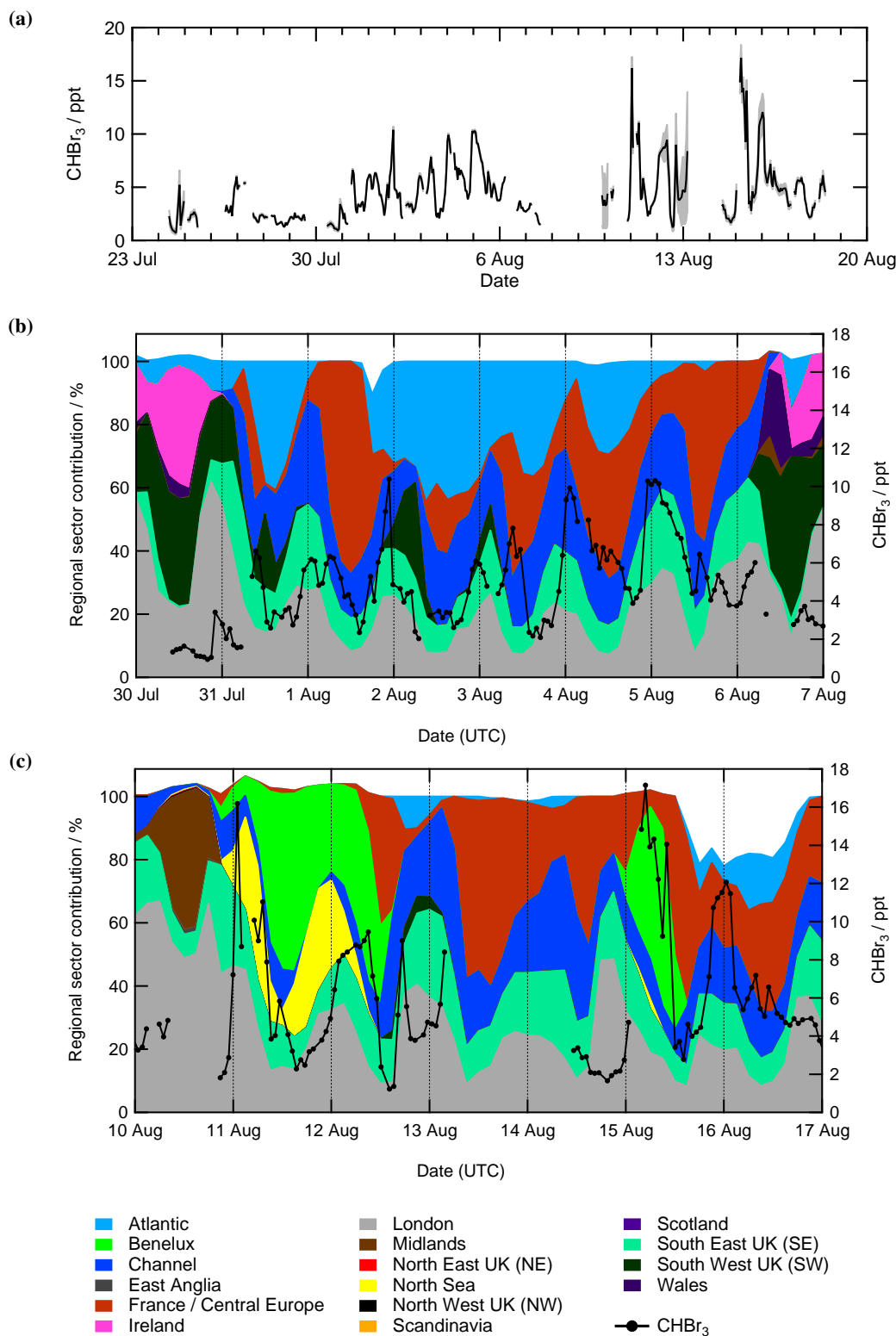


Figure 3.17: Measurements of CHBr₃ made during the ClearfLo campaign summer IOP at Sion Manning school in North Kensington. Data for the whole campaign are shown in (a) with bands surrounding the data indicating analytical uncertainties. Bromoform mixing ratios against time are plotted along with the air mass footprints described in Section 3.6.1 for (b) 30th July to 7th August and (c) 10th to the 17th August.

10th and 17th August are less clearly associated with marine influences. NAME 1-day footprints show that higher mixing ratios are associated with air coming from the coastal regions of Belgium and the Netherlands as in Figure 3.19b. The other four VSLB measured (CH_2Br_2 , CHBr_2Cl , CHBrCl_2 and CH_2BrCl) all follow a similar pattern though with less intense peaks (Figure 3.18). Medians and ranges for CH_2Br_2 , CHBr_2Cl , CHBrCl_2 and CH_2BrCl are 1.24 (0.60–3.0) ppt, 0.69 (0.19–2.83) ppt, 1.07 (0.39–5.3) ppt and 0.17 (0.11–.059) ppt respectively. These are close to global MBL values given in Montzka & Reimann (2011) with the exception of CHBrCl_2 which is higher than the value given by Montzka & Reimann (2011) of 0.3 (0.1–0.9) ppt.

Methyl iodide (CH_3I) has large peaks during the first period of strong marine influence (Figure 3.18e) but less intense peaks during the second period. The median over the IOP period was 1.6 (0.42–5.9) ppt which is higher than the Montzka & Reimann (2011) value of 0.80 (0.1–0.9) ppt. Though marine in origin with sources from marine algae and phytoplankton (e.g. Smythe-Wright et al., 2006), CH_3I also has a non-biological photochemical marine source (e.g. Yokouchi et al., 2008). The peaks in CH_3I do not follow the same pattern as for the VSLB with the largest peaks occurring at different times to those of the VSLB indicating a different source.

Likely sources in the region that might explain the higher mixing ratios of CHBr_3 are seaweeds and power plant cooling water. There are extensive seaweed beds off the coast of Brittany and Normandy. A large proportion of France's seaweed farming takes place at sites around this area (Mesnildrey et al., 2012). It is possible that these seaweeds are the source of bromoform during the 31st July to 7th August period. It is possible that this also provides an explanation for the high mixing ratios encountered later in the campaign. Alternatively, high mixing ratios might be due to power station cooling water from coastal nuclear power stations. Quack & Wallace (2003) estimate a global emission of bromoform-derived bromine of 34 Mmol yr^{-1} from coastal power plants. The french Flamanville nuclear plant is located on the Lower Normandy coast within the air mass foot print in Figure 3.19a. The UK Dungeness B nuclear plant is located on the Kent coast within the air mass foot print in Figure 3.19b. Additionally, the Sizewell nuclear plant is located just outside of the footprint on the Suffolk coast. All of these plants appear to use sea water cooling from the limited information available (Turnpenny et al., 2010; Pacey et al., 2011). Both periods are associated with elevated bromoform. Interestingly, the peak bromoform (and other VSLB) mixing ratios all occur during the night which might indicate that this is not related to biological production, as peak production from seaweeds or phytoplankton would be expected to occur during the day.

3.7 Summary

3.7.1 ClearfLo results

Measurements were made of a range of long- and short-lived halocarbon trace gases during summer 2012 within London, U.K. It would not be expected for London to be a source of CFCs, halons, CH_3CCl_3 or CCl_4 as these compounds have been phased out under the terms of the Montreal Protocol in both developed and developing countries. Results from ClearfLo indicate that this is the case. Northern Hemispheric data for the minor CFCs, CFC-112 and CFC-113a, is not available for comparison. However, comparison to Southern Hemispheric data from Laube et al. (2014) indicate that there is, at least, no local source of these compounds. However, there

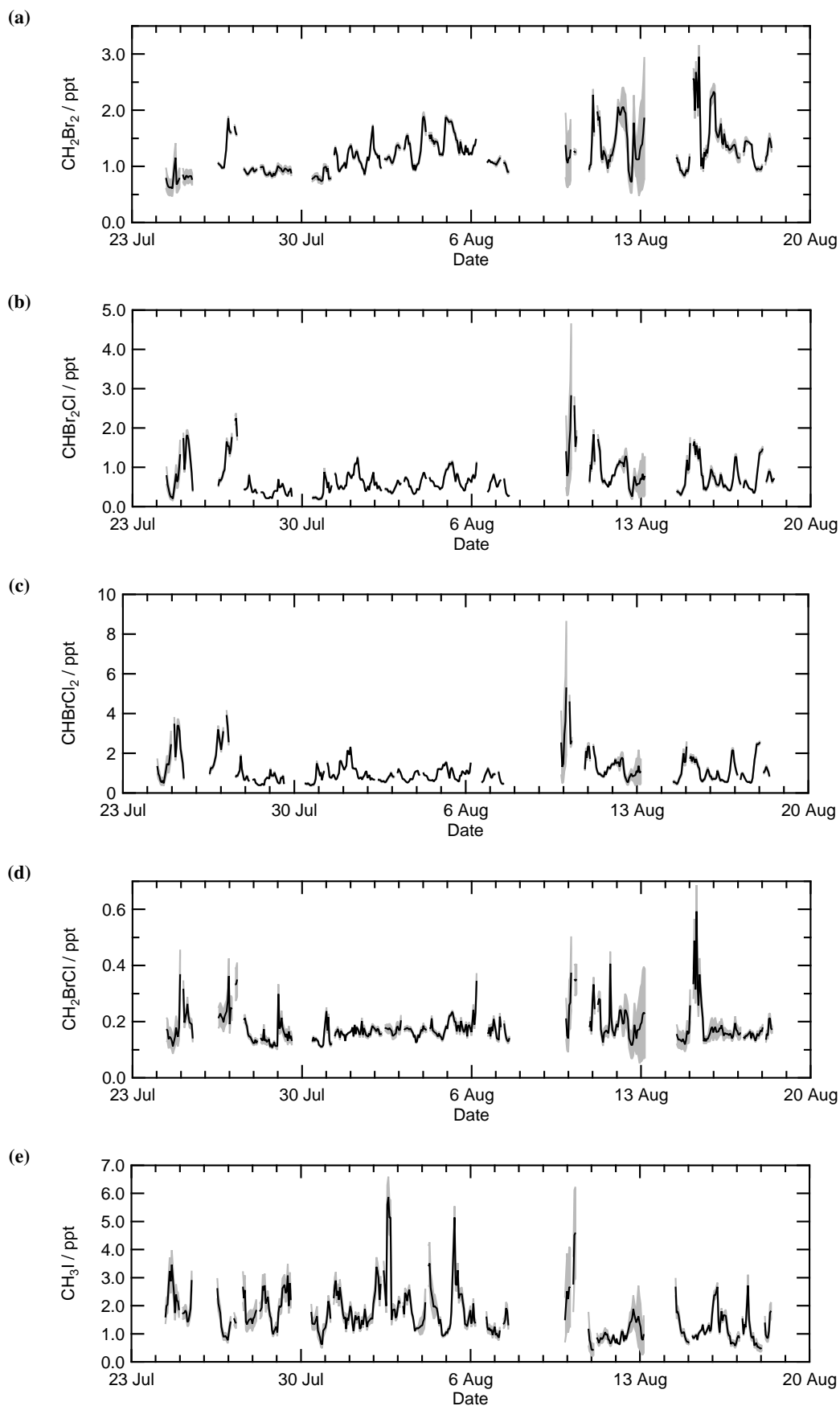


Figure 3.18: Measurements of selected very short-lived biogenic halocarbons made at Sion Manning school during the ClearLo summer IOP for (a) CH_2Br_2 , (b) CHBr_2Cl , (c) CHBrCl_2 , (d) CH_2BrCl and (e) CH_3I . Bands around the data indicate the analytical errors.

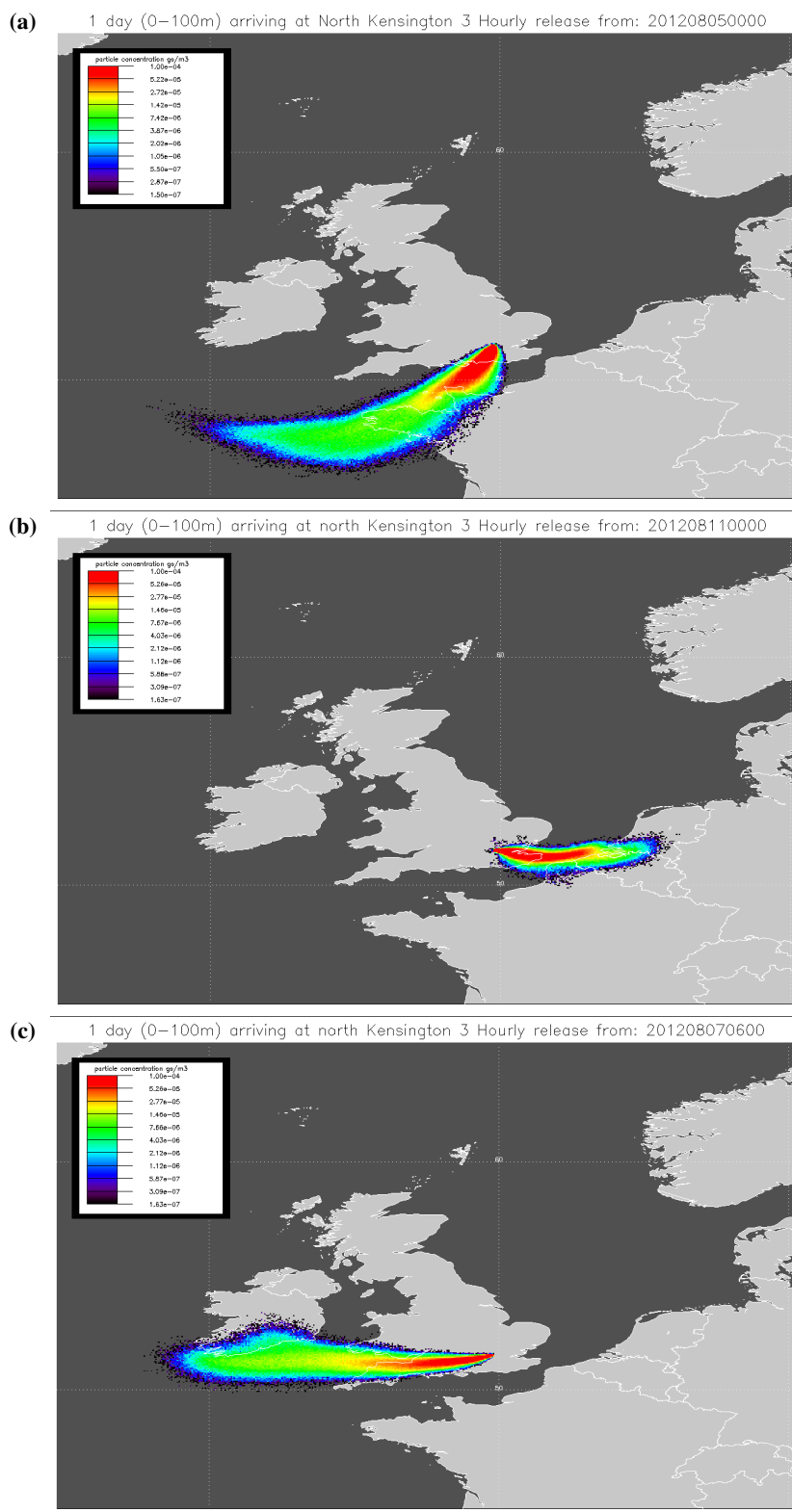


Figure 3.19: NAME 1-day footprints (see Section 3.6.1) for (a) 5th August 00:00 (UTC), (b) 11th August 00:00 (UTC) and (c) 7th August 06:00 (UTC). Colours indicate the concentration of inert tracer particles.

appear to be extant reservoirs of some of these long-lived species, within the U.K., as indicated by the high concentrations presumably from air-conditioning units and fire extinguishers on site (see Section 3.6.2).

In contrast, the HCFCs and HFCs generally appear to be enhanced compared to baseline measurements made at Mace Head. HCFCs were the first stage replacements for the CFCs. HFCs are the subsequent replacement compounds for the HCFCs. HCFC-22, HCFC-141b and HCFC-142b show higher mixing ratios (~ 29 , ~ 6 and ~ 6 ppt greater respectively) than Mace Head measurements. These compounds also show a large degree of variability which probably reflects their usage on a local as well as a regional scale. The minor HCFC-133a is also 0.37 ppt higher than Southern Hemispheric measurements, indicating that there is a Northern Hemispheric source. HFC-134a and HFC-227ea are both nearly double their respective baseline values at Mace Head. This indicates a strong source within London. As mentioned, HFC-134a is the preferred refrigerant for mobile air conditioning i.e. vehicular 'air-con'. HFC-227ea is used predominantly in fire protection systems and is the most dominant HFC used in fire protection in the U.K. (DEFRA, 2012). Emissions of these compounds are likely to increase in the future as the HCFCs are phased out and HFCs are used as replacements.

London does not appear to be a strong source of perfluorinated species. There are Mace Head baseline measurements from the period of only two of the perfluorinated species measured during ClearfLo (C_3F_8 and SF_6). These two species do not have notably higher mixing ratios than the background measurements. ClearfLo values for *c*- C_4F_8 and *n*- C_7H_{16} are in line with a Northern Hemispheric source. However, with little data from the region to compare to, it is not possible to draw a conclusion about London sources. It is unlikely that there are any significant sources of C_3F_8 as ClearfLo measurements closely match those at Mace Head. ClearfLo values for SF_5CF_3 are in line with expected values and indicate no local or Northern Hemispheric emissions.

ClearfLo measurements of CH_2Cl_2 , TCE and PCE indicate strong sources in London, the South West of England or Ireland. Considering the large number of applications for these compounds, it is not surprising that these compounds have higher mixing ratios in London. These compounds are short-lived (see Table 1.1 for atmospheric lifetimes) and as such, are not controlled by the Montreal Protocol. However, CH_2Cl_2 has a long enough lifetime to become distributed throughout the atmosphere. CH_2Cl_2 is growing in the atmosphere (Leedham Elvidge et al., 2014) and may be of significance in the future.

The very short-lived bromocarbons measured during ClearfLo indicate a source close to London. It is likely that this is due either to coastal seaweed beds in the region of Normandy or to sea water cooled, coastal power plants in either France or the U.K. Seaweeds have been implicated as VSLB sources in the tropics. Yokouchi et al. (2005) encountered up to 40 ppt of $CHBr_3$ off the coast of tropical islands. However, airborne measurements of VSLB, e.g. CARIBIC (see Chapter 4) or SHIVA (Sala et al., 2014), have not found especially high concentrations of these compounds in the troposphere. ClearfLo measurements add to the evidence that seaweeds are a strong source of these compounds. Alternatively, the ClearfLo measurements might corroborate power plant cooling as a source of VSLB. These emissions are unlikely to be of significance for stratospheric ozone depletion due to the short lifetimes of the compounds. However, they do highlight the significance of marine emissions on air quality in London.

3.7.2 TOF GC-MS

When purchased in around 2006, the SAI TOF GC-MS instrument was one of the first of its type. It was bought as something of a prototype, particularly for atmospheric measurements, with the expectation that it would achieve similar detection limits, working in the equivalent of full scan mode, to that achieved by the market leading Agilent MSD systems operating in selected ion, electron ionisation mode. The initial aim of this thesis was to test and refine the instrument, with assistance from the manufacturer, and to develop a fully automated system for the measurement of a wide and diverse range of VOCs (halocarbons, hydrocarbons, etc.) in ambient air.

The time-of-flight GC-MS system was assessed for suitability in atmospheric measurement. Instrument sensitivity is not as high as hoped for in an instrument intended to replace a quadrupole mass spectrometer (LODs are, at best, ~ 0.1 ppt). Trends with reproducibility show expected behaviours for most compounds with no apparent mass dependent effects. Long-term sensitivity drift could not be assessed due to the nature of the manual inlet setup. However, drift over the course of one day shows a consistent behaviour for compounds with low LODs. Daily sensitivity changes indicate that there is an exponential drop in sensitivity over the first two samples followed by an approximately linear increase in sensitivity. Although, long-term sensitivity drift could not be assessed, the stability of the instrument tune parameters indicates that there is little long-term drift. Linearity with sample size indicates non-linear behaviour volumes below ~ 750 mL. For most compounds, non-linearities are of the order of $< 10\%$. A preliminary comparison with a dual quadrupole MS system indicates good agreement. Further work is required in order to assess the linearity and sensitivity stability of the system.

The TOF GC-MS does not meet the original specifications for a GC-MS intended as a replacement for quadrupole GC-MS instruments used for atmospheric measurements. The ability to record a large range of ions without losing sensitivity is the main advantage of this instrument. However, instrument sensitivity is often not good enough to positively identify some of the lower mixing ratio compounds of current interest e.g. newer HFCs and PFCs. Additions and upgrades to the TOF MS, e.g. the HV Einzel lens assembly and the 100 kHz sampling mode, were not sufficient to improve the sensitivity. These modifications had additional issues that led to their deactivation. Further work is required in order to fully characterise the sensitivity stability and linearity of the system. Improvements to the usability will likely involve the proper integration of a standalone GC unit and further work with SAI engineers to improve stability, sensitivity and general instrument performance.

The main advantage of this instrument, in its current state, is the large number of ions recorded simultaneously without loss of sensitivity. This could be advantageous for simultaneous analysis of several classes of compounds, e.g. halocarbons and hydrocarbons. The only limitation on this analysis scheme is the ability to calibrate for a large range of compounds. Ideally, a GC \times GC system would be used for such an analysis to improve separation and identification of compounds.

The main limitation on the usability of the TOF instrument is reliability. Instrument software and hardware issues do not provide a stable platform for analysis. As the intended use of this instrument is for automated measurements, particularly in the field, instrument stability is a key factor in usability. Furthermore, the current instrument setup is not practically usable as a field instrument due to the addition of a separate GC unit which makes the instrument footprint larger than practically useful for in-the-field applications. Due to the limitations of the instrument it was

decided that analyses of campaign samples for the CARIBIC and SAMBBA projects (Chapters 4 and 5) would be performed on existing quadrupole instruments.

Very short-lived bromocarbons in CARIBIC

This chapter is based on the paper (Wisher et al., 2014) of which I was the first author. Co-author contributions included the supporting measurements and modelling (acknowledged in the text) as well as discussion on the content.

The main purpose of this study is to provide a minimum estimate of VSLB at the base of the tropical tropopause layer (TTL) in order to better constrain the quantity of bromine entering the stratosphere and the proportional influence of biogenic and anthropogenic emissions on stratospheric bromine levels. As described in Sections 1.5.2.3 and 1.7.2, a discrepancy exists between stratospheric inorganic bromine (Br_y) and the total bromine available from halons and methyl bromide (Dorf et al., 2006, 2008). This Br_y ‘gap’ is presumed to be due to very short-lived bromomethanes (VSLB). Additionally, it was hoped that it would be possible to identify broad tropical source regions for the VSLB, such as the western Pacific, an expected source region for VSLB (e.g. Aschmann et al., 2009; Fueglistaler et al., 2009). Furthermore, due to the short-lived nature of bromomethanes, VSLB can be used to elucidate structure within the transition layer between the extra-tropical troposphere and the lowermost stratosphere, the upper troposphere/lower stratosphere (UTLS).

4.1 The CARIBIC project

The CARIBIC project (Containerised Aircraft for the Regular Investigation of the atmosphere Based on an Instrument Container, www.caribic-atmospheric.com) has, since 2005, made regular deployments of a fully automated container-based atmospheric laboratory aboard a Lufthansa Airlines Airbus A340–600 (Brenninkmeijer et al., 2007). Flights originate in Frankfurt (Germany) with routes to North America, Asia, Africa and South America. At cruising altitudes (approximately 10–12 km), the aircraft typically intersects air masses representative of the free troposphere in the tropics, and both the upper troposphere and lowermost stratosphere (UT/LMS) at mid- to high latitudes. The UT/LMS is of particular interest as this is a complex region of the atmosphere with a limited number of measurements made within it. During each flight, real-time trace-gas and aerosol measurements are made alongside the collection of whole-air samples. A subset of whole-air samples have been analysed for five VSLB; CHBr_3 , CH_2Br_2 , CHBr_2Cl , CHBrCl_2 and

CH₂BrCl (Sect. 4.2).

4.2 Methods

The CARIBIC container instrumentation carries out a number of in situ measurements during each flight (Brenninkmeijer et al., 2007). In addition, whole-air samples are collected for later laboratory analysis. A detailed description of CARIBIC sample collection can be found in Baker et al. (2011b). The whole-air sampler unit consists of a pumping unit and two TRAC (Triggered Retrospective Air Collector) sampling units. Each TRAC contains 14 2.7 L glass sampling flasks with a normal flight consisting of 14 samples taken on the outbound and 14 on the return flight, making a total of 28 samples per round-trip flight. Samples are collected along the flight route at predetermined, evenly spaced sampling intervals of ~ 35 min, or ~ 480 km between samples. Filling times are on average 45 s (30–90 s) corresponding to a spatial coverage of 7–21 km. TRACs are routinely analysed after the flight at different laboratories for non-methane hydrocarbons (Baker et al., 2010), non-halogenated and halogenated greenhouse gases, e.g. N₂O, CH₄, SF₆ and CO₂ (Schuck et al., 2010) and a variety of short- and long-lived halocarbons at the University of East Anglia (e.g. Laube et al., 2010, 2012; Baker et al., 2011a; Lai et al., 2011; Oram et al., 2012; Sturges et al., 2012).

Between June 2009 and May 2011 the container was installed on flights between Frankfurt, Germany (FRA) and Caracas, Venezuela (CCS); between Frankfurt and Bogotá, Columbia (BOG), and between Frankfurt and Cape Town, South Africa (CPT). During November and December 2012 and February 2013 the container was installed on flights between Frankfurt and Bangkok, Thailand (BKK) and between Bangkok and Kuala Lumpur, Malaysia (KUL). Figure 4.1 shows the sampling locations for all Central American flights (FRA-CCS/BOG), South African flights (FRA-CPT) and Southeast Asian flights (FRA-BKK and BKK-KUL). CARIBIC flights are at civil aircraft cruising altitudes and those included in this study were between 6.9 and 12 km and on average at ~ 11 km (~ 220 hPa).

Routine analysis of whole-air samples for halocarbons is normally carried out by conventional gas chromatography mass spectrometry (GC-MS) in electron ionisation mode (EI-GCMS). However, the analysis of VSLB reported here was performed on a subset of CARIBIC samples using a quadrupole GC-MS running in negative ion chemical ionisation (NICI) mode. NICI has been shown to give much improved response for organic compounds containing bromine and iodine atoms (Worton et al., 2008). The GC-MS (Agilent Technologies GC 6890/MS 5973N) was coupled to a thermal desorption pre-concentrator (UNITY2TM and Online Air Server; Markes International Ltd.) as described in Worton et al. (2008). Accurately measured air samples (~ 500 mL, flow rate ~ 40 mL min⁻¹) were dried with a counterflow nafion drier (PermapureTM, 100 mL min⁻¹ counterflow of dry nitrogen) prior to pre-concentration on a packed capillary cold trap at -30 °C and thermally desorbed at a rate > 60 °C s⁻¹ to a maximum of 310 °C for 6 min. Chromatographic separation was achieved using an RTX-502.2 capillary column (105 m \times 320 μ m OD, 1.8 μ m film, RestekTM Corporation) using research grade helium (≥ 99.9995 % purity) as the carrier gas and by temperature-programmed gas chromatography (30 °C hold 2 min, 8 °C min⁻¹ to 150 °C hold 16 min, 20 °C min⁻¹, to 220 °C hold 5 min). The column eluent was subjected to negative ion chemical ionisation in the presence of methane reagent gas (research grade, ≥ 99.9995 %)

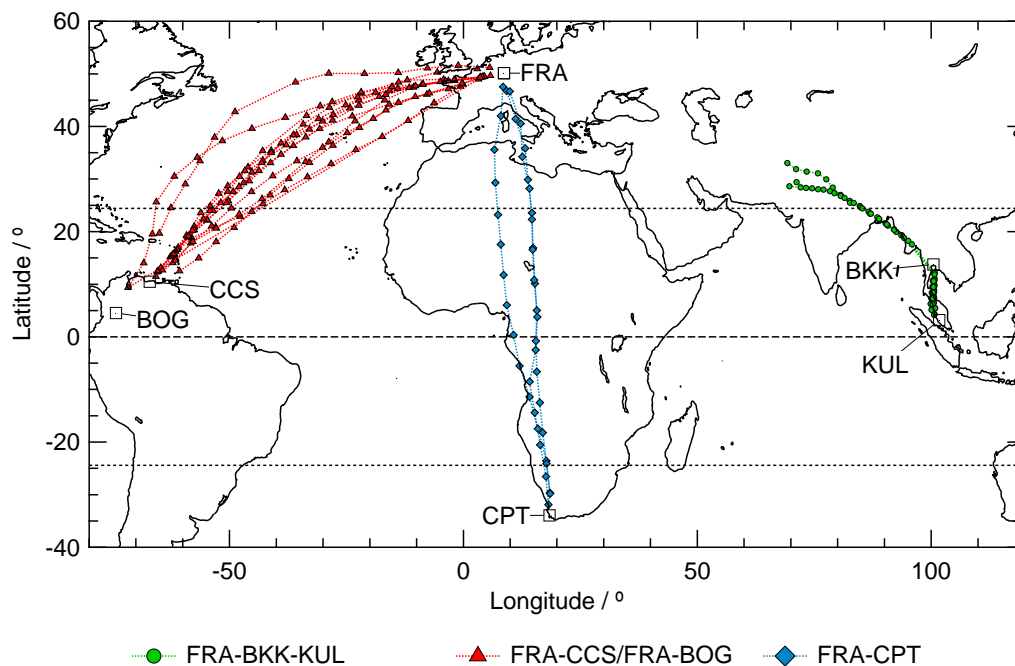


Figure 4.1: Collection locations of whole air samples for CARIBIC flight routes FRA-CCS/BOG, FRA-CPT and FRA-BKK-KUL. For the latter, air sample collection north of approximately 30° N were not analysed at UEA.

Table 4.1: Estimated limits of detection (LOD), compound dependant analytical precisions and mixing ratios at which the precision measurement was made for short-lived bromomethane species considered in this study (see Sect. 4.2.1 for further discussion of the working standard).

Species	Estimated Limit of Detection (LOD) [ppt]	Mean Analytical Precision [%]	Mixing Ratio [ppt]
Bromoform	0.001*	5.3	1.57–2.23
Dibromomethane	0.001*	5.1	1.23
Dibromochloromethane	0.001*	4.3	1.17
Bromodichloromethane	0.0008*	4.3	1.60
Bromochloromethane	0.005	6.1	0.29

All LODs given in parts per trillion (ppt) rounded to one significant figure.

* Values from Worton et al. (2008).

prior to detection by a quadrupole mass selective detector operating in selective ion mode (SIM) and monitoring the Br ion (m/z 79, 81) for brominated compounds. CARIBIC measurements of VSLB are reported as dry-air mole fractions, pmol mol^{-1} (dry air), abbreviated here to ppt (parts per trillion).

Analytical uncertainties were calculated on a per-run basis and are the 1σ standard deviation of the working standard on the respective measurement day. Estimated limits of detection in parts per trillion (ppt), average compound-dependent analytical precisions and the mixing ratios of the working standard at which the measurements were made for the compounds in this study are shown in Table 4.1. For more details on the working standard see Sect. 4.2.1.

A number of trace gases are continuously measured through the same inlet line as used for

collection of TRAC samples. For each TRAC sample, values for continuously measured trace gases are determined by integration over the sampling period. Ozone (O_3) measurements used in this study were measured using a custom-made dual-beam UV-photometer, developed and maintained by the Institute for Meteorology and Climate Research, Karlsruhe, Germany with a time resolution of 4 s and a precision of 0.5 ppb or 0.5 % (whichever is the larger) and a total uncertainty of 1.5 % (Brenninkmeijer et al., 2007; Zahn et al., 2012). Ozone mixing ratios are reported in this study as wet-air mole fractions, nmol mol^{-1} (air), abbreviated here to ppb (parts per billion).

Meteorological analyses and backward trajectory calculations are performed along the flight track using the TRAJKS model, of the Royal Netherlands Meteorological Institute (KNMI; Scheele et al. (1996), see also http://www.knmi.nl/samenw/campaign_support/CARIBIC/). The trajectory model uses as input 6 hourly wind fields at $1^\circ \times 1^\circ$ resolution derived from archived analysis fields from the European Centre for Medium range Weather Forecasting (ECMWF). 5 day back trajectories are calculated along the flight track at 3 min intervals. Additionally, at 6 s time steps, 8 day back trajectories are calculated during the sampling interval of each whole air sample. Additional meteorological parameters, such as potential vorticity (PV), were interpolated along the flight tracks at time intervals of 1 min by linear interpolation in space and time from the archived ECMWF analyses.

4.2.1 Calibration of short-lived halocarbons

Mixing-ratios of short-lived halocarbons are known to drift when stored for long periods in certain types of metal container (e.g. Laube et al., 2008; Hall et al., 2014; Butler et al., 2007, supplemental). Regular comparisons to known standards are necessary to ensure a consistent dataset. Calibration of the bromocarbons is based on individual compound response factors determined by comparison to a working standard with known mixing ratios. The working standard was an aluminium cylinder containing dry ambient air at high pressure. The mixing ratios of halocarbons in the working standard were determined by repeat comparison to calibrated gas standards supplied by the Global Monitoring Division of NOAA-ESRL in 34 L electropolished stainless steel canisters (Essex Cryogenics, St. Louis, MO, US). Mixing ratios in these standards are known to be stable over a period of years (e.g. Hall et al., 2014; Butler et al., 2007, supplemental). These comparisons are performed periodically and allow an assessment of any potential changes in the absolute mixing ratio of halocarbons in our working standard over time.

From comparisons with 3 separate NOAA standards: SX-3546 (comparison performed in 2008); SX-3570 (2010); and SX-3568 (twice in 2012) we estimate that the mixing ratio of CHBr_3 in the working standard has declined by 38 % over the period October 2008–September 2012, whilst that of CH_2Br_2 has remained unchanged (1.23 ± 0.07 ppt, or 5.6 %, 1σ). NOAA calibration data for the 3 mixed bromochloromethanes were only available for the 2010 and 2012 comparisons and our analysis shows that the concentrations of CH_2BrCl and CHBr_2Cl in the working standard have remained approximately constant (0.28 ± 0.004 ppt, or 1.5 %; and 1.18 ± 0.04 ppt, 3.4 % respectively) whilst that of CHBrCl_2 may have increased by 16 %. Calibration factors applied to the CARIBIC data for CHBr_3 have been time-corrected using a quadratic fit to the inter-comparison values. A calibration factor was applied to CH_2Br_2 based on mean values from 2008–2012 comparisons. Calibration factors for CHBr_2Cl , CHBrCl_2 and CH_2BrCl are based on

the mean values of the 2010 and 2012 comparison. Again, note that the differences in calibration scales for these compounds limit this comparison.

The mixing ratios reported here are therefore based on the latest NOAA-ESRL scales for CH_2Br_2 (2004) and CHBr_3 (2003), and on a preliminary NOAA scale for CHBr_2Cl , CHBrCl_2 and CH_2BrCl (Brad Hall, personal communication). The accuracy of the absolute mixing ratio in the working standard, based on combined uncertainties associated with the standard comparisons and NOAA's stated uncertainties was $\pm 6.0\%$ for CHBr_3 , $\pm 7.8\%$ for CH_2Br_2 , $\pm 6.7\%$ for CHBr_2Cl , $\pm 9.9\%$ for CHBrCl_2 and $\pm 9.0\%$ for CH_2BrCl .

4.3 Results and discussion

Samples for the following analysis were categorised into tropospheric samples and those with stratospheric influence. Samples with stratospheric influences were defined as having an O_3 mixing ratio exceeding the seasonally-dependent ozone threshold value determined by Eq. (4.1) (Zahn & Brenninkmeijer (2003), confirmed by Thouret et al., 2006). This excludes the influence of stratospheric air on samples and is independent of seasonal variations in the thermal tropopause (see Sect. 4.3.1.3).

$$\text{O}_3 = 97 + \sin\left(\frac{2\pi(\text{Day of Year} - 30)}{365}\right) \text{ (in ppb)} \quad (4.1)$$

4.3.1 Central American flights

4.3.1.1 Latitudinal distribution and averages

Back trajectories from a typical Central American flight are shown in Fig. 4.2. On this route (FRA-CCS/BOG), the CARIBIC aircraft samples air mainly originating from the west with some air uplifted from the surface at the northern and southern ends of the flight track.

Figure 4.3 shows the latitudinal distributions of VSLB during the Central American flights. There is little latitudinal variation over the range covered with larger mixing ratios in only a small number of samples in the tropics compared to higher latitudes. Notably, there are two samples with higher mixing ratios of CHBr_2Cl , CHBrCl_2 and CH_2BrCl at $10\text{--}20^\circ\text{N}$ with no enhancement in CHBr_3 and negligible enhancement in CH_2Br_2 (see Sect. 4.3.4). CHBr_3 , and to a lesser extent CHBr_2Cl , have lower mean mixing ratios in the region of $20\text{--}40^\circ\text{N}$ though this is not significant within the uncertainties. CHBr_3 and CHBr_2Cl have the shortest local lifetimes of the five VSLB (24 days and 59 days, respectively, Montzka & Reimann, 2011). This indicates that there has been a higher degree of photochemical processing and mixing in these air-masses due to longer range transport from high altitudes in these regions as in the example flight in Fig. 4.2. It is possible that source emission variations could also contribute to lower mixing ratios in this region.

The CARIBIC data can be compared to other recent aircraft studies in the region including CR-AVE, Costa Rica AVE (e.g. Kroon et al., 2008; Aschmann et al., 2009; Hossaini et al., 2010; Ashfold et al., 2012) and HIPPO-1, HIAPER Pole-to-Pole Observations (Wofsy, 2011; Hossaini et al., 2012b, 2013). CR-AVE took place January and February 2006 over the Eastern Pacific and HIPPO-1 took place during January 2009 with some measurements in the region of Central America. HIPPO-1 mixing ratios are on the NOAA scale and are directly comparable to CARIBIC.

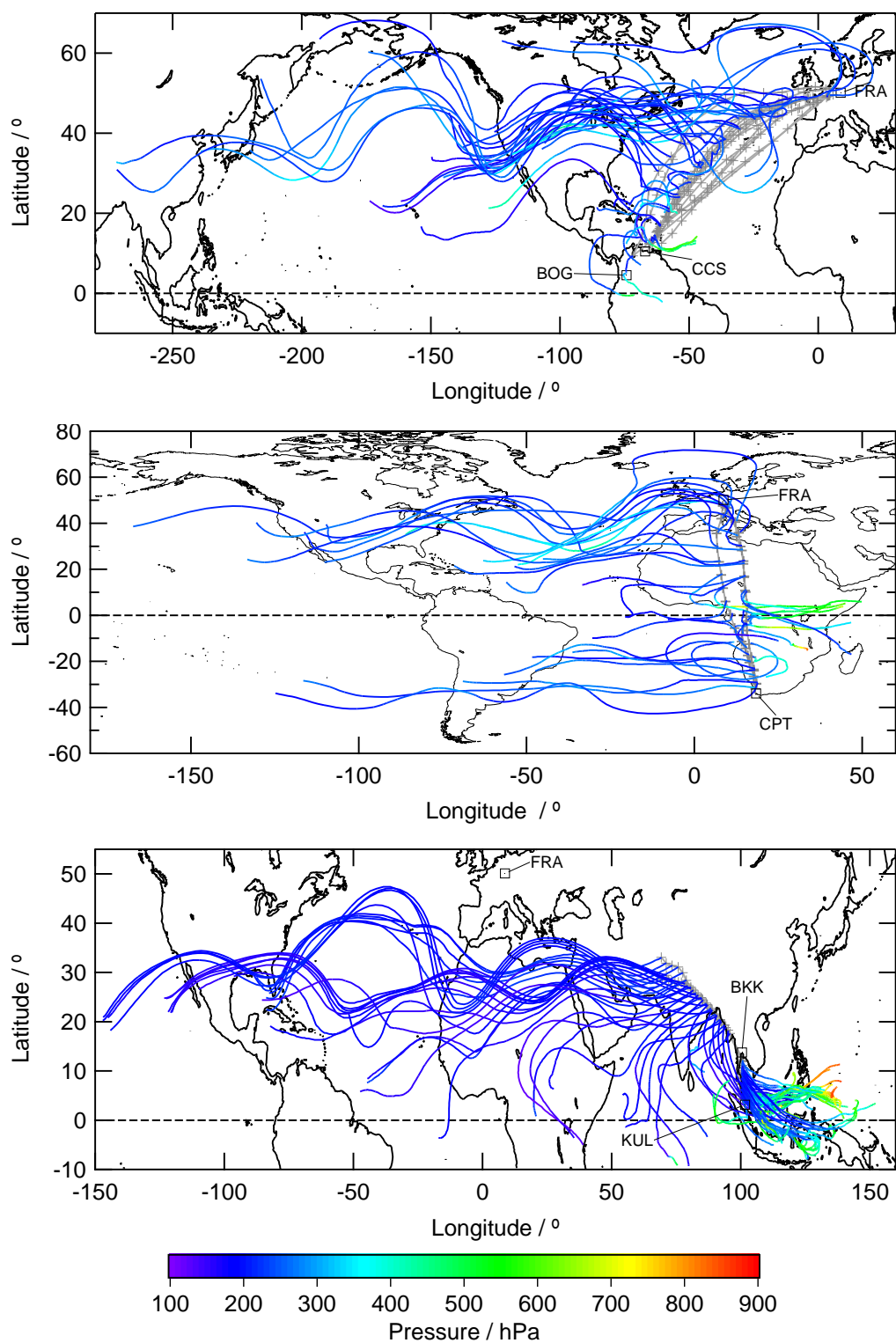


Figure 4.2: 5 day back trajectories for the routes sampled in this study (see http://www.knmi.nl/samenw/campaign_support/CARIBIC/). An example of the air masses sampled along the FRA-CCS route (top); back trajectories for all samples along FRA-CPT (middle) and back trajectories for all samples along FRA-BKK-KUL (bottom).

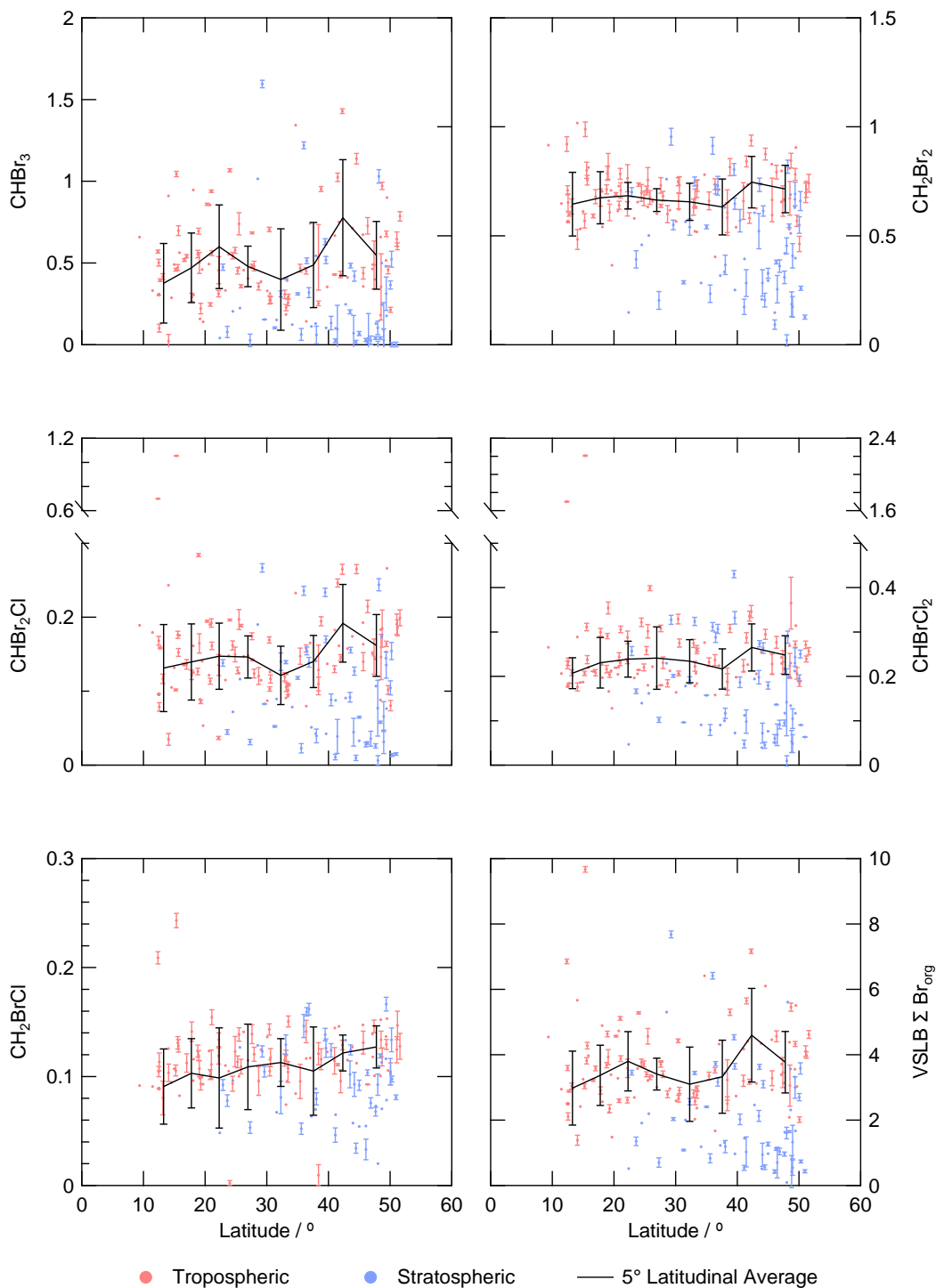


Figure 4.3: Northern-hemispheric latitudinal distributions in Central American flights of VSLB and total VSLB-derived bromine (VSLB Σ Br_{org}) for tropospheric samples, samples classified as having some stratospheric influence (following the definition in Sect. 4.3) and 5° latitudinal means of tropospheric samples above 10 km altitude with 1 σ error bars representing variability. Error bars on individual samples represent analytical uncertainties. All VSLB values on the vertical axes are given in ppt.

HIPPO values are based on a regionally relevant subset of all measurements made during the campaign available from the HIPPO data archive (Wofsy et al., 2012). The calibration scale used in CR-AVE has mixing ratios that are $\sim 10\%$ higher for CHBr_3 and $\sim 20\%$ higher for CH_2Br_2 than the NOAA-ESRL scale (Elliot Atlas, personal communication). Additionally, CARIBIC results can be compared to WMO 2010 (Montzka & Reimann, 2011). WMO 2010 values referred to in this study are 10–12 km upper tropospheric values from Tables 1–7 of WMO 2010. These values are mean values of DC-8 observations made during the TC4, PEM-West A and PEM-West B campaigns (Toon et al., 2010; Hoell et al., 1999, 1997; Schauffler et al., 1999). The minimum and maximum values given in WMO 2010 are based on the smallest mean minus one standard deviation and the largest mean plus one standard deviation respectively, across all campaigns. Again, note that the differences in calibration scales for these compounds limit this comparison.

A summary of the tropical and extra-tropical 10–12.3 km means and medians for the Central American flights with comparison to literature values is shown in Table 4.2. Mean values for the tropical region show good agreement with WMO 2010. CHBrCl_2 has a larger mean and range in CARIBIC than in WMO 2010.

HIPPO-1 mean mixing ratios agree within the uncertainties given. However, CH_2Br_2 is notably higher (0.88 ppt) than in CARIBIC (0.72 ppt) and total VSLB-derived organic bromine ($\text{VSLB } \Sigma \text{Br}_{\text{org}}$) is similar to CARIBIC (3.2 ppt for HIPPO-1 compared to 3.7 ppt for CARIBIC) without the addition of CHBrCl_2 and CH_2BrCl , both of which were unavailable for HIPPO-1. HIPPO-1 samples used in this study were collected further west than the CARIBIC Central American flights which may account for some of the differences in mean mixing ratios. Additionally, this might reflect some seasonality in VSLB, especially CH_2Br_2 , as HIPPO-1 took place in January whereas CARIBIC Central American flights took place during March–September.

Seasonality has been observed for CHBr_3 in the boundary layer (e.g. Carpenter et al., 2005). However, it is uncertain as to whether a seasonal cycle in CHBr_3 , or other VSLB, would be present in the upper troposphere or the regions sampled in this study. Due to the limited temporal coverage of CARIBIC, seasonal cycles cannot be identified or ruled out. Transport processes and the high degree of variability in source emissions of VSLB could also account for these differences.

CR-AVE mean mixing ratios for CHBr_3 (0.69 ppt) and CH_2Br_2 (0.96 ppt) are higher than in CARIBIC. However, when differences in calibration scales are taken into account, the CR-AVE means are more similar, i.e. ~ 0.62 ppt and ~ 0.77 ppt for CHBr_3 and CH_2Br_2 respectively. CR-AVE measurements were made further west than CARIBIC and may be more influenced by Pacific and Gulf of Mexico. Significant differences between standards and calibration methodologies for these compounds are known (e.g. Jones et al., 2011) therefore caution should be exercised when drawing conclusions based on these inter-campaign comparisons. This also applies to South African and Southeast Asian routes (see Sects. 4.3.2 and 4.3.3).

4.3.1.2 Potential temperature

The tropical tropopause layer (TTL) (between 345 K and 380 K potential temperature, approximately 12–17 km altitude) acts as a source region for the stratospheric overworld and for the extra-tropical lowermost stratosphere (Law & Sturges, 2007). Figure 4.4 shows plots of bromocarbons vs. potential temperature (Θ). Also plotted are 5 K binned means $\pm 1 \sigma$ vs. Θ . In the tropics, the five VSLB show little change in mean mixing ratio, within the natural variability, with

increasing Θ . VSLB Σ Br_{org} has a maximum mean mixing ratio of 3.74 ppt at 340–345 K. From 340 K to 355 K (disregarding the points at lower Θ as the means are based on only one or two points), the tropical means are higher than in the extra-tropics. This is a possible indication that vertical transport mechanisms in the tropics are a significant factor in supplying VSLB to the stratosphere although this difference is not significant or very small when the natural variability is taken into account. Back trajectory analysis indicates that enhanced mixing ratios in the tropics associated with uplift from the Gulf of Mexico or Eastern Pacific region. The CARIBIC aircraft has a maximum altitude of ~ 12 km and reaches potential temperatures of ~ 360 K, i.e. just at the entrance to the TTL. Therefore, mixing ratios obtained from CARIBIC in the tropics do not directly represent the quantity of VSLB available for transport from within the TTL into the tropical stratosphere. Rather, they represent an upper limit on organic bromine derived from VSLB available for transport into the stratospheric overworld with the proviso that further photochemical processing and physical transport processes will reduce mixing ratios entering the tropical stratosphere.

In the extra-tropics, there is a seasonal variation in the height of the thermal tropopause (e.g. Gettelman et al., 2011). Therefore, binned means $\pm 1 \sigma$ in Fig. 4.4 are separated, for the extra-tropics, into the two seasonal periods covered by the Central American flights analysed in this study; March, April, May (MAM) and June, July, August and September (JJAS). All five VSLB show an overall decrease in extra-tropical mean mixing ratio during MAM with increasing Θ ; VSLB Σ Br_{org} decreases from ~ 3.7 ppt at 320–325 K to ~ 1.5 ppt at 340–345 K. No data for MAM are available above 345 K. During JJAS, mean mixing ratios are constant, within the uncertainties, up to 340–345 K after which there is a decrease to 355–360 K beyond which there is no data available. VSLB Σ Br_{org} decreases from ~ 3.2 ppt to ~ 0.8 ppt over this range of Θ . This decrease in mixing ratios above ~ 345 K corresponds to the extra-tropical tropopause layer (ExTL). There are a number of samples with enhanced mixing ratios in the extra-tropics. However, back trajectories do not indicate a consistent origin for the air in these samples.

4.3.1.3 Ozone and height above the tropopause

O₃ is measured in situ on CARIBIC flights and provides an alternative tracer when considering UTLS structure and chemistry. Figure 4.5 shows plots of the five VSLB and VSLB Σ Br_{org} against O₃ for all FRA-CCS/BOG samples. Data are coloured to show samples with a degree of stratospheric influence. As stated in Sect. 4.2, tropospheric and stratospherically-influenced samples have been segregated based on a seasonally dependent O₃-threshold. This ‘chemical tropopause’ (CT) lies ~ 800 m below the thermal tropopause (Bethan et al., 1996) and approximates to a CT at 100 ppb O₃ and an upper limit to the mixed ExTL of ~ 500 ppb O₃. Therefore, between the CT and thermal tropopause there is significant impact from stratospheric air. All five VSLB show a sharp decrease in mixing ratio around 100–200 ppb O₃ corresponding to the transition from the troposphere to the ExTL. Above 200 ppb O₃ mixing ratios do not decrease greatly indicating that this layer is still showing some degree of mixing with the troposphere or the influence of quasi-horizontal transport from the tropics. All tropical samples are below the CT due to the restricted altitude range of the aircraft.

An alternate method of viewing the chemical structure within the ExTL is to define a vertical height above the tropopause based on simultaneously measured O₃ mixing ratios. O₃ mixing

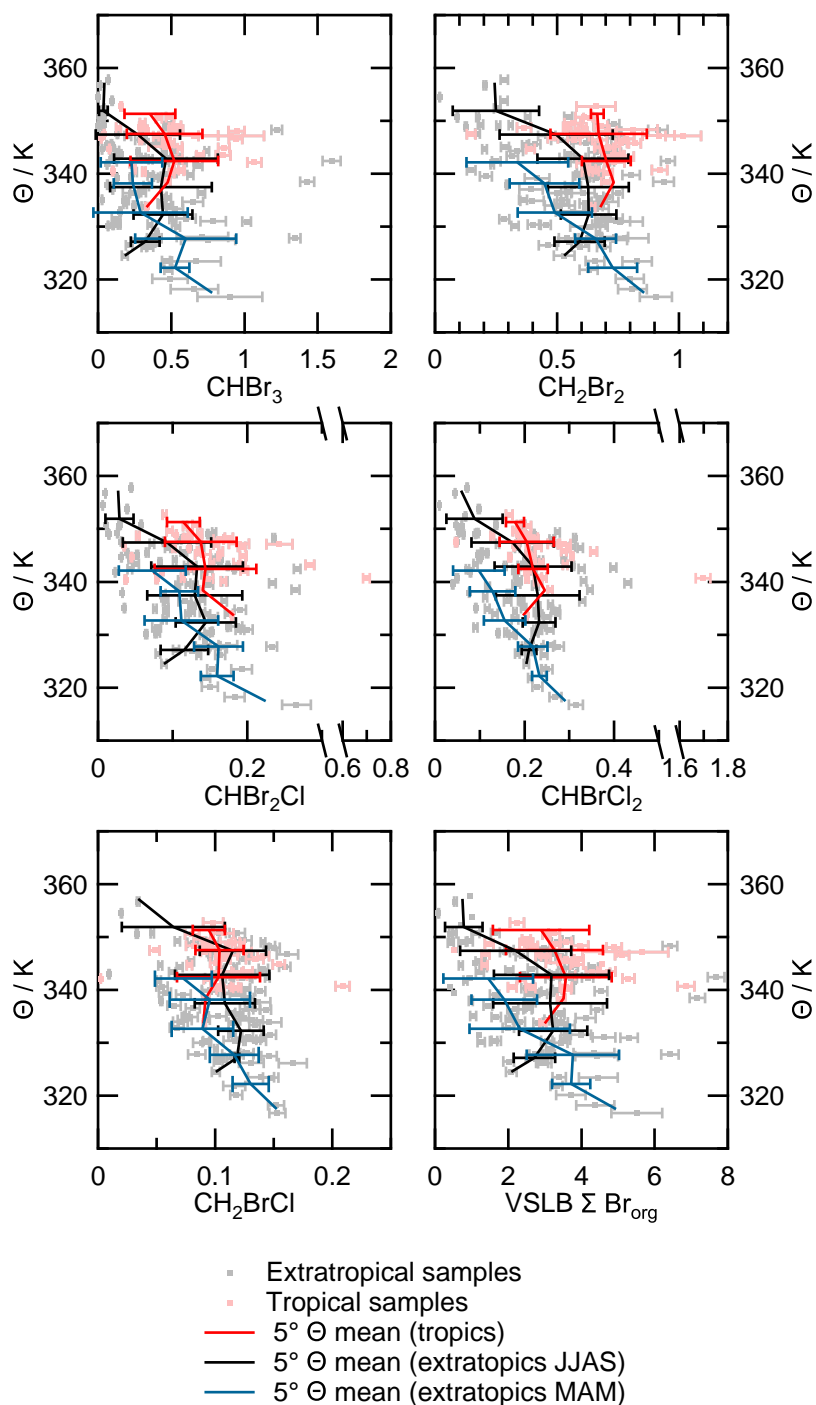


Figure 4.4: Plots of VSLB and total VSLB-derived bromine (VSLB Σ Br_{org}) for Central American flights against potential temperature (Θ) with 5 K means. 5 K means with 1 σ error bars representing variability are separated into extra-tropical from March, April and May (MAM); extra-tropical from June, July, August and September (JJAS) and tropical samples from all months. Where fewer than three data points were available for averaging, error bars have not been added. Error bars on sample data points represent analytical uncertainties. All VSLB values on the horizontal axes are given in ppt.

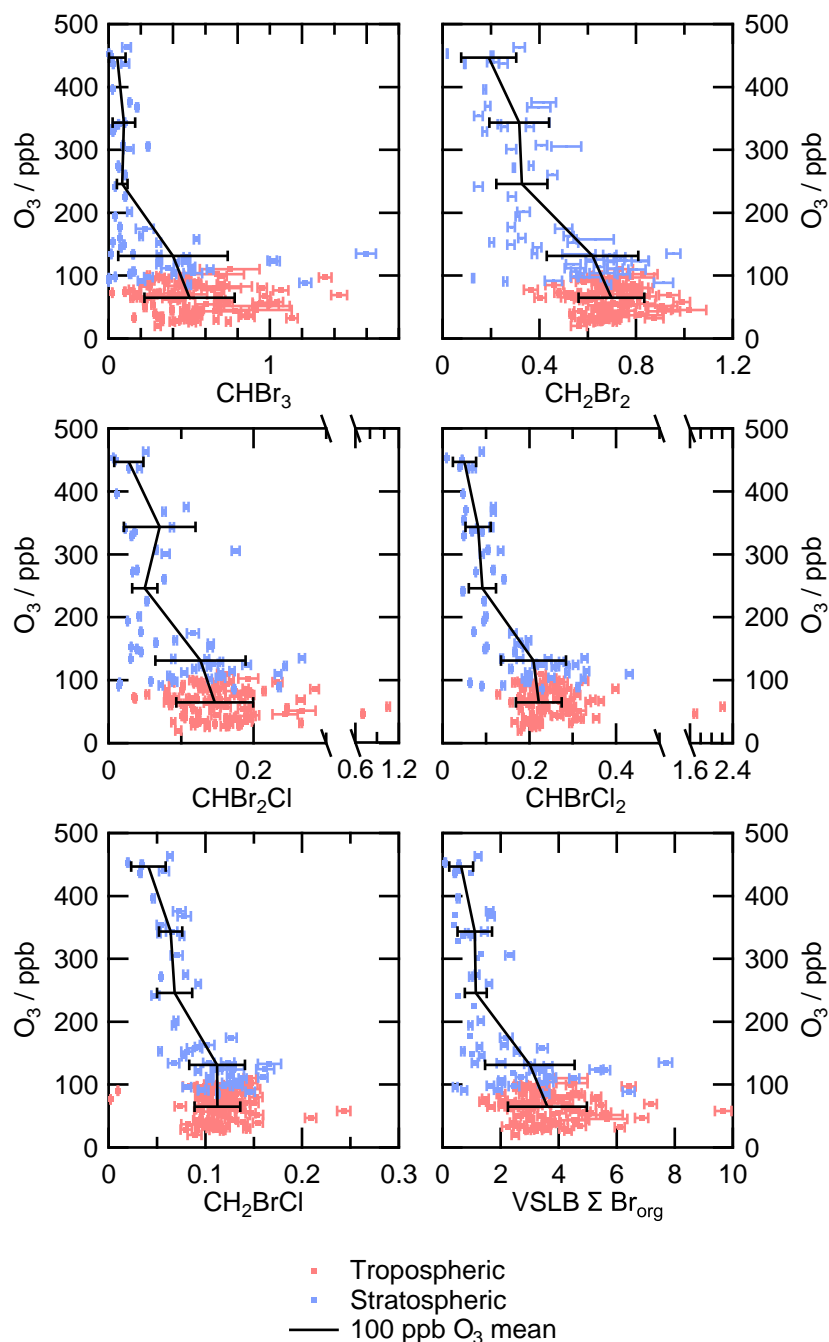


Figure 4.5: Plots of VSLB and total VSLB-derived bromine (VSLB Σ Br_{org}) for all samples on Central American flights against O₃ with 100 ppb binned means $\pm 1 \sigma$ error bars representing variability. Error bars on sample data points represent analytical uncertainties. Data points have been separated by colour into tropospheric samples and those with stratospheric influence (see Sect. 4.3). All VSLB values on the horizontal axes are given in ppt.

Table 4.2: Summary of tropospheric tropical and extra-tropical 10–12.3 km mid-upper tropospheric means and medians for the bromomethanes and total VSLB-derived organic bromine (VSLB Σ Br_{org}) in Central American, South African and Southeast Asian CARIBIC flights (FRA-CCS/BOG, FRA-CPT, FRA-BKK and BKK-KUL) with comparison to literature values. Tropical is defined as between 24.4378° S and 24.4378° N. Values are means with $\pm 1\sigma$, medians in curly brackets and minimum/maximum values in parentheses except for WMO 2010 where medians are not given. Values in square brackets are the number of samples included in the average. All values are given in parts per trillion (ppt).

Campaign			CHBr ₃	CH ₂ Br ₂	CHBr ₂ Cl	CHBrCl ₂	CH ₂ BrCl	VSLB Σ Br _{org}
CARIBIC ¹	Central America	Extra-tropical	0.52 ± 0.27	0.71 ± 0.11	0.15 ± 0.05	0.23 ± 0.05	0.12 ± 0.02	3.6 ± 1.1
		[58]	{0.45}	{0.70}	{0.15}	{0.22}	{0.11}	{3.4}
			(0.14–1.4)	(0.42–0.98)	(0.08–0.27)	(0.15–0.38)	(0.01–0.15)	(1.7–7.2)
	Tropical	0.52 ± 0.26	0.72 ± 0.14	0.17 ± 0.16	0.27 ± 0.32	0.11 ± 0.03	3.7 ± 1.5	
		[36]	{0.49}	{0.71}	{0.14}	{0.21}	{0.10}	{3.5}
			(0.02–1.1)	(0.38–1.1)	(0.04–1.1)	(0.12–2.1)	(0.0–0.24)	(1.4–9.7)
South Africa	Tropical	0.48 ± 0.54	0.68 ± 0.14	0.14 ± 0.10	0.24 ± 0.10	0.10 ± 0.02	3.4 ± 2.1	
	[26]	{0.35}	{0.69}	{0.12}	{0.22}	{0.10}	{2.9}	
		(0.03–2.8)	(0.40–0.87)	(0.05–0.55)	(0.10–0.56)	(0.04–0.14)	(1.4–12)	
Southeast Asia (FRA-BKK)	Tropical > 15° N	0.28 ± 0.19	0.76 ± 0.14	0.10 ± 0.04	0.17 ± 0.03	0.10 ± 0.01	2.8 ± 0.93	
	[18]	{0.25}	{0.79}	{0.10}	{0.16}	{0.10}	{2.8}	
		(0.05–0.58)	(0.49–0.95)	(0.04–0.16)	(0.11–0.22)	(0.09–0.12)	(1.6–4.2)	
Southeast Asia (BKK-KUL)	Tropical 0–15° N	0.56 ± 0.12	0.92 ± 0.08	0.16 ± 0.02	0.21 ± 0.03	0.12 ± 0.01	4.2 ± 0.56	
	[39]	{0.56}	{0.93}	{0.16}	{0.21}	{0.12}	{4.1}	
		(0.15–0.81)	(0.74–1.0)	(0.08–0.19)	(0.16–0.31)	(0.09–0.14)	(2.4–5.2)	
HIPPO-1 ²	Central America	Tropical	0.44 ± 0.07	0.88 ± 0.02	0.13 ± 0.03			3.2 ± 0.33
		[8]	{0.44}	{0.88}	{0.14}	N/A	N/A	{3.2}
			(0.34–0.58)	(0.85–0.92)	(0.09–0.15)			(2.8–3.9)

Continued on next page ...

Table 4.2: *Continued from previous page.*

	Campaign		CHBr ₃	CH ₂ Br ₂	CHBr ₂ Cl	CHBrCl ₂	CH ₂ BrCl	VSLB Σ Br _{org}
HIPPO-4 ²	Southeast Asia	Tropical > 15° N	0.25 ± 0.11	0.69 ± 0.07	0.07 ± 0.02			2.2 ± 0.42
		[10]	{0.27}	{0.68}	{0.08}	N/A	N/A	{2.3}
			(0.00–0.42)	(0.60–0.83)	(0.04–0.09)			(1.26–2.6)
		Tropical 0–15° N	0.80 ± 0.24	0.95 ± 0.09	0.16 ± 0.06			4.4 ± 0.87
		[7]	{0.72}	{0.95}	{0.16}	N/A	N/A	{4.4}
			(0.51–1.2)	(0.83–1.1)	(0.10–0.21)			(3.2–5.9)
CR-AVE ³	East Pacific	Tropical	0.69 ± 0.32	0.96 ± 0.11	0.11 ± 0.02			4.2 ± 1.2
		[24]	{0.59}	{0.96}	{0.11}	N/A	N/A	{3.8}
			(0.32–1.5)	(0.80–1.2)	(0.07–0.14)			(2.7–7.0)
SHIVA ⁴	Southeast Asia	Tropical	0.61 ± 0.11	0.90 ± 0.12	0.19 ± 0.04	0.25 ± 0.04	0.09 ± 0.02	4.35 ± 0.71
			(0.28–1.01)	(0.71–1.22)	(0.12–0.27)	(0.19–0.35)	(0.06–0.26)	(2.75–6.62)
WMO 2010 ⁵		Tropical	0.50	0.86	0.11	0.11	0.09	3.5
			(0.12–1.21)	(0.63–1.21)	(0.01–0.36)	(0.02–0.28)	(0.03–0.16)	(1.7–7.4)

¹ 10–12.3 km mid-upper tropospheric means ±1σ and ranges.

² Wofsy et al. (2012). Averages at 9–12 km altitude. VSLB Σ Br_{org} does not include CHBrCl₂ and CH₂BrCl.

³ VSLB Σ Br_{org} derived from CHBr₃, CH₂Br₂ and CHBr₂Cl only.

⁴ 10–13 km means ±1σ and 2.5–97.5 % ranges from Sala et al. (2014) Table 7.

⁵ 10–12 km. Montzka & Reimann (2011)

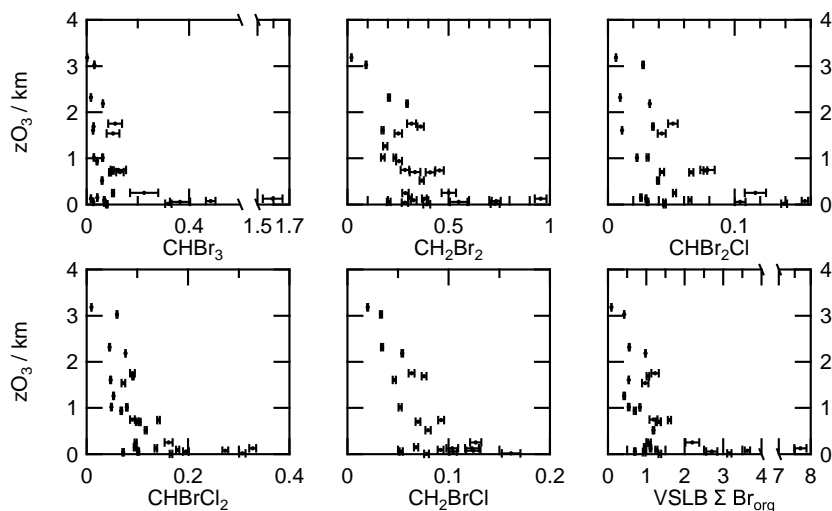


Figure 4.6: Plots of VSLB and VSLB-derived total bromine ($\text{VSLB } \Sigma \text{ Br}_{\text{org}}$) for Central American flights with O_3 -derived height above the thermal tropopause ($z\text{O}_3$) as defined by Zahn & Brenninkmeijer (2003). Error bars represent analytical uncertainties. The tropopause is defined as $z\text{O}_3 = 0$ (see Sect. 4.3.1.3). All VSLB values on the horizontal axes are given in ppt.

ratios can be translated into vertical distance above the thermal tropopause ($z\text{O}_3$) by comparison to monthly mean O_3 sonde-based profiles (Sprung & Zahn, 2010). Being a relatively long-lived tracer, O_3 follows the vertical movement of the tropopause. Therefore, $z\text{O}_3$ removes vertical variations in the thermal tropopause from trace gas profiles as shown in Sprung & Zahn (2010).

Figure 4.6 shows plots for all FRA-CCS/BOG samples of the five VSLB and $\text{VSLB } \Sigma \text{ Br}_{\text{org}}$ with the height above the thermal tropopause as calculated for CARIBIC following the definition given in Zahn & Brenninkmeijer (2003). Due to the limited cruising altitude range of the aircraft, height above the thermal tropopause is only available for extra-tropical samples. There is a high degree of variation within 0.5 km of the tropopause with a lesser degree of variation above 0.5 km. $\text{VSLB } \Sigma \text{ Br}_{\text{org}}$ decreases from a mean value of 2.3 ppt at 0–0.5 km above the tropopause to < 0.5 ppt above 3 km although this number is based on only two samples. This level is at the upper extent of the mixed ExTL layer and puts an upper limit on the quantity of organic-derived bromine entering the lower extra-tropical stratosphere. This, of course, does not give an indication of the quantity of product gases (derived from photochemical processing of VSLB) transported into this region.

4.3.2 South African flights

The South African (FRA-CPT) CARIBIC route partly samples air masses with similar origins to the Central American route (Fig. 4.2 and Sect. 4.3.1). However, there is also greater latitudinal range over FRA-CPT providing the opportunity to sample air masses from both hemispheres as well as air masses from the African continent and further east.

Analyses for three flights were available for CARIBIC route FRA-CPT (one return flight and one out-bound flight). Latitudinal profiles for these flights are shown in Fig. 4.7 with 10° latitudinal means of tropospheric data above 10 km altitude. When all the data is binned latitudinally, there

is some degree of latitudinal gradient in all VSLB with higher values in the northern mid-latitudes declining towards the southern mid-latitudes (see Fig. 4.7). For example, mean CHBr_3 drops from 0.73 ppt to 0.16 ppt and CH_2Br_2 from 0.80 ppt to 0.48 ppt. These two compounds are the main contributors to VSLB $\Sigma \text{Br}_{\text{org}}$ which drops from 4.5 ppt to 1.8 ppt. However, higher mixing ratios in the northern mid-latitudes derive from one FRA-CPT flight leg in February 2011 (the other return flight was in October 2009). Five and eight-day back trajectories shows that air in the northern mid-latitudes originated, on this flight leg, from further south within the Central American tropics rather than from the North American continent and North West Atlantic as in the return flight. Elevated mixing ratios of CHBr_2Cl , CHBrCl_2 and CH_2BrCl at 25–35° S are from the return flight and show a possible influence from the east coast of South America. It is likely that the inter-hemispheric gradient in Fig. 4.7 is a product of regional influences and the limited temporal range of the data rather than representing a larger-scale gradient. For comparison, over all HIPPO campaigns (HIPPO-1 and -4 are summarised in Table 4.2, see also Sects. 4.3.1.1 and 4.3.3) there is no comparable inter-hemispheric gradient over a similar latitudinal and altitudinal range.

If the February 2011 flight leg is excluded from the dataset (as in Fig. 4.7), there is no discernible inter-hemispheric latitudinal gradient. However, there is a possible increase in mixing ratios in all except CH_2BrCl in the tropics, e.g. CHBr_3 is enhanced by up to ~ 0.4 ppt. This increase is small when variability is taken into account with limited sampling. Therefore, these results should be taken as suggesting the possibility of a tropical enhancement over Africa rather than being definitive. This is perhaps present in the latitudinal averages across all data but obscured by the apparent latitudinal gradient. The HIPPO campaigns show increased mixing ratios around the equator compared to the extra-tropics (e.g. CHBr_3 increases from ~ 0.2 ppt at 50° N to ~ 0.6 ppt in the tropics); a similar enhancement to the CARIBIC data. It should be noted that the HIPPO campaign was exclusively in the Pacific region. Therefore, it is not directly comparable to the CARIBIC FRA-CPT route except in discussing global patterns. The source of this tropical enhancement is not clearly given by five-day back trajectories (Fig. 4.2). There is an indication in the back trajectories of strong uplift from the east coast and continental Africa around the equator. One sample in this region shows high levels of CHBr_3 (2.85 ppt), CHBr_2Cl (0.55 ppt) and CHBrCl_2 (0.56 ppt). Back trajectory analysis for this sample indicates possible influence from the east coast of Africa in the region of Somalia and/or the Arabian Sea. This sample is from the February 2011 flight leg but is representative, from back trajectory analysis, of air around the equator.

Mean mixing ratios for the tropical mid-troposphere at 10–12.3 km are presented in Table 4.2. Values for the extra-tropical region are not given due to limited data coverage. The values given in Table 4.2 for CHBr_3 , CHBr_2Cl , CHBrCl_2 and CH_2BrCl agree well, within the uncertainties, with tropical troposphere values for the Central American flights and, therefore, with WMO 2010; CH_2Br_2 is ~ 0.2 ppt lower. Ranges for CHBr_2Cl , CHBrCl_2 and CH_2BrCl are similar to WMO 2010 however, the maximum value for CHBr_3 in CARIBIC is ~ 1.6 ppt higher than in WMO 2010 and maximum CH_2Br_2 is ~ 0.4 ppt lower.

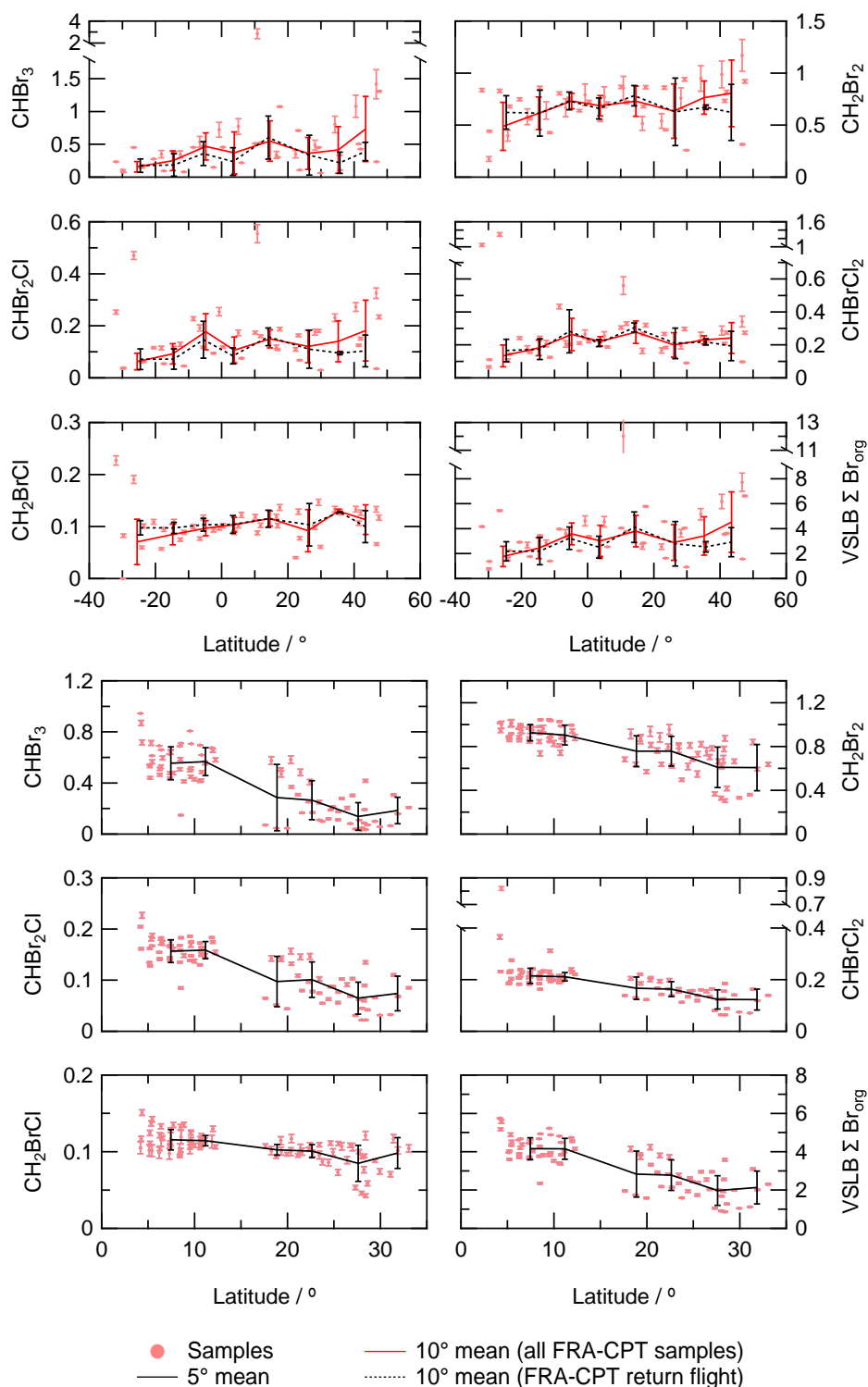


Figure 4.7: Latitudinal distributions in South African (top) and Southeast Asia (bottom) flights of VSLB and total VSLB-derived bromine (VSLB Σ Br_{org}) with 10° (South African flights) and 5° (Southeast Asia) latitudinal means of tropospheric samples above 10 km altitude with 1 σ error bars representing variability. Latitudinal averages for South African flights are shown for all samples and for samples collected on the return flight (see Sect. 4.3.2). All samples in both routes are tropospheric (following the definition in Sect. 4.3) with error bars representing analytical uncertainties. All VSLB values on the horizontal axes are given in ppt.

4.3.3 South-East Asia flights

The tropical West Pacific is considered a potentially important region for transport of VSLB into the stratosphere (e.g. Aschmann et al., 2009). Frequent and intense convection provides an efficient pathway for boundary layer air to be transported to the TTL (e.g. Fueglistaler et al., 2009). Additionally, emissions in the region are poorly sampled, including those of farmed macroalgae species. These could impact on future VSLB emissions due to interest in increasing seaweed aquaculture in the region (Leedham et al., 2013).

Flights between FRA and KUL consist of two legs; FRA-BKK and BKK-KUL (collectively FRA-BKK-KUL). As bottle samples are only collected at cruising altitude and not during take-off or landing, there is a discontinuity in data coverage in the region of Bangkok. This route intersects air masses, over the FRA-BKK leg, with a range of origins (Fig. 4.2). The BKK-KUL leg samples a less diverse range of air masses mainly originating over Indonesia and the South China Sea.

A total of three return flights were analysed along the FRA-BKK-KUL route providing good coverage in a region of the tropics that is considered important for VSLB emissions (e.g. Ashfold et al., 2013). Latitudinal profiles for these flights are shown in Fig. 4.7 with 5° latitudinal means of tropospheric samples above 10 km altitude. All five compounds show distinctly higher mixing ratios within 15° N of the equator than at higher latitudes with CHBr₃ at ~ 0.6 ppt below 15° N compared to ~ 0.3 ppt at 15–30° N. This partly reflects the origins of air masses in this region; back trajectories indicate that most air masses on the BKK-KUL leg of the flight have been uplifted from the South China Sea and Western Pacific Ocean. In contrast, the FRA-BKK leg is dominated by long-range, higher altitude transport from over the Atlantic and North American, European, Asian and African continents with a small number of samples near Bangkok uplifted from Indonesia (see Fig. 4.2). Additionally, as the VSLB are mainly marine sourced, the FRA-BKK leg of the route, which passes over Europe and Asia, might be expected to show relatively lower mixing ratios.

Samples from 0–5° N are from below 10 km altitude and are not included in the latitudinal means however, two of the samples show slightly higher mixing ratios than 5–15° N for CHBr₃, CHBr₂Cl and CHBrCl₂. Back trajectories indicate that the air masses originated off the coast of Malaysia in one case and west of Sumatra in the other.

Average values for the tropical troposphere for the FRA-BKK leg and for the BKK-KUL leg are included in Table 4.2. Values for the extra-tropical region are not given due to limited data coverage. Means over the FRA-BKK leg for CHBr₂Cl, CHBrCl₂ and CH₂BrCl agree well with the Central American and South African flights. CH₂Br₂ (0.76 ppt) is 0.08–0.11 ppt higher and CHBr₃ (0.28 ppt) is ~ 0.2 ppt lower than Central American and South African flights. This reflects the mix of long and short-scale transport from various regions covered on this leg of the flight and is not representative of emissions and vertical transport from tropical regions.

Mean mixing ratios for CHBr₃ (0.56 ppt), CHBr₂Cl (0.16 ppt), CHBrCl₂ (0.21 ppt) and CH₂BrCl (0.12 ppt) for the BKK-KUL leg are similar to the South African and Central American CARIBIC routes and agree well within the errors. However, CH₂Br₂ (0.92 ppt) is 0.24–0.27 ppt higher than in the South African and Central American flights. This indicates that there is a greater emission of CH₂Br₂ in the Southeast Asian Pacific tropics than in either the Western Atlantic or African tropics. Emissions of the other VSLB are more similar. Caveats relating to data limitations, including seasonality, are the same as those discussed in Sect. 4.3.1.1.

The HIPPO-4, HIAPER Pole-to-Pole Observations (Wofsy, 2011; Hossaini et al., 2013) took place in June and July 2011. HIPPO-4 mixing ratios are on the NOAA scale and are directly comparable to CARIBIC. HIPPO values are based on a subset of all measurements made during the campaign available from the HIPPO data archive (Wofsy et al., 2012). Part of the campaign took place in the region of Indonesia and the Philippines, further east than the CARIBIC BKK-KUL leg. Average mixing ratios for this campaign are shown in Table 4.2. All mixing ratios are on the NOAA scale. 0–15° N means for CH₂Br₂, CHBr₂Cl and VSLB Σ Br_{org} agree well with BKK-KUL. CHBr₃ is higher in HIPPO-4 (0.80 ppt) than in BKK-KUL (0.56 ppt) but this is within the variability. Sala et al. (2014) made airborne measurements in the region of Malaysia during November and December 2011 as part of the SHIVA campaign. Mean values at 10–13 km altitude are given in Table 4.2. These values agree very well with CARIBIC BKK-KUL means and indicate that CARIBIC values are representative of this region.

We suggest that there are two possible reasons for this enhancement in tropical CH₂Br₂ between BKK-KUL and Central America or South African flights.

1. The CHBr₃/CH₂Br₂ emission ratio might differ between the regions. The enhancement in CH₂Br₂ in BKK-KUL is not accompanied by a similar enhancement in CHBr₃ and might indicate a lower CHBr₃ emission ratio, relative to CH₂Br₂, in Southeast Asia. This is not the case in the literature where CHBr₃/CH₂Br₂ emission ratios have been reported as broadly consistent over a range of tropical regions (e.g. Brinckmann et al. 2012; Yokouchi et al. 2005; O'Brien et al. 2009). Additionally, CHBr₂Cl is similar across the tropical regions sampled, indicating that the Southeast Asian emission ratio is lower for CHBr₂Cl. The CHBr₂Cl/CH₂Br₂ emission ratio is known to vary regionally, e.g. Brinckmann et al., O'Brien et al. and Yokouchi et al. report varying emission ratios relative to CH₂Br₂ (0.35, 0.46 and 0.7 respectively). Verification of the emission ratios relative to CH₂Br₂ in this study is not possible as measurements were too far removed from source to provide a reliable estimate. This hypothesis is based on the assumption that there is no effect, in our data, of seasonality or inter-annual variability.
2. The local lifetime of CH₂Br₂ might be longer in Southeast Asia. Montzka and Reimann (2011) give the local lifetime (τ_{local}) of CH₂Br₂ as 120 days. This lifetime is dominated by reaction with hydroxyl (OH) radical ($\tau_{\text{OH}} = 123$ days, $\tau_{\text{photolysis}} = 5000$ days). CHBr₃ ($\tau_{\text{local}} = 24$ days) is more influenced by photolysis ($\tau_{\text{OH}} = 76$ days, $\tau_{\text{photolysis}} = 36$ days). Therefore, it could be expected that, within the troposphere, a region of low OH mixing ratios would lead, after significant photochemical processing, to an enhancement in CH₂Br₂ without a significant, concomitant depletion of CHBr₃. The mixed halomethanes could be expected to show a similar behaviour, however, the magnitude of this effect would be too small to discern from the analytical uncertainties. Rex et al. (2014) have identified an "OH minimum area" in the West Pacific through a combination of O₃ measurements, modelled OH mixing ratios and some limited OH measurements. Modelling studies of this "OH minimum area", made by Rex et al. (2014), indicate that the local lifetime of CH₂Br₂ could be increased by up to a factor of three compared to other tropical regions and suggest that this would have a significant effect on the efficiency of transport of CH₂Br₂ from the region into the stratosphere.

4.3.4 Enhancements in the mixed bromochloromethanes

We have observed on a few occasions, enhanced mixing ratios of mixed bromochloromethanes (CHBr_2Cl , CHBrCl_2 and CH_2BrCl) without significant enhancements of CHBr_3 or CH_2Br_2 , e.g. between 10 and 20° N in the Central American flights and 30–40° S in the South African flights. These samples also show enhancements in chloroform (CHCl_3), toluene and benzene. This hints at a possible anthropogenic source of trihalomethanes although a biogenic source cannot be ruled out. Disinfection of seawater, freshwater and wastewater is a known anthropogenic source of halomethanes (Quack & Wallace, 2003, and references therein). However, it would be expected that CHBr_3 would show an enhancement if this was the case. Due to the altitude of the CARIBIC aircraft and the limitations of following a commercial flight-path, it is not possible to attribute these elevated samples to a distinct source. However, we believe that there is some indication of a source of mixed bromochloromethanes that is independent of CHBr_3 and CH_2Br_2 .

4.4 Summary and conclusions

We report the mixing ratios of five brominated VSLB in samples collected on three routes of the CARIBIC aircraft during 2009–2013. Across the three routes analysed, mean tropical mid-UT mixing ratios were: CHBr_3 , 0.43 ppt; CH_2Br_2 , 0.74 ppt; CHBr_2Cl , 0.14 ppt; CHBrCl_2 , 0.23 ppt and CH_2BrCl , 0.11 ppt. Total bromine across all routes in the tropical mid-UT was 3.4 ± 1.5 ppt. These values agree well with values reported in the 2010 WMO O_3 assessment (Montzka & Reimann, 2011). Using a 2008 value of 15.2 ± 0.2 ppt for bromine from Halons and methyl bromide (Montzka & Reimann, 2011), VSLB across all routes accounts for $\sim 19\%$ of total bromine. As the anthropogenic contribution to atmospheric bromine (mainly halons and methyl bromide) is expected to decrease, coupled with the potential changes in emissions due to climate change (e.g. increases in wind speeds, ocean temperatures etc.), emissions of VSLB are likely to become proportionally more significant in the future.

For each of the tropical regions covered in this study, mid-UT VSLB $\Sigma \text{Br}_{\text{org}}$ was 3.7 ppt for FRA-CCS/BOG, 3.4 ppt for the FRA-CPT and 4.2 ppt for BKK-KUL. Mixing ratios of CHBr_3 , CHBr_2Cl , CHBrCl_2 and CH_2BrCl were similar between these three routes: CH_2Br_2 was relatively enhanced in the Southeast Asian flights and is the main contributor to the 0.5–0.8 ppt enhancement of total organic bromine compared to Central American and South African tropical mixing ratios.

The percentage contribution of the three minor VSLB (CHBr_2Cl , CHBrCl_2 and CH_2BrCl) to total organic bromine derived from the species analysed across all routes in the tropical mid-UT was $18 \pm 4.8\%$ (range 11–46); CHBr_3 and CH_2Br_2 together contributed $82 \pm 4.8\%$ (54–89). Individual contributions were $34 \pm 13\%$ (4.7–71) for CHBr_3 , $48 \pm 12\%$ (14–73) for CH_2Br_2 , $7.8 \pm 2.0\%$ (2.8–22) for CHBr_2Cl , $6.9 \pm 3.0\%$ (3.8–25) for CHBrCl_2 and $3.6 \pm 1.3\%$ (0.0–7.2) for CH_2BrCl .

Considering that these measurements were made at 10–12 km, below the tropical tropopause layer (TTL) (~ 12 –17 km), further decomposition will occur during ascent in to the stratospheric overworld. This implies that these values constrain the contribution of VSLB to stratospheric bromine to the lower end of 6 (3–8) ppt of stratospheric BrO required by WMO 2010 to balance the stratospheric bromine budget. Though this study is limited latitudinally, altitudinally and temporally, the large range and number of regular flights means that the CARIBIC passenger

aircraft will continue to be an important source of UTLS and free tropospheric data in the future.

Biomass burning and background emissions in SAMBBA

5.1 The SAMBBA campaign

The South American Biomass Burning Analysis (SAMBBA) field experiment took place during September-October 2012 over Brazil. The main aims of SAMBBA were to quantify and better understand South American burning emissions and the chemical and physical processes associated with burning, to assess the impacts of biomass burning and to evaluate/validate models and remote sensing observations related to biomass burning. These broad aims were mainly focused around processes influencing aerosols in biomass burning. However, a large number of supporting measurements were made during the campaign.

5.2 Analysis and supporting measurements

The main analysis platform utilised in SAMBBA was the Facility for Airborne Measurements (FAAM), modified BAe 146-301 research aircraft as part of the National Center for Atmospheric Science (NCAS) in association with the Met OfficeTM and the Natural Environmental Research Council (NERC).

A number of atmospheric measurements were made on board the aircraft including CO, CO₂, CH₄, O₃, NO_x, PAN, volatile organic compounds (VOCs) and a suite of aerosol measurements. In addition, whole air samples were collected in 128 SilcosteelTM-coated, 3 L bottles for analysis after the campaign. These were filled to ~3 bar with a fill time of ~10–20 s. Analysis at UEA was performed within 4–7 months of collection.

5.2.1 Instrumental set-up and methods

Bottle samples were analysed at UEA using a gas chromatograph-electron ionisation mass spectrometer (GC-EI-MS) with an EntechTM 7100A Pre-concentrator inlet system. Accurately measured samples (~500 mL, flow rate ~100 mL min⁻¹) were dried with a magnesium perchlorate (Mg(ClO₄)₂) drier prior to pre-concentration. Chromatographic separation was achieved using a GC-GasProTM capillary column (30 m × 320 μm, Agilent Technologies) using research

Table 5.1: Compound dependent limits of detection (LOD), mean analytical precisions, mixing ratio in the standard used for calculations of compounds analysed in SAMBBA samples and ion mass-to-charge ratio (m/z) used for quantification. Precisions are the 1σ standard deviation of duplicate samples.

Species	Formula	LOD [ppt]	Precision [%]	Mixing Ratio [ppt]	m/z
Methylchloride	CH ₃ Cl	0.29	2.3	639	52
Methylbromide	CH ₃ Br	0.037	2.5	8.3	96
Methyliodide	CH ₃ I	0.018	10	0.21	142
Dichloromethane	CH ₂ Cl ₂	0.073	3.2	63.9	84
Dibromomethane	CH ₂ Br ₂	0.042	4.7	0.99	174
Chloroform	CHCl ₃	0.19	4.1	11.7	83
Bromoform	CHBr ₃	0.021	5.7	0.75	173
Carbon tetrachloride	CCl ₄	0.10	3.5	90.9	117
CFC-12	CCl ₂ F ₂	0.030	2.4	535.1	85
PCE	C ₂ Cl ₄	0.020	5.3	3.74	166
Chlorobenzene*	C ₆ H ₅ Cl	-	4.4	N/A	112
Carbonylsulfide	COS	0.063	2.8	555	60

* Chlorobenzene is not calibrated in the standard. Therefore, values for LOD, blank and standard mixing ratio have not been reported.

grade helium (≥ 99.9995 % purity) as the carrier gas and by temperature-programmed gas chromatography (-10 °C hold 2 min, 10 °C min⁻¹ to 145 °C, 20 °C min⁻¹ to 200 °C hold 2 min). The column eluent was subjected to electron ionisation prior to detection by a quadrupole mass selective detector operating in single ion mode. SAMBBA bottle measurements are reported here as dry-air mole fractions, pmol mol⁻¹ (dry air), abbreviated here to ppt (parts per trillion).

Mixing ratios were determined by comparison with a working standard with known mixing ratios. The working standard was a 34 L electro-polished stainless steel canister (SX706070, Essex Cryogenics, St. Louis MO, US). Analytical uncertainties were calculated on a per-run basis and are the 1σ standard deviation of duplicate samples on the respective day of measurement (see below). Estimated limits of detection (LODs) in parts per trillion (ppt), average compound-dependent analytical precisions and the mixing ratios of the working standard are shown in Table 5.1.

Due to the nature of the EntechTM pre-concentration system it is not possible to trap a sample of carrier gas without passing the gas through the inlet system. This makes attribution of a blank impurity to the carrier gas or the trapping system impractical. A system blank was assessed by accurately sampling 1 L research grade N₂ (≥ 99.9995 % purity) through the system using the same inlet and sampling methodology as for air samples with comparison to a 1 L sample of the working standard. Blanks assessed in this manner were typically <0.8 % for compounds reported in this study. As blank contamination cannot be attributed to the N₂ gas or the system, they have not been applied to calculation of precision values or to correction of sample mixing ratios.

5.2.2 Carbon monoxide measurements

During the campaign CO data was collected using a high time resolution Aerolaser instrument by FAAM. High-frequency measurements were subsequently averaged to the bottle-filling period for each bottle sample collected (James Lee, UoY). CO measurements were repeated at the University of East Anglia on a subset of bottle samples collected during the campaign ~ 6 – 7 months after

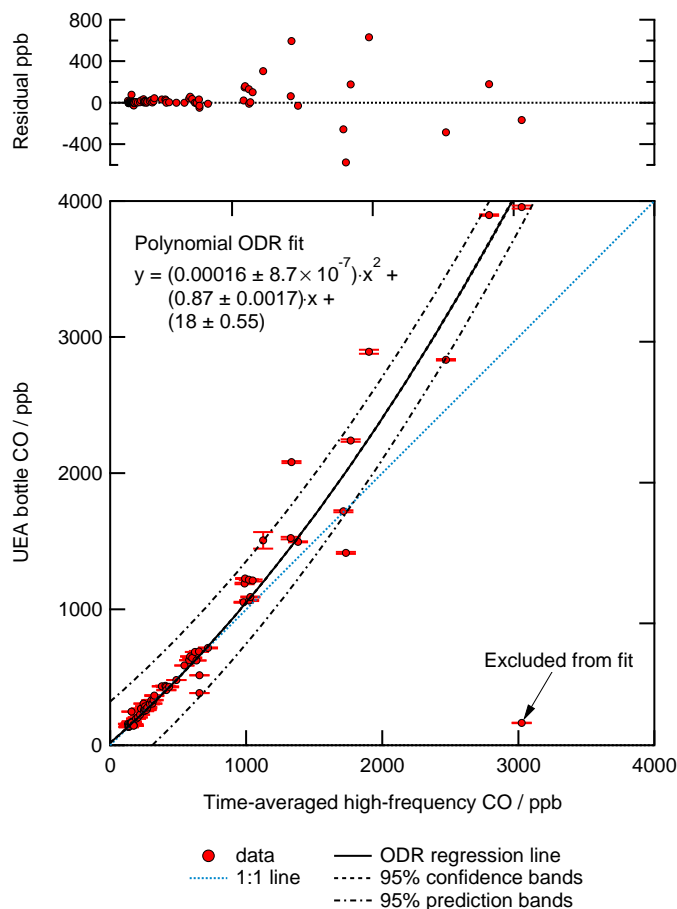


Figure 5.1: Comparison of CO data derived from time-averaged in situ high-frequency measurements and bottle measurements. Error bars on the bottle data represent precision and are $\pm 1\sigma$. Included is a 3rd order polynomial orthogonal distance regression (ODR) fit to the data. 95% confidence and prediction bands are shown as well as the equation of the fit line. Errors in the fit are $\pm 1\sigma$. The labelled outlier was excluded from the fit.

collection. The bottles chosen for analysis included those used for sampling biomass burning plus a small subset of background samples. CO bottle measurements were performed using a modified commercial Reduction Gas Analyser (RGA3, Trace Analytical, Inc., California, USA) which includes gas chromatography followed by reduction of mercuric oxide and detection of mercury vapour by UV absorption. Further details including calibration, non-linearity characterisation and further instrumental details can be found in Forster et al. (2012).

Plotting time-averaged and bottle measurements against each other should closely fit an idealised 1:1 line. However, as can be seen in Figure 5.1, time-averaged CO data underestimates bottle CO at mixing ratios above ~ 1000 ppb. Also shown in Figure 5.1 is a 3rd order polynomial orthogonal distance regression (ODR) fit to the data that closely approximates this trend. Additionally, there is one significant outlier in the time-averaged CO data that is not present in the bottle CO. This is probably due to an error in averaging the high-frequency CO data.

Bottle sampling often takes place over a longer time-scale (~ 20 s) than the transit time of the aircraft across the burning plume (plumes were on the order of ~ 10 s across). Therefore, time-averaged and bottle CO data can be a mixture of background air and plume air. Hypothetically, and particularly during higher CO mixing ratios, a small discrepancy between the averaging period

and the actual sampling period could lead to a discrepancy between measurements. Taking this into account it is possible that the in situ CO data were averaged over a shorter period than bottle sample collection, leading to an underestimation of higher mixing ratios of CO. However, high-frequency CO data show that a number of plume shapes were sampled during the bottle-filling period. This makes inappropriate assignment of the time-averaging period an unlikely explanation for the discrepancy as it would be expected that this would be dependent on the plume shape sampled.

It is also possible that non-linearities in either the high-frequency measurements or the bottle measurements could have led to the discrepancy. This is unlikely in the bottle data as linearity has been quantified and instrument calibration is performed using a range of six CO standards. Four standards are on the NOAA2004 range for CO (61.8 ppb, 105.2 ppb, 192.9 ppb and 201.7 ppb) with two high range standards (1400 ppb and 5005 ppb) determined using an aerolaser instrument via linear extrapolation of the NOAA2004 range (further details can be found in Forster et al., 2012). Additionally, non-linearities in the high-frequency instrument are considered unlikely.

A further possibility is production or loss of CO in the bottles during storage which would cause a discrepancy during inter-comparison. The comparison in Figure 5.1 indicates that growth in the bottles is a possibility. This cannot be ruled out as bottle CO measurements were made over a period of 2 days and we were unable to perform repeat measurements to assess growth in the bottles due to time restrictions. However, at higher mixing ratios, growth in the bottles would have to account for ~ 1 ppm of CO. This is a large quantity of CO and seems unlikely to be the sole cause of the discrepancy. Furthermore, there is no evidence for CO growth in samples below 1 ppm CO, where there is close to linear agreement between the two datasets (see Figure 5.1).

Due to the relatively small temporal scale of the fire plumes encountered, any discrepancies in the timestamps recorded for the high-frequency data and bottle filling period could have a significant effect on comparability of mixing ratios. Similarly, differences in the time-lag between air entering the aircraft inlet and reaching the instrument or bottle-pack and internal time-lags within the instrument could be significant.

Finally, it is likely that bottles do not fill evenly throughout the filling period. As bottles are evacuated prior to use, filling is probably faster earlier in the filling period than later when the pressure in the bottles exceeds atmospheric pressure. However, as mentioned in regard to the time-averaging period, a number of peak shapes were sampled. No pattern can be observed that would match the expected rate of filling of bottles e.g. a larger discrepancy when the highest mixing ratios were sampled at the beginning of the bottle filling. The rate of filling of bottle samples was not quantified in this study but this might be useful in future studies.

In conclusion, a number of factors may be responsible for the disagreement in bottle and time-averaged high-frequency CO measurements. This highlights the limitations of aircraft-based bottle measurements of narrow plumes. Future studies should take account of the difficulties in utilising these measurements. Further investigation of CO stability in bottles would be useful in ruling out growth of CO. Additionally, similar aircraft-based studies would be improved by utilising bottle measurements of all reference species of interest (i.e. CO, CO₂, CH₄) instead of relying on in situ time-averaged data.

In this study bottle-derived CO has been used in the calculation of normalised emission ratios (NEMRs) to eliminate errors arising from comparison of high-frequency and bottle data. However,

for calculations of emission factors and modified combustion efficiencies, time-averaged CO, CO₂ and CH₄ data have been utilised. This has been done to minimise factors arising from inter-comparison of high-frequency and bottle data. A comparison of NEMRs derived from time-averaged and bottle measurements can be found in Table 5.2 and is discussed further in Section 5.4.2.2.

5.3 Emission ratios and emission factors

Reporting absolute mixing ratios of a species in a fire-plume does not give an accurate impression of the strength of fire emissions due to mixing of background air into the plume and variation in the burning phase of the fire i.e. smouldering and flaming combustion. To account for this variation, emission ratios are utilised to quantify emissions from fires. Emission ratios (ERs) are the ratio of a substance of interest to a reference species (e.g. CO or CO₂). This only represents the ‘true’ emission from a fire at the source and is not usually practical to measure in the field (Akagi et al., 2011). To this end, fire emission information is commonly represented using normalised emission ratios (NEMR, see Section 5.3.1) and emission factors (EF, Section 5.3.2). These metrics of fire emission remove the influence of mixing by referencing a co-emitted gas (in the case of NEMR) or the quantity of fuel burned (in the case of EF). In practice, EFs based exclusively on atmospheric observations are usually derived from NEMRs.

There is a degree of disagreement in the literature about the appropriate term for emission ratio. To clarify, in this work, emission ratio (ER) refers to the uncorrected ratio of species usually only used for measurements at source, and normalised emission ratio (NEMR) is used for the ratio of excess mixing ratios of two species.

5.3.1 Normalised emission ratio (NEMR)

Normalised emission ratios (NEMRs) can be obtained by two methods:

1. By taking the ratio of the fire-plume enhancement in a species of interest to the enhancement in a simultaneously measured reference gas (e.g. CO or CO₂).
2. By determining the gradient of a linear regression line of the enhancements in the species of interest and the reference gas.

Enhancements, also termed excess mixing ratios, are calculated by subtracting a background value from the measured value of the species and often denoted ‘ΔX’. These values represent the degree of plume dilution (Yokelson et al., 1999). For example the emission ratio of compound X relative to CO is given by Equation 5.1 (e.g. Andreae & Merlet, 2001).

$$ER_X = \frac{\Delta X}{\Delta CO} = \frac{[X]_{\text{plume}} - [X]_{\text{ambient}}}{[CO]_{\text{plume}} - [CO]_{\text{ambient}}} \quad (5.1)$$

Commonly, NEMRs are reported relative to CO for compounds emitted in the smouldering phase of a fire, and relative to CO₂ for compounds emitted during the burning phase. The smouldering phase of a fire is oxidatively poor and would be expected to be the source of more reduced compounds such as halocarbons and hydrocarbons (e.g. Andreae & Merlet, 2001). CO is also dominantly released during smouldering combustion and is therefore suitable as a reference

gas for other gases emitted in this phase. Correlations of smouldering-derived gases with CO₂ are relatively poor compared to correlations with CO (Lobert et al., 1999). This is due to the variability in the proportion of flaming combustion between and within fires resulting in variable smouldering-derived trace gas to CO₂ ratios. The burning phase of a source fire can be quantified by defining a combustion efficiency (see Section 5.3.3).

As the majority of biomass carbon is released in the form of CO₂, the NEMR of a gas to CO₂ can be utilised to estimate the emission of trace gas from fires based on the amount of biomass burned. This is possibly the most suitable parameter for regional and global emission estimates. Smouldering species are often related to CO₂ for this purpose either by calculating an NEMR from the regression slope for the species relative to CO₂ (assuming a strong correlation exists) or by deriving NEMRs relative to CO and multiplying that with the average CO/CO₂ NEMR for the fire e.g. Equation 5.2 (Andreae & Merlet, 2001).

$$ER_X = \frac{\Delta X}{\Delta CO_2} = \frac{\Delta X}{\Delta CO} \times \frac{\Delta CO}{\Delta CO_2} \quad (5.2)$$

During airborne observations, NEMRs derived on an individual sample basis are only sensible when the sampling time is less than or similar to the transit time across a plume. Practically, this is only possible with high frequency instruments as transit times across a plume in aircraft studies can be on the order of seconds. Furthermore, determination of a suitable background mixing ratio for the species of interest and the reference species is necessary. When sampling time exceeds the plume transit time or when it is not possible to determine representative background levels (e.g. when distant from source), NEMRs can be determined from the gradient of a linear regression slope between the mixing ratio of the species versus the reference gas (Andreae et al., 1996; Ferek et al., 1998).

Regression calculations should use the least orthogonal distance regression (ODR) method as there are errors in both the dependent and independent variables (Cantrell, 2008). Regression-derived NEMRs are usually calculated from enhancements in the species of interest and enhancements of a relatively non-reactive reference species where background measurements are available. Enhancements are used to account for mixing with background air during plume evolution.

5.3.2 Emission factor (EF)

In theory and in laboratory conditions, EF is the ratio of grams of carbon in species *X* emitted from a fire to grams of carbon in the fuel.

$$EF_X = \frac{[C]_X}{[C]_{fuel}} \quad (5.3)$$

Concentrations given in Equation 5.3 are mass concentrations. In the field, it is not usually feasible to know the carbon content of the fuel being burned. Therefore, for field campaigns, the EF is normally calculated by taking the ratio of carbon in species *X* to the carbon in all measured species and multiplying that by a factor approximating the carbon content of woody fuels as in Equation 5.4 (Ferek et al., 1998; Yokelson et al., 1999).

$$EF_X = F_C \cdot \frac{[X]}{[C]_{CO_2} + [C]_{CO} + [C]_{CH_4} + [C]_{NMHC} + [C]_{PC\dots}} \quad (5.4)$$

Where F_C is the fraction of carbon in the fuel. $[X]$ is the mass concentration of species X . $[C]_{CO_2} + [C]_{CO} + [C]_{CH_4} \dots$ is the sum of the mass concentrations of all measured carbon-containing species. EFs are normally expressed either in units of grams of X emitted per kilogram carbon burned e.g. g/kgC or grams of carbon in X per kilogram of carbon burned e.g. g(C)/kg(C). The expressions for EF when using molar mixing ratios and NEMRs are given in Equations 5.5 and 5.6 (Simpson et al., 2011).

$$EF_X \left(\frac{g}{kg} \right) = F_C \cdot \frac{M_X}{M_C} \cdot \frac{C_X}{C_T} \quad (5.5)$$

where

$$\frac{C_X}{C_T} = \frac{\frac{\Delta C_X}{\Delta CO}}{\sum_{Y=1}^n \left(nC_Y \cdot \frac{\Delta C_Y}{\Delta CO} \right)} \quad (5.6)$$

Where $\Delta C_X/\Delta CO$ is the NEMR of species X to CO. nC_Y is the number of carbon atoms in compound Y and the sum is over all carbon-containing species as in Equation 5.4 (Simpson et al., 2011). Equation 5.6 assumes that NEMRs have been calculated relative to CO, however, CO₂ or another species could be used.

5.3.3 Modified combustion efficiency (MCE)

Combustion efficiency (CE) is the molar ratio of fuel carbon emitted as CO₂ from a fire to total excess carbon (Equation 5.7, Sinha, 2003).

$$CE = \frac{\Delta C_{CO_2}}{\Delta C_{CO_2} + \Delta C_{CO} + \Delta C_{CH_4} + \Delta C_{NMHC} + \Delta C_{PC}} \quad (5.7)$$

It is difficult to measure all the species required for CE in the field. Therefore, modified combustion efficiency (MCE, Equation 5.8) is often used as an indicator of the stage of a fire's combustion. MCE ranges from near 0.8 for smoldering combustion to 0.99 for 100 % flaming combustion. Since CH₄, NMHC and PM are emitted in relatively small quantities compared to CO₂ and CO, the difference between CE and MCE is only a few percent (Sinha, 2003).

$$MCE = \frac{\Delta CO_2}{\Delta CO_2 + \Delta CO} \quad (5.8)$$

5.4 Results and discussion

5.4.1 Flight classification

Bottle samples were collected on eight flights mainly in the region of Porto Velho, Brazil where the aircraft was based. These included flights to sample regional haze, forest fire burning emissions, background emissions (including one flight from Porto Velho to Manaus) and cerrado fire emissions (one local flight in the region of Palmas). These flights fall into four categories (bottle sample locations are shown in Figure 5.2).

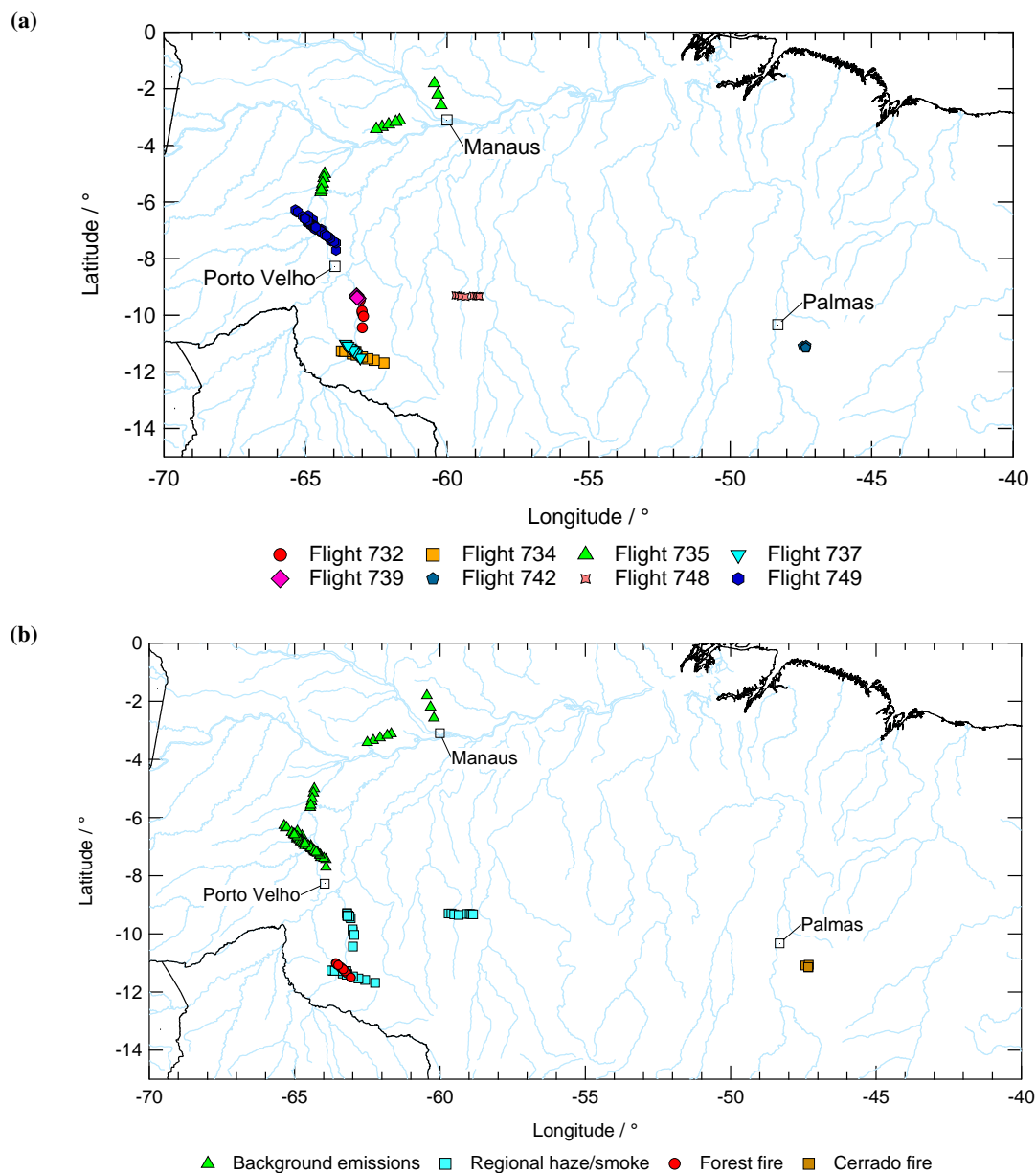


Figure 5.2: Locations of bottle samples (a) grouped by flight number and (b) grouped into the four categories described in Section 5.4.1.

Forest fires

Consisting of one flight where a forest fire plume was sampled multiple times close to source, flight 737 (see Figures 5.2 and 5.3a).

Cerrado fires

Consisting of one flight where a number of cerrado savannah fires were sampled close to source, flight 742 (see Figures 5.2 and 5.3b).

Regional haze/smoke

Consisting of four flights in the region of Porto Velho where smoke from forest fires, either as regional haze or from identified fires, was present but was not sampled close to source (see Figure 5.2).

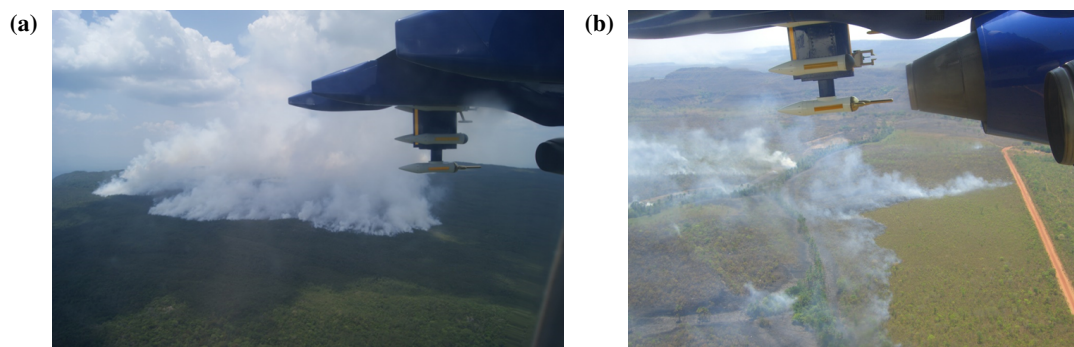


Figure 5.3: Photographs taken from the FAAM aircraft of (a) the forest fire sampled during flight 737 (courtesy of Jim McQuaid) and (b) cerrado savannah fires sampled during flight 742 (courtesy of Alex Wellpot).

Background flights

Consisting of two flights in the region between Porto Velho and Manaus over forest where no fires were observed (see Figure 5.2).

5.4.2 Biomass burning

Positive trends with increasing CO in biomass burning samples were observed for the methyl halides (CH_3Cl , CH_3Br and CH_3I), carbonyl sulfide (COS) and chlorobenzene. These are discussed further in Sections 5.4.2.2, 5.4.2.5 and 5.4.2.4 respectively.

Of the species measured in bottle samples (see Table 5.1 and Figure 5.4) the other halocarbons of interest do not show a positive trend with CO. It is not surprising that CFCs and HCFCs are not emitted from biomass burning; Yokelson et al. (2008) reported an emission factor of 2.8 mg kg^{-1} for CFC-12 without any further comment and Simpson et al. (2011) reported a small plume enhancement of HCFC-141b but could not find any evidence that fire-induced convection was a contributing factor. To my knowledge, no other studies have found evidence for biomass burning emissions of CFCs or HCFCs. However, this data confirms that CHCl_3 , CH_2Cl_2 and naturally occurring short-lived bromocarbons, i.e. CHBr_3 , CH_2Br_2 , CHBr_2Cl , CHBrCl_2 and CH_2BrCl , are not emitted from biomass burning at least in the Amazon basin and cerrado savannah regions of Brazil. CHCl_3 has been previously reported as having a minor source from biomass burning (Keene et al., 1999; Lobert et al., 1999). Similarly, CH_2Cl_2 was reported as having biomass burning sources (e.g. Simmonds et al., 2006). However, as suggested by Simpson et al. (2011), it is likely that CHCl_3 and CH_2Cl_2 are not emitted from biomass burning.

In the following discussion, calculations of NEMRs used bottle CO mixing ratios. EFs and MCEs used CO mixing ratios derived from time-averaged 1 Hz data (as discussed in Section 5.2.2). Bottle CH_4 and CO_2 values were derived from time-averaged 1 Hz in situ measurements.

5.4.2.1 Halomethane background mixing ratios

Background mixing ratios were derived from samples collected during background emission flights (see Figure 5.2). These samples had consistently low CO mixing ratios (130–180 ppb), although this mixing ratio range is higher than the monthly mean, in the region of the background flights, for September 2012 of ~ 80 ppb (NASA Earth Observations (NEO), 2012). It is possible

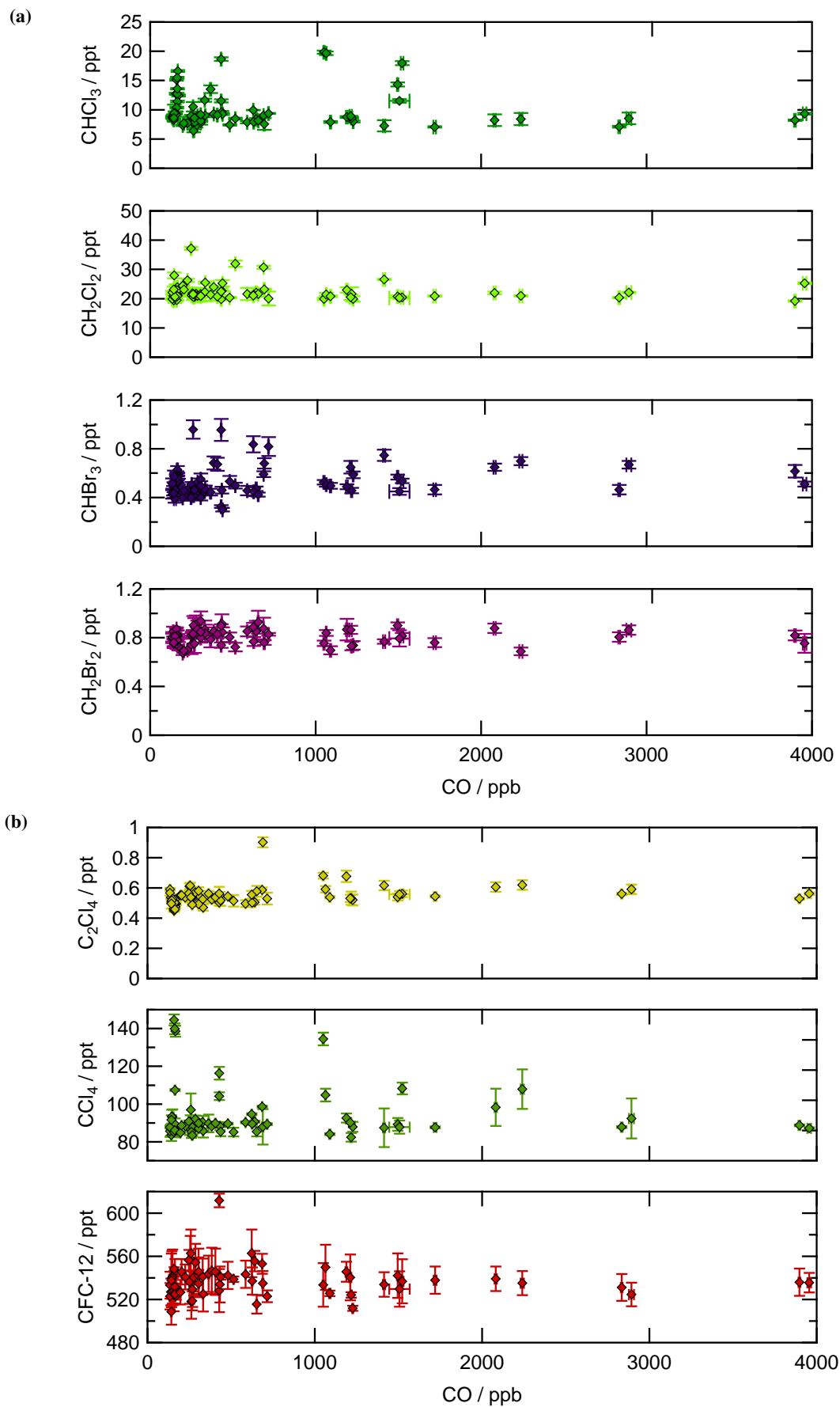


Figure 5.4: Plots against CO for (a) CHCl₃, CH₂Cl₂, CHBr₃ and CH₂Br₂ and (b) PCE (C₂Cl₄), CCl₄ and CFC-12 (CF₂Cl₂). Error bars represent analytical uncertainties.

that these background samples were somewhat influenced by regional biomass burning emissions. However, there is no indication, in bottle samples, of elevated levels of burning or anthropogenic tracers such as hydrocarbons (see Section 5.4.3.1 for further details). It is possible that there is some photochemical production of CO from biogenic emissions, such as isoprene. This is discussed further in Section 5.4.3.1. Baseline CO mixing ratios close to biomass burning plumes were similar to background sample CO.

MeCl, MeBr and MeI background mixing ratios were ~ 620 – 720 ppt, ~ 7 – 10 ppt and ~ 0.5 – 1.5 ppt respectively. Background mixing ratios are defined here as the mean of background samples. This gives values for CO, MeCl, MeBr and MeI of 150 ppb, 670 ppt, 8.3 ppt and 0.88 ppt respectively, rounded to two significant figures.

5.4.2.2 Halomethane normalised emission ratios (NEMRs)

Over the range of CO mixing ratios sampled (~ 130 – 4000 ppb) MeCl increases from ~ 645 to ~ 1400 ppt, MeBr ~ 7.8 – 27 ppt and MeI ~ 0.6 – 7.2 ppt.

Normalised emission ratios (NEMRs) have been calculated by taking the gradient of a linear fit to the enhancement of the species of interest (ΔMeX) versus the enhancement of CO (ΔCO) in fire plume samples. Fits are orthogonal distance regressions (ODRs) weighted by the analytical errors of the data. Orthogonal distance regression analysis minimizes the orthogonal distance of residuals rather than the square of residuals and is more suited to datasets where there are errors in both variables (Cantrell, 2008). ODR fits were performed using the inbuilt function in Igor ProTM. There are a number of different options for the application of a linear fit to the data.

1. Linear fit to the data weighted by data errors without further constraints.
2. Linear fit to the data weighted by data errors with the y-intercept forced through the origin. As only enhancements over background mixing ratios are considered in NEMR estimates, ΔMeX would be expected to be 0 at $\Delta\text{CO} = 0$. This relies on a well-defined background.
3. Linear fit to the data weighted by data errors including negative values of ΔMeX and ΔCO . As ΔMeX could not be practically determined on a flight-by-flight basis, it is possible that background ΔMeX (determined from a set of background flights) are not representative for biomass burning flights. Using negative values eliminates errors arising from poor background estimation. This is equivalent to a linear fit to MeX vs CO.
4. Linear fit combining negative values of ΔMeX with the y-intercept forced through the origin i.e. a combination of the two methods given above.

A comparison of methyl halide NEMRs of forest fires, derived from the linear fit methods outlined above and from averaging of individual sample $\Delta\text{MeX}/\Delta\text{CO}$ is shown in Table 5.2. Means of individual sample $\Delta\text{X}/\Delta\text{CO}$ are given as ‘Mean’ in Table 5.2. Errors in the fit method are $\pm 1\sigma$ of the fit line. Errors in the mean values are $\pm 1\sigma$ and represent the variability of $\Delta\text{MeX}/\Delta\text{CO}$. The averaging method overestimates NEMR_{CO} compared to the linear fit method. Additionally, the errors are larger for the averaging method. A large range of individual sample NEMRs were sampled over the course of the forest fire flight (flight 737). This is reflective of the variability of emission of these compounds as a function of the burning state of the fire (discussed below). Given the limitations of aircraft-based plume sampling (see Section 5.3.1), I consider the

Table 5.2: Comparison of NEMR_{CO} calculation methods and available CO datasets for forest fire samples (flight 737). Linear regression values are calculated as the gradient of an least orthogonal distance regression fits to enhancements in CO and MeX weighted by the errors in the data (see Section 5.3.1). Fits were repeated with the fit forced through the origin ($a = 0$), with negative values of ΔMeX and ΔCO (neg. Δ) and with both constraints ($a = 0, \text{neg.}\Delta$). For these values errors are the 1σ standard deviation of the fit. Mean values are the mean of individual sample $\Delta\text{X}/\Delta\text{CO} \pm 1\sigma$. All values are given to 2 significant figures.

CO dataset	Method	$\text{NEMR}_{\text{CO}}/\times 10^{-6}$		
		CH_3Cl	CH_3Br	CH_3I
Bottle CO	Lin. reg.	180 ± 5.1	5.0 ± 0.10	1.4 ± 0.042
	$a = 0$	180 ± 5.0	5.3 ± 0.091	1.4 ± 0.036
	neg. Δ	180 ± 5.2	5.0 ± 0.010	1.5 ± 0.038
	$a = 0, \text{neg.}\Delta$	180 ± 5.0	5.3 ± 0.091	1.3 ± 0.035
	Mean	210 ± 170	14 ± 29	1.7 ± 0.48
Time-av. CO	Lin.reg.	240 ± 11	6.5 ± 0.22	1.7 ± 0.069
	$a = 0$	230 ± 8.3	6.8 ± 0.20	1.7 ± 0.057
	neg. Δ	240 ± 10	6.5 ± 0.22	1.9 ± 0.068
	$a = 0, \text{neg.}\Delta$	220 ± 8.2	6.8 ± 0.20	1.7 ± 0.057
	Mean	190 ± 73	12 ± 17	1.9 ± 0.53

linear regression method of deriving NEMRs, $a = 0$ (Table 5.2) where a well-defined background measurement is available, more appropriate for this study.

Given the discussion in Section 5.2.2, both methods for deriving NEMRs have been repeated using bottle-derived CO measurements and time-averaged, in situ 1 Hz CO data (see Table 5.2). NEMRs derived from time-averaged CO data are higher than those from bottle-derived CO. This is to be expected from the comparison in Figure 5.1. As NEMRs are derived from plume enhancements, lower CO values, where there is little to no discrepancy, are selectively removed. At higher CO mixing ratios, CO is underestimated in time-averaged data leading to a higher ratio of methyl halide to CO. Errors for fits to time-averaged data are higher than those for bottle CO, indicating that time-averaged measurements are less reliable than bottle measurements.

Figure 5.5 shows the results of ODR fits for ΔMeCl , ΔMeBr and ΔMeI against ΔCO for forest fire, cerrado fire and regional haze/smoke. For each fit line in Figure 5.5, 95 % confidence intervals are shown. This is plotted to give an indication of the statistical significance of the fit lines and is the complement of a significance level of 0.05 i.e. non-overlapping confidence intervals imply a statistically significant difference between fit lines. It should be noted that samples of regional haze/smoke cover a smaller range of CO values than samples collected near the source of a fire. Linear regressions for ΔMeCl indicate that cerrado and forest fires sampled have significantly different NEMRs (300×10^{-6} for cerrado fires and 180×10^{-6} for forest fires). NEMRs for MeBr indicate that there is also a significant difference in NEMRs between forest ($\text{NEMR} = 5.3 \times 10^{-6}$) and cerrado fires ($\text{NEMR} = 4.1 \times 10^{-6}$). However, in contrast with MeCl, forest fires have stronger emissions than cerrado fires. Methyl iodide shows no significant difference between forest and cerrado fires. However, the data for this compound are more scattered. This is probably as a result of the comparatively short lifetime of methyl iodide.

Normalised emissions ratios for regional haze/smoke samples are not significantly different from cerrado fires, in the case of MeCl, or from forest fires, in the case of MeBr. The difference

between fit lines for MeBr in cerrado and regional haze/smoke is small enough to not be appreciably different given the limited number of samples. For MeI haze/smoke samples, the NEMR is lower than cerrado or forest fires by $0.54\text{--}0.64 \times 10^{-6}$.

There have been a limited number of studies of Brazilian biomass burning in the literature. Table 5.3 summarises literature values for NEMR with comparison to values derived in this study. Values from Blake et al. (1996) are from 800 km NNE of Brasilia mainly over cerrado savannah vegetation. Additionally, the boundary layer is described as being "... affected by a grassland and rainforest fires and, though somewhat unclear, it appears that the given NEMRs are derived from samples from all of these vegetation types. SAMBBA NEMR_{CO} for MeCl in forest fires is lower at 180×10^{-6} compared to 529×10^{-6} in Ferek et al. (1998). SAMBBA MeBr (5.3×10^{-6}) and MeI (1.4×10^{-6}) are also lower than Ferek et al. (1998) (10×10^{-6} and 5×10^{-6} respectively). This could reflect the mixture of sources sampled in Ferek et al. (1998). MeCl NEMR_{CO} for SAMBBA cerrado savannah fire is lower by 550×10^{-6} than the value given in Blake et al. (1996). MeBr is 6.5×10^{-6} lower and MeI 1.3×10^{-6} lower. This is possibly due to sampling of haze over the cerrado rather than direct emissions or the lack of defined background values for CO or the species of interest. Andreae & Merlet (2001) do not report NEMR_{CO}. Comparison of cerrado emissions is complicated by the variability of vegetation in this region. Ward et al. (1992) describes cerrado vegetation as "... a continuum along a soil fertility and fire gradient from open tropical grassland ... to forest ...". Furthermore, emission ratios of halogenated compounds are affected by the halogen content of biomass fuel (e.g. Lobert et al., 1999). It should be noted that differences in calibration scales, methods of sample collection and analysis limit inter-comparison with literature values.

Methyl halides are thought to be mainly emitted during smoldering phase of a fire (e.g. Ferek et al., 1998). To probe this, the modified combustion efficiency (MCE) can be used as an indicator of the degree of smoldering/flaming combustion (see Section 5.3.3). Lower values are indicative of smoldering combustion whereas higher values indicate flaming combustion. Figure 5.6 shows plots of ΔMeX ($X = \text{Cl, Br or I}$) against MCE for samples from forest fires. All three methyl halides show a negative trend in plume enhancements with decreasing MCE. This confirms that methyl halides, in the case of Amazonian forest fires, are emitted more strongly from smoldering fires. Cerrado savannah fire samples were all taken in plumes with a high MCE (0.92–0.95) with higher plume enhancements than forest fires. However, the trend with MCE for cerrado fires is uncertain as only three samples had CO₂ data available to calculate MCEs from.

5.4.2.3 Halomethane emission factors (EFs)

Emission factors for this study are based on the mass balance method outlined in Section 5.3.2. A number of species were measured in the bottled samples, including non-methane hydrocarbons (NMHCs), and particulates. However, limited data availability requires that EFs are reported relative to total carbon derived from CO, CO₂ and CH₄ only. This is known to be accurate to within a few percent of the total carbon emitted in all carbon-containing species (e.g. Simpson et al., 2011; Akagi et al., 2013).

Emission factors for the methyl halides are given in Table 5.3 in units of milligrams emitted of the species of interest per kilogram of dry matter burned (mg kg^{-1}). This requires knowledge of

Table 5.3: Emission ratios relative to CO and CO₂ (NEMR_{CO} and NEMR_{CO₂} respectively), emission factors (EF) and modified combustion efficiencies (MCE) from the literature. NEMRs for this study include are derived from a linear orthogonal distance regression (ODR) fit with y-intercept forced through the origin of $\Delta\text{CH}_3\text{X}$ (X = Cl, Br or I) against ΔCO (derived from bottle measurements). EFs are in units of milligrams species per kilogram dry matter burned (mg kg^{-1}) and use CO, CO₂ and CH₄ derived from time-averaged high-frequency measurements (see Section 5.2.2 for discussion of bottle and high-frequency measurements). EFs for methyl halides are the mean of all plume samples with ranges in parentheses as they show a strong trend with MCE (see text).

Compound	NEMR _{CO} × 10 ⁻⁶	NEMR _{CO₂} × 10 ⁻⁶	EF/ mg kg ⁻¹	MCE	Source	Comments
CH ₃ Cl	180 ± 5.0	-	61 (25–98)	0.76–0.98	This study	Forest fire
	300 ± 3.3	-	60 (44–71)	0.92–0.95		Cerrado fire
	290 ± 11	-	-	-		Regional haze/smoke
	520 ± 170	-	~ 110 *	-	Ferek et al. (1998)	Brazil
	-	-	20-180	-	Andreae & Merlet (2001)	Tropical forest
	-	-	53	-	Akagi et al. (2011)	Tropical Forest
	850 ± 60	27 ± 4	-	-	Blake et al. (1996)	Brazil (Cerrado/haze)
	-	-	75 ± 29	-	Andreae & Merlet (2001)	Savannah & grassland
	-	-	55	-	Akagi et al. (2011)	Savannah
	980 ± 40	21 ± 2	-	-	Andreae et al. (1996)	Southern Africa
	1040 ± 130	53 ± 3	-	-		
1010 ± 60	14 ± 8	-	-			
CH ₃ Br	5.3 ± 0.091	-	1.8 (0.35–2.7)	0.76–0.98	This study	Forest fire
	4.1 ± 0.076	-	0.87 (0.52–1.1)	0.92–0.95		Cerrado fire
	5.0 ± 0.23	-	-	-		Regional haze/smoke
	10 ± 3	-	~ 8.5 *	-	Ferek et al. (1998)	Brazil
	-	-	7.8 ± 3.5	-	Andreae & Merlet (2001)	Tropical forest

Continued on next page ...

Table 5.3: *Continued from previous page.*

Compound	NEMR _{CO} × 10 ⁻⁶	NEMR _{CO₂} × 10 ⁻⁶	EF/mg kg ⁻¹	MCE	Source	Comments
	-	-	2.83	-	Akagi et al. (2011)	Tropical Forest
	10.6 ± 0.8	0.37 ± 0.04	-	-	Blake et al. (1996)	Brazil (Cerrado/haze)
	-	-	2.1 ± 1.0	-	Andreae & Merlet (2001)	Savannah & grassland
	-	-	0.853	-	Akagi et al. (2011)	Savannah
	8.3 ± 0.4	0.11 ± 0.04	-	-	Andreae et al. (1996)	Southern Africa
CH ₃ I	1.4 ± 0.036	-	0.59 (0.24–0.97)	0.76–0.98	This study	Forest fire
	1.3 ± 0.032	-	0.31 (0.19–0.43)	0.92–0.95		Cerrado fire
	0.76 ± 0.026	-	-	-		Regional haze/smoke
	5 ± 2	-	~ 8 *	-	Ferek et al. (1998)	Brazil
	-	-	6.8	-	Andreae & Merlet (2001)	Tropical forest
	-	-	2.50	-	Akagi et al. (2011)	Tropical Forest
	1.2 ± 0.2	0.037 ± 0.010	-	-	Blake et al. (1996)	Brazil (Cerrado/haze)
	-	-	0.5 ± 0.2	-	Andreae & Merlet (2001)	Savannah & grassland
	-	-	0.506	-	Akagi et al. (2011)	Savannah
	2.6 ± 0.3	0.09 ± 0.05	-	-	Andreae et al. (1996)	Southern Africa
COS	150 ± 4.3	-	15 ± 3.1	0.76–0.98	This study	Forest fire
	62 ± 0.41	-	24 ± 7.9	0.92–0.95		Cerrado fire
	220 ± 9.1	-	-	-		Regional haze/smoke
	-	-	25	-	Akagi et al. (2011)	Tropical Forest

* Approximate values taken from a figure.

the proportion of carbon in the fuel in order to convert from grams of emitted species per kilogram emitted carbon, i.e. $[\text{MeX}]/[\text{CCO}] + [\text{CCO}_2] + [\text{CCH}_4]$, to grams of emitted species per kilogram dry vegetative matter. As this was not possible to determine in the field, a carbon content of 450 g/kg biomass was applied. This is representative to within a few percent (e.g. Yokelson et al., 2008).

EFs for CH_3Cl are broadly similar to the literature e.g. 61 mg kg^{-1} for forest fires compared to 20–180 mg kg^{-1} in Andreae & Merlet (2001) and 53 mg kg^{-1} in Akagi et al. (2011). EFs for CH_3Br are lower than Andreae & Merlet (2001) by $\sim 5 \text{ mg kg}^{-1}$. However, there is good agreement with Akagi et al. (2011). Akagi et al. (2011) is based in part in the same datasets as Andreae & Merlet (2001) and on Sinha (2004) which reports EFs for fires in African miombo woodland ecosystems. Miombo woodland is described in Sinha (2004) as a wooded savannah ecosystem. Hence, EFs reported in Akagi et al. (2011) for CH_3Br and CH_3I in forest fires might be misleading and not be suitable for direct comparison with SAMBBA data. SAMBBA data for all three methyl halides show no substantial difference in EF between forest fires and cerrado savannah fires. However, for cerrado fires, fewer samples were available with the supporting data necessary for EF calculations. Additionally, cerrado fire samples were exclusively from flaming fires (MCE 0.92–0.95) whereas forest fire samples cover a range of combustion phases (MCE 0.76–0.98).

Emission factors of methyl halides are expected to show a negative trend with MCE i.e. increasing plume enhancement with decreasing MCE. This is due to the preferential emission of these compounds from smoldering combustion in which a higher proportion of CO is emitted (e.g. Ferek et al., 1998). Figure 5.7 shows plots of methyl halides against MCE for samples of forest fires. All three methyl halides show a negative linear trend in EF. This implies that knowledge of the CO emission field or detail of the fire behaviour across different vegetation types and regions is necessary for accurate estimation of large scale emissions of these compounds. This also indicates that, in some cases, broad vegetation type definitions, such as ‘tropical forest’ or ‘savannah’ may not reflect the variability of fire emissions accurately enough.

5.4.2.4 Chlorobenzene burning emissions

Chlorobenzene increases from ~ 3.8 –160 % of the working standard (Figure 5.8). As this was uncalibrated in the standard, absolute mixing ratios cannot be assigned to this compound and NEMRs and EFs cannot be calculated. The methods and equipment required to create a gas standard of this relatively high boiling-point gas (132°C ; Lindstrom & Mallard, 2015) were not available for this analysis.

To my knowledge there is only one report of chlorobenzene in biomass burning plumes. Evtyugina et al. (2013) sampled Portuguese prescribed wildfires 10–200 m downwind and reported average plume mixing ratios of 400 ppt (maximum 3000 ppt) compared to a background of 25 ppt. However, no further comment is given on this result and details given on calibrations indicate that these mixing ratios may only be a rough estimate.

The tropospheric lifetime of chlorobenzene is approximately 2 weeks (Atkinson et al., 1985) and is, therefore, termed a very short-lived substance (VSLs). VSLs may be significant for stratospheric ozone depletion in regions that act as sources for the tropical tropopause layer (TTL) and hence, the stratospheric overworld (see Sections 1.5.2.3 and Chapter 4 for more detail). Chlorobenzene is unlikely to have a large impact on the stratospheric chlorine loading. However,

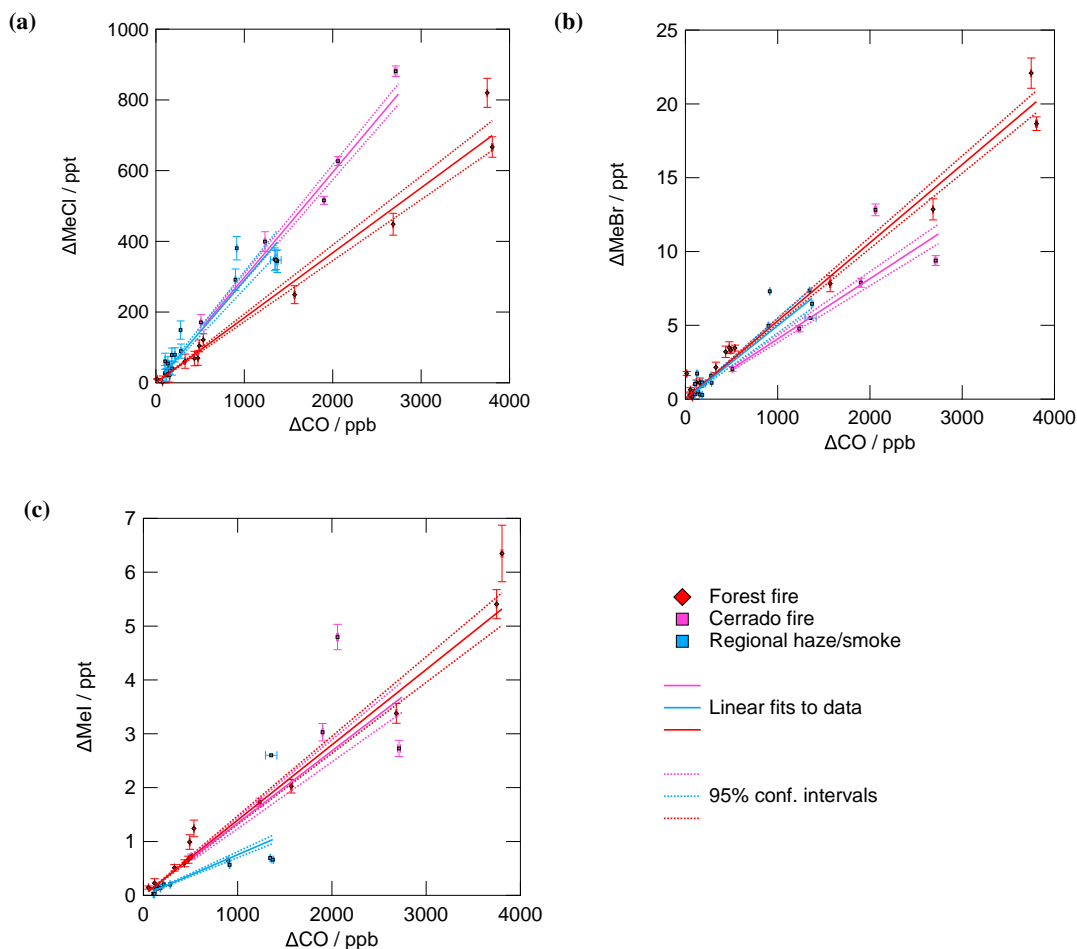


Figure 5.5: Comparison of NEMRs from forest fire, cerrado fire and regional haze/smoke samples for (a) MeCl, (b) MeBr and (c) MeI. Error bars represent analytical uncertainties. Fit lines are orthogonal distance regression fits, weighted by sample errors and forced through the origin. Also shown are 95 % confidence intervals for the fit lines.

as the tropics are the main source region for VSLs to the TTL, it is possible that this compound might have some impact on chlorine in this region of the atmosphere. Further work is needed to quantify this compound and its fire emissions.

5.4.2.5 Carbonyl sulfide NEMRs and EFs

Carbonyl sulfide (COS) shows a positive linear trend with CO, with COS increasing from ~ 380 – 1000 ppt over ~ 130 – 4000 ppb CO. Figure 5.9 shows linear fits to ΔCOS versus ΔCO for samples from forest fires, cerrado savannah fires and regional haze/smoke. As for NEMR calculations in Section 5.4.2.2, fit lines are ODR linear fits to the data weighted by analytical errors in the data. However, as can be seen in Figure 5.9, ΔCOS is offset from zero by up to ~ 200 ppt when ΔCO is close to zero. Unlike NEMR calculations for the halomethanes, forcing the y-intercept through the origin would not give a reasonable estimate of the gradient. Therefore, the linear fits applied in Figure 5.9 are not forced through origin. The offset of ΔCOS and range of values at low ΔCO could indicate non-biomass burning source of COS or that, during biomass burning flights, background air entrained into the plume was not truly representative of background air in the region i.e. there was some other less localised burning impacting the region.

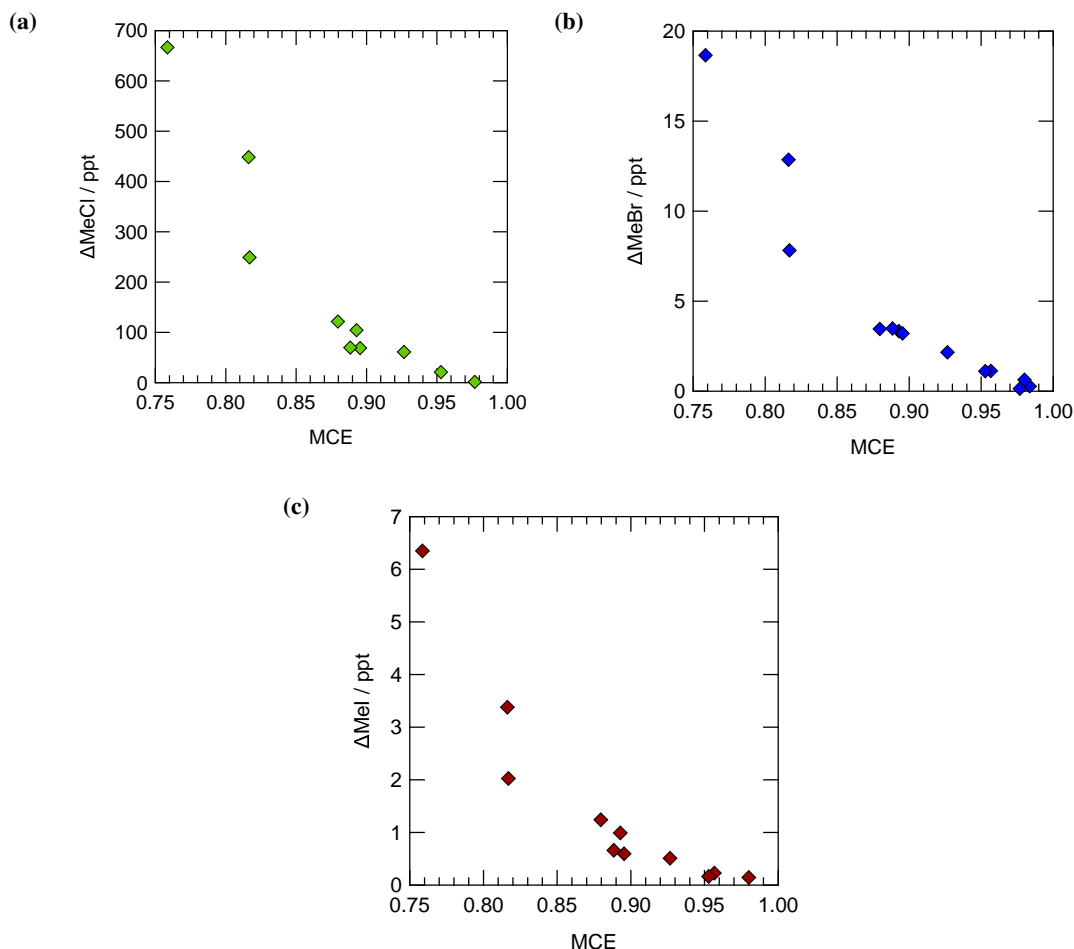


Figure 5.6: Enhancements in methyl halides plotted against modified combustion efficiency (MCE) defined as $\Delta\text{CO}_2/\Delta\text{CO}_2 + \Delta\text{CO}$. (a) ΔMeCl , (b) ΔMeBr and (c) ΔMeI . Lower values of MCE indicate smoldering combustion, higher values indicate flaming combustion.

Background mixing ratios were derived samples collected during background emission flights (see Figure 5.2). COS varied between 350–470 ppt over the range of CO encountered (~ 130 –180 ppb) with a mean $\pm 1\sigma$ of 410 ± 26 ppt rounded to two significant figures. Figure 5.10 shows COS collected during background flights plotted against latitude. Variation in background COS cannot account for the large offset in ΔCOS . The main source of COS is oceanic and the main sink is uptake by vegetation (Montzka et al., 2007). COS also has a seasonal cycle primarily driven by seasonality in oceanic emissions and vegetative uptake. Seasonal variation in the southern hemisphere clean background air ranges between ~ 460 –510 ppt with a minimum in July–September and maximum during Jan–Mar. Additional sources include biomass burning, soil processes and wetlands. Mean background mixing ratios are 81 ppt lower than the southern hemispheric surface mean of 491 ppt (200–2005) and 74 ppt lower than the Cape Grim mean for 2000–2005 (Montzka et al., 2007). The lower mixing ratios encountered over the Brazilian rainforest suggest that, during background flights, COS mixing ratios are strongly influenced by vegetative uptake which is the largest sink for COS (see Table 1.5).

Elevated COS seen at low CO during biomass burning flights could either be due to diffuse burning emissions with highly variable COS emission ratios, or to variations in biogenic emission/uptake. It is unlikely that burning emissions have highly variable emission ratios as shown by the strong linear relationships shown in Figure 5.9. Low COS enhancements (e.g.

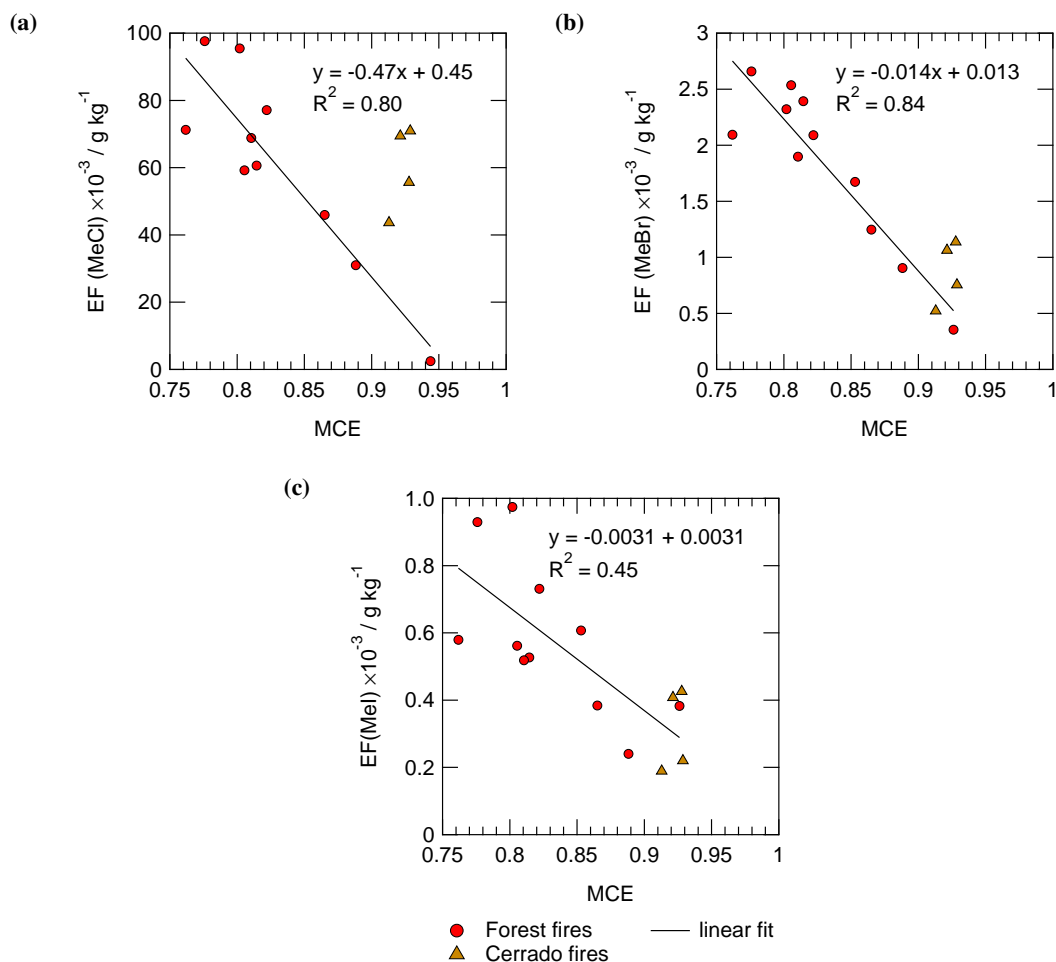


Figure 5.7: Emission factors (EFs) with units of grams MeX per kilogram dry fuel plotted against modified combustion efficiency (MCE) for (a) MeCl, (b) MeBr and (c) MeI in forest fires and cerrado fires. Low values of MCE indicate smoldering combustion, higher values indicate flaming combustion. Fits to the data are least squares linear regressions.

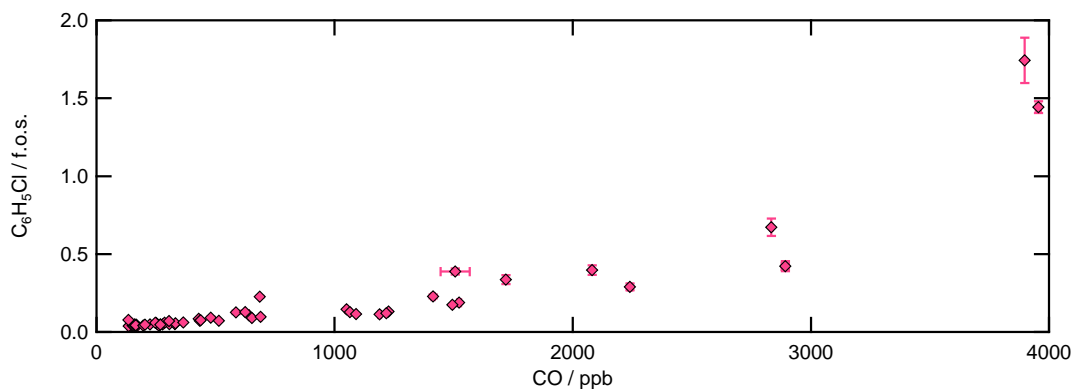


Figure 5.8: Chlorobenzene, as a fraction relative to standard (f.o.s.) plotted against CO for all bottle samples collected during the campaign.

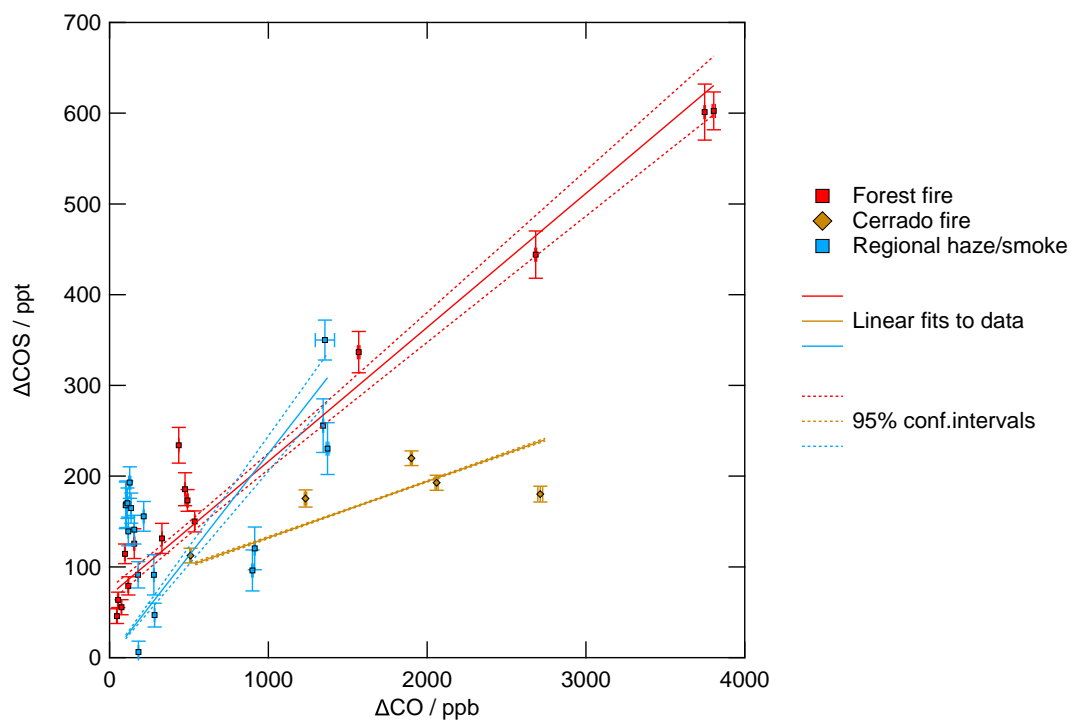


Figure 5.9: Plots of ΔCOS against ΔCO for forest fire, cerrado savannah and regional haze/smoke samples and. Error bars represent analytical uncertainties. Fit lines in are orthogonal distance regression fits, weighted by sample errors and forced through the origin. Also shown are 95 % confidence intervals for the fit lines.

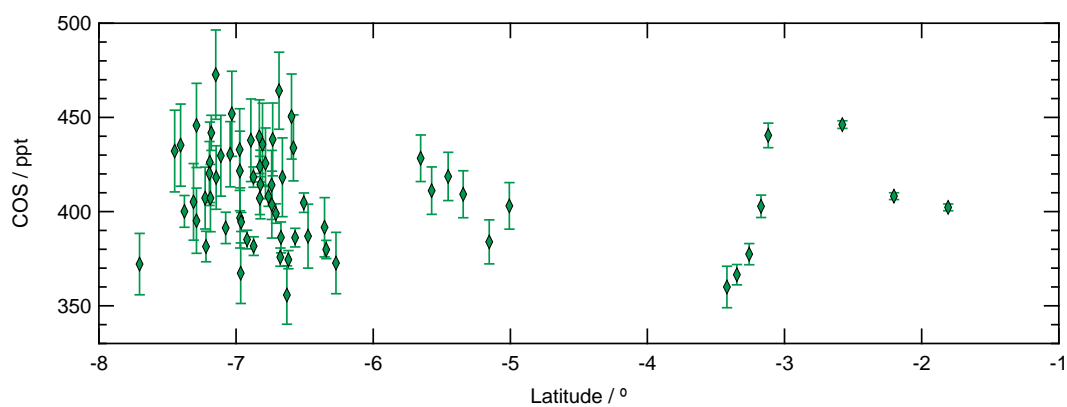


Figure 5.10: COS plotted against latitude for samples collected on background flights. Error bars represent analytical uncertainties.

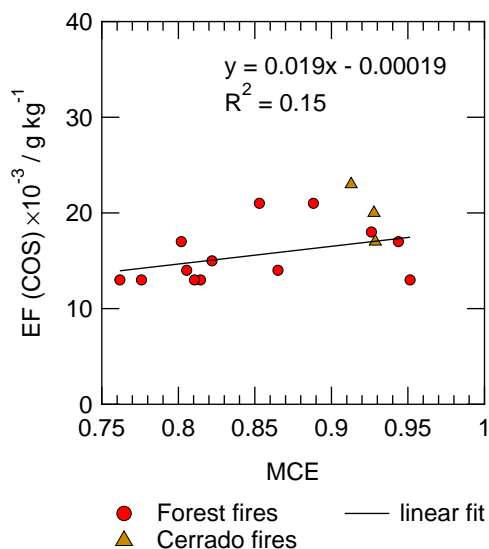


Figure 5.11: Emission factor (EF) versus modified combustion efficiency (MCE) for forest and cerrado fires. Low values of MCE indicate smoldering combustion. Fits to the data are least squares linear regressions.

$\Delta\text{COS} < 200$ ppt) were encountered at 300–2500 m altitude. However, sampling coverage over the altitude range is not sufficient to discern a clear altitudinal gradient and, hence, evidence of increased production or reduced uptake. NEMRs and EFs for COS are given in Table 5.3. EFs for cerrado fires are 9 mg kg^{-1} higher than for forest fire samples. 95 % confidence bands shown in Figure 5.9 indicate that the fit lines are significantly different. EFs for COS agree well with Akagi et al. (2011). The value for COS in Akagi et al. (2011) is derived from measurements of a planned fire reported in Yokelson et al. (2007) The higher COS emission factor for cerrado fires implies that these savannah regions are potentially more significant for COS fire emissions than has previously been accounted for.

As shown in Figure 5.9, COS shows a strong trend with CO in biomass burning plumes. COS also shows a strong trend with CO_2 (not shown here). However, as shown in Figure 5.11, there is no distinct trend with MCE.

5.4.2.6 Regional and global biomass burning emission estimates

As suggested in Section 5.4.2.3, accurate and fine-grained regional and global emissions require detailed information on the burning state and/or CO field in addition to the burned area of fires. However, reasonable ‘first-guess’ estimates of annual biomass burning emissions, i.e. a mass quantity per year, can be made by multiplying the mean emission factor for a compound by the quantity of biomass consumed. Fire emissions are dependant on the vegetation type burned (see Section 5.4.2). Therefore, estimates of the quantity of biomass burned annually have to be either regionally specific or based on globally distinct vegetation types. Table 5.4 shows regional emission estimates based on South American savannah and forest burning figures given in Bond (2004). Biomass burning estimates in Bond (2004) give consumption figures of 808 Tg and 585 Tg dry matter per year for South American savannah and forest respectively. Errors on these estimates of biomass burning are not quantified but can be assumed to be large. As the biomass burning figures are based on data from the mid-1990s, these aren’t truly representative of biomass burned

Table 5.4: Regional estimates of biomass burning emissions from South America and the contribution to global biomass burning emissions. Emissions estimates are based on biomass consumption figures given in Bond (2004) and emission factors given in Table 5.3. Ranges given for halomethanes reflect variability in emissions with the burning phase of a fire (see Section 5.4.2.3). Values are means $\pm 1\sigma$ for COS. Emissions estimates are given in units of Ggyr^{-1} . The contribution to global biomass burning emissions is also given as a percentage (Contribution / %).

Compound	South America		Contribution / %
	Forest / Ggyr^{-1}	Savannah / Ggyr^{-1}	
CH_3Cl	36 (15–57)	48 (36–57)	6–29 ¹
CH_3Br	1.1 (0.20–1.6)	0.70 (0.42–0.89)	3.7–19 ¹
CH_3I	0.35 (0.14–0.57)	0.25 (0.15–0.35)	4.3 ²
COS	8.8	19	10 ²

¹ Based on global emissions summarised in Gebhardt et al. (2008) and references therein.

² Based on global emissions estimates given in Andreae & Merlet (2001).

in the year of the SAMBBA campaign (2012). However, if forest and savannah burning remain constant on average, this provides a reasonable estimate. Emissions given in Table 5.4 are based on the average emission factors given in Table 5.3. As emission factors for methyl halides are dependent on the MCE of the fire (see Section 5.4.2.3), a range of emission estimates has been given for the range of MCE values given in Table 5.4. COS is not dependant on MCE in the same way so a range has not been given for regional estimates.

Also shown in Table 5.4 is the percentage of global biomass burning emissions represented by South American fires i.e. the sum of regional emissions from forest and savannah fires. Global biomass burning figures are taken, in the case of CH_3Cl and CH_3Br , from Gebhardt et al. (2008) which summarises source estimates from Clerbaux & Cunnold (2007) and Montzka & Fraser (2003). There are large uncertainties associated with global biomass burning estimates. Gebhardt et al. (2008) gives a range of emissions of $325\text{--}1125 \text{ Ggyr}^{-1}$ for CH_3Cl and $10\text{--}40 \text{ Ggyr}^{-1}$ for CH_3Br . This is reflected in a range of percentage contributions of 6–29 % for CH_3Cl and 3.7–19 % for CH_3Br with median values of $\sim 17\%$ and $\sim 11\%$. These contributions of CH_3Cl and CH_3Br represent a considerable proportion of biomass burning emissions of these two stratospherically significant compounds. Additionally, South America biomass burning emissions represent approximately 0.6–5 % of global CH_3Cl emissions and 0.6–2.3 % of total global CH_3Br emissions based on global estimates given in Gebhardt et al. (2008). Global biomass burning figures for CH_3I and COS are taken from Andreae & Merlet (2001). South American biomass burning represents $\sim 4\%$ of global biomass burning CH_3I emissions based on a value of 14 Ggyr^{-1} from Andreae & Merlet (2001). However, global emissions might be as little as 3 Ggyr^{-1} (Andreae et al., 1996) and are not well quantified. South American COS emissions contribute 10 % to global biomass burning emissions based on Andreae & Merlet's value for global biomass burning emissions of 270 Ggyr^{-1} . It should be noted that error or variability estimates have not been included in Table 5.4 as there are large and difficult to quantify uncertainties in the estimation of the quantity of biomass burning consumed. Future refinements may be possible based on satellite measurements of fires.

Global biomass burning emissions can be estimated using an analogous process to that used for regional estimates. As there are a limited number of biomass burning emissions measurements

Table 5.5: Global emission estimates of biomass burning from tropical forests and savannah based on biomass consumption estimates from Akagi et al. (2011). Estimates are derived from the mean emission factors given in Table 5.3.

Source type		CH ₃ Cl	CH ₃ Br	CH ₃ I	COS
Tropical forest	This study	81	2.4	0.78	20
	Andreae & Merlet (2001)	100	10	9.0	50
	Akagi et al. (2011)	70	3.8	3.3	33
Savannah	This study	200	2.9	1.0	81
	Andreae & Merlet (2001)	240	6	1.6	50
	Akagi et al. (2011)	190	2.9	1.7	-

All values given in units of Ggyr⁻¹.

of halomethanes and COS, scaling up of regionally limited measurements is frequently the best estimate available. However, due to the influence of vegetations types and the type of burning on emissions of these compounds, it is more reasonable to limit global estimates to global terrestrial biomes similar to those where the measurements were made. In the case of this study, this means scaling up burning emissions from the Amazonian rainforest to global tropical forest and Cerrado savannah emissions to global savannah. Table 5.5 shows global biomass burning estimates for tropical forest and savannah emissions. These estimates are based on the emission factors given in Table 5.3 and global biomass consumption estimates from Akagi et al. (2011). Akagi et al. (2011) biomass consumption estimates are based on the average of values from Andreae & Merlet (2001) and Bond (2004) in the case of savannah, and Andreae & Merlet (2001) in the case of tropical forest.

Global biomass burning emission estimates for tropical forest (81 Ggyr⁻¹) and savannah (200 Ggyr⁻¹) for CH₃Cl show good agreement with the literature values given in Table 5.5. CH₃Br (2.4 Ggyr⁻¹ and 2.9 Ggyr⁻¹ for tropical forest and savannah respectively) also shows good agreement with literature values especially with Akagi et al. (2011). The SAMBBA emission estimate for CH₃I from tropical forest fires (0.78 Ggyr) is lower than literature values by 2.52–8.22 Ggyr⁻¹. Savannah fire emissions of CH₃I (1.0 Ggyr⁻¹) have a better agreement with the literature values of 1.6 and 1.7 Ggyr⁻¹. As mentioned in Section 5.4.2, Akagi et al. (2011) tropical forest values may not be comparable to Amazonian rainforest. Emissions factors for CH₃Cl and CH₃Br are more similar between tropical forest and savannah environments than for CH₃I (see Table 5.3). Therefore, the differences in emission estimates for CH₃I may be explained by the inclusion of African savannah woodland in tropical forest emission estimates from Akagi et al. (2011). COS values, derived from SAMBBA, are lower than the literature by 13–30 Ggyr⁻¹ for tropical forest but is higher than Andreae & Merlet (2001) by 31 Ggyr⁻¹ for savannah fires. Akagi et al. (2011) does not provide a value for savannah emissions. In summary, global biomass burning emission estimates based on SAMBBA data agree well with the most recent summaries of biomass burning emissions with the exception of tropical forest emissions of CH₃I and COS. However, given the large uncertainties in annual quantities of biomass burned, it is possible that the observed agreements between this study and literature values are coincidental.

5.4.3 Background measurements

In addition to burning emissions, tropical forests are potential sources of a range of trace gases that may be of significance in atmospheric composition. Of the compounds discussed in this section MeCl, MeBr and CHCl₃ have been previously reported as having terrestrial sources. CHBr₃ and CH₂Br₂ are mainly marine in origin with the only reported terrestrial source being from rice paddies. Though mostly anthropogenic in origin, with 90 % of emissions in the northern hemisphere, Montzka & Reimann (2011) indicate that PCE and CH₂Cl₂ might have an unidentified natural source in the southern hemisphere. MeI is also mainly marine in origin with a few poorly quantified terrestrial sources, e.g. rice paddies, peatlands etc. (see Section 1.5.3.1).

Background measurements are based on two flights (735 and 749, see Section 5.4.1). Flight 749 consisted of 53 samples collected between ~130 km north to ~320 km NNW of Porto Velho. Flight 735 consisted of 11 samples collected on route between Porto Velho and Manaus, and an additional three samples collected between ~50–140 km north of Manaus (see Figure 5.2a). All samples were collected over the Amazonian forest. Background mean mixing ratios and ranges for the compounds discussed in this section are summarised in Table 5.6.

Table 5.6: Mean mixing ratios from background flight measurements made during SAMBBA. SAMBBA values are means $\pm 1\sigma$ standard deviation with minimum and maximum values in parentheses beneath. Monthly means for September 2012 ($\pm 1\sigma$) of baseline data from three AGAGE (Advanced Global Atmospheric Gases Experiment) sites are given for comparison as well as the AGAGE global monthly mean (Prinn et al., 2000; O’Doherty et al., 2001; Cox et al., 2003; Simmonds et al., 2004; Prinn et al., 2014). All values are molar mixing ratios in parts per trillion (ppt).

	CH ₃ Cl	CH ₃ Br	CH ₃ I	CH ₂ Cl ₂
Mace Head, Ireland (53°N, 10°W)	492 \pm 13	8.7 \pm 0.27	-	32 \pm 1.2
Ragged Point, Barbados (13°N, 59°W)	523 \pm 7.5	7.2 \pm 0.14	-	25 \pm 3.1
SAMBBA (1–9°S, 59–67°W)	669 \pm 26 (626–734)	8.3 \pm 0.41 (7.4–9.7)	0.88 \pm 0.33 (0.37–2.1)	22 \pm 3.8 (17–45)
Cape Grim, Tasmania (40.68°S, 144.69°E)	529 \pm 2.9	6.3 \pm 0.093	-	-
Global Monthly Mean	526 \pm 11	7.0 \pm 0.45	-	22 \pm 5.5
	CHCl ₃	CH ₂ Br ₂	CHBr ₃	PCE
Mace Head, Ireland (53°N, 10°W)	10 \pm 0.75	-	-	1.5 \pm 0.098
Ragged Point, Barbados (13°N, 59°W)	6.5 \pm 0.66	-	-	0.74 \pm 0.17
SAMBBA (1–9°S, 59–67°W)	10 \pm 2.2 (7.6–17)	0.79 \pm 0.059 (0.67–0.95)	0.53 \pm 0.13 (0.13–1.1)	0.49 \pm 0.036 (0.40–0.59)
Cape Grim, Tasmania (40.68°S, 144.69°E)	-	-	-	0.58 \pm 0.021
Global Monthly Mean	7.68 \pm 1.4	-	-	0.87 \pm 0.25

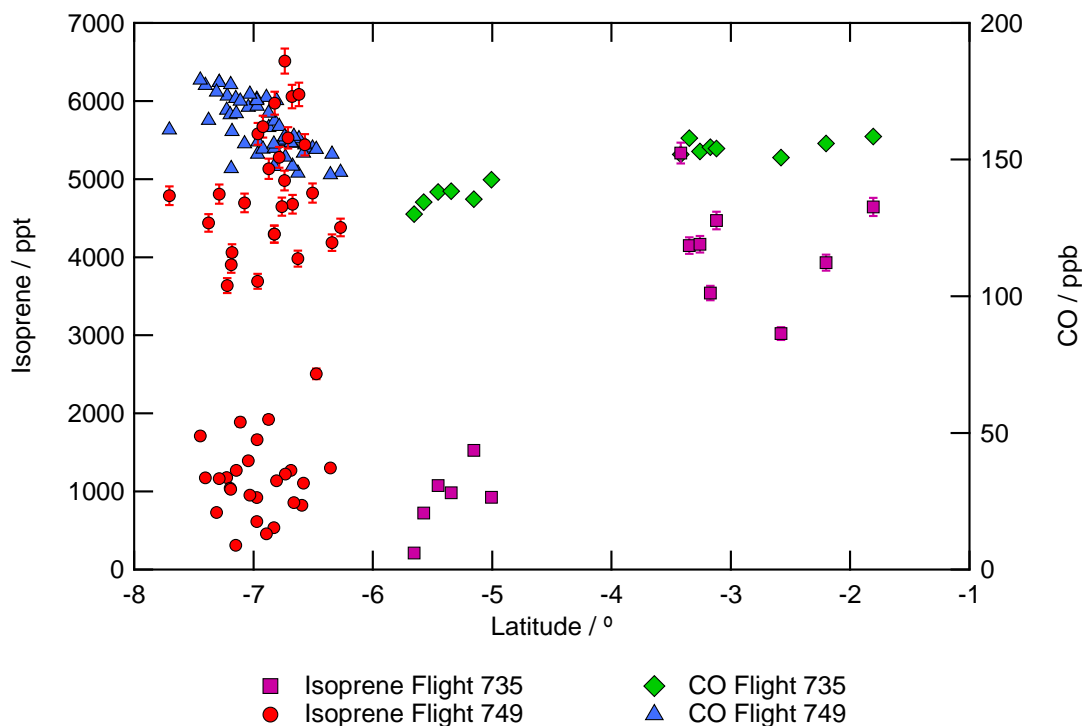


Figure 5.12: Isoprene and carbon monoxide (CO) plotted against latitude for background flights (735 and 749). Error bars represent analytical uncertainties. CO data are derived from time-averaged high-frequency measurements due to greater data coverage on these flights. At low CO mixing ratios, these measurements agree well with bottle measurements (See Section 5.2.2 for further details).

5.4.3.1 Carbon monoxide

Carbon monoxide measurements during the background flights were in the range of 140–180 ppb. Within this range CO shows an enhancement, in some samples during flight 749, of ~ 20 ppb. Furthermore, there is a positive trend with increasing latitude over the samples from flight 735 (see Figure 5.12).

A clean background might be expected to have a CO mixing ratio of ~ 60 ppb but this would only be expected in the remote marine atmosphere. Satellite measurements indicate that monthly mean CO for September 2012, in the region of the background flights, was ~ 80 ppb at an altitude of ~ 365 m (NASA Earth Observations (NEO), 2012). It is unlikely that SAMBBA background measurements are influenced by biomass burning. No enhancement in hydrocarbons indicative of biomass burning, such as alkanes, benzene and toluene, were enhanced in the background flight bottle samples analysed by the University of York. Additionally, there were no noticeable enhancements in the methyl halides that were otherwise found to be associated with biomass burning in this region (Section 5.4.2.2).

The enhancements in CO might be explained by direct or indirect biogenic emissions. Isoprene measurements made on bottle samples by the University of York, along with time-averaged high frequency CO measurements, are shown in Figure 5.12. Mixing ratios of up to 6 ppb of isoprene can be seen in some samples. Additionally, these enhancements follow a similar pattern with latitude as CO in flight 735. Isoprene has a strong diurnal response to temperature thought to be a protective response to heat stress (e.g. Kansal, 2009; Sharkey et al., 2008). Figure 5.13 shows the bottle isoprene measurements plotted against local time-of-day. Flight 735 (Figure 5.13a) shows

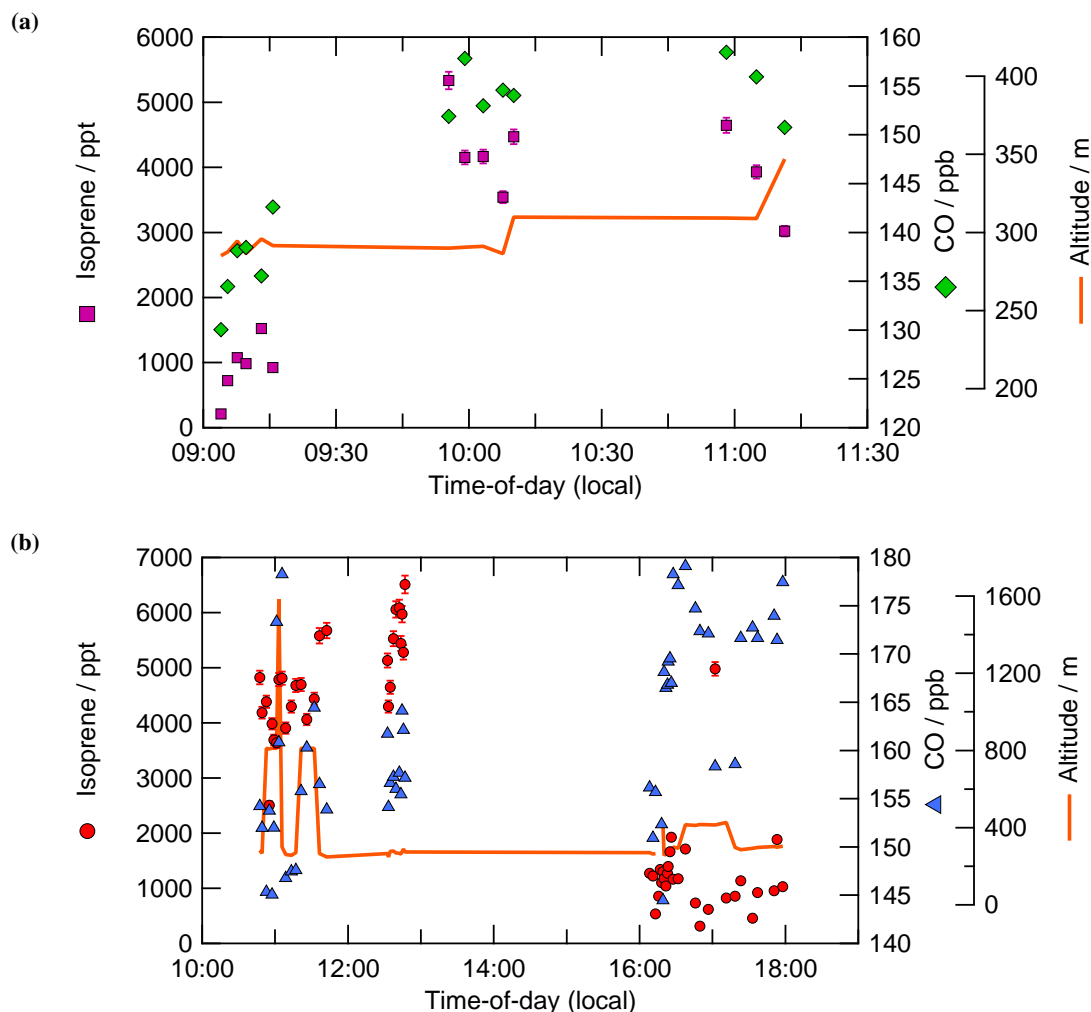


Figure 5.13: Plots of (a) isoprene and CO for flight 735 and (b) isoprene and CO for flight 749 against local time-of-day. Error bars represent analytical uncertainties. CO data are derived from time-averaged high-frequency measurements due to greater data coverage on these flights. At low CO mixing ratios, these measurements agree well with bottle measurements (See Section 5.2.2 for further details).

an increase in of ~ 3 ppb isoprene, following a similar pattern to the CO increase of ~ 20 ppb. However, Flight 749 does not show a similar pattern between isoprene and CO (Figure 5.13b), with the highest CO (~ 175 ppb) measured when isoprene was at the lowest mixing ratio during the flight (~ 1 ppt). Andreae et al. (2012) indicate that biogenic sources (direct emissions and photochemical degradation of volatile organic species) could account for ~ 10 ppb of CO in the planetary boundary layer (PBL). This might explain the enhancements in background measurements during SAMBBA. However, there are additional factors such as entrainment from the free troposphere with changes in the boundary layer, or advection from upwind sources which cannot be further examined with the data available and are beyond the scope of this study.

5.4.3.2 Methyl chloride

Methyl chloride is the most abundant chlorine-containing gas in the atmosphere and contributes 16% of the chlorine from long-lived gases in the troposphere (Montzka & Reimann, 2011). Due to the predominantly natural source of MeCl, mixing ratios might be expected to be higher near to source in the productive tropical regions. Umezawa et al. (2014) indicate that strong tropical

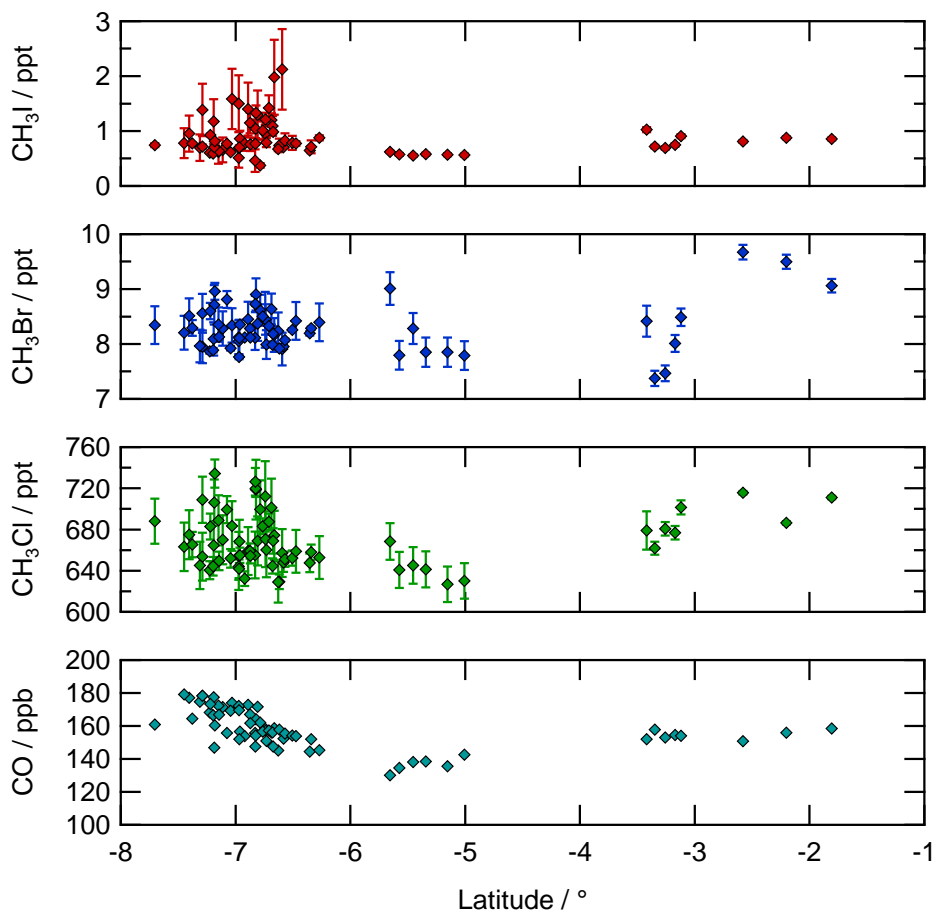


Figure 5.14: MeCl, MeBr, MeI and CO plotted against latitude for samples of background emissions (see Figure 5.2a). Error bars represent analytical uncertainties. CO data are derived from time-averaged high-frequency measurements due to greater data coverage on these flights. At low CO mixing ratios, these measurements agree well with bottle measurements (See Section 5.2.2 for further details).

sources and outflow of air to the extra-tropics is the main controller of the global-scale distribution of MeCl in the atmosphere. Recently, evidence has been growing for a significant source from tropical plants (e.g. Gebhardt et al., 2008; Yokouchi et al., 2007; Saito et al., 2008). Smaller tropical contributions have been identified from mangroves (Manley et al., 2007; Yokouchi et al., 2007), fungus (Moore et al., 2005; Mead et al., 2008a) and abiotic production from dead or senescent plant material (Hamilton et al., 2003). Xiao et al. (2010) estimate global emissions for 2000–2004 of $4.10 \pm 0.47 \text{ Tgyr}^{-1}$ using a 3-D global chemistry transport model. They also estimate that tropical terrestrial sources account for $2.3 \pm 0.3 \text{ Tgyr}^{-1}$ or $\sim 55\%$ of global emissions.

The mean mixing ratio of CH_3Cl in the background flights was $669 \pm 26 \text{ ppt}$, 146 ppt more than the background mean for September 2012 (526.0 ppt) measured at Ragged Point, Barbados (Table 5.6), the nearest monitoring station to the SAMBBA sampling region. A latitudinal plot of CH_3Cl can be found in Figure 5.14. Our observations support terrestrial vegetation in this region as a source of CH_3Cl .

5.4.3.3 Methyl bromide

The main sources of CH_3Br are the ocean and biomass burning (42 and 29 Ggyr^{-1} respectively) with smaller anthropogenic contributions from fumigation and leaded gasoline (14.3 and $<5.7 \text{ Ggyr}^{-1}$). Numerous other biogenic sources, totalling 17.1 Ggyr^{-1} , have been identified, of which some terrestrial sources remain unquantified (Montzka & Reimann, 2011).

CH_3Br has an inter-hemispheric gradient with an annual mean hemispheric difference of 1.2 ppt in 2008 (Montzka & Reimann, 2011). This is also reflected in the AGAGE monthly means for September 2012 given in Table 5.6 with a monthly mean baseline value of 8.7 ppt in the northern hemisphere (Mace Head) and 6.3 ppt in the southern hemisphere (Cape Grim). The inter-hemispheric gradient is due to the use of CH_3Br as a fumigant with larger emissions in the northern hemisphere. Declining production, as a result of the Montreal Protocol (Yvon-Lewis et al., 2009), has decreased the inter-hemispheric gradient. Southern hemispheric mixing ratios have been reduced to 60–70 % of pre-industrial levels in 2008 from a peak of 8 ppt (Montzka & Reimann, 2011).

Mean SAMBBA CH_3Br (8.3 ppt) is 1.1 ppt above the mean monthly baseline mixing ratio measured at Ragged Point, Barbados. This $\sim 15\%$ enhancement could indicate a potential biogenic source over the Brazilian rainforest. This enhancement is unlikely to be due to biomass burning as no enhancement is observed in CH_3Cl , CH_3I or CO as was seen in known biomass burning samples (see Section 5.4.2.2). It is possible that this enhancement could have a similar source to that of CHCl_3 discussed further in Section 5.4.3.5. However, it is also possible that CH_3Br is being used as a fumigant in agricultural land clearance. The highest mixing ratio samples observed during background flights (~ 9.5 ppt, see Figure 5.14) coincide with areas of forest clearance (see Figure 5.18). Depending on the usage of the land in the region, it is possible that these emissions are anthropogenic in origin if CH_3Br is used to sterilise soils for crops or crops themselves.

5.4.3.4 Methyl iodide

The dominant source of CH_3I to the atmosphere is from the ocean. Butler et al. (2007) estimate equal fluxes from the open ocean (270 GgIyr^{-1}) and coastal regions (280 GgIyr^{-1}). Photochemical processes in the surface ocean are thought to be the main oceanic source (e.g. Happell & Wallace, 1996). Additional marine sources have been identified in picoplankton production (Smythe-Wright et al., 2006) and an abiotic process (Williams et al., 2007). Sive et al. (2007) identified fluxes from terrestrial sources in mid-latitudes of 33 Ggyr^{-1} .

CH_3I in SAMBBA varies over the range ~ 0.6 – 2.1 ppt with elevated values occurring at 6–8°S. CH_3I has a relatively short local lifetime of 7 days (Montzka & Reimann, 2011) and high spatial and temporal variability (Montzka & Reimann, 2011). Therefore, a range of background mixing ratios is expected. If the analytical errors are taken into account, variability is small (see Figure 5.14). CH_3I is not routinely monitored at a site close to the SAMBBA sampling region. Montzka & Reimann (2011) give global marine boundary layer (MBL) mixing ratios of 0.80 ppt (range 0.3–1.9) with the dominate source from the ocean. Therefore, our measurements are in line with the expected background of CH_3I , and do not indicate a terrestrial source from the South American rainforest.

5.4.3.5 Chloroform

Figure 5.15a shows the latitudinal distribution of CHCl_3 during background flights. Mean CHCl_3 during these flights was 10 ± 2.2 ppt. However, at $4\text{--}6^\circ\text{S}$ the majority of samples have mixing ratios of $\sim 8\text{--}10$ ppt. 6 samples at $4\text{--}6^\circ\text{S}$ show enhancements of $\sim 3\text{--}6$ ppt. Samples at $0\text{--}4^\circ\text{S}$ show similar enhancements of $\sim 3\text{--}6$ ppt. Figure 5.15b shows the location of samples collected during background emission flights coloured by CHCl_3 mixing ratio. Gebhardt et al. (2008) reported mean mixing ratios for CHCl_3 of 8.2 ppt (range 6.6–11.2) in the boundary layer (given as up to 1400 m) in bottle samples collected over the rainforest of Suriname on the north-eastern coast of South America. The maximum mixing ratio encountered in SAMBBA background flights was 16.6 ppt, which is ~ 6 ppt higher than the maximum reported by Gebhardt et al. (2008). Samples collected during SAMBBA were collected below 1600 m altitude with only one sample above 1000 m and were all collected within the boundary layer. Mean CHCl_3 during the SAMBBA background flights was 10.2 ± 2.2 ppt which is in good agreement with Gebhardt et al. (2008) within the variability of the measurement.

Northern hemispheric mean monthly baseline CHCl_3 for September 2012 was 10 ppt (Table 5.6). Northern hemispheric mixing ratios are higher than for the southern hemisphere due to anthropogenic emissions from the production of HCFC-22, fluoropolymers, paper and pulp bleaching and water chlorination (Montzka & Reimann, 2011). Mean monthly baseline CHCl_3 for September at Ragged Point, Barbados was 6.5 ppt (Table 5.6), ~ 3.5 ppt lower than the SAMBBA mean. Southern hemispheric measurements made at Cape Grim (1998–2000) give a background mixing ratio of CHCl_3 of 6.3 ± 0.2 ppt with annual cycle of amplitude 1.1 ppt (Cox et al., 2003). This suggests that SAMBBA measurements over the Brazilian rainforest are close to a source of CHCl_3 .

Bottle samples along the two background flights, 735 and 749, were collected on 19th September between 13:00–15:30 UTC (09:00–11:30 local time) and on 3rd October 2012 between 14:30–22:00 UTC (10:30–18:00 local time) respectively. Figure 5.16 shows CHCl_3 plotted against time-of-day (local time) for flights 735 and 749. CHCl_3 enhancements in both flights are clustered between $\sim 10:00$ and 12:00. This could be indicative of a possible diurnal cycle in CHCl_3 emissions. However, this study incompletely covered only two diurnal cycles. Therefore, this is not conclusive and may be heavily influenced by factors such as wind direction, altitude and sampling location.

Flight 735, from Porto Velho to Manaus, shows increasing mixing ratios of CHCl_3 along the route towards Manaus. Maximum mixing ratios were encountered north of Manaus reaching 16.6 ppt at 140 km north of Manaus. Figure 5.17 shows the location of samples taken during flight 735. Also shown are 3-day back trajectories calculated using the HYSPLIT online back-trajectory model for each group of samples collected (Draxler & Rolph, 2013). Back-trajectories are $1^\circ \times 1^\circ$ matrices centred on each cluster of samples. All samples on flight 735 were collected at 250–350 m altitude. Over the course of the flight, regional scale flow is from approximately the same north-easterly direction. Due to the north-easterly flow, it is unlikely that pollution from Manaus is impacting the mixing ratios of CHCl_3 over the course of flight 735. Additionally, samples with the highest CHCl_3 mixing ratios were collected 50–140 km north of Manaus making it unlikely that flight 735 was sampling anthropogenic emissions of CHCl_3 . A lack of significant enhancements in dichloromethane (CH_2Cl_2) and perchloroethene (C_2Cl_4) also suggest no great

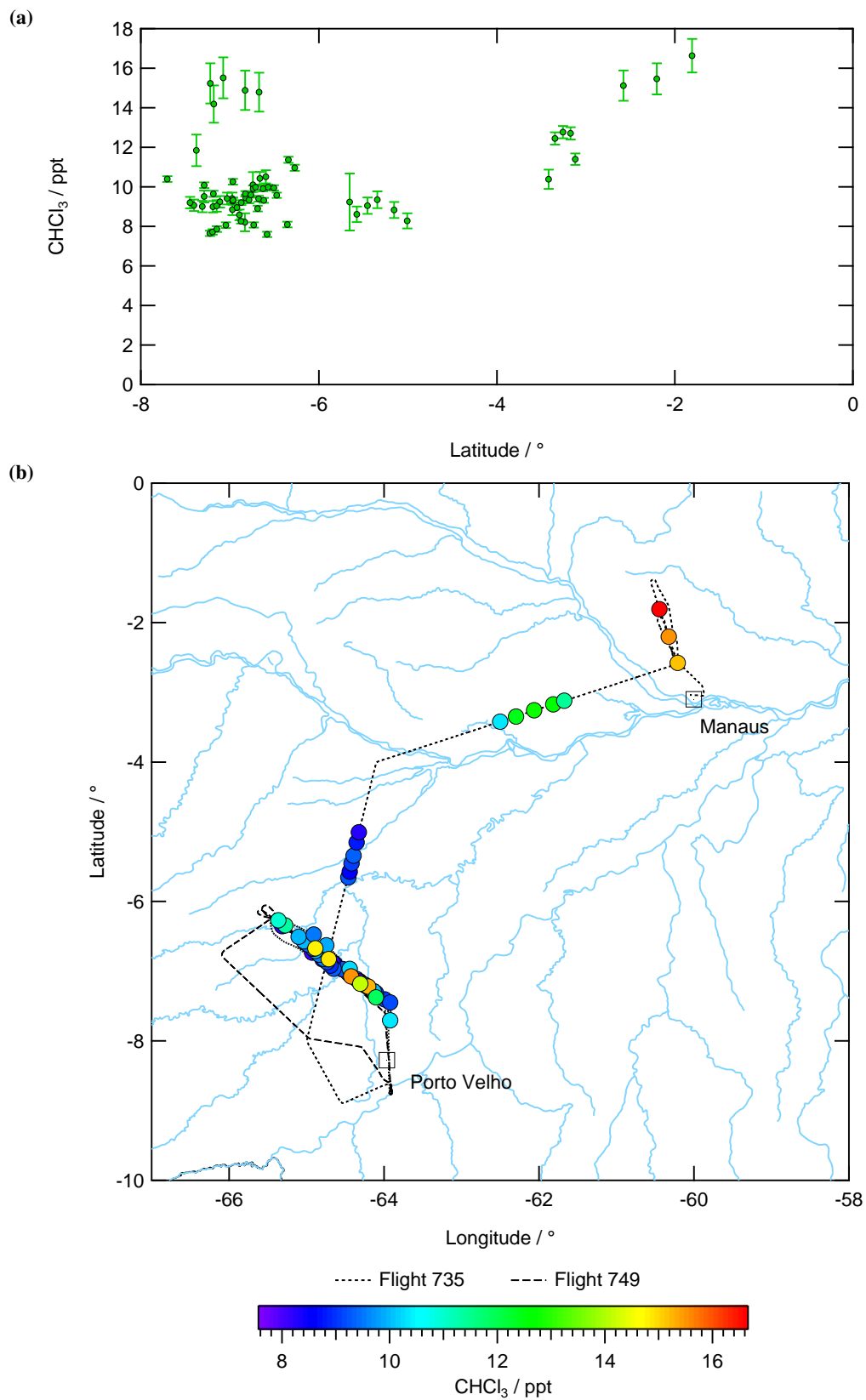


Figure 5.15: Plots for CHCl₃ in background emission samples (a) against latitude and (b) locations of samples coloured by CHCl₃ mixing ratio. Error bars represent analytical uncertainties.

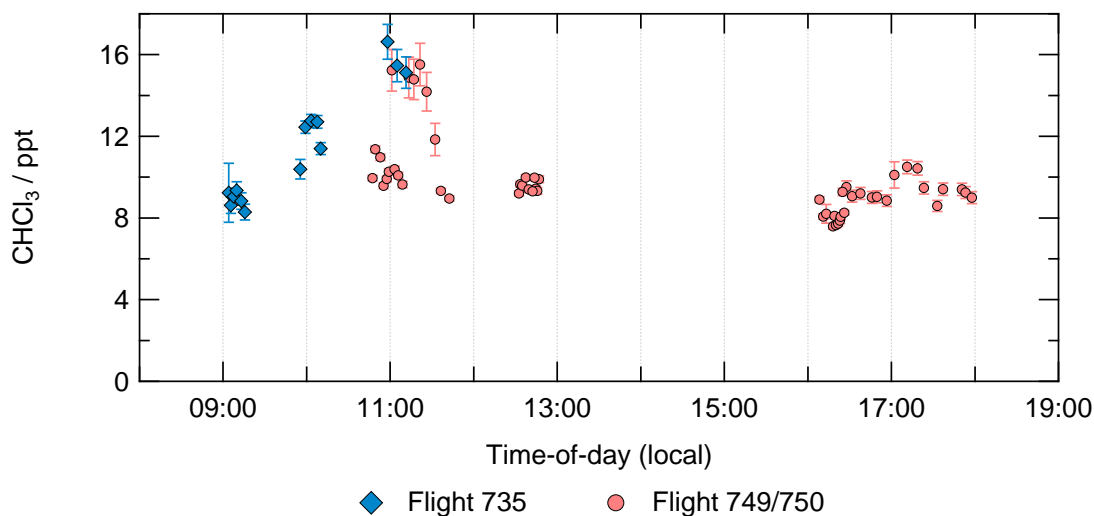


Figure 5.16: Plot of CHCl_3 against time-of-day for the background flights. Time of day is local time (UTC – 4 hours).

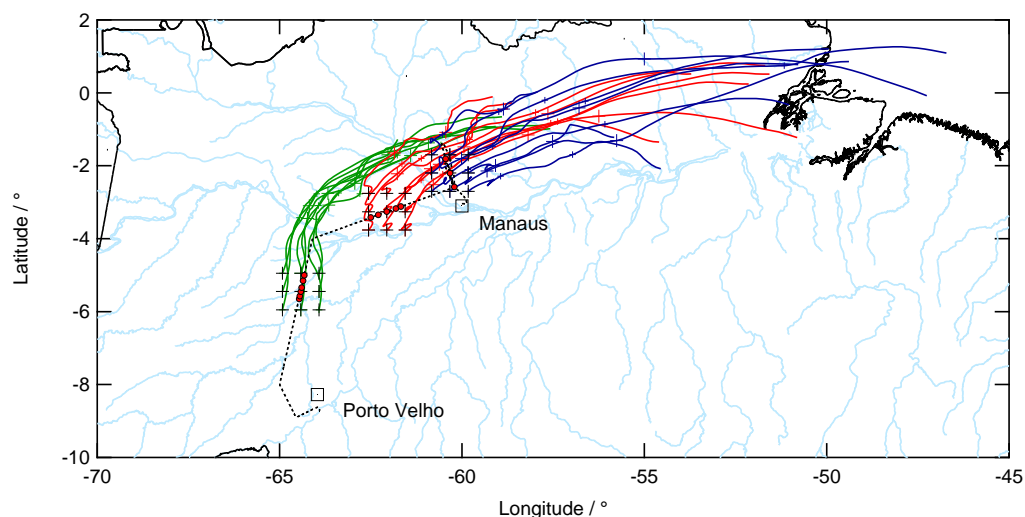


Figure 5.17: HYSPLIT matrix 3-day back-trajectories for samples collected during flight 735.

local anthropogenic influence.

Figure 5.18 shows the samples north of Manaus which contained the highest CHCl_3 mixing ratios superimposed on a satellite image of the region (courtesy of Google MapsTM). Several features are visible in the satellite image: the Rio Negro runs from the left of the image to Manaus at the bottom-centre where it becomes the Rio Amazonas; a major road runs roughly north from Manaus with large areas of cleared forest and/or agricultural land either side; in the top-right of the image is the Balbina reservoir with the Balbina dam at its south-eastern extreme. Given the regional flow indicated in Figure 5.17, and the local features indicated in the satellite image, a number of possible hypotheses for the elevated mixing ratios encountered along flight 735 are possible.

A Upwind burning. It is possible that burning upwind of the sampling location has enhanced CHCl_3 mixing ratios. No burning was observed in the region of the samples. NO_x and CO

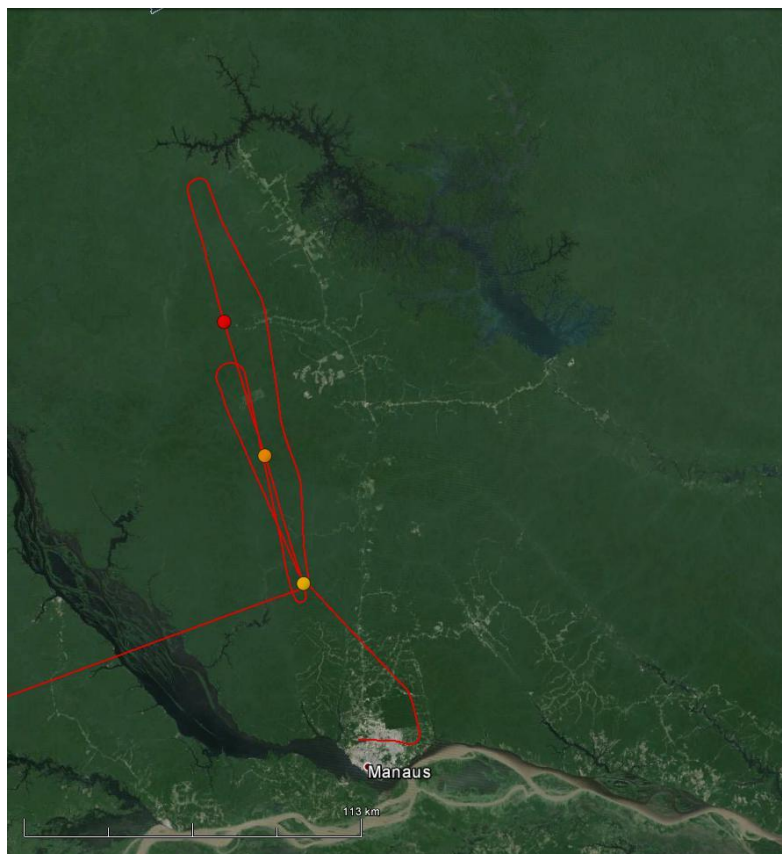


Figure 5.18: Map showing location of samples collected north of Manaus. The body of water in the top right is the Balbina reservoir. The river running from the middle-left to Manaus is the Rio Negro which forms, in part, the Rio Amazonas beyond Manaus. Map courtesy of Google Maps™.

measurements made during the flight do not indicate a strong influence of biomass burning in bottle samples. CO is in the range 140–180 ppb, which is greater than an expected clean background of ~ 60 ppb. This implies some possible influence from regional haze. However, results from biomass burning flights in this study do not indicate that CHCl_3 is emitted from burning of vegetation in the region (see Section 5.4.2 and Figure 5.4b). Therefore, it is unlikely that burning is responsible for elevated CHCl_3 in background flights.

B The Amazon delta. The open ocean is the largest source of CHCl_3 ($270\text{--}450 \text{ Ggyr}^{-1}$). Pulp and paper manufacture, water treatment and other industrial sources account for $43\text{--}89 \text{ Ggyr}^{-1}$ (Gebhardt et al., 2008). Given the regional north-easterly flow during flight 735, it is possible that elevated CHCl_3 could be associated with natural or anthropogenic emissions from the delta region of the Rio Amazonas, or emissions from the Atlantic Ocean.

C The Balbina dam. The Balbina reservoir (directly north-east of the highest CHCl_3 mixing ratios, Figure 5.18) is the largest hydroelectric reservoir in the Amazon. It was formed by impounding the Uatamà river in 1987 and has an average flooded area of 1770 km^2 and a generating capacity of 250 MW (Fearnside, 1989; Kemenes et al., 2007). The Balbina dam has a relatively low energy return of $\sim 0.14 \text{ W m}^{-2}$ (Fearnside, 1989) and generates a large quantity of greenhouse gases (e.g. Kemenes et al., 2007, 2011). Total annual CO_2 equivalent greenhouse emissions (CO_2 and CH_4) have been estimated at $3 \text{ Tg(C)}/\text{yr}$ or approximately the equivalent global warming potential as 54 % of the fossil fuel consumption of São Paulo

(Kemenes et al., 2011). The large area and shallow depth (average 7 m, Kemenes et al., 2007) of the reservoir means that wetland soil processes could be expected to be important in this region. CHCl_3 emissions have been linked to soil processes and are thought to mainly arise as a by-product of chlorination of humic material by hypochlorous acid. This acid is generated by the chloroperoxidase enzyme which is thought to be fungal in origin (McCulloch, 2003, and references therein). Given the quantity of deadwood in the reservoir (e.g. Abril et al., 2013) and the wetland conditions, this is a potentially strong source. Abril et al. (2013) indicate that most greenhouse gases are emitted during the first 5–10 years of dam operation. Therefore, as the Balbina reservoir was flooded 25 years before the SAMBBA campaign, chloroform emissions may have been higher shortly after flooding than at the time of the SAMBBA campaign if similar physical and biological processes are responsible. Therefore, it is possible that flooded regions of tropical forest, i.e. projects similar to the Balbina reservoir, represent a source of CHCl_3 to the atmosphere.

D Forest clearance and agriculture. Soil processes are the second largest source of CHCl_3 after open oceans, accounting for $120\text{--}320\text{ Ggyr}^{-1}$ (Gebhardt et al., 2008). CHCl_3 emissions from soils have been found, in temperate forests, to be dependent on the humic content of soils with higher concentrations associated with a soil covering of wood chips or humic material (Hoekstra et al., 2001). Additionally, Hoekstra et al. indicate that high concentrations of CHCl_3 can be found in deeper soil layers and hypothesise that this is due to transport of CHCl_3 precursors and subsequent formation of CHCl_3 in these layers. I hypothesise that, if similar soil processes are present in the Amazonian basin (Hoekstra et al. are careful to point out that this may not be the case due to the limitations of the study), soil disturbance by logging or agricultural work (such as ploughing) might lead to increased production of CHCl_3 . This could either be as a result of increased input of humic material (in the form of wood-chips, discarded brush and logs), or by the disturbance of deep soil layers and the exposure of buried humic material to the soil surface.

Hypothesis A is unlikely due to the lack of evidence from burning in other species measured. Furthermore, no evidence for CHCl_3 from the burning of natural vegetation was found during this study. The regional flow implied from back-trajectories indicates that all bottle samples collected along flight 735 have a similar upwind source. Mixing ratios of CHCl_3 decrease from 16 to 8 ppt between samples north of Manaus and those collected at the south-western extreme of the flight. This makes Hypothesis B unlikely unless a strong anthropogenic source in the Amazon delta region is invoked. Emissions from the Balbina dam (Hypothesis C) would be expected to coincide with elevated levels of CH_4 as the dam has been shown to be a source of methane (Abril et al., 2013; Kemenes et al., 2011, 2007). However, there is no consistent pattern in CH_4 that could explain elevated CHCl_3 (see Figure 5.19a). Emissions associated with soil disturbance would be expected to coincide with those of other species emitted from soils for instance NO_x (i.e. $\text{NO}_2 + \text{NO}$). Figure 5.19b shows high frequency NO_x data plotted with bottle CHCl_3 against local time-of-day. Enhancements of $\text{NO}_x \sim 50$ ppt above the local background appear to coincide with CHCl_3 measurements. Additionally CH_3Br is enhanced by ~ 1 ppt above the mean for background flights for the most northerly samples (Figure 5.14). As mentioned in Section 5.4.3.3, this could be linked to agricultural soil fumigation and could strengthen the argument for soil emissions linked with either the Balbina dam or forest clearance/agriculture.

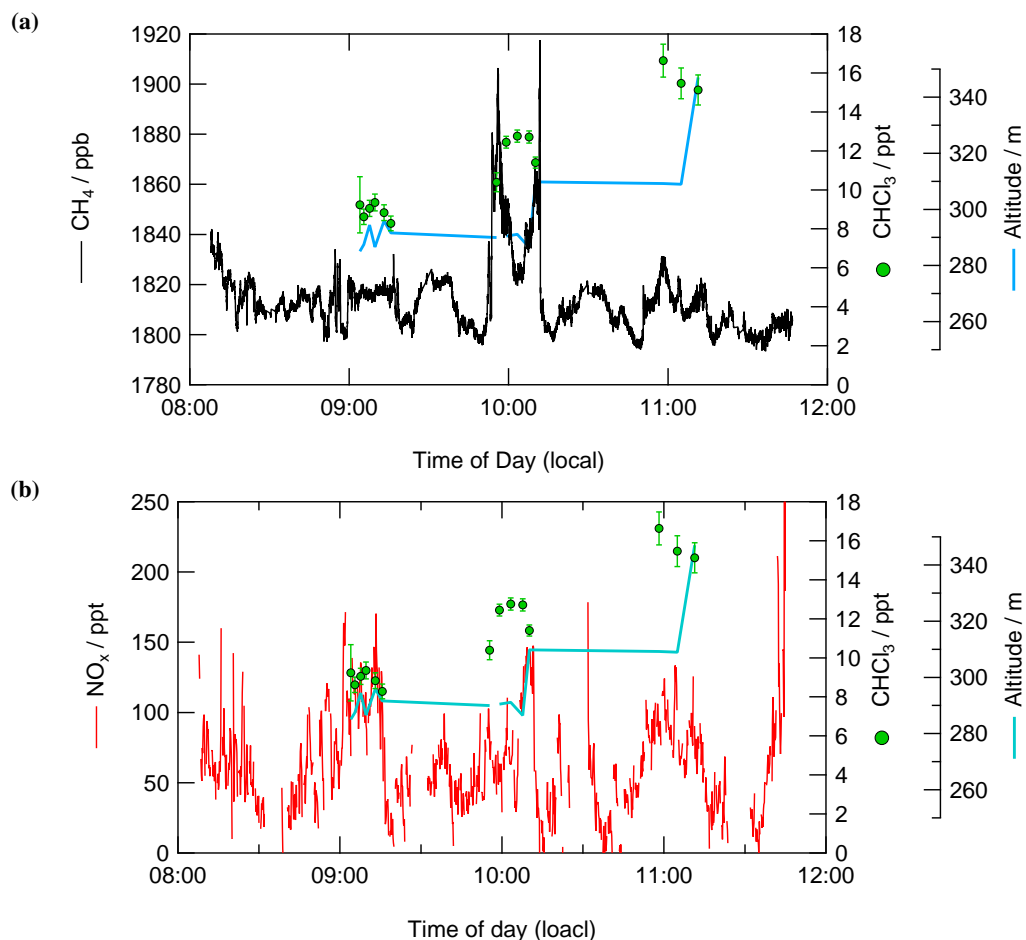


Figure 5.19: CHCl_3 in bottle samples and high frequency, in situ measurements plotted against local time-of-day for (a) CH_4 and (a) NO_x . Error bars on CHCl_3 data represent analytical uncertainties.

However, without CHCl_3 measurements in background NO_x conditions, a correlation cannot be implied. Further work would be needed in order to attribute the source of CHCl_3 enhancements in this region. Non-methane hydrocarbons measured during background flights, by the University of York, do not show any enhancements that would indicate biomass burning or anthropogenic sources.

5.4.3.6 Dichloromethane

CH_2Cl_2 is mainly anthropogenic in origin ($\sim 90\%$, Montzka & Reimann, 2011) with a strong inter-hemispheric gradient e.g. baseline means for 1998–2004 give 30.8 ppt in the northern hemisphere and 8.74 ppt in the southern hemisphere (Simmonds et al., 2006). The tropical MBL mixing ratio given in Montzka & Reimann (2011) is 17.5 ppt as a mean over several campaigns spanning 1994–2001. Leedham Elvidge et al. (2014) report an increase in northern hemispheric CH_2Cl_2 , between 1998 and 2012, of 38–69% (equating to 7–9 ppt in background regions and 12–15 ppt in regions of stronger emission). This increase in CH_2Cl_2 might be attributable to an increase in the use of CH_2Cl_2 as a feedstock for HFC-32 (CH_2F_2) which is used in a 50%/50% mixture with HFC-125 (C_2HF_5) named R-410a as a replacement for HFC-22 (CHClF_2).

Mean baseline mixing ratios for September 2012, as measured by AGAGE, were 32 ppt and 25 ppt for the northern hemisphere and tropics respectively (Table 5.6). The global mean for

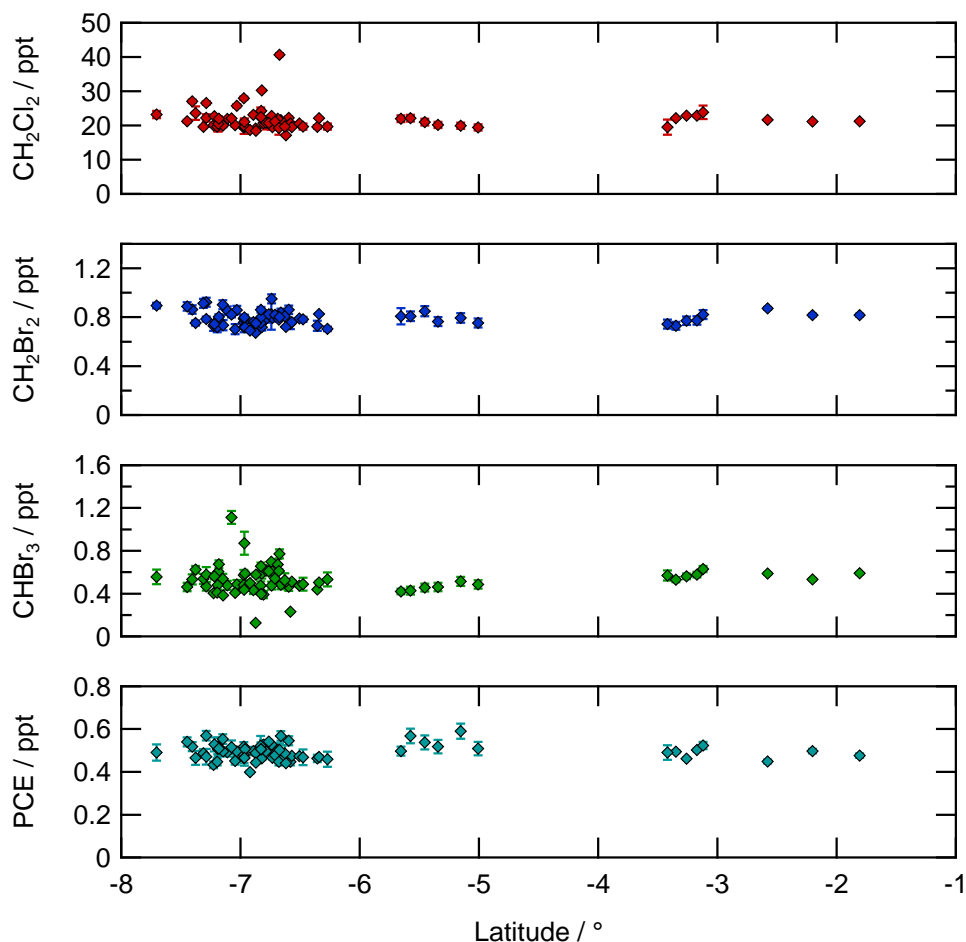


Figure 5.20: CH_2Cl_2 , CH_2Br_2 , CHBr_3 and PCE plotted against latitude for background flights (see Figure 5.2b). Error bars represent analytical uncertainties.

the period was 22 ppt. Mean CH_2Cl_2 from background emission flights in this study was 22 ppt with little latitudinal variation (see Figure 5.20). This is ~ 3 ppt lower than the AGAGE tropical measurements at Ragged Point, Barbados. Therefore, it is unlikely that there is a terrestrial source of CH_2Cl_2 from Amazonian rainforest.

5.4.3.7 Dibromomethane and bromoform

CH_2Br_2 and CHBr_3 are mainly marine in origin with a small contribution from drinking water purification and power plant cooling water (Montzka & Reimann, 2011). Rice paddies (e.g. Law & Sturges, 2007) and peatlands (Carpenter et al., 2005) have also been indicated as terrestrial sources of bromoform. To my knowledge, measurements of CH_2Br_2 and CHBr_3 have not been made or reported over tropical forests before. Montzka & Reimann (2011) give MBL mixing ratios of 0.5–2.4 and 0.7–1.5 ppt. Measurements from this study are at the lower end of this range, suggesting that the South American tropical forest is not a source of these compounds.

5.4.3.8 Perchloroethene, PCE

Perchloroethene (PCE) is thought to be predominantly anthropogenic in origin with 90 % of emissions in the northern hemisphere. As industrial inventories indicate that only 1 % of emissions are in the southern hemisphere, Montzka & Reimann (2011) indicate that there may be other sources such as biomass burning. Mean mixing ratios are ~ 0.26 ppt lower than Simmonds et al. (2006) measured at Cape Grim 2000–2004. Therefore it is unlikely that South American forest is a source of PCE. Additionally, measurements of biomass burning plumes (Figure 5.4b) do not indicate a biomass burning source in this region either.

5.5 Summary

Fire emissions for fires in Brazilian forest and cerrado savannah were evaluated for a range of halocarbons and carbonyl sulfide (COS). Of the compounds analysed, CH_3Cl , CH_3Br , CH_3I and COS were found in fire plumes from both forest and cerrado fires. Normalised emission ratios (NEMRs) relative to CO, emission factors (EFs) and modified combustion efficiencies were calculated for these compounds.

The EF for CH_3Cl in forest fires was found to agree well with the latest summary of emission factors in Akagi et al. (2011). EFs for CH_3Br , CH_3I and COS were found to be lower than those given by Akagi et al. (2011). The forest fire smoke plume was sampled close to the source. This suggests that EFs calculated here accurately represent forest fire emissions from South American rainforest.

In addition to the forest fire plume, emissions from a number of cerrado savannah fires were sampled close to source. EFs for CH_3Cl , CH_3Br and CH_3I agree well with values from Akagi et al. (2011) for savannah fires. EFs for COS in cerrado fires have not been, to the author's knowledge, reported before in the literature. SAMBBA data indicate that cerrado fires are a stronger source of COS than Brazilian forest fires by ~ 60 %.

Regional emission estimates indicate that South American biomass burning contributes a significant quantity of halomethanes and COS to global emissions. Scaling up regional emission to global scale tropical forest and savannah has inherently large uncertainties. However, bearing in mind that these are rough estimates with large uncertainties, there is good agreement between global emission estimates based on SAMBBA data and estimates in Akagi et al. (2011) and Andreae & Merlet (2001), the exception being CH_3I , with lower emissions than suggested in the literature. There have been limited measurements of halomethanes and COS biomass burning fire emissions in the literature. The measurements in this study represent a significant addition to knowledge of biomass burning emissions. It should be noted that calculations of NEMRs, EFs and emission estimates are based on a small number of samples, especially in the case of cerrado fires.

Background measurements of halomethanes over the South American rainforest indicate terrestrial sources of CH_3Cl , CH_3Br and CHCl_3 . Terrestrial sources have been identified in the literature for all three of these compounds. However, higher mixing ratios in CHCl_3 encountered during background flights indicate a localised source and a number of hypotheses were given for this enhancement. These included upwind burning, anthropogenic emissions, emissions from the Balbina reservoir and forest clearance/agriculture. Unfortunately, due to the nature of airborne sampling, it was not possible to rule out any of these hypotheses. However, it is more likely that

these emissions are linked to the Balbina reservoir or local agriculture and forest clearance.

Conclusions and future research

6.1 Outline of major research findings

6.1.1 TOF GC-MS

- The TOF GC-MS instrument is suitable, in terms of performance, for measurements of atmospheric trace gases under certain conditions i.e. high mixing ratio, low precision analysis.
 - LODs are at best ~ 0.1 ppt. This a factor 10–100 times less sensitive than expected.
 - Mean reproducibility is $\sim 4\%$. Ideally this would be $< 1\%$.
 - Daily sensitivity drift is within expectations and requires discarding the first two samples of a daily run.
 - The TOF GC-MS shows a linear response, within a few percent, to sample volume.
 - A preliminary comparison to in situ measurements made on a quadrupole instrument in London indicates good initial agreement.
- In its current state, the TOF GC-MS is most suited to measurements in polluted atmospheres.
- The main limitation on usability of the TOF GC-MS is instrument reliability.

6.1.2 Halocarbons in London

- Long-lived halocarbons currently banned under the terms of the Montreal Protocol, such as CFCs and halons, do not have significant sources from London or the surrounding region (e.g. continental Europe).
- The measured short- and long-term replacement compounds, the HCFCs and HFCs respectively, are present at higher concentrations in London in background air.
 - HCFC-22, HCFC-141b and HCFC-142b are all higher than the expected background. HCFC-133a also appears to be elevated.
 - HFC-134a and HFC-227ea are almost double their Northern Hemispheric baseline values. This is attributable to refrigeration, air-conditioning and fire-suppression applications. These enhancements might have sources in continental Europe as well as from London.

- Emission banks exist in the U.K. for CFCs and halons as well as for HCFCs as evidenced by on site contamination presumably from air-conditioning units and fire-extinguishers.
- The PFCs and other perfluorinated compounds do not show notable enhancements over background values.
- Strong sources of CH_2Cl_2 , TCE and PCE are indicated in London.
- Air arriving in London shows the influence of strong sources of very short-lived bromomethanes. These are likely to be linked to either seaweed beds off the coast of Normandy, France or to nuclear power plant cooling water from power plants in the U.K. or Europe.

6.1.3 Very short-lived bromocarbons in the upper troposphere

- Total mid-upper tropospheric tropical bromine available from the five VSLB analysed is at the lower end of the range required to balance the stratospheric bromine budget.
- Tropical CHBr_3 , CHBr_2Cl , CHBrCl_2 and CH_2BrCl show little variation at 10–12 km in the tropics.
- The region of Southeast Asia and the Western Pacific show higher concentrations of CH_2Br_2 relative to other tropical regions.
 - Two possibilities are proposed for this Southeast Asian enhancement in CH_2Br_2 : regional variation in $\text{CHBr}_3/\text{CH}_2\text{Br}_2$ emission ratio or, an increase in the local lifetime of CH_2Br_2 in the region of Southeast Asia.
- An anthropogenic source of trihalomethanes, independent of CHBr_3 or CH_2Br_2 , has been tentatively identified.
- VSLB in the mid-latitude UTLS might provide a tool for probing the structure of this region of the atmosphere.

6.1.4 Biomass burning and background emissions over Brazil

6.1.4.1 Biomass burning

- Brazilian forest fire emission estimates for CH_3Cl agree well with measurements from the literature. Forest fire emissions of CH_3Br , CH_3I and COS were found to be lower than the current best estimate (Akagi et al., 2011) by approximately 36, 76 and 40 % respectively.
- Brazilian savannah fire emission estimates for methyl halides are similar to those previously reported in the literature. Savannah fire emissions of COS were found to be higher, by ~60 %, than forest fire emissions.
- Regional annual emission estimates indicate that South America biomass burning contributes approximately 17 %, 11 %, 4 % and 10 % of global biomass burning emissions of CH_3Cl , CH_3Br , CH_3I and COS respectively. These estimate are subject to large uncertainties.

- Global annual emission estimates of tropical forest fire and savannahs show a good agreement with the literature for CH_3Cl and CH_3Br . Estimates for CH_3I are considerably lower than the literature for forest fires but are in better agreement for savannah fires. These estimates are subject to large uncertainties.
- Global COS biomass burning emission estimates are lower than the literature for tropical forest fires by $13\text{--}30 \text{ Ggyr}^{-1}$ but higher than the literature for savannah fires by $\sim 31 \text{ Ggyr}^{-1}$. COS for Brazilian Cerrado have not, to the author's knowledge, been reported before.

6.1.4.2 Background rainforest emissions

- Background measurements over the South American rainforest confirm terrestrial sources of CH_3Cl , CH_3Br and CHCl_3 .
 - Emissions from a localised source of CHCl_3 were identified in background measurements. Proposed hypotheses for emissions source were upwind burning, anthropogenic emissions, emissions from the Balbina reservoir and forest clearance/agriculture. Though it was not possible to rule out any of these possibilities or positively identify the source, it is most likely that these emissions are linked to the Balbina reservoir and/or local agriculture and forest clearance.

6.2 Discussion and future work

6.2.1 TOF-GC MS

The TOF GC-MS did not meet the expectations, when purchased, of an instrument with similar or better performance to that of the industry leading quadrupole MS. However, the performance is such that it could still be used for atmospheric measurements, if current reliability issues can be resolved. The TOF GC-MS might find use in polluted atmospheres where the large number of ions recorded would allow for easier deconvolution of overlapping signals and identification of compound interferences. Certain analyses might not currently be possible, such as for low mixing ratio compounds in clean atmospheric environments.

Improvements to reproducibility and, to a lesser extent, sensitivity, are required to make the TOF a serviceable instrument. Reproducibility might be improved by refinement of the existing inlet system and GC-to-MS transfer line. Sensitivity improvements will require further alterations or upgrades in collaboration with the manufacturers. A replacement detector might improve the sensitivity in the short term as it is possible that the current detector is reaching the end of its operational lifetime, where detector gain can be reduced. These changes might also improve the linearity of the system at low sample volumes and concentrations by reducing losses to the inlet and GC parts of the instrument. Additionally, linearity would be better characterised by analysis of a static dilution series. This would give a better indication of whether the possible non-linearities observed with a volume series (see Section 3.4.6) are the result of analyte concentration or sample size. A further comparison, preferably in a realistic field situation or, at least, between measurements made on the same bottle samples would provide a better indication of the limitations of the TOF GC-MS.

The main advantage of the TOF GC-MS remains the large number of ions analysed without decreasing sensitivity. However, positive identification of compounds, through the analysis of fragmentation patterns, can still be difficult in practise. This is especially the case in polluted environments where a large number of compounds with overlapping ions might be present. Two routes of improvement might provide solutions: a software solution for mass spectral deconvolution or the implementation of GC×GC. Both methods have associated advantages and disadvantages. For instance deconvolution software can be inefficient for large numbers of compounds and may not be able to separate all compounds of interest. Similarly, the GC×GC technique available for the TOF GC-MS, dual jet cryojet modulation, uses liquid N₂ and would not be suitable for field deployment.

The future application of the GC-TOF is not certain at the time of writing. However, a number of uses can be envisaged for the instrument. As discussed previously, the GC-TOF would be particularly well suited to atmospheric analysis in polluted environments, such as urban centres, due to the large number of simultaneously detectable compounds, each with full mass spectra to aid identification. This would be most pertinent if the range of compounds of interest was expanded beyond halocarbons to include species such as hydrocarbons. Perhaps more interesting is the potential to make measurements of more exotic species, such as minor halocarbons, sulfur-containing compounds, or previously unidentified atmospheric trace gases. The advantages of GC-TOF would also make it suitable for analysis of biological emissions, e.g. direct emissions from plants, phytoplankton etc., where mixing ratios are much higher than in the atmosphere. The GC-TOF instrument could also be used as a detector in parallel with a quadrupole MS e.g. an NICI quadrupole GC-MS in a setup similar to that used in Chapter 3 for in situ analysis during the ClearfLo campaign. NICI GC-MS increases the sensitivity towards high electron affinity compounds such as halocarbons (see Section 2.2.3.2). However, NICI is a 'soft' ionisation technique, with little or no ion fragmentation, and requires that a quadrupole instrument be run in single ion monitoring (SIM) with a limited number of ions to maximise sensitivity. The increased sensitivity comes with a necessary decrease in the mass spectral information acquired i.e. the ability to identify compounds from ion fragments. A parallel TOF detector with its high m/z range might aid positive identification of compounds while the NICI detector provides the higher sensitivities required for low abundance species. There would be an additional benefit, in a parallel TOF detector, of being able to analyse a large number of low electron affinity compounds in addition to those analysed by NICI. There is also the possibility of converting the GC-TOF into an NICI instrument by using an alternate ion source. This would provide a higher sensitivity analysis for electronegative compounds whilst giving more information on ion fragmentation to aid positive identification and co-elutants/interferences.

Alternately, the GC-TOF could find a role in preparatory work such as that undertaken for compound identification, analytical method development and calibration. Recently, for instance, as-yet unpublished work was undertaken at UEA to develop methods of analysing, identifying and calibrating a number of isoprene nitrates (e.g. $\text{CH}_2=\text{CH}-\text{C}(\text{CH}_3)(\text{ONO}_2)-\text{CH}_2\text{OH}$, Lockwood et al. (2010)). Numerous preparatory tests and calibrations involving synthesised isoprene nitrates with analysis on a quadrupole GC-MS were required due to the high reactivity of these compounds. A TOF MS would have simplified positive identification of compounds and contaminants and would also have allowed for a better and faster assessment of the consequences of methodology

changes e.g. break-down products.

The TOF is mainly limited in its application by the unreliability of hardware and software. An additional limitation is the low sensitivity of the instrument which effectively rules out a number of atmospheric analyses, such as upper tropospheric or stratospheric measurements where a large number of compounds of interest are present at low mixing ratios. It is doubtful that sensitivity will be improved with further work. In spite of these shortcomings, the GC-TOF is currently usable under laboratory conditions, i.e. not for fieldwork. Better integration with a GC and an alternate, preferably automated, inlet system would be required for useful analysis. Furthermore, software updates may aid usability, stability and control of the instrument and some hardware replacements, such as a new detector, might aid instrument performance. At the time of writing, the next step in restoring the TOF is to separate it from the provided GC and use it as a standalone MS with a known GC system before using it in one of the applications mentioned above.

6.2.2 Halocarbons in London

Preliminary analysis of measurements made for the ClearLo campaign indicate that London is largely adherent to the terms of the Montreal Protocol. The higher concentrations of HCFCs and HFCs measured indicate, not unexpectedly, that these compounds are being heavily used in London. The HCFCs will be phased out of production and usage by 2030, however, these results highlight the importance of continued and regular monitoring of these compounds in the atmosphere for the purposes of future regulation and policy-making. Perhaps the more significant of the two, for future regulation, are the HFCs. It might be envisaged that London, and presumably the rest of the U.K., will continue to adhere to the terms of the Montreal Protocol and reduce the consumption of HCFCs. The long-term replacement compounds, the HFCs, are likely to be produced and used in ever larger quantities. Though the effects of stratospheric ozone depletion will be diminished by this switch-over, the high GWPs of HFCs will have an increasing impact on global warming. Similarly, PFCs and other perfluorinated compounds require continued monitoring for the purposes of feeding into appropriate legislation lest they become a more significant threat to future global warming. Though current atmospheric levels of these compounds are currently small, their very long lifetimes and high GWPs imply that caution should be exercised to limit the growth of these compounds as their emissions effectively represent a permanent change to the atmosphere on human time-scales.

Short-lived chlorinated compounds in London indicate strong sources, likely to be a combination of local and regional emissions from continental Europe. These results highlight that short-lived chlorocarbons should be closely monitored in the future, especially as levels of CH_2Cl_2 are increasing in the atmosphere. The short-lived bromomethanes and iodomethanes measured in London show that there are strong marine influences on air quality in London. Emissions of bromomethanes, especially bromoform, are likely to be sourced from seaweed beds off the coast of Normandy, France or from nuclear power plant cooling water.

A more detailed analysis is necessary in order to determine the proportional influence of emissions from London or continental Europe on levels of anthropogenic halocarbons. It will not be possible to derive an accurate emission inventory due to the lack of reliable upwind background measurements for comparison. A more detailed back trajectory analysis might provide information on likely sources of short-lived chlorocarbons, and comparison to measurements made during

winter might further elucidate those sources. Future measurements of halocarbons in London, or other urban centres, should include upwind baseline measurements and a downwind site might be preferable for capturing emissions. The ClearLo results indicate that urban emissions, especially for short-lived compounds, might be important for future halocarbon inventory monitoring and source apportionment.

6.2.3 VSLB in the mid-upper troposphere

Results from the CARIBIC project show that total bromine, derived from the five most significant naturally sourced bromocarbons, is on average ~ 3.4 ppt in the tropical mid-upper troposphere (10–12 km altitude). This value lies at the lower end of the assumed inorganic bromine (Br_y) derived from VLS in the stratosphere, 6 (3–8) ppt. As measurements were not made at the lower bound of the ~ 12 –17 km range of the TTL, the VSLB are likely to be degraded further before they reach the stratosphere. This implies that the contribution of VSLB to stratospheric Br_y has been overestimated in the past. Further refinements in the methods used to model Br_y from stratospheric BrO observations are expected to lower the required contribution of VSLB to stratospheric bromine (e.g. Kreyer et al., 2013). Closure of this Br_y gap is likely to come from a combination of improved modelling and further measurements over the full range of the troposphere from surface to TTL.

Of the five VSLB measured, only CH_2Br_2 showed a notable variation in mixing ratio between the tropical areas that the CARIBIC aircraft overflew. Measurements over Southeast Asia and the Western Pacific showed higher concentrations of CH_2Br_2 . Two possible explanations were offered: a higher $\text{CHBr}_3/\text{CH}_2\text{Br}_2$ emission ratio or locally low hydroxyl radical (OH) concentrations. Of the two explanations, lower OH mixing ratios over the Western Pacific appears more likely in light of evidence from Rex et al. (2014). Lower OH concentrations would lead to longer local lifetimes for compounds dominated by OH reactions and hence, to reduced tropospheric removal rates. Therefore, a larger proportion of these compounds could be transported to the TTL and from there into the stratosphere. If there is an ‘OH hole’ over Southeast Asia the implications for transport into the stratosphere would be similar for other halocarbons, such as the HCFCs. Hydroxyl radical concentrations can be probed by analysis of the reaction kinetics of hydrocarbon pairs with similar well-defined sources and constant emissions ratios but differing OH reaction rates (e.g. Jobson et al., 1999). Assuming that the emission ratios of CHBr_3 and CH_2Br_2 are relatively constant in the tropics, an analogous process might be possible for pairs of VSLB. This would be complicated by the competing and sometimes dominant, as is the case for CHBr_3 , photolysis reaction and this would require calculation of photolysis rates during the passage of air from the surface to the aircraft. The well-defined back-trajectories, and relatively short transport times from the surface of air collected over Southeast Asia might help to constrain the photolysis rate somewhat. Assuming a co-located source, a comparison could be made to hydrocarbon pair results.

Further measurements of VSLB, and other halocarbons, over Southeast Asia are necessary in the future to gain a better understanding of emissions and processing of VSLB in this region. This would also help to identify possible anthropogenic sources of trihalomethanes. Current instrumental set-up does not allow for the accurate measurement of all bromocarbons, especially the halons. Future CARIBIC measurements will aim to create a complete bromine budget in the

mid- to upper-troposphere including all halons as well as short-lived bromocarbons. Another key factor for measurement improvement that requires frequent reassessment, is the comparison of calibration scales between laboratories. Measurement comparisons are limited, to some extent, by the potential offsets of differing calibration scales. This is the case for all measurement comparisons made in this work. Short-lived compounds, due to their instability in some containers, are also affected by concentration drift and require routine reanalysis in order to provide accurate mixing ratios.

6.2.4 Brazilian biomass burning and background emissions

Measurements of biomass burning emissions made during the SAMBBA campaign show that current estimates for tropical fire emissions are representative for CH_3Cl in Brazil. However, tropical forest fire emissions of CH_3Br , CH_3I and COS in Brazil are overestimated by the most up-to-date and commonly referred to summary of compounds emitted from biomass burning i.e. Akagi et al. (2011). Savannah emissions of CH_3Cl and CH_3I agree well with the literature and CH_3Br is slightly lower than literature values. Measurements of COS from Cerrado savannah fires have not been reported before in literature to the author's knowledge. Cerrado fire emissions were found to be higher, per kilogram of dry matter burned, than Brazilian forest fires. These results highlight that burning emissions are not always accurately represented by averaging over broad ecological environments such as tropical forest or savannah. Emissions are dependent on the specific ecological environment, the biome, and largely controlled by the type and density of vegetation. Some compounds might be more variable between similar biomes than others, i.e. CH_3Cl appears to be more accurately represented in global means than CH_3Br and CH_3I . This is probably dependent on factors such as the halogen content of the vegetation and the variability of burning characteristics, e.g. smoldering and flaming combustion. Future global estimates for burning emissions of methyl halides, and other halocarbons, need to take this variability into account and integrate accurate representations of fire distribution and type. There do not appear, in SAMBBA results, to be fire emissions of other major halocarbons, long- or short-lived, in contrast to some reports in the literature. Further investigation of these compounds from a range of environments is needed to confirm this.

Regional annual emission estimates indicate that South America is an important contributor to global biomass burning emissions. Crucially, fire emissions from this region are located where trace-gases can be rapidly convected into the TTL and, consequently, have an impact on stratospheric mixing ratios. Fire emissions in South America are heavily influenced by human activities such as slash-and-burn forest clearance and might be considered to be anthropogenic and natural in origin. Depending on whether human forest clearance increases or decreases in the future, fire emissions and the effects on stratospheric halocarbon levels might be of increasing importance. As such, monitoring and better quantifying emissions from this region will be of continuing importance. SAMBBA measurements indicate that the cerrado savannah, and perhaps other savannah biomes, are an important source of COS that requires further investigation to better quantify emission estimates.

Background forest emissions from the Brazilian rainforest confirm a terrestrial source of CH_3Cl , CH_3Br and CHCl_3 . A localised source of CHCl_3 was identified as possibly being linked to soil processes in wetlands or agricultural soil disturbance. Though short-lived, these CHCl_3

emissions are, similarly to the burning emissions discussed above, in a location of rapid transport to the TTL. This adds to the impact of anthropogenic activity in the Amazon rainforest provided the source is from agricultural soil disturbance. If the source is from the wetland habitat created by the Balbina reservoir, this has ramifications for future hydroelectric power generation in Brazil. The Balbina dam was a controversial hydroelectric project, from ecological, power generation and human perspectives. Construction is currently under way on a similarly controversial hydroelectric plant on the Rio Xingu in Pará, Brazil; the Belo Monte Dam and its flow-regulating dam the Altamira/Babaquara Dam. Together, these dams will flood 6580 km² of Amazon rainforest, a flooded area more than 3.5 times larger than that of the Balbina reservoir, as well as displacing a large number of indigenous people and greatly affecting the local ecosystem (Fearnside, 2006; Kemenes et al., 2007). Emissions from soil systems and wetland habitats need to be further investigated and quantified to derive an accurate emission inventory for CHCl₃. A more in-depth investigation of emissions and fluxes from large-scale, man-made wetlands, such as the Balbina and Belo Monte reservoir systems would further the understanding and impacts of these structures and inform the decision-making processes for similar future projects. This would also apply to gases other than the halocarbons such as greenhouse gases (e.g. CH₄, CO₂ and N₂O).

References

- Abril G, Parize M, Pérez MAP & Filizola N. “Wood decomposition in Amazonian hydropower reservoirs: An additional source of greenhouse gases.” *J. South Am. Earth Sci.*, **44**, 104–107, **2013**, URL <http://dx.doi.org/10.1016/j.jsames.2012.11.007>.
- Akagi SK, Yokelson RJ, Burling IR, Meinardi S, Simpson I, Blake DR, McMeeking GR, Sullivan A, Lee T, Kreidenweis S, Urbanski S, Reardon J, Griffith DWT, Johnson TJ & Weise DR. “Measurements of reactive trace gases and variable O₃ formation rates in some South Carolina biomass burning plumes.” *Atmos. Chem. Phys.*, **13** (3), 1141–1165, **2013**, URL <http://dx.doi.org/10.5194/acp-13-1141-2013>.
- Akagi SK, Yokelson RJ, Wiedinmyer C, Alvarado MJ, Reid JS, Karl T, Crouse JD & Wennberg PO. “Emission factors for open and domestic biomass burning for use in atmospheric models.” *Atmos. Chem. Phys.*, **11** (9), 4039–4072, **2011**, URL <http://dx.doi.org/10.5194/acp-11-4039-2011>.
- Anderson JG, Wilmouth DM, Smith JB & Sayres DS. “UV dosage levels in summer: increased risk of ozone loss from convectively injected water vapor.” *Science*, **337** (6096), 835–9, **2012**, URL <http://dx.doi.org/10.1126/science.1222978>.
- Andreae MO, Artaxo P, Beck V, Bela M, Freitas S, Gerbig C, Longo K, Munger JW, Wiedemann KT & Wofsy SC. “Carbon monoxide and related trace gases and aerosols over the Amazon Basin during the wet and dry seasons.” *Atmos. Chem. Phys.*, **12**, 6041–6065, **2012**, URL <http://dx.doi.org/10.5194/acp-12-6041-2012>.
- Andreae MO, Atlas EL, Harris GW, Helas G, de Kock A, Koppmann R, Maenhaut W, Manø S, Pollock WH, Rudolph J, Scharffe D, Schebeske G & Welling M. “Methyl halide emissions from savanna fires in southern Africa.” *J. Geophys. Res.*, **101** (D19), 23,603–23,613, **1996**.
- Andreae MO & Merlet P. “Emission of trace gases and aerosols from biomass burning.” *Global Biogeochem. Cycles*, **15** (4), 955–966, **2001**, URL <http://dx.doi.org/10.1029/2000GB001382>.
- Aschmann J, Sinnhuber BM, Atlas EL & Schauflier SM. “Modeling the transport of very short-lived substances into the tropical upper troposphere and lower stratosphere.” *Atmos. Chem. Phys.*, **9** (23), 9237–9247, **2009**, URL <http://dx.doi.org/10.5194/acp-9-9237-2009>.
- Ashfold MJ, Harris NRP, Atlas EL, Manning AJ & Pyle JA. “Transport of short-lived species into the Tropical Tropopause Layer.” *Atmos. Chem. Phys.*, **12** (14), 6309–6322, **2012**, URL <http://dx.doi.org/10.5194/acp-12-6309-2012>.
- Ashfold MJ, Harris NRP, Manning aJ, Robinson aD, Warwick NJ & Pyle Ja. “Estimates of tropical bromoform emissions using an inversion method.” *Atmos. Chem. Phys.*, **13** (8), 20,463–20,502, **2013**, URL <http://dx.doi.org/10.5194/acpd-13-20463-2013>.
- Atkinson R, Aschmann SM, Winer AM & Pitts JN. “Atmospheric gas phase loss processes for chlorobenzene, benzotrifluoride, and 4-chlororbenzotrifluoride, and generalization of predictive techniques for atmospheric lifetimes of aromatic compounds.” *Arch. Environ. Contam. Toxicol.*, **14**, 417–425, **1985**.
- Baker AK, Rauthe-Schöch A, Schuck TJ, Brenninkmeijer CAM, van Velthoven PFJ, Wisher A & Oram DE. “Investigation of chlorine radical chemistry in the Eyjafjallajökull volcanic plume

- using observed depletions in non-methane hydrocarbons.” *Geophys. Res. Lett.*, **38** (13), 1–6, **2011a**, URL <http://dx.doi.org/10.1029/2011GL047571>.
- Baker AK, Schuck TJ, Slemr F, van Velthoven P, Zahn A & Brenninkmeijer CAM. “Characterization of non-methane hydrocarbons in Asian summer monsoon outflow observed by the CARIBIC aircraft.” *Atmos. Chem. Phys.*, **11** (2), 503–518, **2011b**, URL <http://dx.doi.org/10.5194/acp-11-503-2011>.
- Baker AK, Slemr F & Brenninkmeijer CAM. “Analysis of non-methane hydrocarbons in air samples collected aboard the CARIBIC passenger aircraft.” *Atmos. Meas. Tech.*, **3**, 311–321, **2010**.
- Bell N. “Methyl iodide: Atmospheric budget and use as a tracer of marine convection in global models.” *J. Geophys. Res.*, **107** (D17), 4340, **2002**, URL <http://dx.doi.org/10.1029/2001JD001151>.
- Bennett M, Blinova O, Derwent R, McCulloch A, Yamabe M, Shevlin J & Vink T. “HFCs and PFCs: current and future supply, demand and emissions, plus emissions of CFCs, HCFCs and Halons.” In: G Hayman & L Kuijpers (editors), “IPCC/TEAP Spec. Rep. Safeguarding Ozone Layer Glob. Clim. Syst.”, chapter 11, page 34. Cambridge University Press, Cambridge, UK, **2005**.
- Bethan S, Vaughan G & Reid SJ. “A comparison of ozone and thermal tropopause heights and the impact of tropopause definition on quantifying the ozone content of the troposphere.” *Q. J. R. Meteorol. Soc.*, **122**, 929–944, **1996**.
- Blake NJ, Blake DR, Sive BC, Chen Ty, Sherwood Rowland F, Collins Jr JE, Sachse GW & Anderson BE. “Biomass burning emissions and vertical distribution of atmospheric methyl halides and other reduced carbon gases in the South Atlantic region.” *J. Geophys. Res.*, **101**, 151–164, **1996**, URL <http://dx.doi.org/10.1029/96JD00561>.
- Bohnenstengel SI, Belcher SE, Aiken A, Allan JD, Allen G, Bacak A, Bannan TJ, Barlow JF, Beddows DC, Bloss WJ, Booth AM, Chemel C, Coceal O, Di Marco CF, Dubey MK, Faloon KH, Fleming ZL, Furger M, Gietl JK, Graves RR, Green DC, Grimmond CSB, Halios CH, Hamilton JF, Harrison RM, Heal MR, Heard DE, Helfter C, Herndon SC, Holmes RE, Hopkins JR, Jones AM, Kelly FJ, Kotthaus S, Langford B, Lee JD, Leigh RJ, Lewis AC, Lidster RT, Lopez-Hilfiker FD, McQuaid JB, Mohr C, Monks PS, Nemitz E, Ng NL, Percival CJ, Prévôt ASH, Ricketts HMA, Sokhi R, Stone D, Thornton JA, Tremper AH, Valach AC, Visser S, Whalley LK, Williams LR, Xu L, Young DE & Zotter P. “Meteorology, air quality, and health in London: The ClearLo project.” *Bull. Am. Meteorol. Soc.*, **2014**, URL <http://dx.doi.org/10.1175/BAMS-D-12-00245.1>.
- Bond TC. “A technology-based global inventory of black and organic carbon emissions from combustion.” *J. Geophys. Res.*, **109** (D14), D14,203, **2004**, URL <http://dx.doi.org/10.1029/2003JD003697>.
- Brenninkmeijer CAM, Crutzen PJ, Boumard F, Dauer T, Dix B, Ebinghaus R, Filippi D, Fischer H, Franke H, Frieß U, Heintzenberg J, Helleis F, Hermann M, Kock HH, Koeppel C, Lelieveld J, Leuenberger M, Martinsson BG, Miemczyk S, Moret HP, Nguyen HN, Nyfeler P, Oram D, O’Sullivan D, Penkett S, Platt U, Pucek M, Ramonet M, Randa B, Reichelt M, Rhee TS, Rohwer J, Rosenfeld K, Scharffe D, Schlager H, Schumann U, Slemr F, Sprung D, Stock P, Thaler R, Valentino F, van Velthoven P, Waibel A, Wandel A, Waschitschek K, Wiedensohler A, Xueref-Remy I, Zahn A, Zech U & Ziereis H. “Civil Aircraft for the regular investigation of the atmosphere based on an instrumented container: The new CARIBIC system.” *Atmos. Chem. Phys.*, **7** (18), 4953–4976, **2007**, URL <http://dx.doi.org/10.5194/acp-7-4953-2007>.
- Brinckmann S, Engel A, Bönisch H, Quack B & Atlas EL. “Short-lived brominated hydrocarbons — observations in the source regions and the tropical tropopause layer.” *Atmos. Chem. Phys.*, **12**, 1213–1228, **2012**, URL <http://dx.doi.org/10.5194/acp-12-1213-2012>.
- Butler JH, King DB, Lobert JM, Montzka SA, Yvon-Lewis SA, Hall BD, Warwick NJ, Mondeel DJ, Aydin M & Elkins JW. “Oceanic distributions and emissions of short-lived halocarbons.” *Global Biogeochem. Cycles*, **21**, **2007**, URL <http://dx.doi.org/10.1029/>

- 2006GB002732.
- Campbell JM, Collings BA & Douglas DJ. “A new linear ion trap time-of-flight system with tandem mass spectrometry capabilities.” *Rapid Commun. Mass Spectrom.*, **12** (20), 1463–1474, **1998**, URL [http://dx.doi.org/10.1002/\(SICI\)1097-0231\(19981030\)12:20<1463::AID-RCM357>3.0.CO;2-H](http://dx.doi.org/10.1002/(SICI)1097-0231(19981030)12:20<1463::AID-RCM357>3.0.CO;2-H).
- Cantrell CA. “Technical Note: Review of methods for linear least-squares fitting of data and application to atmospheric chemistry problems.” *Atmos. Chem. Phys.*, **8**, 5477–5487, **2008**, URL <http://dx.doi.org/10.5194/acpd-8-6409-2008>.
- Carpenter LJ, Jones CE, Dunk RM, Hornsby KE & Woeltjen J. “Air-sea fluxes of biogenic bromine from the tropical and North Atlantic Ocean.” *Atmos. Chem. Phys.*, **9**, 1805–1816, **2009**.
- Carpenter LJ, Wevill DJ, O’Doherty S, Spain G & Simmonds PG. “Atmospheric bromoform at Mace Head, Ireland: seasonality and evidence for a peatland source.” *Atmos. Chem. Phys.*, **5** (11), 2927–2934, **2005**, URL <http://dx.doi.org/10.5194/acp-5-2927-2005>.
- Chameides WL & Davis DD. “Iodine : Its possible role in tropospheric photochemistry.” *J. Geophys. Res.*, **85**, 7383–7398, **1980**, URL <http://dx.doi.org/10.1029/JC085iC12p07383>.
- Chapman S. “A theory of upper-atmospheric ozone.” *Mem. R. Meteorol. Soc.*, **3** (26), 103–125, **1930**.
- Clerbaux C & Cunnold DM. “Long-lived Compounds.” In: “Scientific Assessment of Ozone Depletion 2006, Global Ozone Research Monitoring Project Report No. 50,” February, chapter 1, pages 1.1–1.63. World Meteorological Organization (WMO), Geneva, Switzerland, **2007**.
- Cox ML, Sturrock G, Fraser P, Siems S, Krummel P & O’Doherty S. “Regional sources of methyl chloride, chloroform and dichloromethane identified from AGAGE observations at Cape Grim, Tasmania, 19982000.” *J. Atmos. Chem.*, **45**, 79–99, **2003**.
- Crutzen PJ, Leroy E H, Krasnec JP, Pollock WH & Seiler W. “Biomass burning as a source of atmospheric gases CO, H₂, N₂O, CH₃Cl and COS.” *Nature*, **282**, 253–256, **1979**.
- Cunnold DM, Weiss RF, Prinn RG, Hartley D, Simmonds PG, Fraser PJ, Miller B, Alyea FN & Porter L. “GAGE/AGAGE measurements indicating reductions in global emissions of CCl₃F and CC₁₂F₂ in 1992-1994.” *J. Geophys. Res.*, **102** (D1), 1259–1269, **1997**.
- Dallüge J, Roose P & Brinkman UAT. “Evaluation of a high-resolution time-of-flight mass spectrometer for the gas chromatographic determination of selected environmental contaminants.” *J. Chromatogr. A*, **970** (1-2), 213–23, **2002**.
- DEFRA. “Department for Environment and Rural Affairs; Guidance for fire protection sectors; Guidance: F gas and ozone regulations; Information sheet FP 2: Usage.” (retrieved 20/11/14), **2012**, URL https://www.gov.uk/government/uploads/system/uploads/attachment_data/file/182562/fgas-fp2-usage.pdf.
- Dessens O, Zeng G, Warwick N & Pyle JA. “Short-lived bromine compounds in the lower stratosphere ; impact of climate change on ozone.” *Atmos. Sci. Lett.*, **10**, 201–206, **2009**, URL <http://dx.doi.org/10.1002/asl.236>.
- Dorf M, Butler JH, Butz A, Camy-Peyret C, Chipperfield MP, Kritten L, Montzka SA, Simmes B, Weidner F & Pfeilsticker K. “Long-term observations of stratospheric bromine reveal slow down in growth.” *Geophys. Res. Lett.*, **33** (24), 2–5, **2006**, URL <http://dx.doi.org/10.1029/2006GL027714>.
- Dorf M, Butz A, Camy-Peyret C, Chipperfield MP, Kritten L & Pfeilsticker K. “Bromine in the tropical troposphere and stratosphere as derived from balloon-borne BrO observations.” *Atmos. Chem. Phys. Discuss.*, **8** (4), 12,999–13,015, **2008**, URL <http://dx.doi.org/10.5194/acpd-8-12999-2008>.
- Draxler RR & Rolph GD. “HYSPLIT (HYbrid Single-Particle Lagrangian Integrated Trajectory) Model access via NOAA ARL READY Website, NOAA Air Resources Laboratory, College Park, MD.”, **2013**, URL <http://www.arl.noaa.gov/HYSPLIT.php>.
- Evyugina M, Calvo AI, Nunes T, Alves C, Fernandes AP, Tarelho L, Vicente A & Pio C. “VOC emissions of smouldering combustion from Mediterranean wildfires in central Portugal.” *Atmos.*

- Environ.*, **64**, 339–348, **2013**, URL <http://dx.doi.org/10.1016/j.atmosenv.2012.10.001>.
- Farman JC, Gardiner BG & Shanklin JD. “Large losses of total ozone in Antarctica reveal seasonal ClO_x/NO_x interaction.” *Nature*, **315 (6016)**, 207–210, **1985**, URL <http://dx.doi.org/10.1038/315207a0>.
- Fearnside PM. “Brazil’s Balbina Dam : Environment versus the legacy of the pharaohs in Amazonia.” *Environ. Manage.*, **13 (4)**, 401–423, **1989**.
- Fearnside PM. “Dams in the Amazon: Belo Monte and Brazil’s hydroelectric development of the Xingu River Basin.” *Environ. Manage.*, **38 (1)**, 16–27, **2006**, URL <http://dx.doi.org/10.1007/s00267-005-0113-6>.
- Ferek RJ, Reid JS, Hobbs PV, Blake DR & Liousse C. “Emission factors of hydrocarbons, halocarbons, trace gases and particles from biomass burning in Brazil.” *J. Geophys. Res.*, **103 (D24)**, 32,107–32,118, **1998**.
- Fleming ZL, Monks PS & Manning AJ. “Review: Untangling the influence of air-mass history in interpreting observed atmospheric composition.” *Atmos. Res.*, **104-105**, 1–39, **2012**, URL <http://dx.doi.org/10.1016/j.atmosres.2011.09.009>.
- Forster GL, Sturges WT, Fleming ZL, Bandy BJ & Emeis S. “A year of H₂ measurements at Weybourne Atmospheric Observatory, UK.” *Tellus B*, **64 (17771)**, **2012**, URL <http://dx.doi.org/10.3402/tellusb.v64i0.1777>.
- Forster P, Ramaswamy V, Artaxo P, Berntsen T, Betts R, Fahey DW, Haywood J, Lean J, Lowe DC, Myhre G, Nganga J, Prinn R, Raga G, Schulz M, Dorland RV & Contributing. “Changes in atmospheric constituents and in radiative forcing.” In: T Nakajima & V Ramanathan (editors), “Contribution of Working Group I to the fourth assessment report of the Intergovernmental Panel on Climate Change,” chapter 2, pages 131–234. Cambridge University Press, Cambridge, United Kingdom and New York, NY, USA, **2007**.
- Fraser P, Cunnold D, Alyea F, Weiss R, Prinn R, Simmonds P, Miller B & Langenfelds R. “Lifetime and emission estimates of 1,1,2-trichlorotrifluoroethane (CFC-113) from daily global background observations June 1982-June 1994.” *J. Geophys. Res.*, **101 (D7)**, 12,585–12,599, **1996**, URL <http://dx.doi.org/10.1029/96JD00574>.
- Fueglistaler S, Dessler AE, Dunkerton TJ, Folkins I, Fu Q & Mote PW. “Tropical tropopause layer.” *Rev. Geophys.*, **47 (RG1004)**, **2009**, URL <http://dx.doi.org/10.1029/2008RG000267>.
- Gebhardt S, Colomb A, Hofmann R, Williams J & Lelieveld J. “Halogenated organic species over the tropical South American rainforest.” *Atmospheric Chem. Phys.*, **8**, 3185–3197, **2008**.
- Gottelman A, Hoor P, Pan LL, Randel WJ, Hegglin MI & Birner T. “The Extratropical upper troposphere and lower stratosphere.” *Rev. Geophys.*, **49**, 1–31, **2011**, URL <http://dx.doi.org/10.1029/2011RG000355>.
- Guilhaus M, Mlynski V & Selby D. “Perfect timing: time-of-flight mass spectrometry.” *Rapid Commun. Mass Spectrom.*, **11 (9)**, 951–962, **1997**, URL [http://dx.doi.org/10.1002/\(SICI\)1097-0231\(19970615\)11:9<951::AID-RCM785>3.3.CO;2-8](http://dx.doi.org/10.1002/(SICI)1097-0231(19970615)11:9<951::AID-RCM785>3.3.CO;2-8).
- Guilhaus M, Selby D & Mlynski V. “Orthogonal acceleration time-of-flight mass spectrometry.” *Mass Spectrom. Rev.*, **19 (2)**, 65–107, **2000**, URL [http://dx.doi.org/10.1002/\(SICI\)1098-2787\(2000\)19:2<65::AID-MAS1>3.0.CO;2-E](http://dx.doi.org/10.1002/(SICI)1098-2787(2000)19:2<65::AID-MAS1>3.0.CO;2-E).
- Hall BD, Engel A, Mühle J, Elkins JW, Artuso F, Atlas EL, Aydin M, Blake DR, Brunke EG, Chiavarini S, Fraser PJ, Happell J, Krummel PB, Levin I, Loewenstein M, Maione M, Montzka SA, O’Doherty S, Reimann S, Rhoderick G, Saltzman ES, Scheel HE, Steele LP, Vollmer MK, Weiss RF, Worthy D & Yokouchi Y. “Results from the International Halocarbons in Air Comparison Experiment (IHALACE).” *Atmos. Meas. Tech.*, **7**, 469–490, **2014**, URL <http://dx.doi.org/10.5194/amtd-6-8021-2013>.
- Hamilton J, Webb P, Lewis AC, Hopkins J, Smith S & Davy P. “Partially oxidised organic components in urban aerosol using GCXGC-TOF/MS.” *Atmos. Chem. Phys.*, **4 (2)**, 1393–1423, **2004**, URL <http://dx.doi.org/10.5194/acpd-4-1393-2004>.

- Hamilton JF. "Using comprehensive two-dimensional gas chromatography to study the atmosphere." *J. Chromatogr. Sci.*, **48** (4), 274–82, **2010**.
- Hamilton JTG, McRoberts WC, Keppler F, Kalin RM & Harper DB. "Chloride methylation by plant pectin: an efficient environmentally significant process." *Science* (80-.), **301** (5630), 206–9, **2003**, URL <http://dx.doi.org/10.1126/science.1085036>.
- Happell J & Wallace D. "Methyl iodide in the Greenland/Norwegian Seas and the tropical Atlantic Ocean: Evidence for photochemical production." *Geophys. Res. Lett.*, **23** (16), 2105–2108, **1996**.
- Hepach H, Quack B, Ziska F, Fuhlbrügge S, Atlas EL, Krüger K, Peeken I & Wallace DWR. "Drivers of diel and regional variations of halocarbon emissions from the tropical North East Atlantic." *Atmos. Chem. Phys.*, **14** (3), 1255–1275, **2014**, URL <http://dx.doi.org/10.5194/acp-14-1255-2014>.
- Hoekstra EJ, Duyzer JH, de Leer EWB & Brinkman UAT. "Chloroform - concentration gradients in soil air and atmospheric air, and emission fluxes from soil." *Atmos. Environ.*, **35**, 61–70, **2001**.
- Hoell JM, Davis DD, Jacob DJ, Rodgers MO, Newell RE, Fuelberg HE, McNeal RJ, Raper JL & Bendura RJ. "Pacific Exploratory Mission in the tropical Pacific :PEM-Tropics A, August-September 1996." *J. Geophys. Res.*, **104**, 5567–5583, **1999**, URL <http://dx.doi.org/10.1029/1998JD100074>.
- Hoell JM, Davis DD, Liu SC, Newell RE, Akimoto H, McNeal RJ & Bendura RJ. "The Pacific Exploratory Mission-West Phase B: February-March, 1994." *J. Geophys. Res.*, **102**, 28,223–28,239, **1997**, URL <http://dx.doi.org/10.1029/97JD02581>.
- Holloway AM & Wayne RP. *Atmospheric Chemistry*. Royal Society of Chemistry, Cambridge, UK, Cambridge, UK, 1st edition. ISBN 9781847558077, **2010**.
- Hossaini R, Chipperfield MP, Dhomse S, Ordóñez C, Saiz-Lopez A, Abraham NL, Archibald AT, Braesicke P, Telford P, Warwick N, Yang X & Pyle JA. "Modelling future changes to the stratospheric source gas injection of biogenic bromocarbons." *Geophys. Res. Lett.*, **39** (L20813), **2012a**, URL <http://dx.doi.org/10.1029/2012GL053401>.
- Hossaini R, Chipperfield MP, Feng W, Breider TJ, Atlas EL, Montzka SA, Miller BR, Moore F & Elkins J. "The contribution of natural and anthropogenic very short-lived species to stratospheric bromine." *Atmos. Chem. Phys.*, **12** (1), 371–380, **2012b**, URL <http://dx.doi.org/10.5194/acp-12-371-2012>.
- Hossaini R, Chipperfield MP, Monge-Sanz BM, Richards NaD, Atlas EL & Blake DR. "Bromoform and dibromomethane in the tropics: a 3-D model study of chemistry and transport." *Atmos. Chem. Phys.*, **10** (2), 719–735, **2010**, URL <http://dx.doi.org/10.5194/acp-10-719-2010>.
- Hossaini R, Mantle H, Chipperfield MP, Montzka SA, Hamer P, Ziska F, Quack B, Krüger K, Tegtmeier S, Atlas E, Sala S, Engel A, Bönisch H, Keber T, Oram D, Mills G, Ordóñez C, Saiz-Lopez A, Warwick N, Liang Q, Feng W, Moore F, Miller BR, Marécal V, Richards NAD, Dorf M & Pfeilsticker K. "Evaluating global emission inventories of biogenic bromocarbons." *Atmos. Chem. Phys.*, **13** (23), 11,819–11,838, **2013**, URL <http://dx.doi.org/10.5194/acp-13-11819-2013>.
- Hu L, Yvon-Lewis SA, Butler JH, Lobert JM & King DB. "An improved oceanic budget for methyl chloride." *J. Geophys. Res. Ocean.*, **118**, 715–725, **2013**, URL <http://dx.doi.org/10.1029/2012JC008196>.
- Huang L, Zhu L, Pan X, Zhang J, Ouyang B & Hou H. "One potential source of the potent greenhouse gas SF₅CF₃: the reaction of SF₆ with fluorocarbon under discharge." *Atmos. Environ.*, **39**, 1641–1653, **2005**, URL <http://dx.doi.org/10.1016/j.atmosenv.2004.11.013>.
- Hübschmann HJ. *Handbook of GC/MS*. Wiley-VCH Verlag GmBH, Weinheim, 2nd edition. ISBN 978-3-527-31427-0, **2009**.

- James AT & Martin AJP. "Gas-liquid partition chromatography : the separation and micro-estimation of volatile fatty acids from formic acid to dodecanoic acid." *Biochem. J.*, **50**, 679–690, **1952**.
- Jobson BT, McKeen SA, Parrish DD, Fehsenfeld FC, Blake DR, Goldstein AH, Schauffler SM & Elkins JW. "Trace gas mixing ratio variability versus lifetime in the troposphere and stratosphere: Observations." *J. Geophys. Res.*, **104 (D13)**, 16,091, **1999**, URL <http://dx.doi.org/10.1029/1999JD900126>.
- Jones A, Thomson D, Hort M & Devenish B. "The U.K. Met Office's Next-Generation Atmospheric Dispersion Model, NAME III." In: C Borrego & AL Norman (editors), "Air Pollut. Model. Its Appl. XVII," chapter 62, pages 580–589. Springer US. ISBN 978-0-387-28255-8, **2007**, URL http://dx.doi.org/10.1007/978-0-387-68854-1_62.
- Kallio M, Jussila M, Rissanen T, Anttila P, Hartonen K, Reissell A, Vreuls R, Adahchour M & Hyotylainen T. "Comprehensive two-dimensional gas chromatography coupled to time-of-flight mass spectrometry in the identification of organic compounds in atmospheric aerosols from coniferous forest." *J. Chromatogr. A*, **1125 (2)**, 234–43, **2006**, URL <http://dx.doi.org/10.1016/j.chroma.2006.05.050>.
- Kansal A. "Sources and reactivity of NMHCs and VOCs in the atmosphere: a review." *J. Hazard. Mater.*, **166 (1)**, 17–26, **2009**, URL <http://dx.doi.org/10.1016/j.jhazmat.2008.11.048>.
- Keene WC, Khalil MAK, Erickson DJ, McCulloch A, Graedel TE, Lobert JM, Aucott ML, Gong SL, Harper DB, Kleiman G, Midgley P, Moore RM, Seuzaret C, Sturges WT, Benkovitz CM, Koropalov V, Barrie LA & Li YF. "Composite global emissions of reactive chlorine from anthropogenic and natural sources: Reactive Chlorine Emissions Inventory." *J. Geophys. Res.*, **104 (D7)**, 8429–8440, **1999**, URL <http://dx.doi.org/10.1029/1998JD100084>.
- Kemenes A, Forsberg BR & Melack JM. "Methane release below a tropical hydroelectric dam." *Geophys. Res. Lett.*, **34 (12)**, L12,809, **2007**, URL <http://dx.doi.org/10.1029/2007GL029479>.
- Kemenes A, Forsberg BR & Melack JM. "CO₂ emissions from a tropical hydroelectric reservoir (Balbina, Brazil)." *J. Geophys. Res.*, **116 (G3)**, G03,004, **2011**, URL <http://dx.doi.org/10.1029/2010JG001465>.
- Kreytz S, Camy-Peyret C, Chipperfield MP, Dorf M, Feng W, Hossaini R, Kritzen L, Werner B & Pfeilsticker K. "Atmospheric test of the $J(\text{BrONO}_2)/k_{\text{BrO}+\text{NO}_2}$ ratio: implications for total stratospheric Br_y and bromine-mediated ozone loss." *Atmos. Chem. Phys.*, **13**, 6263–6274, **2013**, URL <http://dx.doi.org/10.5194/acp-13-6263-2013>.
- Kroon M, Petropavlovskikh I, Shetter R, Hall S, Ullmann K, Veefkind JP, McPeters RD, Browell EV & Levelt PF. "OMI total ozone column validation with Aura-AVE CAFS observations." *J. Geophys. Res.*, **113 (D15)**, D15S13, **2008**, URL <http://dx.doi.org/10.1029/2007JD008795>.
- Lai SC, Baker AK, Schuck TJ, Slemr F, Brenninkmeijer CAM, van Velthoven P, Oram DE, Zahn A & Ziereis H. "Characterization and source regions of 51 high-CO events observed during Civil Aircraft for the Regular Investigation of the Atmosphere Based on an Instrument Container (CARIBIC) flights between south China and the Philippines, 20052008." *J. Geophys. Res.*, **116 (D20)**, 2005–2008, **2011**, URL <http://dx.doi.org/10.1029/2011JD016375>.
- Laitinen T, Martín SH, Parshintsev J, Hyotylainen T, Hartonen K, Riekkola ML, Kulmala M & Pavón JLP. "Determination of organic compounds from wood combustion aerosol nanoparticles by different gas chromatographic systems and by aerosol mass spectrometry." *J. Chromatogr. A*, **1217 (1)**, 151–9, **2010**, URL <http://dx.doi.org/10.1016/j.chroma.2009.11.028>.
- Laube JC, Engel A, Bönisch H, Möbius T, Worton DR, Sturges WT, Grunow K & Schmidt U. "Contribution of very short-lived organic substances to stratospheric chlorine and bromine in the tropics a case study." *Atmos. Chem. Phys.*, **8 (3)**, 8491–8515, **2008**, URL <http://dx.doi.org/10.5194/acpd-8-8491-2008>.
- Laube JC, Hogan C, Newland MJ, Mani FS, Fraser P J, Brenninkmeijer CAM, Martinerie P, Oram

- DE, Röckmann T, Schwander J, Witrant E, Mills GP, Reeves CE & Sturges WT. “Distributions, long term trends and emissions of four perfluorocarbons in remote parts of the atmosphere and firn air.” *Atmos. Chem. Phys.*, **12**, 4081–4090, **2012**, URL <http://dx.doi.org/10.5194/acp-12-4081-2012>.
- Laube JC, Martinerie P, Witrant E, Blunier T, Schwander J, Brenninkmeijer CAM, Schuck TJ, Bolder M, Röckmann T, van der Veen C, Bönisch H, Engel A, Mills GP, Newland MJ, Oram DE, Reeves CE & Sturges WT. “Accelerating growth of HFC-227ea (1,1,1,2,3,3,3-heptafluoropropane) in the atmosphere.” *Atmos. Chem. Phys.*, **10** (13), 5903–5910, **2010**, URL <http://dx.doi.org/10.5194/acp-10-5903-2010>.
- Laube JC, Newland MJ, Hogan C, Brenninkmeijer CAM, Fraser PJ, Martinerie P, Oram DE, Reeves CE, Röckmann T, Schwander J, Witrant E & Sturges WT. “Newly detected ozone-depleting substances in the atmosphere.” *Nat. Geosci.*, **7** (4), 266–269, **2014**, URL <http://dx.doi.org/10.1038/ngeo2109>.
- Law KS & Sturges WT. “Halogenated Very Short-Lived Substances.” In: “Scientific Assessment of Ozone Depletion 2006, Global Ozone Research Monitoring Project Report No. 50,” February, chapter 2, pages 2.1–2.57. World Meteorological Organization (WMO), Geneva, Switzerland, **2007**.
- Lee-Taylor J & Redeker KR. “Reevaluation of global emissions from rice paddies of methyl iodide and other species.” *Geophys. Res. Lett.*, **32** (L15801), **2005**, URL <http://dx.doi.org/10.1029/2005GL022918>.
- Leedham EC, Hughes C, Keng FSL, Phang SM, Malin G & Sturges WT. “Emission of atmospherically significant halocarbons by naturally occurring and farmed tropical macroalgae.” *Biogeosciences*, **10** (6), 3615–3633, **2013**, URL <http://dx.doi.org/10.5194/bg-10-3615-2013>.
- Leedham Elvidge EC, Oram DE, Laube JC, Baker AK, Montzka SA, Humphrey S, O’Sullivan DA & Brenninkmeijer CAM. “Increasing concentrations of dichloromethane, CH₂Cl₂, inferred from CARIBIC air samples collected 1998–2012.” *Atmos. Chem. Phys. Discuss.*, **14**, 20,721–20,765, **2014**, URL <http://dx.doi.org/10.5194/acpd-14-20721-2014>.
- Levin I, Naegler T, Heinz R, Osusko D, Cuevas E, Engel A, Ilmberger J, Langenfelds RL, Neininger B, Rohden CV, Steele LP, Weller R, Worthy DE & Zimov Sa. “The global SF₆ source inferred from long-term high precision atmospheric measurements and its comparison with emission inventories.” *Atmos. Chem. Phys.*, **10** (6), 2655–2662, **2010**, URL <http://dx.doi.org/10.5194/acp-10-2655-2010>.
- Liebl H. *Applied Chared Particle Optics*. Springer Science & Business Media. ISBN 9783540719250, **2008**.
- Lindstrom P & Mallard WG. ““Mass Spectra” by NIST Mass Spec Data Center, S.E. Stien (director).” In: “NIST Chem. WebBook, NIST Stand. Ref. Database Number 69,” National Institute of Standards and Technology, Gaithersburg MD, 20899, <http://webbook.nist.gov> (retrieved 17/11/2014), **2014**.
- Lindstrom P & Mallard WG. ““Boiling Point Data” by R.L. Brown and S.E. Stein.” In: “NIST Chem. WebBook, NIST Stand. Ref. Database Number 69,” National Institute of Standards and Technology, Gaithersburg MD, 20899, <http://webbook.nist.gov> (retrieved 16/03/2015), **2015**.
- Lobert JM, Keene C, Logan A & Yevich R. “Global chlorine emissions from biomass burning: Reactive Chlorine Emissions Inventory.” *J. Geophys. Res.*, **104**, 8373–8389, **1999**.
- Lockwood AL, Shepson PB, Fiddler MN & Alaghmand M. “Isoprene nitrates: preparation, separation, identification, yields, and atmospheric chemistry.” *Atmos. Chem. and Phys.*, **10** (13), 6169–6178, **2010**, URL <http://dx.doi.org/10.5194/acp-10-6169-2010>.
- Mäkelä JM, Hoffmann T, Holzke C, Väkevä M, Suni T, Mattila T, Aalto PP, Tapper U, Kauppinen EI & O’Dowd CD. “Biogenic iodine emissions and identification of end-products in coastal ultrafine particles during nucleation bursts.” *J. Geophys. Res. Atmos.*, **107**, **2002**, URL <http://dx.doi.org/10.1029/2001JD000580>.
- Manley SL, Wang NY, Walser ML & Cicerone RJ. “Coastal salt marshes as global methyl halide

- sources from determinations of intrinsic production by marsh plants." *Global Biogeochem. Cycles*, **20 (GB3015)**, 2006, URL <http://dx.doi.org/10.1029/2005GB002578>.
- Manley SL, Wang NY, Walser ML & Cicerone RJ. "Methyl halide emissions from greenhouse-grown mangroves." *Geophys. Res. Lett.*, **34**, 2007, URL <http://dx.doi.org/10.1029/2006GL027777>.
- McCulloch A. "Chloroform in the environment: occurrence, sources, sinks and effects." *Chemosphere*, **50 (10)**, 1291–308, 2003.
- McCulloch A, Aucott ML, Graedel TE, Kleiman G, Midgley PM & Li YF. "Industrial emissions of trichloroethene, tetrachloroethene, and dichloromethane : Reactive Chlorine Emissions Inventory." *J. Geophys. Res.*, **104 (D7)**, 8417–8427, 1999, URL <http://dx.doi.org/10.1029/1999JD900011>.
- Mead MI, Khan MaH, Nickless G, Greally BR, Tainton D, Pitman T & Shallcross DE. "Leaf cutter ants: a possible missing source of biogenic halocarbons." *Environ. Chem.*, **5 (1)**, 5, 2008a, URL <http://dx.doi.org/10.1071/EN07068>.
- Mead MI, White IR, Nickless G, Wang KY & Shallcross DE. "An estimation of the global emission of methyl bromide from rapeseed (*Brassica napus*) from 1961 to 2003." *Atmos. Environ.*, **42 (2)**, 337–345, 2008b, URL <http://dx.doi.org/10.1016/j.atmosenv.2007.09.020>.
- Mesnildrey L, Jacob C, Frangouides K, Reunavot M & Leseur M. "Seaweed industry in France, Report Interreg program NETALAGAE." *Les Publ. du Pôle Halieut. AGROCAMPUS OUEST No. 9.*, page 34, 2012.
- Metz B, Kuijpers L, Solomon S, Andersen SO, Davidson O, Pons J, de Jager D, Kestin T, Manning M & Meyer L (editors). *IPCC/TEAP Special Report: Safeguarding the Ozone Layer and the Global Climate System: Issues Related to Hydrofluorocarbons and Perfluorocarbons*. Cambridge University Press, UK, Cambridge UK, 2005.
- Mlynski V & Guilhaus M. "Matrix-assisted Laser/Desorption Ionization Time-of-flight Mass Spectrometer with Orthogonal Acceleration Geometry: Preliminary Results." *Rapid Commun. Mass Spectrom.*, **10 (12)**, 1524–1530, 1996, URL [http://dx.doi.org/10.1002/\(SICI\)1097-0231\(199609\)10:12<1524::AID-RCM674>3.0.CO;2-P](http://dx.doi.org/10.1002/(SICI)1097-0231(199609)10:12<1524::AID-RCM674>3.0.CO;2-P).
- Molina M & Rowland F. "Stratospheric sink for chlorofluoromethanes: chlorine atom-catalysed destruction of ozone." *Nature*, **249**, 810–812, 1974.
- Montzka SA, Calvert P, Hall BD, Elkins JW, Conway TJ, Tans PP & Sweeney C. "On the global distribution, seasonality, and budget of atmospheric carbonyl sulfide (COS) and some similarities to CO₂." *J. Geophys. Res.*, **112 (D9)**, D09,302, 2007, URL <http://dx.doi.org/10.1029/2006JD007665>.
- Montzka SA & Fraser PJ. "Controlled Substances and Other Source Gases." In: CE Ennis (editor), "Scientific Assessment Ozone Depletion 2002, Global Ozone Research Monitoring Project Report No. 47," chapter 1, pages 1.1–1.71. World Meteorological Organization (WMO), Geneva, Switzerland, 2003.
- Montzka SA, Myers RC, Butler JH, Elkins JW, Lock LT, Clarke AD & Goldstein AH. "Observations of HFC-134a in the remote troposphere." *Geophys. Res. Lett.*, **23 (2)**, 169–172, 1996, URL <http://dx.doi.org/10.1029/95GL03590>.
- Montzka SA & Reimann S. "Chapter 1: Ozone-Depleting Substances (ODSs) and related chemicals." In: CE Ennis (editor), "WMO (World Meteorological Organization Scientific Assessment Ozone Depletion 2010 Global Research Monitoring Project - Report No. 52," 52, chapter 1. World Meteorological Organization, Geneva, Switzerland, 2011.
- Moore RM, Gut A & Andreae MO. "A pilot study of methyl chloride emissions from tropical woodrot fungi." *Chemosphere*, **58 (2)**, 221–5, 2005, URL <http://dx.doi.org/10.1016/j.chemosphere.2004.03.011>.
- Mühle J, Ganesan AL, Miller BR, Salameh PK, Harth CM, Greally BR, Rigby M, Porter LW, Steele LP, Trudinger CM, Krummel PB, O'Doherty S, Fraser PJ, Simmonds PG, Prinn RG & Weiss RF. "Perfluorocarbons in the global atmosphere: tetrafluoromethane, hexafluoroethane, and octafluoropropane." *Atmos. Chem. Phys.*, **10 (11)**, 5145–5164, 2010, URL <http://dx.doi.org/10.1029/2009JD013001>.

- doi.org/10.5194/acp-10-5145-2010.
- NASA Earth Observations (NEO). “Carbon Monoxide (1 month - Terra/MOPITT).” Retrieved 17/11/2014, **2012**, URL http://neo.sci.gsfc.nasa.gov/view.php?datasetId=MOP_CO_M&year=2012.
- Newland MJ, Reeves CE, Oram DE, Laube JC, Sturges WT, Hogan C, Begley P & Fraser PJ. “Southern hemispheric halon trends and global halon emissions, 1978–2011.” *Atmos. Chem. Phys.*, **13** (11), 5551–5565, **2013**, URL <http://dx.doi.org/10.5194/acp-13-5551-2013>.
- NOAA: ESRL. “Earth System Research Laboratory Global Monitoring Divisions Central Calibration Laboratory: NOAA Calibration Scales for Various Trace Gases.”, **2008**, URL <http://www.esrl.noaa.gov/gmd/cc1/cc1.html>.
- O’Doherty S, Cunnold DM, Manning A, Miller BR, Wang RHJ, Krummel PB, Fraser PJ, Simmonds PG, McCulloch A, Weiss RF, Salameh P, Porter LW, Prinn RG, Huang J, Sturrock G, Ryall D, Derwent RG & S A Montzka. “Rapid growth of hydrofluorocarbon 134a and hydrochlorofluorocarbons 141b, 142b, and 22 from Advanced Global Atmospheric Gases Experiment (AGAGE) observations at Cape Grim, Tasmania, and Mace Head, Ireland.” *J. Geophys. Res.*, **109** (D06310), **2004**, URL <http://dx.doi.org/10.1029/2003JD004277>.
- O’Doherty S, Simmonds PG, Cunnold DM, Wang HJ, Sturrock GA, Fraser PJ, Ryall D, Derwent RG, Weiss RF, Salameh P, R MB & Prinn RG. “In situ chloroform measurements at Advanced Global Atmospheric Gases Experiment atmospheric research stations from 1994 to 1998.” *J. Geophys. Res.*, **106**, 20,429–20,444, **2001**, URL <http://dx.doi.org/10.1029/2000JD900792>.
- Oram DE, Mani FS, Laube JC, Newland MJ, Reeves CE, Sturges WT, Penkett SA, Brenninkmeijer CAM, Röckmann T & Fraser P J. “Long-term tropospheric trend of octafluorocyclobutane (c-C₄F₈ or PFC-318).” *Atmos. Chem. Phys.*, **12**, 261–269, **2012**, URL <http://dx.doi.org/10.5194/acp-12-261-2012>.
- Ozel M, Ward M, Hamilton J, Lewis AC, Raventos-Duran T & Harrison R. “Analysis of organic nitrogen compounds in urban aerosol samples using GC×GC-TOF/MS.” *Aerosol Sci. Technol.*, **44** (2), 109–116, **2010**, URL <http://dx.doi.org/10.1080/02786820903410105>.
- Pacey N, Beadle I, Heaton A & Newsome L. “Chemical discharges from nuclear power stations: historical releases and implications for Best Available Techniques.” Technical report, Environment Agency, Bristol, U.K. (retrieved 27/11/14), **2011**, URL https://www.gov.uk/government/uploads/system/uploads/attachment_data/file/290827/scho0911bubz-e-e.pdf.
- Prinn RG, Weiss RF, Fraser PG, Simmonds PJ, Cunnold DM, Alyea FN, O’Doherty S, Salameh P, Miller BR, Huang J, Wang RHJ, Hartley DE, Harth C, Steele LP, Sturrock G, Midgley PM & McCulloch A. “A history of chemically and radiatively important gases in air deduced from ALE/GAGE/AGAGE.” *J. Geophys. Res.*, **105** (D14), 17,751–17,792, **2000**, URL <http://dx.doi.org/10.1029/2000JD900141>.
- Prinn RG, Weiss RF, Fraser P J, Simmonds PG, Alyea FN & Cunnold DM. “The ALE/GAGE/AGAGE database, Dataset DB-1001.”, **2014**, URL <http://dx.doi.org/10.3334/CDIAC/atg.db1001>, [File names: RPB-medusa.mon, CGO-medusa.mon, MHD-medusa.mon, global_mean_ms.txt].
- Quack B & Wallace D. “Air-sea flux of bromoform: Controls, rates, and implications.” *Global Biogeochem. Cycles*, **17** (1), 1023, **2003**, URL <http://dx.doi.org/10.1029/2002GB001890>.
- Read KA, Mahajan AS, Carpenter LJ, Evans MJ, Faria BVE, Heard DE, Hopkins JR, Lee JD, Moller SJ, Lewis AC, Mendes L, McQuaid JB, Oetjen H, Saiz-Lopez A, Pilling MJ & Plane JMC. “Extensive halogen-mediated ozone destruction over the tropical Atlantic Ocean.” *Nature*, **453** (7199), 1232–5, **2008**, URL <http://dx.doi.org/10.1038/nature07035>.
- Rex M, Wohltmann I, Ridder T, Lehmann R, Rosenlof K, Wennberg P, Weisenstein D, Notholt J, Krüger K, Mohr V & Tegtmeier S. “A Tropical West Pacific OH minimum and implications for stratospheric composition.” *Atmos. Chem. Phys.*, **14**, 4827–4841, **2014**.

- Rhew RC, Miller BR & Weiss RF. "Natural methyl bromide and methyl chloride emissions from coastal salt marshes." *Nature*, **403**, 292–295, **2000**.
- Riese M, Ploeger F, Rap A, Vogel B, Konopka P, Dameris M, Forster P & Foster P. "Impact of uncertainties in atmospheric mixing on simulated UTLS composition and related radiative effects." *J. Geophys. Res.*, **117** (D16305), D16,305, **2012**, URL <http://dx.doi.org/10.1029/2012JD017751>.
- Saito T, Yokouchi Y, Kosugi Y, Tani M, Philip E & Okuda T. "Methyl chloride and isoprene emissions from tropical rain forest in Southeast Asia." *Geophys. Res. Lett.*, **35** (19), L19,812, **2008**, URL <http://dx.doi.org/10.1029/2008GL035241>.
- Saiz-Lopez A, Plane JMC, Baker AR, Carpenter LJ, von Glasow R, Gómez Martín JC, McFiggans G & Saunders RW. "Atmospheric Chemistry of Iodine." *Chem. Rev.*, **2011**, URL <http://dx.doi.org/10.1021/cr200029u>.
- Sala S, Bönisch H, Keber T, Oram DE, Mills G & Engel A. "Deriving an atmospheric budget of total organic bromine using airborne in situ measurements from the western Pacific area during SHIVA." *Atmos. Chem. Phys.*, **14** (13), 6903–6923, **2014**, URL <http://dx.doi.org/10.5194/acp-14-6903-2014>.
- Schauffler SM, Atlas EL, Blake DR, Flocke F, Lueb RA, Lee-Taylor JM, Stroud V & Travnicek W. "Distributions of brominated organic compounds in the troposphere and lower stratosphere." *J. Geophys. Res.*, **104** (D17), 21,513–21,535, **1999**, URL <http://dx.doi.org/10.1029/1999JD900197>.
- Scheele MP, Siegmund PC & Van Velthoven PFJ. "Sensitivity of trajectories to data resolution and its dependence on the starting point: In or outside a tropopause fold." *Meteorol. Appl.*, **3**, 267–273, **1996**, URL <http://dx.doi.org/10.1002/met.5060030308>.
- Schuck TJ, Brenninkmeijer CAM, Baker AK, Slemr F, Velthoven PFJV & Zahn A. "Greenhouse gas relationships in the Indian summer monsoon plume measured by the CARIBIC passenger aircraft." *Atmos. Chem. Phys.*, **10**, 3965–3984, **2010**.
- Sharkey TD, Wiberley AE & Donohue AR. "Isoprene emission from plants: why and how." *Ann. Bot.*, **101** (1), 5–18, **2008**, URL <http://dx.doi.org/10.1093/aob/mcm240>.
- Simmonds PG, Derwent RG, Manning AJ, Fraser PJ, Krummel PB, O'Doherty S, Prinn RG, Cunnold DM, Miller BR, Wang HJ, Ryall DB, Porter LW, Weiss RF & Salameh PK. "AGAGE Observations of Methyl Bromide and Methyl Chloride at Mace Head, Ireland, and Cape Grim, Tasmania, 19982001." *J. Atmos. Chem.*, **47** (3), 243–269, **2004**, URL <http://dx.doi.org/10.1023/B:JOCH.0000021136.52340.9c>.
- Simmonds PG, Manning AJ, Cunnold DM, McCulloch A, O'Doherty S, Derwent RG, Krummel PB, Fraser PJ, Dunse B, Porter LW, Wang RHJ, Grealley BR, Miller BR, Salameh P, Weiss RF & Prinn RG. "Global trends, seasonal cycles, and European emissions of dichloromethane, trichloroethene, and tetrachloroethene from the AGAGE observations at Mace Head, Ireland, and Cape Grim, Tasmania." *J. Geophys. Res.*, **111** (D18), D18,304, **2006**, URL <http://dx.doi.org/10.1029/2006JD007082>.
- Simpson IJ, Akagi SK, Barletta B, Blake NJ, Choi Y, Diskin GS, Fried A, Fuelberg HE, Meinardi S, Rowland FS, Vay Sa, Weinheimer AJ, Wennberg PO, Wiebring P, Wisthaler A, Yang M, Yokelson RJ & Blake DR. "Boreal forest fire emissions in fresh Canadian smoke plumes: C₁-C₁₀ volatile organic compounds (VOCs), CO₂, CO, NO₂, NO, HCN and CH₃CN." *Atmos. Chem. Phys.*, **11** (13), 6445–6463, **2011**, URL <http://dx.doi.org/10.5194/acp-11-6445-2011>.
- Sinha P. "Emissions of trace gases and particles from savanna fires in southern Africa." *J. Geophys. Res.*, **108** (D13), 8487, **2003**, URL <http://dx.doi.org/10.1029/2002JD002325>.
- Sinha P. "Emissions from miombo woodland and dambo grassland savanna fires." *J. Geophys. Res.*, **109** (D11), D11,305, **2004**, URL <http://dx.doi.org/10.1029/2004JD004521>.
- Sinnhuber B, Sheode N, Sinnhuber M, Chipperfield MP & Feng W. "The contribution of anthropogenic bromine emissions to past stratospheric ozone trends: a modelling study." *Atmos. Chem. Phys.*, **9**, 2863–2871, **2009**.

- Sive BC, Varner RK, Mao H, Blake DR, Wingenter OW & Talbot R. "A large terrestrial source of methyl iodide." *Geophys. Res. Lett.*, **34** (17), L17,808, **2007**, URL <http://dx.doi.org/10.1029/2007GL030528>.
- Smythe WR & Mattauch J. "A new mass spectrometer." *Phys. Rev.*, **40**, 429–433, **1932**.
- Smythe-Wright D, Boswell SM, Breithaupt P, Davidson RD, Dimmer CH & Eiras Diaz LB. "Methyl iodide production in the ocean: Implications for climate change." *Global Biogeochem. Cycles*, **20** (3), n/a–n/a, **2006**, URL <http://dx.doi.org/10.1029/2005GB002642>.
- Solomon S, Qin D, Manning M, Chen Z, Marquis M, Averyt K, Tignor M & Miller H (editors). *Contribution of Working Group I to the Fourth Assessment Report of the Intergovernmental Panel on Climate Change (IPCC)*. Cambridge University Press, Cambridge, United Kingdom and New York, NY, USA. ISBN 0521880092, **2007**, URL <http://dx.doi.org/volume>.
- Sprung D & Zahn A. "Acetone in the upper troposphere / lowermost stratosphere measured by the CARIBIC passenger aircraft : Distribution , seasonal cycle , and variability." *J. Geophys. Res.*, **115** (D16301), 1–12, **2010**, URL <http://dx.doi.org/10.1029/2009JD012099>.
- Sturges WT, Oram DE, Laube JC, Reeves CE, Newland MJ, Hogan C, Martinerie P, Witrant E, Brenninkmeijer CAM, Schuck TJ & Fraser PJ. "Emissions halted of the potent greenhouse gas SF₅CF₃." *Atmos. Chem. Phys.*, **12** (8), 3653–3658, **2012**, URL <http://dx.doi.org/10.5194/acp-12-3653-2012>.
- Tanaka PL, Riemer DD, Chang S, Yarwood G, McDonald-Buller EC, Apel EC, Orlando JJ, Silva PJ, Jimenez JL, Canagaratna MR, Neece JD, Mullins CB & Allen DT. "Direct evidence for chlorine-enhanced urban ozone formation in Houston, Texas." *Atmos. Environ.*, **37** (9-10), 1393–1400, **2003**, URL [http://dx.doi.org/10.1016/S1352-2310\(02\)01007-5](http://dx.doi.org/10.1016/S1352-2310(02)01007-5).
- Thouret V, Cammas JP, Sauvage B, Athier G, Zbinden R, Nédélec P, Simon P & Karcher F. "Tropopause referenced ozone climatology and inter-annual variability (1994–2003) from the MOZAIC programme." *Atmos. Chem. Phys.*, **6** (4), 1033–1051, **2006**, URL <http://dx.doi.org/10.5194/acp-6-1033-2006>.
- Toon OB, Starr DO, Jensen EJ, Newman PA, Platnick S, Schoeberl MR, Wennberg PO, Wofsy SC, Kurylo MJ, Maring H, Jucks KW, Craig MS, Vasques MF, Pfister L, Rosenlof KH, Selkirk HB, Colarco PR, Kawa SR, Mace GG, Minnis P & Pickering KE. "Planning, implementation, and first results of the Tropical Composition, Cloud and Climate Coupling Experiment (TC4)." *J. Geophys. Res.*, **115** (D10), **2010**, URL <http://dx.doi.org/10.1029/2009JD013073>.
- Turnpenny AWH, Coughlan J, Ng B, Crews P, Bamber RN & Rowles P. "Cooling water options for the new generation of nuclear power stations in the UK." Technical report, Environment Agency, Bristol, U.K., **2010**, URL https://www.gov.uk/government/uploads/system/uploads/attachment_data/file/291077/scho0610bsot-e-e.pdf (accessed 27/11/14).
- Umezawa T, Baker AK, Oram DE, Sauvage C, O'Sullivan D, Rauthe-Schöch A, Montzka SA, Zahn A & Brenninkmeijer CAM. "Methyl chloride in the upper troposphere observed by the CARIBIC passenger aircraft observatory: Large-scale distributions and Asian summer monsoon outflow." *J. Geophys. Res. Atmos.*, **119** (March), 5542–5558, **2014**, URL <http://dx.doi.org/10.1002/2013JD021396>.
- Vogt L, Gröger T & Zimmermann R. "Automated compound classification for ambient aerosol sample separations using comprehensive two-dimensional gas chromatography-time-of-flight mass spectrometry." *J. Chromatogr. A*, **1150** (1-2), 2–12, **2007**, URL <http://dx.doi.org/10.1016/j.chroma.2007.03.006>.
- Wallace JM & Hobbs PV. *Atmospheric Science an Introductory Survey*. Academic Press Inc. (London Ltd.), London, U.K., 1st edition. ISBN 0127329501, **1977**.
- Ward DE, Susott RA, Kauffmann JB, Babbitt RE, Cummings DL, Dias B, Holben BN, Kaufman YJ, Rasmussen RA & Setzer AW. "Smoke and fire characteristics for cerrado and deforestation burns in Brazil: BASEB experiment." *J. Geophys. Res.*, **97**, 14,601–14,619, **1992**.
- Watson JT & Sparkman OD. *Introduction to Mass Spectrometry: Instrumentation, Applications and Strategies for Data Interpretation*. John Wiley & Sons, Ltd., Chichester, 4th edition. ISBN

- 9780470516348, **2007**.
- Wayne RP. *Chemistry of Atmospheres*. Oxford University Press, New York, USA, 2nd edition. ISBN 0198555717, **1996**.
- White ML, Varner RK, Crill PM & Mosedale CH. “Controls on the seasonal exchange of CH₃Br in temperate peatlands.” *Global Biogeochem. Cycles*, **19 (GB4009)**, **2005**, URL <http://dx.doi.org/10.1029/2004GB002343>.
- Whitehead DC. “The Distribution and Transformations of Iodine in the Environment.” *Environ. Int.*, **10**, 321–339, **1985**.
- Wiley WC & McLaren IH. “Time-of-flight mass spectrometer with improved resolution.” *Rev. Sci. Instrum.*, **26 (12)**, 1150–1157, **1955**, URL <http://dx.doi.org/10.1063/1.1715212>.
- Williams J, Gros V, Atlas EL, Maciejczyk K, Batsaikhan A, Schöler HF, Forster C, Quack B, Yassaa N, Sander R & Van Dingenen R. “Possible evidence for a connection between methyl iodide emissions and saharan dust.” *J. Geophys. Res. Atmos.*, **112**, **2007**, URL <http://dx.doi.org/10.1029/2005JD006702>.
- Wisher A, Oram DE, Laube JC, Mills GP, van Velthoven PFJ, Zahn A & Brenninkmeijer CAM. “Very short-lived bromomethanes measured by the CARIBIC observatory over the North Atlantic, Africa and Southeast Asia during 2009–2013.” *Atmos. Chem. Phys.*, **14 (7)**, 3557–3570, **2014**, URL <http://dx.doi.org/10.5194/acp-14-3557-2014>.
- Wofsy SC. “HIAPER Pole-to-Pole Observations (HIPPO): fine-grained, global-scale measurements of climatically important atmospheric gases and aerosols.” *Philos. Trans. R. Soc. A*, **369 (1943)**, 2073–86, **2011**, URL <http://dx.doi.org/10.1098/rsta.2010.0313>.
- Wofsy SC, Daube BC, Jimenez R, Kort E, Pittman JV, Park S, Commane R, Xiang B, Santoni G, Jacob D, Fisher J, Pickett-Heaps C, Wang H, Wecht K, Wang QQ, Stephens BB, Shertz S, Watt A, Romashkin P, Campos T, Haggerty J, Cooper WA, Rogers D, Beaton S, Hendershot R, Elkins JW, Fahey DW, Gao RS, Moore F, Montzka SA, Schwarz JP, Perring AE, Hurst D, Miller BR, Sweeney C, Oltmans S, Nance D, Hintsä E, Dutton G, Watts LA, Spackman JR, Rosenlof KH, Ray EA, Hall B, Zondlo MA, Diao M, Keeling R, Bent J, Atlas EL, Lueb R & Mahoney MJ. “HIPPO Combined Discrete Flask and GC Sample GHG, Halo-, Hydrocarbon Data (R_20121129).”, **2012**, URL [http://dx.doi.org/http://dx.doi.org/10.3334/CDIAC/hippo_012\(Release:20121129\)\[FileNames:HIPPO_discrete_continuous_merge_20121129.tbl\]](http://dx.doi.org/http://dx.doi.org/10.3334/CDIAC/hippo_012(Release:20121129)[FileNames:HIPPO_discrete_continuous_merge_20121129.tbl]).
- Worton DR, Mills GP, Oram DE & Sturges WT. “Gas chromatography negative ion chemical ionization mass spectrometry: application to the detection of alkyl nitrates and halocarbons in the atmosphere.” *J. Chromatogr. A*, **1201 (1)**, 112–9, **2008**, URL <http://dx.doi.org/10.1016/j.chroma.2008.06.019>.
- Worton DR, Sturges WT, Schwander J, Mulvaney R, Barnola JM & Chappellaz J. “20th century trends and budget implications of chloroform and related tri- and dihalomethanes inferred from firn air.” *Atmos. Chem. Phys.*, **6**, 2847–2863, **2006**, URL <http://dx.doi.org/10.5194/acp-6-2847-2006>.
- Xiao X, Prinn RG, Fraser PJ, Simmonds PG, Weiss RF, O’Doherty S, Miller BR, Salameh PK, Harth CM, Krummel PB, Porter LW, Mühle J, Grealley BR, Cunnold D, Wang R, Montzka SA, Elkins JW, Dutton GS, Thompson TM, Butler JH, Hall BD, Reimann S, Vollmer MK, Stordal F, Lunder C, Maione M, Arduini J & Yokouchi Y. “Optimal estimation of the surface fluxes of methyl chloride using a 3-D global chemical transport model.” *Atmos. Chem. Phys.*, **10 (12)**, 5515–5533, **2010**, URL <http://dx.doi.org/10.5194/acp-10-5515-2010>.
- Yokelson RJ, Christian TJ, Karl TG & Guenther A. “The tropical forest and fire emissions experiment: laboratory fire measurements and synthesis of campaign data.” *Atmos. Chem. Phys.*, **8**, 3509–3527, **2008**.
- Yokelson RJ, Goode JG, Ward DE, Susott RA, Babbitt RE, Wade DD, Bertschi I, Griffith DWT & Hao WM. “Emissions of formaldehyde, acetic acid, methanol, and other trace gases from biomass fires in North Carolina measured by airborne Fourier transform infrared spectroscopy.” *J. Geophys. Res.*, **104 (D23)**, 109–125, **1999**, URL <http://dx.doi.org/10.1029/1999JD000000>.

- 1029/1999JD900817.
- Yokelson RJ, Karl T, Artaxo P, Blake DR, Christian TJ, Griffith DWT, Guenther A & Hao WM. “The Tropical Forest and fire emissions experiment: overview and airborne fire emission factor measurements.” *Atmos. Chem. Phys.*, **7** (3), 6903–6958, **2007**, URL <http://dx.doi.org/10.5194/acpd-7-6903-2007>.
- Yokouchi Y, Hasebe F, Fujiwara M, Takashima H, Shiotani M, Nishi N, Kanaya Y, Hashimoto S, Fraser P, Toom-Sauntry D, Mukai H & Nojiri Y. “Correlations and emission ratios among bromoform, dibromochloromethane, and dibromomethane in the atmosphere.” *J. Geophys. Res.*, **110** (D23), D23,309, **2005**, URL <http://dx.doi.org/10.1029/2005JD006303>.
- Yokouchi Y, Ikeda M, Inuzuka Y & Yukawa T. “Strong emission of methyl chloride from tropical plants.” *Nature*, **416** (6877), 163–5, **2002**, URL <http://dx.doi.org/10.1038/416163a>.
- Yokouchi Y, Osada K, Wada M, Hasebe F, Agama M, Murakami R, Mukai H, Nojiri Y, Inuzuka Y, Toom-Sauntry D & Fraser P. “Global distribution and seasonal concentration change of methyl iodide in the atmosphere.” *J. Geophys. Res.*, **113** (D18), 1–9, **2008**, URL <http://dx.doi.org/10.1029/2008JD009861>.
- Yokouchi Y, Saito T, Ishigaki C & Aramoto M. “Identification of methyl chloride-emitting plants and atmospheric measurements on a subtropical island.” *Chemosphere*, **69** (4), 549–53, **2007**, URL <http://dx.doi.org/10.1016/j.chemosphere.2007.03.028>.
- Yvon-Lewis SA, Saltzman ES & Montzka SA. “Recent trends in atmospheric methyl bromide: analysis of post-Montreal Protocol variability.” *Atmos. Chem. Phys.*, **9**, 5963–5974, **2009**.
- Zahn A & Brenninkmeijer CAM. “New directions: a chemical tropopause defined.” *Atmos. Environ.*, **37** (3), 439–440, **2003**, URL [http://dx.doi.org/10.1016/S1352-2310\(02\)00901-9](http://dx.doi.org/10.1016/S1352-2310(02)00901-9).
- Zahn A, Weppner J, Widmann H, Schlote-Holubek K, Burger B, Kühner T & Franke H. “A fast and precise chemiluminescence ozone detector for eddy flux and airborne application.” *Atmos. Meas. Tech.*, **5** (2), 363–375, **2012**, URL <http://dx.doi.org/10.5194/amt-5-363-2012>.

List of figures

1.1	Example of the vertical temperature profile in the atmosphere. Courtesy of Wallace & Hobbs (1977).	2
2.1	van Deemter curves for nitrogen, helium and hydrogen carrier gases. The values given are based on a $250\ \mu\text{m} \times 30\ \text{m}$ column with a film thickness of $0.25\ \mu\text{m}$. Adapted from Hübschmann (2009).	25
2.2	Schematic of a quadrupole mass filter, showing ion trajectories. Only ions of one m/z value have a stable enough trajectory to reach the detector. Courtesy of Watson & Sparkman (2007).	26
2.3	Schematic representation of a linear time-of-flight mass spectrometer.	27
2.4	An illustration of spectral skewing due to dynamic changes in analyte partial pressure in an instrument that scans across an m/z range, from low to high masses, during GC elution (distortion has been exaggerated for clarity). During the leading and trailing portions of the peak, where the concentration of the eluent is rapidly changing, the mass spectrum is distorted (Scans #1 and #3). For instance, during a spectral acquisition on the leading edge of the peak, higher masses are recorded at slightly higher eluent concentration than the lower masses, skewing the mass spectrum towards higher m/z . The equivalent occurs on the trailing edge but with mass spectra skewed towards lower m/z . Adapted from Watson & Sparkman (2007).	29
2.5	Schematic of an orthogonal TOF mass spectrometer with reflectron. Ion packets are cut out of a continuous, collimated ion beam before ion separation.	30
2.6	Schematic of a reflectron ion mirror. Ions retain their original velocity (high, normal or low) but are detected at the same time because of the difference in residence time in the reflectron.	31
2.7	Typical mass spectrum for methyl bromide, CH_3Br . Intensities are given relative to the most intense ion in this case m/z 79. Based on data from the NIST Chemistry WebBook (Lindstrom & Mallard, 2014).	33
3.1	Photograph of the time-of-flight gas chromatography mass spectrometer (GC-TOF) provided by SAI (Scientific Analysis Instruments) Ltd. The left-hand panel houses the time-of-flight mass spectrometer (TOF), the central panel houses the gas chromatograph (GC) and the right-hand panel houses the GC control panel with a void that can be utilised for housing a controlling computer workstation.	40
3.2	Diagrammatic representation of the inlet system used for the GC-TOF. The MPC drier is a glass tube packed with magnesium perchlorate.	41
3.3	Screen-shot of the software output for selected ions acquired at constant temperature showing oscillations in the baseline. These oscillations are assumed to have been caused by pressure fluctuations due to either poor thermo-regulation in the GC oven or poor pressure regulation from the GC electronic pressure control.	42
3.4	Internal layout of the TOF MS showing the location of key elements.	43

3.6	Example mass spectra for CFC-115 (top) and H-1211 (bottom). Signal intensity is given in ion counts.	48
3.11	Locations of ClearfLo measurement sites. Urban observations were made at several locations in central London (main map). Measurements were also undertaken at three rural locations (see inset). UEA measurements were undertaken at the Sion Manning school site at the middle left of the main map. Image courtesy of Bohnenstengel et al. (2014).	59
3.14	Diagrammatic map of the areas used for determining the potential source region contributions at the Sion Manning school site using the NAME 1-day model.	70
3.15	Regional influences of air arriving at the Sion Manning school site. Air mass footprints are derived from the NAME particle dispersion model (Jones et al., 2007). The contribution of each geographical region represents the proportion of released particles found within 100 m of the surface of each region over a 1-day backwards mode model run following a process similar to that described in Fleming et al. (2012), Section 5. The geographical regions defined for this analysis are shown in Figure 3.14.	71
4.1	Collection locations of whole air samples for CARIBIC flight routes FRA-CCS/BOG, FRA-CPT and FRA-BKK-KUL. For the latter, air sample collection north of approximately 30° N were not analysed at UEA.	91
4.2	5 day back trajectories for the routes sampled in this study (see http://www.knmi.nl/samenw/campaign_support/CARIBIC/). An example of the air masses sampled along the FRA-CCS route (top); back trajectories for all samples along FRA-CPT (middle) and back trajectories for all samples along FRA-BKK-KUL (bottom).	94
4.3	Northern-hemispheric latitudinal distributions in Central American flights of VSLB and total VSLB-derived bromine ($\text{VSLB } \Sigma \text{ Br}_{\text{org}}$) for tropospheric samples, samples classified as having some stratospheric influence (following the definition in Sect. 4.3) and 5° latitudinal means of tropospheric samples above 10 km altitude with 1 σ error bars representing variability. Error bars on individual samples represent analytical uncertainties. All VSLB values on the vertical axes are given in ppt.	95
4.4	Plots of VSLB and total VSLB-derived bromine ($\text{VSLB } \Sigma \text{ Br}_{\text{org}}$) for Central American flights against potential temperature (Θ) with 5 K means. 5 K means with 1 σ error bars representing variability are separated into extra-tropical from March, April and May (MAM); extra-tropical from June, July, August and September (JJAS) and tropical samples from all months. Where fewer than three data points were available for averaging, error bars have not been added. Error bars on sample data points represent analytical uncertainties. All VSLB values on the horizontal axes are given in ppt.	98
4.5	Plots of VSLB and total VSLB-derived bromine ($\text{VSLB } \Sigma \text{ Br}_{\text{org}}$) for all samples on Central American flights against O_3 with 100 ppb binned means $\pm 1 \sigma$ error bars representing variability. Error bars on sample data points represent analytical uncertainties. Data points have been separated by colour into tropospheric samples and those with stratospheric influence (see Sect. 4.3). All VSLB values on the horizontal axes are given in ppt.	99
4.6	Plots of VSLB and VSLB-derived total bromine ($\text{VSLB } \Sigma \text{ Br}_{\text{org}}$) for Central American flights with O_3 -derived height above the thermal tropopause (z_{O_3}) as defined by Zahn & Brenninkmeijer (2003). Error bars represent analytical uncertainties. The tropopause is defined as $z_{\text{O}_3} = 0$ (see Sect. 4.3.1.3). All VSLB values on the horizontal axes are given in ppt.	102

4.7	Latitudinal distributions in South African (top) and Southeast Asia (bottom) flights of VSLB and total VSLB-derived bromine (VSLB Σ Br _{org}) with 10° (South African flights) and 5° (Southeast Asia) latitudinal means of tropospheric samples above 10 km altitude with 1 σ error bars representing variability. Latitudinal averages for South African flights are shown for all samples and for samples collected on the return flight (see Sect. 4.3.2). All samples in both routes are tropospheric (following the definition in Sect. 4.3) with error bars representing analytical uncertainties. All VSLB values on the horizontal axes are given in ppt.	104
5.1	Comparison of CO data derived from time-averaged in situ high-frequency measurements and bottle measurements. Error bars on the bottle data represent precision and are $\pm 1\sigma$. Included is a 3 rd order polynomial orthogonal distance regression (ODR) fit to the data. 95% confidence and prediction bands are shown as well as the equation of the fit line. Errors in the fit are $\pm 1\sigma$. The labelled outlier was excluded from the fit.	111
5.2	Overview of SAMMBA sample locations and grouping.	116
5.4	Plots against CO for halocarbons measured during SAMBBA excluding the methyl halides.	118
5.5	Comparison of NEMRs for forest fire, cerrado fire and regional haze/smoke	125
5.6	Trends of methyl halide enhancements with MCE in forest fires.	126
5.7	Emission factors in forest fires for methyl halides against MCE.	127
5.8	Chlorobenzene, as a fraction relative to standard (f.o.s.) plotted against CO for all bottle samples collected during the campaign.	127
5.9	Plots of Δ COS against Δ CO for forest fire, cerrado savannah and regional haze/smoke samples and. Error bars represent analytical uncertainties. Fit lines are orthogonal distance regression fits, weighted by sample errors and forced through the origin. Also shown are 95% confidence intervals for the fit lines.	128
5.10	COS plotted against latitude for samples collected on background flights. Error bars represent analytical uncertainties.	128
5.11	Emission factor (EF) versus modified combustion efficiency (MCE) for forest and cerrado fires. Low values of MCE indicate smoldering combustion. Fits to the data are least squares linear regressions.	129
5.12	Isoprene and carbon monoxide (CO) plotted against latitude for background flights (735 and 749). Error bars represent analytical uncertainties. CO data are derived from time-averaged high-frequency measurements due to greater data coverage on these flights. At low CO mixing ratios, these measurements agree well with bottle measurements (See Section 5.2.2 for further details).	133
5.14	MeCl, MeBr, MeI and CO plotted against latitude for samples of background emissions (see Figure 5.2a). Error bars represent analytical uncertainties. CO data are derived from time-averaged high-frequency measurements due to greater data coverage on these flights. At low CO mixing ratios, these measurements agree well with bottle measurements (See Section 5.2.2 for further details).	135
5.20	CH ₂ Cl ₂ , CH ₂ Br ₂ , CHBr ₃ and PCE plotted against latitude for background flights (see Figure 5.2b). Error bars represent analytical uncertainties.	143

List of tables

1.1	Global mean mixing ratios (MR), atmospheric lifetimes, ozone depletion potentials (ODP) and 100-year time horizon global warming potentials (GWP_{100}) for compounds discussed in this work. Due to their short lifetimes and high spatial and temporal variability, short-lived compounds cannot be assigned a single ODP or GWP. Lifetimes for long-lived compounds are global lifetimes. Those for the short-lived compounds are local lifetimes and do not represent global lifetimes. Mixing ratios are global mean values for 2012 from AGAGE measurements (Prinn et al., 2000) unless otherwise stated. ODPs and lifetimes have been taken from Montzka & Reimann (2011) except where indicated.	8
1.2	Estimated sources and sinks for methyl chloride (CH_3Cl) based on Clerbaux & Cunnold (2007) and references therein.	12
1.3	Estimated sources and sinks of chloroform ($CHCl_3$) based on McCulloch (2003).	13
1.4	Estimated sources and sinks of methyl bromide (CH_3Br) based on Montzka & Reimann (2011) and references therein.	15
1.5	Estimated sources and sinks of carbonyl sulfide (COS) based on Montzka et al. (2007).	17
2.1	Comparison of the limit-of-detection (LOD) for similar analyses made with negative ion chemical ionisation (NICI) and electron ionisation (EI) sources. The sensitivity enhancement is given as the ratio of LODs from the two techniques (NICI/EI). Compounds have been grouped to highlight the effects of functional group e.g. Cl, Br, I or ONO_2 , and in the case of halocarbons, the number of halogen atoms in the molecule. Based on data from Worton et al. (2008).	35
3.1	List of compounds identified in real air samples using GC-TOF	52
3.2	Compounds analysed insitu and in bottle samples for the ClearfLo project.	64
3.3	Table of mean values of ClearfLo bottle samples analysed by TOF GC-MS and in situ data analysed by NICI/EI GC-MS. In situ data are based on a linear interpolation between the two closest samples to the bottle sample. Variabilities are given as $\pm 1\sigma$ standard deviation of the mean. Halon 1211 and CH_2Cl_2 in situ values are from the NICI channel of the dual GC-MS.	69
3.4	Means $\pm 1\sigma$ standard deviations and medians with ranges in parentheses for dual NICI/EI GC-MS compounds measured during the summer IOP of ClearfLo at Sion Manning school in North Kensington. Errors on the mean represent variability.	73
4.1	Estimated limits of detection (LOD), compound dependant analytical precisions and mixing ratios at which the precision measurement was made for short-lived bromomethane species considered in this study (see Sect. 4.2.1 for further discussion of the working standard).	91

- 4.2 Summary of tropospheric tropical and extra-tropical 10–12.3 km mid-upper tropospheric means and medians for the bromomethanes and total VSLB-derived organic bromine (VSLB Σ Br_{org}) in Central American, South African and Southeast Asian CARIBIC flights (FRA-CCS/BOG, FRA-CPT, FRA-BKK and BKK-KUL) with comparison to literature values. Tropical is defined as between 24.4378° S and 24.4378° N. Values are means with $\pm 1\sigma$, medians in curly brackets and minimum/maximum values in parentheses except for WMO 2010 where medians are not given. Values in square brackets are the number of samples included in the average. All values are given in parts per trillion (ppt). 100
- 5.1 Compound dependent limits of detection (LOD), mean analytical precisions, mixing ratio in the standard used for calculations of compounds analysed in SAMBBA samples and ion mass-to-charge ratio (m/z) used for quantification. Precisions are the 1σ standard deviation of duplicate samples. 110
- 5.2 Comparison of NEMR_{CO} calculation methods and available CO datasets for forest fire samples (flight 737). Linear regression values are calculated as the gradient of an least orthogonal distance regression fits to enhancements in CO and MeX weighted by the errors in the data (see Section 5.3.1). Fits were repeated with the fit forced through the origin ($a = 0$), with negative values of Δ MeX and Δ CO (neg. Δ) and with both constraints ($a = 0, \text{neg.}\Delta$). For these values errors are the 1σ standard deviation of the fit. Mean values are the mean of individual sample $\Delta X/\Delta CO \pm 1\sigma$. All values are given to 2 significant figures. 120
- 5.3 Emission ratios relative to CO and CO₂ (NEMR_{CO} and NEMR_{CO₂} respectively), emission factors (EF) and modified combustion efficiencies (MCE) from the literature. NEMRs for this study include are derived from a linear orthogonal distance regression (ODR) fit with y-intercept forced through the origin of Δ CH₃X (X = Cl, Br or I) against Δ CO (derived from bottle measurements). EFs are in units of milligrams species per kilogram dry matter burned (mg kg^{-1}) and use CO, CO₂ and CH₄ derived from time-averaged high-frequency measurements (see Section 5.2.2 for discussion of bottle and high-frequency measurements). EFs for methyl halides are the mean of all plume samples with ranges in parentheses as they show a strong trend with MCE (see text). 122
- 5.4 Regional estimates of biomass burning emissions from South America and the contribution to global biomass burning emissions. Emissions estimates are based on biomass consumption figures given in Bond (2004) and emission factors given in Table 5.3. Ranges given for halomethanes reflect variability in emissions with the burning phase of a fire (see Section 5.4.2.3). Values are means $\pm 1\sigma$ for COS. Emissions estimates are given in units of Ggyr^{-1} . The contribution to global biomass burning emissions is also given as a percentage (Contribution / %). . . . 130
- 5.5 Global emission estimates of biomass burning from tropical forests and savannah based on biomass consumption estimates from Akagi et al. (2011). Estimates are derived from the mean emission factors given in Table 5.3. 131
- 5.6 Mean mixing ratios from background flight measurements made during SAMBBA. SAMBBA values are means $\pm 1\sigma$ standard deviation with minimum and maximum values in parentheses beneath. Monthly means for September 2012 ($\pm 1\sigma$) of baseline data from three AGAGE (Advanced Global Atmospheric Gases Experiment) sites are given for comparison as well as the AGAGE global monthly mean (Prinn et al., 2000; O’Doherty et al., 2001; Cox et al., 2003; Simmonds et al., 2004; Prinn et al., 2014). All values are molar mixing ratios in parts per trillion (ppt). 132

Major abbreviations and chemical formulae

BKK	Bangkok, Thailand
BOG	Bogotá, Columbia
Bromoform	Tribromomethane, CHBr_3
CCS	Caracas, Venezuela
CE	Combustion efficiency
CFC	Chlorofluorocarbon
CFC-11	CCl_3F
CFC-112	$\text{C}_2\text{Cl}_4\text{F}_2$
CFC-113	$\text{C}_2\text{Cl}_3\text{F}_3$
CFC-113a	CCl_3CF_3
CFC-115	C_2ClF_5
CFC-12	CCl_2F_2
Chloroform	Trichloromethane, CHCl_3
CPT	Cape Town, South Africa
CT	Chemical tropopause
EF	Emission factor
EI	Electron ionisation
ER	Emission ratio
FRA	Frankfurt, Germany
GC	Gas chromatography
$\text{GC} \times \text{GC}$	Two-dimensional gas chromatography
GC-MS	Gas chromatography mass spectroscopy
GWP	Global warming potential
H-1202	CBr_2F_2
H-1211	CBrClF_2
H-1301	CBr_3F
H-2402	$\text{C}_2\text{Br}_2\text{F}_4$
HCFC	Hydrochlorofluorocarbon
HCFC-133a	$\text{C}_2\text{H}_2\text{ClF}_3$
HCFC-141b	$\text{CH}_3\text{CCl}_2\text{F}$
HCFC-142b	CH_3ClF_2
HCFC-22	CHClF_2
HFC	Hydrofluorocarbon
HFC-134a	$\text{C}_2\text{H}_2\text{F}_4$
HFC-152a	CH_3CHF_2
HFC-227ea	CF_3CHCF_3
IOP	Intensive observation period
ITCZ	Inter-tropical convergence zone

LOD	Limit of detection
MBL	Marine boundary layer
MCE	Modified combustion efficiency
MeBr	Methyl bromide, bromomethane, CH ₃ Br
MeCl	Methyl chloride, chloromethane, CH ₃ Cl
MeI	Methyl iodide, iodomethane, CH ₃ I
Methyl chloroform	1,1,1-Trichloroethane, CH ₃ CCl ₃
MPC	Magnesium perchlorate, Mg(ClO ₄) ₂
MS	Mass spectrometer
NEMR	Normalised Emission Ratio
NH	Northern Hemisphere/Hemispheric
NICI	Negative ion chemical ionisation
NMHC	Non-methane hydrocarbon
oa-TOF	Orthogonal time-of-flight
ODP	Ozone depletion potential
ODS	Ozone depleting substance
PCE	Perchloroethene, C ₂ Cl ₄
PFC	Perfluorocarbon
PFC-218	C ₃ F ₈
PFC-C318	<i>c</i> -C ₄ F ₈
QMF	Quadrupole mass filter
re-TOF	Reflectron time-of-flight
RMS-S/N	Root mean squared signal-to-noise ratio
SH	Southern Hemisphere/Hemispheric
SIM	Single ion monitoring
TCE	Trichloroethene, C ₂ HCl ₃
TOF	Time-of-flight
TTL	Tropical tropopause layer
UTLS	Upper troposphere/lower stratosphere
VOC	Volatile organic compound
VSLB	Very short-lived bromomethanes
VSLs	Very short-lived substances